Stochastische modellering van radicalaire polymerisaties

Stochastic Modeling of Radical Polymerizations

Paul Van Steenberge

Promotoren: prof. dr. M.-F. Reyniers, prof. dr. ir. G. B. Marin
Proefschrift ingediend tot het behalen van de graad van
Doctor in de Ingenieurswetenschappen: Chemische Technologie

Vakgroep Chemische Proceskunde en Technische Chemie
Voorzitter: prof. dr. ir. G. B. Marin
Faculteit Ingenieurswetenschappen en Architectuur
Academiejaar 2012 - 2013

ISBN 978-90-8578-564-4
NUR 952
Wettelijk depot: D/2012/10.500/90

BEGELEIDINGSCOMMISSIE

Promotoren

prof. dr. Marie-Françoise Reyniers
Laboratorium voor Chemische Technologie
Vakgroep Chemische Proceskunde en Technische Chemie
Universiteit Gent

prof. dr. ir. Guy B. Marin
Laboratorium voor Chemische Technologie
Vakgroep Chemische Proceskunde en Technische Chemie
Universiteit Gent

Universiteit Gent
Vakgroep Chemische Proceskunde en Technische Chemie
Laboratorium voor Chemische Technologie

Technologiepark 918/Krijgslaan 281 S5
9000 Gent
België

Onderzoek gefinancierd met een specialisatiebeurs van het Instituut voor de Aanmoediging van Innovatie door Wetenschap en Technologie in Vlaanderen (IWT-Vlaanderen).

EXAMENCOMMISSIE

Leescommissie

prof. dr. Peter Adriaensens
Onderzoeksgroep Toegepaste en Analytische Chemie
Vakgroep Chemie
Universiteit Hasselt

prof. dr. Filip Du Prez
Polymer Chemistry Research Group
Vakgroep Organische Chemie
Universiteit Gent

dr. ir. Dagmar D'hooge [secretaris]
Laboratorium voor Chemische Technologie
Vakgroep Chemische Proceskunde en Technische Chemie
Universiteit Gent

Andere leden

prof. dr. ir. Guy B. Marin [promotor]
Laboratorium voor Chemische Technologie
Vakgroep Chemische Proceskunde en Technische Chemie
Universiteit Gent

prof. dr. Marie-Françoise Reyniers [promotor]
Laboratorium voor Chemische Technologie
Vakgroep Chemische Proceskunde en Technische Chemie
Universiteit Gent

prof. dr. Dirk Vanderzande
Onderzoeksgroep Organische en Bio-Polymere Chemie
Vakgroep Chemie
Universiteit Hasselt

prof. dr. Piet Iedema
Van 't Hoff Institute For Molecular Sciences
Universiteit van Amsterdam

prof. dr. ir. Hendrik Van Landeghem [voorzitter]
Vakgroep Technische Bedrijfsvoering
Universiteit Gent

Contents

Preface

I would like to thank

Prof. M.-F. Reyniers and Prof. G. B. Marin, my supervisors, for their excellent guidance,

Prof. D. Vanderzande, Prof. P. Adriaensens for interesting discussions,

Prof. F. Du Prez, Prof. P. Iedema, Prof. H. Van Landeghem as jury members,

Dr. D. D'hooge for greatly appreciated help,

Dr. J. Vandenbergh for dedicated experiments,

all LCT colleagues,

my parents, my dearest friends and you for reading this.

Paul H. M. Van Steenberge

December 2012

Nederlandse samenvatting

Industriële processen om polymeermaterialen te produceren maken vaak gebruik van radicalaire polymerisaties. De materiaaleigenschappen worden bepaald door de microstructuur van het polymeer, die kan gesimuleerd worden door kinetische modellen als de reactiekinetiek gekend is. Het doel van dit doctoraat is de ontwikkeling van een kinetisch model, met behulp van de Monte Carlo techniek, dat de optimalisatie toelaat van de polymeermicrostructuur resulterend uit twee ladingsgewijs bedreven radicalaire (co)polymerisaties: enerzijds de polymerisatie van *p*-quinodimethanen tot precursor poly(p-fenyleen vinyleen) (PPVs) en anderzijds de atoom transfer radicalaire copolymerisatie (ATRP). Voor de PPV synthese worden de *p*-quinodimethanen in situ verkregen door 1,6-eliminatie van de premonomeren 1-(chloromethyl)-4-[(n-octylsulfinyl)methyl]benzeen (en derivaten) en 2,5-bis(N,N-diethyldithiocarbamaat-methyl)-1-(3,7-dimethyloctyloxy)-4-methoxybenzeen via respectievelijk de sulfinyl en de dithiocarbamaat (DTC) precursor route. Voor het ATRP-proces zijn de comonomeren acrylaten en methacrylaten.

Hoofdstuk 1 is een inleiding over de modellering van de microstructuur van polymeren. De belangrijkste aanpakken tot modellering worden geclassificeerd volgens het detail waarin de polymeermicrostructuur beschreven wordt, de manier waarop transportfenomenen in rekening gebracht worden en de gebruikte numerieke techniek.

In Hoofdstuk 2 wordt de NaOtBu geïnduceerde 1,6-eliminatie van 1-(chloromethyl)-4-[(n-octylsulfinyl)methyl]benzeen en de daaropvolgende homopolymerisatie tot precursor PPV voor het eerst gemodelleerd. PPVs (en andere conjugeerde polymeren) worden gebruikt in opto-elektronische toepassingen en de efficiëntie van energie-omzetting wordt beïnvloed door de microstructuur (ketenlengtedistributie of gemiddelde ketenlengte en structuurdefecten). Snelheidscoëfficiënten in het model zijn gebaseerd op UV-vis (ultraviolet-visueel) spectroscopie en literatuur data. Het ontwikkelde kinetisch model is in overeenstemming met gaschromatografie (GC) en gelpermeatiechromatografie (GPC) data en berekent de ketenlengtedistributie, wat toelaat de opbrengst of de (gemiddelde) ketenlengte en het gehalte structurele defecten te optimaliseren. De uiteindelijke polymeeropbrengst en gemiddelde ketenlengte en gehalte structurele defecten worden enkel bepaald door de verhouding van de initiële base tot premonomeerconcentratie. Tevens wordt aangetoond dat intramoleculaire recombinatie van oligomere radicalen en intermoleculaire recombinatie van macroradicalen verwaarloosbaar zijn.

In Hoofdstuk 3 wordt het kinetisch model voor de voor PPV precursorspolymeervorming beschreven in Hoofdstuk 2 uitgebreid om het effect van de moleculaire structuur (aromatische kern, polarisator, uittredende groep en substituenten op de aromatische ring) op de polymeeropbrengst en de microstructuur van de PPV derivaten te beschrijven. Er wordt aangetoond dat de intermediaire *p*-quinodimethaan derivaten reageren op een tijdschaal van seconden tot minuten afhankelijk van hun moleculaire structuur, wat de snelheid van de dimerisatie (radicalaire initiatie) van de polymerisatie sterk beïnvloedt. In het bijzonder voor het effect van de substituenten op de aromatische ring, voldoen de gebruikte snelheidscoëfficiënten aan structuur-reactiviteitsrelaties. Deze laatste worden bepaald uit gerapporteerde ab initio data en UV-vis data. Bovendien wordt er duidelijk aangetoond dat enkel indien het effect van de moleculaire structuur op de dimerisatiesnelheid groot is, PPVs met elektronzuigende groepen lage ketenlengtes en PPVs met elektrongevende groepen hoge ketenlengtes vertonen. In een volgende stap wordt het kinetisch model uitgebreid naar copolymerisaties. Er wordt aangetoond dat de gemiddelde ketenlengte en het gehalte structurele defecten van PPVs met elektrongevende groepen lineair beïnvloed kan worden door kleine toevoegingen van premonomeren met elektronzuigende groepen tijdens de polymerisatie.

In Hoofdstuk 4 wordt het kinetisch model voor de sulfinyl route uitgebreid naar de dithiocarbamaat route, waarin zowel de uittredende groep als de polarisator dithiocarbamaat groepen zijn. In tegenstelling tot de sulfinyl route kan ook de polarisator uittreden tijdens de 1,6-eliminatie, waardoor een tweede monomeer gevormd wordt. Dit tweede monomeer is een structuurisomeer van het eerste monomeer en copolymerisatie van beide isomere monomeren kan leiden tot regioreguliere PPVs. Deze regioregulariteit is voordelig voor de performantie van opto-elektronische toestellen en dus is het belangrijk de oorsprong van de regioregulariteit te onderzoeken. De graad van regioregulariteit wordt bepaald door de gebruikte base voor de 1,6-eliminatie en wordt gemeten met proton Nucleaire Magnetische Resonantie (^{1}H NMR), wat een monomeersequentietypedistributie van lengte 3 oplevert, de zogenaamde triadedistributie. De uitbreiding van het kinetisch model uit Hoofdstuk 3 omvat het beschrijven van de vorming van de triaden door macroradicalen te onderscheiden op basis van de voorlaatste monomeereenheid. Het kinetische model is in overeenstemming met GC, GPC en de NMR triadedistributie. Er wordt aangetoond dat wanneer de base lithium bis(trimethylsilyl)amide (LHMDS) is, regioreguliere polymeren gevormd worden door sterische hinder tijdens de 1,6-eliminatie, terwijl voor de base KtBuO, regiorandom PPVs

gevormd worden. In het bijzonder werd vastgesteld, op basis van gesimuleerde en experimentele triadedistributies, dat voor de LHMDS base de 1,6-eliminatie reactiviteit van de ongehinderde protonen van het premonomeer driemaal hoger is dan die van de gehinderde protonen.

In Hoofdstuk 5 wordt de optimalisatie van de microstructuur van gradiëntcopolymeren onderzocht. Gradientcopolymeren zijn de belangrijkste kandidaten voor verbeterde schok-werende en dempende materialen dankzij hun breed glastransitietemperatuursbereik. Gradiënten in de monomeersequentie van copolymeerketens zijn aanwezig wanneer het geïncorporeerde monomeer gradueel varieert van het eerste monomeer aan het ene keteneinde naar het tweede monomeer aan het andere keteneinde. Gradiëntcopolymeren worden gesynthetiseerd via ladingsgewijs bedreven atoom transfer radicalaire polymerisatie (ATRP), één van de belangrijkste gecontroleerde radicalaire polymerisatietechnieken. De gradiëntkwaliteit is niet experimenteel toegankelijk, hoewel dit een belangrijke moleculaire eigenschap is. Het ontwikkelde kinetisch model verbetert modellen uit de literatuur door individuele macromoleculen te volgen, alsook hun monomeersequentie. Aan de hand hiervan kan een vergelijking gemaakt worden met de waarschijnlijkheden van de monomeren in een ideaal gradiëntprofiel van een polymeerketen, wat leidt tot een maat voor de gradiëntkwaliteit. Het effect van de polymerisatiecondities (reactiviteit en concentraties van het katalytisch systeem, beoogde ketenlengte) op de gradiëntkwaliteit wordt onderzocht voor de ladingsgewijs bedreven ATRP van acrylaten en methacrylaten. Er wordt vastgesteld dat de gradiëntkwaliteit stijgt wanneer de PDI daalt. In het bijzonder wordt een lineair verband tussen de PDI en de gradiëntkwaliteit vastgesteld bij volledige monomeerconversie over een breed PDI bereik ($1 < PDI < 2$). Bij lagere conversie (0.85; fractioneel) geldt een lineair verband over een nauwer PDI bereik ($1 < PDI < 1.2$) omdat het tweede comonomeer onvoldoende ingebouwd wordt, wat leidt tot gradiënten van slechte kwaliteit. Er wordt besloten dat de gradiëntkwaliteit kan verbeterd worden door de conversie en de controle over de ATRP te verhogen.

In Hoofdstuk 6 worden algemene conclusies geformuleerd en toekomstperspectieven geformuleerd. De algemene conclusies werden hierboven samengevat, terwijl de toekomstperspectieven vermelden dat het kinetisch ATRP model uitgebreid kan worden naar niet-lineair polymerisatie en gedispergeerde-fase polymerisatie in uniforme mengsels. Het nut van parallellisering voor deze modellen wordt besproken.

English summary

Industrial processes to produce plastics often involve radical polymerizations. The material properties are determined by the polymer microstructure, which can be simulated by kinetic models if the reaction kinetics are known. The objective of this PhD is the development of a kinetic Monte Carlo model which allows the optimization of the polymer microstructure resulting from two radical (co)polymerizations: polymerization of *p*-quinodimethanes toward precursor poly(p-phenylene vinylene)s (PPVs) and batch atom transfer radical polymerization (ATRP). For PPV synthesis, the *p*-quinodimethanes are obtained in situ via 1,6-elimination of the premonomers 1-(chloromethyl)-4-[(n-octylsulfinyl)methyl]benzene (and derivatives) and 2,5-bis(N,N-diethyldithiocarbamate-methyl)-1-(3,7-dimethyloctyloxy)-4-methoxybenzene respectively via the sulfinyl and the dithiocarbamate (DTC) precursor routes. For the ATRP, acrylates and methacrylates are considered as comonomers.

In Chapter 1, an introduction to modeling of the polymer microstructure is given. The most important modeling approaches are classified with respect to the detail in which polymer microstructure is described, the way transport phenomena are accounted for and the applied numerical technique.

In Chapter 2, the NaOtBu induced 1,6-elimination of 1-(chloromethyl)-4-[(n-octylsulfinyl)methyl]benzene and the ensuing homopolymerization toward precursor PPV is modeled for the first time. PPVs (and other conjugated polymers) are used in opto-electronic applications and the energy conversion efficiency is influenced by the microstructure (chain length distribution or average chain length and structural defects). Rate coefficients in the model are based on UV-vis (ultraviolet-visual) spectroscopy and literature data. The presented kinetic model is in agreement with gas chromatography (GC) and gel permeation chromatography (GPC) data and calculates the chain length distribution, allowing to optimize the yield or the (average) chain length and the structural defect content. The final polymer yield, average chain length and structural defect content are only determined by the ratio of the initial base to premonomer concentration. It is also shown that intramolecular recombination of oligomer radicals and intermolecular recombination of macroradicals are of negligible importance.

In Chapter 3, the modeling of the PPV precursor polymer formation described in Chapter 2 is extended to account for the effect of the molecular structure (aromatic moiety, polarizer,

leaving group and substituents on the aromatic moiety) on the polymer yield and microstructure of PPV derivatives. It is found that the intermediate *p*-quinodimethane derivatives react on a time scale of seconds to minutes depending on their molecular structure, strongly affecting the dimerization (radical initiation) rate of the polymerization. In particular for the effect of substituents on the aromatic moiety, rate coefficients obey structure-reactivity relations determined from reported ab initio data and UV-vis rate data. Moreover, it is demonstrated that, only when the effect of the molecular structure on the dimerization reaction is large, PPVs possessing electron withdrawing groups possess low chain lengths and PPVs possessing electron donating groups possess high chain lengths. In a next step, the kinetic model is extended toward copolymerizations. It is shown that the average chain length and structural defect content of PPVs with electron donating groups can be affected by small additions of premonomers with electron withdrawing groups during polymerization.

In Chapter 4, the kinetic model for the sulfinyl route is extended to the dithiocarbamate route, in which both leaving group and polarizer are dithiocarbamate groups. In contrast with the sulfinyl route, the polarizer group may be expelled during 1,6-elimination, forming a second monomer. The second monomer is an structural isomer of the first monomer, and copolymerization of both isomeric monomers may lead to regioregular PPVs. Such regioregularity is beneficial for opto-electronic device performance and the origin of regioregularity must be investigated to optimize regioregular polymers for such devices. The degree of regioregularity is determined by the base used for the 1,6-elimination and measured by ^{1}H NMR, yielding a monomer sequence type distribution of length 3, the so-called triad distribution. The extension of the kinetic model involves tracking the formation of such triads by distinguishing macroradicals based on their penultimate monomer unit. The kinetic model is in agreement with GC, GPC and the NMR triad distribution. It is shown that if the base is lithium bis(trimethylsilyl)amide (LHMDS) regioregular polymers are formed due to steric hindrance during 1,6-elimination, while in case the base is KtBuO regiorandom PPVs are formed. In particular, based on comparison of calculated and experimental triad distribution, it is determined that, for LHMDS, the 1,6-elimination reactivity via the unhindered protons of the premonomer is three times higher than via the hindered protons.

In Chapter 5, the optimization of the microstructure of gradient copolymers is investigated. Gradient copolymers are the most important candidates toward improved shock absorbing and damping materials due to their broad glass transition temperature range. Gradients in the monomer sequence of copolymer chains are present when the monomer incorporation

gradually shifts from the first monomer at one chain end to the second monomer at the other chain end. Gradient copolymers are synthesized via batch atom transfer radical polymerization (ATRP), one of the most important controlled radical polymerization techniques. It must be stressed that the quality of gradient copolymers is not experimentally accessible, although it is an important molecular property. The developed kinetic model improves on literature models by individually tracking macromolecules and their monomer sequence. The monomer sequences are then compared to the monomer probabilities of an ideal gradient profile, providing a measure for the gradient quality. The effect of the polymerization conditions (catalytic system reactivity and concentrations, targeted chain length) on the gradient quality is investigated for the batch ATRP of acrylates and methacrylates. It is found that when the PDI decreases, gradient quality increases. In particular, a linear correlation between PDI and gradient quality is found at a conversion of 1 over a wide PDI range ($1 < PDI < 2$). At lower conversions (0.85), the correlation holds over a narrow PDI range ($1 < PDI < 1.2$) because the second comonomer is incorporated insufficiently, leading to gradients of bad quality. The gradient quality can be improved by achieving higher conversion and better control over the ATRP.

In Chapter 6, general conclusions are given and future prospects formulated. The general conclusions are essentially discussed above, while the future prospects mention that the kinetic model for the ATRP can be extended to non-linear polymerization and dispersed phase polymerization in uniform reaction media. The merits of parallelization for these models is discussed.

List of symbols

Roman symbols

A	absorbance in UV-vis spectrum [-]
A	pre-exponential factor in Arrhenius expression [$L \cdot mol^{-1} \cdot s^{-1}$]
A	monomer A [-]
A	absorption in the UV-vis spectrum [-]
Ar	arylene [-]
B	monomer B [-]
C	macroscopic concentration [$mol \cdot L^{-1}$]
Cu(I)	copper with oxidation number 1 [-]
Cu(II)	copper with oxidation number 2 [-]
E1cb(irr)	irreversible first order elimination mechanism in which the conjugate base of the substrate is formed [-]
E2	second order elimination mechanism [-]
E	energy in Arrhenius expression [$kJ \cdot mol^{-1}$]
Et	ethyl group [-]
F(t)	copolymer composition, i.e. the monomer fraction incorporated in the copolymer at a given time t [-]
f	initial molar premonomer fraction in the premonomer feed [-]
f	ratio of rate coefficients [-]
f	initiator efficiency [-]
f(t)	comonomer fraction in the monomer mixture at a given time t [-]

H	benzylic proton close to OC_1 group in 2,5-bis(N,N-diethyldithiocarbamate-methyl)-1-(3,7-dimethyloctyloxy)-4-methoxybenzene [-]
h	discrete vector function describing the number of molecular combinations leading to every reaction [-]
I	initiator radical [-]
i	chain length [-]
j	chain length [-]
k	rate coefficient of a reaction with overall order n [$L^{n-1}\cdot mol^{1-n}\cdot s^{-1}$]
k	number of a simulated polymer chain [-]
$\tilde{k}$	single-event rate coefficient of a reaction with overall order n [$L^{n-1}\cdot mol^{1-n}\cdot s^{-1}$]
L	ligand [-]
L	leaving group [-]
l	optical path length [m]
l	monomer position in a polymer chain (l=1, …, i) [-]
ln	natural logarithm [-]
log	logarithm [-]
M	monomer [-]
M	number of reaction families [-]
M	average molar mass [$g\cdot mol^{-1}$]
M	metal [-]
MeOH	methanol [-]

N_A	Avogadro constant [mol^{-1}]
n	number of molecules [-]
n	oxidation state [-]
n	number of events [-]
OC_1	methoxy group [-]
OC_{10}	3,7-dimethyloctyloxy group [-]
ODMO	3,7-dimethyloctyloxy group [-]
OM	methoxy [-]
P	polarizer in precursor route for conjugated polymers [-]
P	dead polymer molecule [-]
P	reaction probability (scaled with all reactions) [-]
P_1	byproduct of nucleophilic addition in the sulfinyl route [-]
PreM	premonomer [-]
p(i,l)	probability at monomer position l in a polymer chain with length i [-]
p(k,l)	probability at monomer position l in a polymer chain k [-]
pKa,H_2O	acid dissociation coefficient at logarithmic scale ($-\log_{10}$ Ka) [-]
pyrH	hydrogen of a pyridine moiety [-]
R	alkyl group [-]
R	reaction rate [s^{-1}]
R	radical [-]
R^2	correlation coefficient [-]
RO^-	alkoxide base [-]

r	reaction rate [s^{-1}]
r	monomer reactivity ratio
r	random number between 0 and 1 [-]
S'(k,l)	cumulative (with respect to l) amount of monomer units evaluated from right to left [-]
S(k,l)	cumulative (with respect to l) amount of monomer units evaluated from left to right [-]
T	triad [-]
t	time [s]
V	simulated reaction volume [L]
X	halogen atom [-]
x	fractional conversion [-]
x	average chain length [-]
Y	yield [-]
Z	RAFT Z group [-]

Greek symbols

α,ω-macro-diradical	linear macrodiradical possessing radical centers at each chain end [-]
Δt	time step parameter in Guggenheim method [s]
ε	extinction coefficient of p-quinodimethane in sBuOH [$L \cdot mol^{-1} \cdot m^{-1}$]
μ	selected reaction channel [-]
ν	generic reaction channel [-]
ρ	Hammett reaction constant [-]

σ	Hammett substituent constant for the aromatic groups [-]
τ	elapsed time between two reaction events [s]

Subscripts

(H,H)	absence of substituents on the aromatic moiety
(L=Br)	pertaining to a rate coefficient in the sulfinyl route when Br is the leaving group
(L=Cl)	pertaining to a rate coefficient in the sulfinyl route when Cl is the leaving group
(OC_1,OC_{10})	OC_1 and OC_{10} substituents on the aromatic moiety
(OC_1,OC_1)	two OC_1 substituents on the aromatic moiety
(OC_{10},OC_{10})	two OC_{10} substituents on the aromatic moiety
(OR,OR)	OC_1 or OC_{10} substituents on the aromatic moiety
(P=SOC_8)	pertaining to a rate coefficient in the sulfinyl route when SOC_8 is the polarizer
(P=SO_2C_8)	pertaining to a rate coefficient in the sulfinyl route when SO_2C_8 is the polarizer
0	initiator
1	pertaining to a rate coefficient used in the Guggenheim method defined as $k_{E2}[RO^-]_0$
1	pertaining to a benzylic proton close to an OC_1 group in 2,5-bis(N,N-diethyldithiocarbamate-methyl)-1-(3,7-dimethyloctyloxy)-4-methoxybenzene [-]
1	pertaining to the first monomer reactivity ratio k_{pAA}/k_{pAB}
2	pertaining to a rate coefficient used in the Guggenheim method defined as $k_{NA}[RO^-]_0$

2	pertaining to a benzylic proton close to an OC_{10} group in 2,5-bis(N,N-diethyldithiocarbamate-methyl)-1-(3,7-dimethyloctyloxy)-4-methoxybenzene [-]
2	pertaining to the second monomer reactivity ratio k_{pBB}/k_{pBA}
A	generic molecule A
A	(pre)monomer A
A, ideal, A to B	pertaining to monomer A in an ideal A to B gradient profile
A, ideal, B to A	pertaining to monomer A in an ideal B to A gradient profile
a	(energy of) activation
a	pertaining to a 1,6-elimination rate coefficient for which the proton H_a is abstracted
a=b	pertaining to a rate coefficient for 1,6-elimination which is equal for both protons H_a and H_b
a=b,H,H	pertaining to a rate coefficient for 1,6-elimination ($k_{E2,a=b}$) in case no OC_1 or OC_{10} groups are present
a=b,X,Y	pertaining to a rate coefficient for 1,6-elimination ($k_{E2,a=b}$) in case OC_1 or OC_{10} groups are present
a,chem	pertaining to a chemical rate coefficient for activation
a,chem,AX	pertaining to activation of acrylic secondary dormant macroradical
a,chem,BX	pertaining to activation of methacrylate tertiary dormant macroradical
a,da,p,t	pertaining to a rate coefficient for activation, deactivation, propagation, termination
app	pertaining to an apparent rate coefficient
B	pertaining to a rate coefficient for 1,6-elimination from premonomer B in the sulfinyl route when two premonomers are present
B, ideal, B to A	pertaining to monomer B in an ideal B to A gradient profile

B, ideal, A to B	pertaining to monomer B in an ideal A to B gradient profile
Br	pertaining to a rate coefficient for 1,6-elimination in the sulfinyl route when Br is the leaving group
b	pertaining to a 1,6-elimination rate coefficient for which the proton H_b is abstracted
Cl	pertaining to a rate coefficient for 1,6-elimination in the sulfinyl route when Cl is the leaving group
chem	pertaining to a chemical rate coefficient
cyc	pertaining to a rate coefficient for cyclization of small diradicals
da,chem	pertaining to a chemical rate coefficient for deactivation
d,p,t,tr	pertaining to a rate coefficient for dissociation, propagation, termination and transfer
E2	1,6-elimination
E2,1	pertaining to a single-event rate coefficient for 1,6-elimination in the dithiocarbamate route for which the proton H_1 is abstracted
E2,2	pertaining to a single-event rate coefficient for 1,6-elimination in the dithiocarbamate route for which the proton H_2 is abstracted
exp	pertaining to a continuum rate coefficient
H	pertaining to a rate coefficient for 1,6-elimination in the sulfinyl route in absence of substituents on the aromatic moiety
H,1	structurally equivalent unhindered hydrogens in a premonomer without identical substituents on the aromatic moiety [-]
H,2	structurally equivalent hindered hydrogens in a premonomer without identical substituents on the aromatic moiety [-]
H,H	pertaining to a rate coefficient without substituents on the aromatic moiety

HML,A	premonomer A
HML,B	premonomer B
h	hindered
h,h	pertaining to an initiation by dimerization rate coefficient for which two bond forming carbon atoms are hindered by OC_{10} groups
ideal	ideal reference gradient
ini	initiation
ini	pertaining to a rate coefficient for initiation by dimerization of two monomers
ini,3	pertaining to a termolecular initiation by simultaneous dimerization and propagation of p-quinodimethanes
ini,AA	pertaining to a rate coefficient for initiation by dimerization of two monomers A
ini,AB	pertaining to a rate coefficient for initiation by dimerization of monomer A and B
ini,BB	pertaining to a rate coefficient for initiation by dimerization of two monomers B
ini(H,H)	pertaining to an initiation by dimerization rate coefficient in absence of substituents on the aromatic moiety
inst	instantaneous
K*t*BuO(**1**)	pertaining to a rate coefficient for 1,6-elimination from 1,4-Bis(N,N-diethyldithiocarbamate-methyl)-benzene in the dithiocarbamate route when KtBuO is the base
LHMDS(**1**)	pertaining to a rate coefficient for 1,6-elimination from 1,4-Bis(N,N-diethyldithiocarbamate-methyl)-benzene in the dithiocarbamate route when LHMDS is the base

LHMDS	pertaining to a rate coefficient for 1,6-elimination from 1,4-Bis(N,N-diethyldithiocarbamate-methyl)-benzene in the dithiocarbamate route when LHMDS is the base
MC	pertaining to a Monte Carlo rate coefficient
M	monomer
m	monomer
m	mass
max	maximum
meta	meta position with respect to the polarizer
NA	nucleophilic addition
NA,H	pertaining to a rate coefficient for conjugate nucleophilic addition in the sulfinyl route in absence of substituents on the aromatic moiety
NA,X	pertaining to a rate coefficient for conjugate nucleophilic addition in the sulfinyl route when X is the substituent on the aromatic moiety
n	base of the logarithm
n	number of molecules
ortho	ortho position with respect to the polarizer
p	propagation
p	pertaining to a radical propagation rate coefficient
p0,chem	pertaining to a chemical initiator radical propagation
pAA	pertaining to a radical propagation rate coefficient for addition of monomer A to a macroradical ending in monomer A
pAB	pertaining to a radical propagation rate coefficient for addition of monomer B to a macroradical ending in monomer A

pBA	pertaining to a radical propagation rate coefficient for addition of monomer A to a macroradical ending in monomer B
pBB	pertaining to a radical propagation rate coefficient for addition of monomer B to a macroradical ending in monomer B
p,AA	pertaining to a radical propagation rate coefficient for addition of monomer A to a macrodiradical ending in monomer A
p,AB	pertaining to a radical propagation rate coefficient for addition of monomer B to a macrodiradical ending in monomer A
para	para position with respect to the polarizer
p,BA	pertaining to a radical propagation rate coefficient for addition of monomer A to a macrodiradical ending in monomer B
p,BB	pertaining to a radical propagation rate coefficient for addition of monomer B to a macrodiradical ending in monomer B
prop	propagation
R2	initiator diradical
R3	diradicals with chain length 3
R4	diradicals with chain length 4
rc	macoradical termination by recombination
Rtot	pertaining to the total number of macroradicals
s	steric
t	transition
t	total
u	unhindered
u,h	pertaining to an initiation by dimerization rate coefficient for which one bond forming carbon atom is hindered by a OC_{10} group

u,u	pertaining to an initiation by dimerization rate coefficient for which two bond forming carbon atoms are close to OC_1 groups
X	substituent on the aromatic moiety
X,Y	pertaining to a rate coefficient characterized by substituents X and Y on the aromatic moiety
Y	substituent on the aromatic moiety
y	number of ligands

Acronyms

AFM	Atomic Force Microscopy
ATRP	Atom Transfer Radical Polymerization
CC-CLD	Chemical Composition – Chain Length Distribution
CCD	Chemical Composition Distribution
CF3	trifluoromethyl
CFD	Computational Fluid Dynamics
CLD	Chain Length Distribution
CN	cyano
CN-PPV	poly(2,5,2’,5’-tetrahexyloxy-7,8’-dicyanodi-*p*-phenylene vinylene)
CRP	Controlled Radical Polymerization
DCM	dichloromethane
DTC	dithiocarbamate
EDG	Electron Donating Group
EWG	Electron Withdrawing Group
FET	Field Effect Transistor
FRP	Free Radical Polymerization

GC	Gas Chromatography
GD	Gradient Deviation (of a single polymer chain), ranging from 0 to 1
GD*	number gradient deviation, ranging from 0 to 0.175
GD_1	first gradient evaluation method
GD_2	second gradient evaluation method
GD_3	third gradient evaluation method
GD_4	fourth gradient evaluation method
GD_5	fifth gradient evaluation method
GD_k*	unscaled gradient deviation using k-th gradient evaluation method
GD_{nosec}*	unscaled gradient deviation in which the gradient deviation of a single chain is proportional with i^{-1} instead of i^{-2}
GPC	Gel Permeation Chromatography
HDPE	high-density polyethylene
HML	premonomer
HOMO	Highest Occupied Molecular Orbital
IUPAC	International Union of Pure and Applied Chemistry
kMC	kinetic Monte Carlo
KtBuO	potassium tert-butoxide
LCB-CLD	Long Chain Branching – Chain Length Distribution
LDPE	low-density polyethylene
LHMDS	lithium bis(trimethylsilyl)amide
LUMO	Lowest Unoccupied Molecular Orbital
MDMO-PPV	poly(2-methoxy-5-(3',7'-dimethyloctyloxy)-1,4-phenylene vinylene)

MMF	monomethylformamide
MSTD	Monomer Sequence Type Distribution
Na*t*BuO	sodium tert-butoxide
nBuA	n-butyl acrylate
NIR	Near Infra-Red
NMP	Nitroxide Mediated Polymerization
NMR	Nuclear Magnetic Resonance
OFET	Organic Field Effect Transistor
OLED	Organic Light Emitting Diode
OPV	Organic Photovoltaic Cell
P3BT	poly(3-butylthiophene)
P3OT	poly(3-octylthiophene)
PCBM	phenyl-C_{61}-butyric acid methyl ester
PDI	polydispersity index
PPV	poly(p-phenylene vinylene)
PPX	poly(p-xylylene)
PPyV	poly(p-pyridyl vinylene)
PSD	Particle (droplet) Size Distribution
PTV	poly(2,5-thiophenediyl vinylene)
QSSA	Quasi-Steady State Approximation/Assumption
RAFT	Reversible Addition Fragmentation chain Transfer
RAFT-CLD-T	Reversible Addition Fragmentation chain Transfer-Chain Length Dependent-Termination

sBuOH	sec-butanol
SCB-CLD	Short Chain Branching – Chain Length Distribution
SEC	Size Exclusion Chromatography
SLD	Segment Length Distribution
TCL	Targeted Chain Length
TFT	Thin Film Transistor
THF	tetrahydrofuran
UV-vis	Ultra Violet-visual

Chapter 1: Introduction

Synthetic polymers are mainly used to manufacture plastic materials for commercial purposes. Crucial in the related industrial processes is a good control over the polymer microstructure, since the latter influences the mechanical, morphological, rheological, solubility and thermal properties of the polymer and consequently its processability and final application.[1,2] Optimization of existing industrial polymerization processes and the development of new polymer materials therefore requires a detailed insight in the relation between polymerization conditions and the polymer microstructure. As will be illustrated in this PhD thesis, kinetic modeling can be efficiently applied to achieve this goal.

In this chapter the most important microstructural polymer properties are first discussed. Next, the synthetic procedures for the studied radical polymerization techniques are introduced. Then, an overview is given of the modeling techniques available to describe the polymer microstructure for these processes. Finally, the objectives of this PhD thesis are defined and an outline of the remaining chapters is presented.

1.1. Polymer microstructure

A first important polymer microstructural property is the chain length distribution (CLD), which can be modeled as a probability density function. The CLD is often described for simplicity by the number average chain length x_n, i.e. the mean value, and the polydispersity index (PDI), i.e. a measure for the width. For many applications, a sufficiently high x_n is necessary to ensure a sufficiently high strength of the polymeric material.[1] On the other hand, rheological properties of the material which are important for processability are determined by the PDI. For polymers used for bulk plastics manufacturing, the PDI has to be rather high. A typical value for the PDI in free radical polymerization (FRP) is 2.[2]

The polymer microstructure is also determined by the topology of the polymer chains. For example, otherwise linear polymers may possess short or long chain branches (see Figure 1 for a simplified representation of a polymer chain with 5 branches). The effect of branches in the polymer microstructure on the polymer properties is illustrated by the difference in tensile strength between low-density and high-density polyethylene (LD/HDPE).[3,4] LDPE is a weaker material than HDPE since it possesses a high amount of (short) branches and a lower degree of crystallinity.

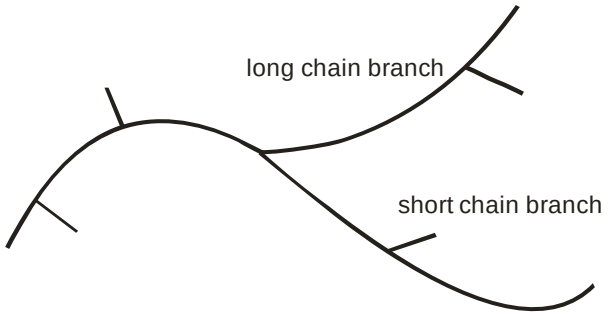

Figure 1: Long and short chain branches (simplified representation for clarity)

The location of substituents in the polymer backbone is also important for the polymer microstructure. E.g. if substituents are present at the same position with respect to the polymer backbone, the polymer is termed regioregular (Figure 2 top). If the location of the substituents is random, the polymer is regiorandom (Figure 2 bottom). Regioregularity affects the polymer morphology[5,6] and is thus an important characteristic of the polymer microstructure.

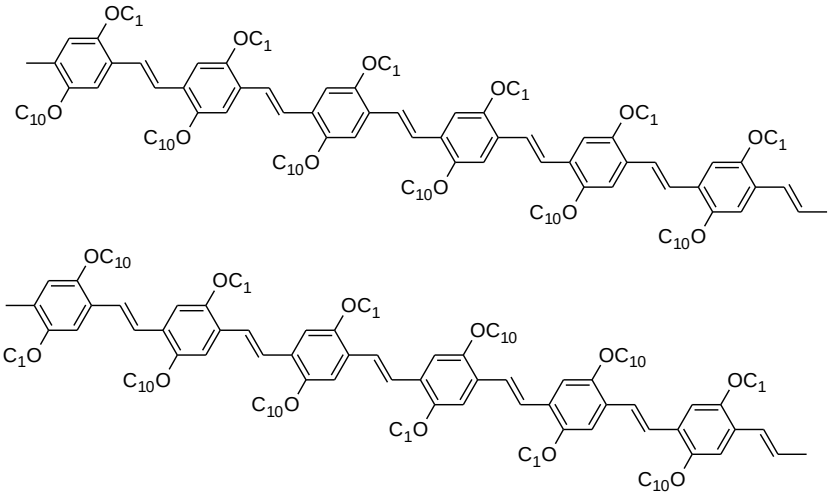

Figure 2: top: regioregular polymer; bottom: regiorandom polymer; shown for poly(2-methoxy-5-(3',7'-dimethyloctyloxy)-1,4-phenylene vinylene) (MDMO-PPV); OC_1: methoxy group; OC_{10}: 3,7-dimethyloctyloxy group

More complicated microstructures result when the polymer consists of more than one type of repeating unit, i.e. a copolymer. In such case, the microstructure also depends on the monomer sequence of every chain. Depending on the monomer sequence a block, alternating, statistical or gradient copolymer chain may result (Figure 3), and different properties are obtained. E.g. gradient copolymers possess a broad glass transition temperature range and hence are better candidates for damping (i.e. reducing oscillatory amplitude) and shock absorbing materials than other types of copolymers with the same monomer composition.[7]

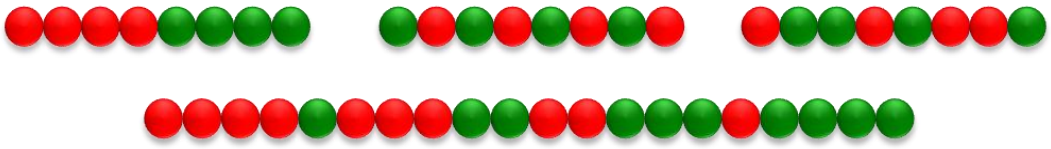

Figure 3: top: block, alternating and statistical copolymer chain; bottom: gradient copolymer chain

For copolymer microstructures, the CLD can be extended to a chemical composition – chain length distribution (CC-CLD)[2], which is a bivariate distribution of the polymer chains with respect to their chain length and chemical composition (Figure 4). In case only the composition is important, this CC-CLD is replaced by one of its two marginal distributions, the so-called chemical composition distribution[8] (CCD), which is a univariate distribution of the polymer chains with respect to their chemical composition (e.g. 50% comonomer A). Like the CLD, both the CC-CLD and CCD can modeled as probability density functions.

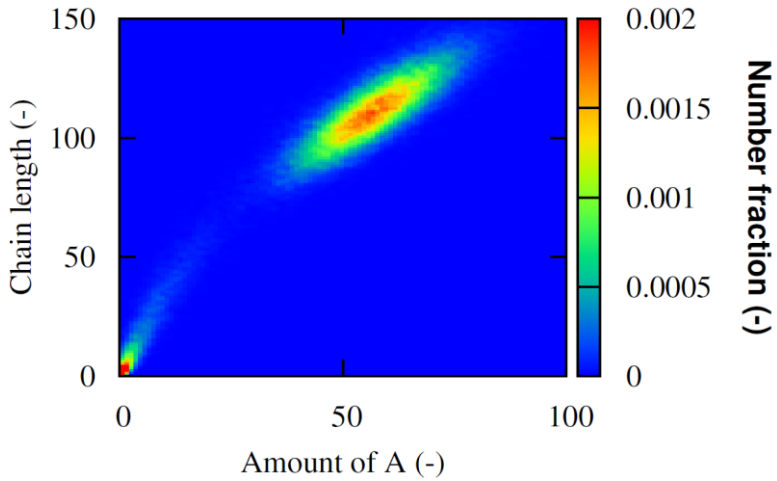

Figure 4: Chemical composition – chain length distribution (CC-CLD) for a copolymer

Aside from the CC-CLD and CCD, which characterize the distributed nature of polymer chains, also the distributed nature of monomer sequences may be characterized by probability density functions. A segment is defined as a sequence of monomers of the same type (a block). The segment length distribution[9-11] (SLD), as shown in Figure 5, describes the distribution of segments with respect to their length. Experimentally, UV-vis may allow qualitative tracking of segments of small length (~5 units).[12] The consideration of SLDs is in particular important for the controlled synthesis of gradient copolymers.[9-11,13]

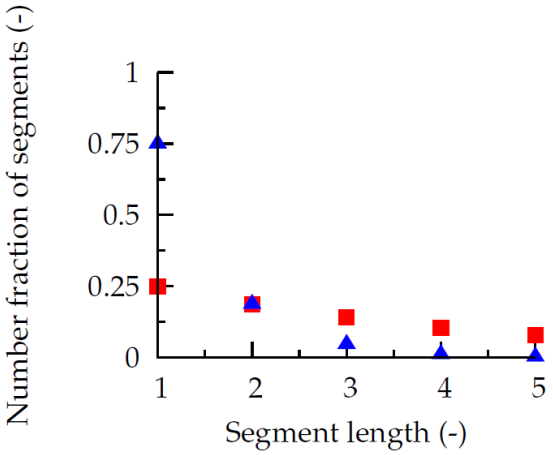

Figure 5: Segment length distribution for one of the repeating unit types in the copolymer

A second way of characterizing the distributed nature of monomer sequences is considering monomer sequences of fixed length but with variable composition and order, resulting in the so-called monomer sequence type distribution (MSTD). Note that the number of types of monomer sequences is a permutation with repetition, i.e. the number of types of monomer sequences is given by n^r in which n is the number of repeating units and r the length of the sequence in monomer units. To the best of our knowledge, such MSTDs have not been modeled thus far. However, nuclear magnetic resonance (NMR) has been used to determine the microstructure of the polymer and in particular the immediate vicinity of monomer units in a polymer backbone. For copolymers, the MSTD of length 2 has been determined using NMR, resulting in so-called diad fractions.[14] Similarly, for regioregular polymers resulting from copolymerization of isomeric comonomers, the MSTD of length 3 has also been determined using NMR, resulting in so-called triad fractions.[6] An example of the MSTD of length 3 is shown in Figure 6, which is a simulation result as a function of the kinetics of the polymerization.

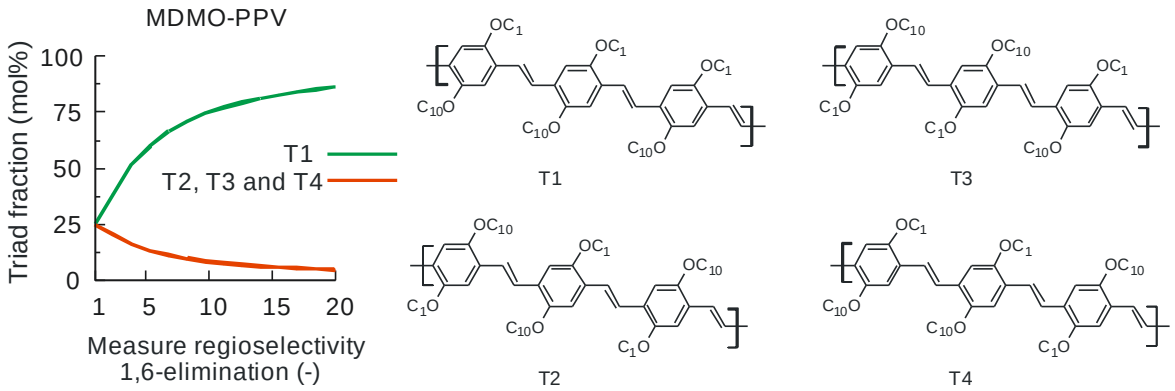

Figure 6: Monomer sequence type distribution (MSTD) of length 3, the so-called triad distribution; Shown for poly(2-methoxy-5-(3',7'-dimethyloctyloxy)-1,4-phenylene vinylene) (MDMO-PPV); OC_1: methoxy group; OC_{10}: 3,7-dimethyloctyloxy group

Next to monomer composition and connectivity, the polymer microstructure is also determined by defects. The influence of defects can be illustrated by polymers possessing alternating double and single carbon-carbon bonds, forming conjugated systems. Such conjugated polymers exhibit opto-electronic properties and are used in plastic/organic electronics.[15] Structural defects interrupt the conjugation and are known to affect device performance. Hence, controlling the occurrence of such defects is important for the optimization of e.g. organic solar cells and organic light emitting diodes. Another example is the lowering of the thermal stability of poly(vinyl chloride) in case internal allylic and tertiary chlorine groups are present.[16]

Finally, the polymer microstructure is determined by the presence of functional groups (e.g. unsaturations), which allow further chemical modification. Based on such groups, the microstructures discussed above may be combined toward more complex microstructures, e.g. brush and comb polymers, which are characterized by very high branching degrees along the polymer backbone (e.g. Figure 7). The microstructure of these molecular brushes or combs may consist of block, alternating, statistical or gradient branches, depending on the application envisaged. Often it is desired that their SEC-determined PDI is low, to achieve "predictable" material properties.[17] Note that in the case of non-linear topology, the SEC-determined PDI is not directly related to the width of the CLD since it is also affected by the branching degree.

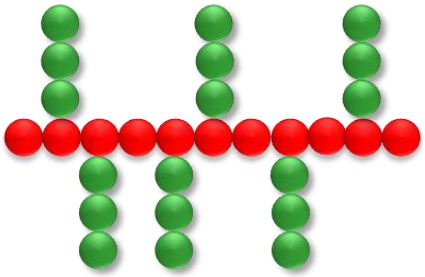

Figure 7: Polymer backbone with high branching degree

1.2. Polymerization techniques

Depending on the application, specific polymer properties are necessary and hence different synthetic approaches have been developed. Two main polymerization techniques can be distinguished[2]: (i) step-growth polymerizations, in which polymer growth takes place by reaction between macromolecules containing certain functional groups and (ii) chain-growth polymerizations, in which the polymers grow one monomer unit at a time. Within the chain-growth polymerizations, a distinction can be made between anionic, cationic, coordination (Ziegler-Natta, Phillips or metallocene catalyzed) and radical polymerizations. The latter are especially popular due to the large number of vinyl monomers that can be polymerized and the mild reaction conditions required. In this PhD thesis, radical polymerizations are considered with focus on formation of the polymer microstructure. In what follows the main characteristics of radical polymerizations are discussed. It is clearly demonstrated that, depending on the desired microstructure, different polymerization procedures are used.

$$I_2 \xrightarrow{f,\, k_d} 2\,I$$

$$I + M \xrightarrow{k_{p0}} R_1$$

$$R_i + M \xrightarrow{k_{pi}} R_{i+1}$$

$$R_i + R_j \xrightarrow{k_{tc,ij}} P_{i+j}$$

$$R_i + R_j \xrightarrow{k_{td,ij}} P_i + P_j$$

Figure 8: Principle of free radical polymerization; f: initiator efficiency; $k_{d,p,t}$: rate coefficient for dissociation, propagation, termination; I_2: radical initiator; M: monomer; P: dead polymer molecule; i, j: chain length

In conventional free radical polymerization (FRP), a radical initiator is typically heated to form initiator radicals, which start the chain reaction by adding monomer units, forming growing chains (Figure 8). Throughout the polymerization, radicals may terminate, forming dead polymer molecules.[17] The radical lifetime in FRP is typically 1 s.[17] Hence, dead polymer molecules and growing chains are created throughout the entire polymerization as long as new initiator radicals are formed, i.e. when a sufficiently high amount of conventional radical initiator is initially present. Consequently, the microstructure of the individual polymer chains differs greatly, both in composition and chain length, leading to broad CLDs and high PDIs.[18] Typical monomers which are used for FRP polymer products are vinyl monomers, such as styrene, acrylates, methacrylates, acrylamides, etc.

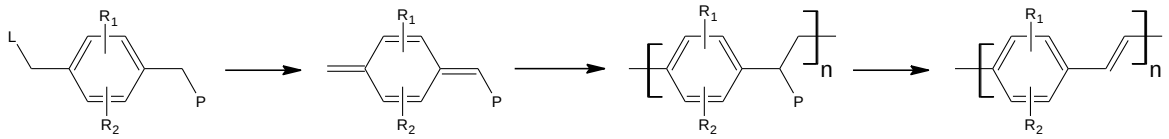

premonomer monomer precursor polymer conjugated polymer

Figure 9: Precursor route toward conjugated polymers; monomer = p-quinodimethane

However, if opto-electronic properties are necessary, conjugation along the polymer backbone is required, which cannot be easily obtained by such monomers via a radical mechanism. In that case, the radical polymerization of quinodimethanes (Figure 9) has been exploited allowing the formation of a conjugated polymer with high average chain length after backbone elimination of the precursor polymer,.[19] As shown in Figure 9, via this precursor route vinylene bonds are formed in several steps. Since the reactivity of p-quinodimethanes is high, the monomer needs to be formed in situ, i.e. a premonomer is used. For completeness, it is mentioned here that conjugated polymers with low average chain length are obtained using so-called direct routes, in which the vinylene bond is formed in one step via electrochemical polymerization, transition metal catalyzed coupling, step-growth polymerization or ring opening polymerization.[19]

It should be emphasized that the radical polymerization behavior of p-quinodimethanes is different from typical FRP processes. p-Quinodimethanes polymerize spontaneously at ambient temperature. Shortly after the p-quinodimethanes are formed, they dimerize forming diradical dimers, which act as chain initiators. General consensus is that polymer growth occurs via both chains ends, the growing macroradicals are termed α,ω-macrodiradicals.

Upon recombination of α,ω-macrodiradicals, the formed macromolecule is a longer α,ω-macrodiradical, which can continue growing by either monomer addition or further recombination. The optimization of conjugated materials hence necessitates kinetic models which are able to describe such binary[20] polymer growth.

In case end-group functionality X is required or when it is desired that individual polymer chains possess a comparable microstructure, mediating agents can be added to the conventional FRP, i.e. a controlled radical polymerization (CRP) is performed. The principle of one of the major CRP techniques, i.e. atom transfer radical polymerization (ATRP), is given in Figure 10. For well-chosen mediating agents, a (pseudo-)equilibrium between growing and dormant macromolecules can be established allowing an effective reduction of the radical concentration and the suppression of the formation of dead polymer molecules, which preserves the end-group functionality X of the polymer chains (Figure 10). These mediating agents allow to deactivate the macroradicals on the ~millisecond time scale (Table 1), forming dormant molecules, which can be reactivated on the time scale of minutes (Table 1) allowing further growth and thus an extension of the radical life time. Contrary, in FRP radicals a polymer chain typically is obtained after 1s in one sequence of propagation steps.

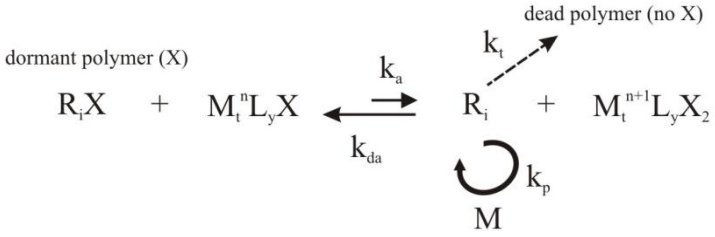

Figure 10: ATRP mechanism; termination leads to loss of X

Note that in Table 1 also the time scales are given for termination and propagation and a distinction is made between intrinsic and diffusional contributions. The apparent time scale follows after summation of these time scales. From low conversions onwards, termination becomes diffusion controlled[21] as evidenced by the significant increase of the apparent time scale for termination. Similarly, at high conversions deactivation becomes diffusion controlled,[21] which can be derived from a comparison of the apparent time scales for deactivation at low and high conversion.

Table 1: Time scales in a typical controlled ATRP process.

	0% conversion	50% conversion	90% conversion
Propagation (chemical)	10^{-4} s	$2\ 10^{-4}$ s	10^{-3} s
Propagation (diffusional)	10^{-11} s	$2\ 10^{-11}$ s	10^{-10} s
Propagation (apparent)	10^{-4} s	$2\ 10^{-4}$ s	10^{-3} s
Termination (chemical)	10^{-2} s	10^{0} s	$8\ 10^{-1}$ s
Termination (diffusional)	10^{-4} s	10^{3} s	10^{6} s
Termination (apparent)	10^{-2} s	10^{3} s	10^{6} s
Deactivation (chemical)	10^{-4} s	10^{-4} s	10^{-4} s
Deactivation (diffusional)	10^{-6} s	10^{-5} s	10^{1} s
Deactivation (apparent)	10^{-4} s	10^{-4} s	10^{1} s
Activation (chemical)	10^{2} s	10^{2} s	10^{2} s
Activation (diffusional)	10^{-6} s	10^{-5} s	10^{1} s
Activation (apparent)	10^{2} s	10^{2} s	10^{2} s

As shown in Figure 11, CRPs are distinguished based on the type of mediating agent used. In nitroxide mediated polymerization (NMP), a nitroxide radical reversibly forms a labile bond with the growing macroradicals. In atom transfer radical polymerization (ATRP), a halogen atom is transferred between a macroradical and transition metal complex. In reversible addition fragmentation chain transfer polymerization (RAFT), macroradicals may add to a RAFT chain transfer agent, forming stable radical adducts which may fragment at a later stage, continuing their growth. Ideally, in all these CRPs a simultaneous growth of all macromolecules takes place as polymerization proceeds. Hence, the CCD of the copolymer is much narrower than the CCD for the same copolymer obtained via FRP. Moreover, in case initiation is completed at low conversion a PDI close to unity is obtained, indicating a unique value for the chain length and coinciding number, mass and z average chain lengths of the CLD. For completeness, it is mentioned that for copper based CRPs a distinction can be made in case Cu(0) species are present and/or formed. An ATRP-like system results if comproportionation of the ATRP deactivator and Cu(0) is dominant, whereas in case disproportionation of the ATRP activator is the main reaction path, a so-called single electron transfer/living radical polymerization (SET/LRP) can be obtained.[22,23]

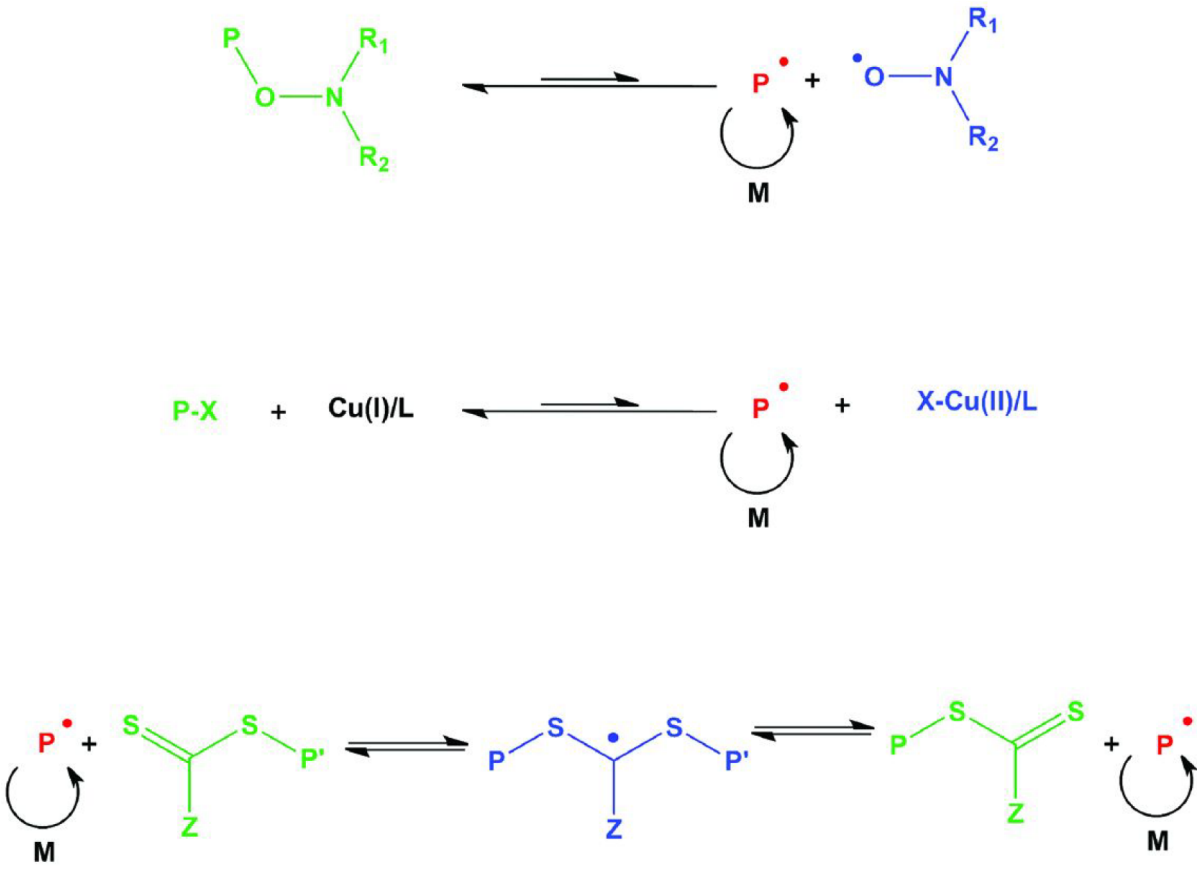

Figure 11: Principle of controlled radical polymerization: Nitroxide Mediated Polymerization (NMP, top), Atom Transfer Radical Polymerization (ATRP, center), Reversible Addition Fragmentation chain Transfer polymerization (RAFT, bottom)

1.3. Modeling of polymer microstructure originating from radical polymerizations

In this PhD thesis, it is shown that modeling of the polymer microstructure is a valuable tool to optimize radical polymerization processes in bulk and solution and that, in particular cases, information that is experimentally inaccessible can be obtained. Depending on the modeling technique, a different level of detail of the polymer microstructure is possible. A number of simple representations of the polymer microstructure has already been introduced above. In general, not all representations can be accessed by any modeling technique. In other words, a more detailed microstructural requires a more complex modeling technique. Therefore certain optimization strategies can only be performed in case the proper modeling technique is selected. In the remainder of this section, more complicated representations of the polymer microstructure and their relation to the modeling technique are discussed. At the same time, an overview is presented of the state of the art of microstructural modeling. In general, current modeling techniques for bulk and solution polymerization differ in the simulated

microstructure characteristics, i.e. the model complexity, the description of transport phenomena and the mathematical framework (stochastic or deterministic) describing the time evolution of the polymerization. In what follows, these three aspects are discussed.

1.3.1. Model complexity

To calculate the entire microstructure of a polymer, every macromolecule has to be tracked during the polymerization with respect to chain length, monomer sequence, defect/branching length and location, and functional groups. However, a high computational cost results in case such detailed description is targeted. The earliest (co)polymerization models were largely limited by computational resources and therefore more simplified models were developed instead.

In the simplest models for linear polymers, the description of the polymer microstructure is limited to the calculation of averages of the complete CLD: x_n, x_m and x_z.[16,24-49] Despite its low level of detail, this approach is very popular for two reasons: i) a relatively easy but simplified numerical technique, i.e. the so-called method of moments (see further), is available to calculate the averages of the complete CLD and ii) based on these simulated averages, certain polymer properties, such as the dynamic viscosity, can be assessed using empirical correlations.[50,51]

However, recent research[52-56] has indicated that even for a reliable calculation of these averages (and the polymerization rate) the calculation of the complete CLD is required due to the chain length dependency of the rates of reactions involving macrospecies. For example, termination involving long macroradicals is suppressed at high conversion due to the chain length dependency of the apparent rate coefficients. In addition, chain length dependency of the intrinsic chemical rate coefficients can theoretically influence the CLD. Apart from chain length dependent reaction kinetics, the moment averages are also insufficient for an optimization of polymers displaying multimodal CLDs.[52]

Therefore, new modeling methods have been developed which take into account explicitly the (chain length) distributed nature of the macromolecules. For linear and weakly branched polymers, a distinction is made between univariate descriptions and multivariate descriptions. It should be noted that neither of the latter track the individual polymer chains. In the univariate description, calculated distributions are only dependent on one stochastic variable (e.g. chain length), whereas in the multivariate description several stochastic variables (e.g. chain length, branching content and composition) are considered. Finally, more elaborated

modeling strategies allow individual tracking of individual (co)polymer molecules. Such methods are able to track the microstructure of each polymer molecule. In particular, this strategy allows the treatment of complex polymer topology. In what follows these methods are discussed.

1.3.1.1. Univariate distributions

Most modeling studies consider besides a calculation of the polymerization rate only the calculation of chain length characteristics, i.e. a univariate description with the chain length as the variable.[18,21,52,53,55-56] It should be noted that for branched polymers a univariate description with the chain length as variable is approximate: two branched polymer chains having the same total chain length, i.e. containing the same number of monomer units, are likely different with respect to their microstructure.

Compared to a calculation of averages only, the simulation of the complete CLD allows a more detailed study of the effect of polymerization conditions and reaction kinetics on the polymer microstructure. For example, Bentein et al.[56] showed that calculation of the complete CLD in nitroxide mediated polymerization (NMP) of styrene allows a reliable interpretation of the importance of (chain) transfer reactions and chain length dependent diffusional limitations (Figure 12). Similarly, He et al.[57] used CLD calculations to understand the NMP of styrene and Saliakas et al.[52] demonstrated that the industrial bulk FRP toward poly(methyl methacrylate) requires the calculation of the complete CLD.

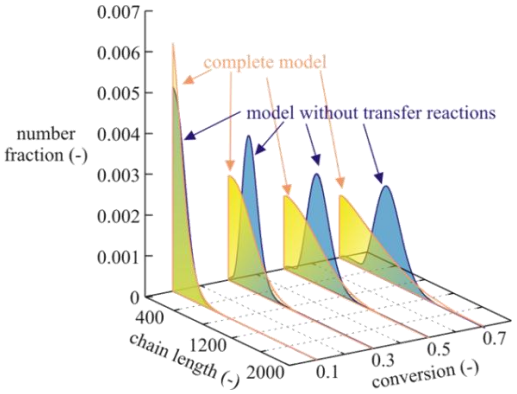

Figure 12: Importance of (chain) transfer reactions in NMP of styrene for the CLD as a function of conversion; data taken from from Bentein et al.[56]

Besides the CLD, for copolymerization also the copolymer composition is of importance. In a univariate description only the overall copolymer composition is simulated, i.e. the total amount of each comonomer in all copolymer chains. In contrast to homopolymerizations, compositional drift (i.e. the deviation of the copolymer composition from the monomer composition in the feed) can occur in copolymerizations.[58,59] If two comonomers are present, such compositional drift during the polymerization is typically described by a relation between $f_A(t)$, the fraction of comonomer A in the monomer mixture at a given time t, and $F_{A,inst}(t)$, the instantaneous copolymer composition, i.e. the fraction of monomer A incorporated in the copolymer at the same time. The most popular relation between f_A and $F_{A,inst}$ is the so-called Mayo-Lewis equation[2]:

$$F_{A,inst} = \frac{r_1 f_A^2 + f_A f_B}{r_1 f_A^2 + 2 f_A f_B + r_2 f_B^2}$$

in which r_1 and r_2 are the corresponding monomer reactivity ratios k_{pAA}/k_{pAB} and k_{pBB}/k_{pBA} with p denoting propagation. The wide-spread use of the Mayo-Lewis equation is related to its easy-to-use application and the limited number of parameters to be determined. It should however be stressed that the Mayo-Lewis equation is approximate since it is based on propagation kinetics only and the quasi-steady state approximation (QSSA) for both macroradical types. Also, only the last monomer unit in the growing macroradical is taken into account to describe the propagation kinetics, i.e. a terminal model is used.
Alternatively, the relation between f_A and $F_{A,inst}$ can be calculated via an empirical expression or using a kinetic model. For example, Wang and Hutchinson[60] used a kinetic model to implement penultimate models for starved feed copolymerizations of *n*-butyl methacrylate, styrene and *n*-butyl acrylate at elevated temperature. These authors illustrated that $F_{A,inst}$ depends strongly on the applied initial monomer fractions.

Finally, it should be mentioned that in univariate descriptions the presence of branching and defect formation[16,21] is described on an average basis, similar to the copolymer composition.[60] However, in principle, macromolecules with the former microstructural characteristics are distributed with respect to number of defects, branches and comonomers. If the description of these microstructural properties on a global basis is insufficient, then these microstructural properties must be considered on a molecular basis, using the multivariate descriptions discussed in the next paragraph.

1.3.1.2. Multivariate distributions

A typical example for a multivariate description of a homopolymerization is the calculation of the amount of branches per chain length present. E.g. Konkolowicz et al.[61] calculated the short chain branching – chain length distribution (SCB-CLD) to explain the difference in branching frequency between poly(*n*-butyl acrylate) made by FRP and ATRP. This multivariate description of a homopolymerization is shown in Figure 13. Similarly, Krallis and Kiparissides[62] calculated the long chain branching – chain length distribution (LCB-CLD) of poly(vinyl acetate) and LDPE, by tracking for each chain length the number of long chain branches, allowing a direct product evaluation.

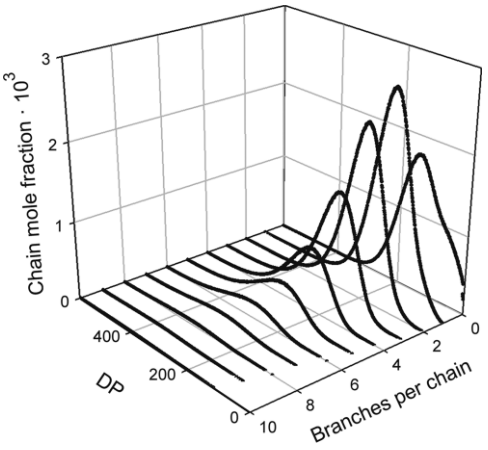

Figure 13: Example of multivariate description: short chain branching – chain length distribution (SCB-CLD); data from Konkolewicz et al.[61]

The most frequently used multivariate description for a copolymerization is the chemical composition – chain length distribution (CC-CLD) as introduced above. This distribution allows to calculate the chemical composition distribution (CCD), of which the broadness is an indication of the compositional homogeneity of the chains, irrespective of their chain length. For FRP, compositional heterogeneity is obtained, whereas compositional homogeneity results for CRPs.[18]

Szymanski[63] showed that the CC-CLD in living polymerization depends not only on the monomer reactivity ratios $r_1 = k_{pAA}/k_{pAB}$ and $r_2 = k_{pBB}/k_{pBA}$ but also on the reactivity ratio k_{AA}/k_{BB}. Furthermore, Krallis et al.[64] calculated the CC-CLD and CCD for bulk FRP of styrene with methyl methacrylate up to high conversions allowing computer-aided design of the related industrial process.

Hence, it can be concluded that the CC-CLD is an important copolymer property. However, in case not only information on composition but also on other microstructural characteristics is needed, the CC-CLD does not offer enough detail. For complex microstructures, such as gradient copolymers, (hyper)branched polymers, polymer brushes and polymer networks a large number of stochastic variables is needed. In particular for gradient copolymers, not only the chain length, but also the position in the chain and either the local segment length or local copolymer composition have to be included as variables.[9-11] However, multivariate methods become memory inefficient if the number of variables is too large, explaining the very recent research efforts to develop methods in which the microstructure of the individual polymer chains is tracked during the polymerization, as explained in the next section.

1.3.1.3. Individual tracking of macromolecules

For the description of the polymer structure using individual tracking of macromolecules, the reaction event history of every chain has to be tracked during the polymerization, taking into account the possible presence of multiple reactive centers. For example, Meimaroglou et al.[65] developed a stochastic algorithm to calculate the microstructure of highly branched low-density polyethylene (LDPE) polymer chains produced in solution and a high-pressure tubular reactor.

In this method, the LDPE homopolymer chain in Figure 14 was stored as [3,3,6,3,7,16,8,4,10] allowing an easy identification of the branching location and length. These authors reported that the number of long-chain branches and their length can be controlled both by the temperature and solvent concentration. In addition, based on this representation of the LDPE microstructure, the mean radius of gyration and the branching factor were calculated using a random-walk molecular simulator.

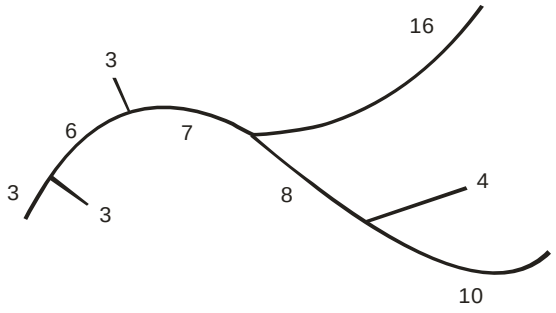

Figure 14: LPDE polymer chain translated to an description[65] using individual tracking of macromolecules

The potential of individual tracking of macromolecules can also be illustrated by its possibility to track monomer sequences. For example, Wang and Broadbelt[9-11,13] calculated the segment length distribution (SLD) in NMP gradient copolymers. A copolymer chain fragment …AABBBBABAA… was stored in vector notation […, 2, 4, 1, 2, ...]. Calculating the segment lengths for each position on the chain and for every chain length, allowed to obtain the number average segment length (and segment dispersity) as function of the position along the normalized chain length.

Hence, it can be concluded that both univariate or multivariate distributions can be obtained from methods tracking polymer chains individually. Therefore, in this PhD thesis this method was selected in case a detailed description of the copolymer was desired.

1.3.2. Transport phenomena

During a polymerization process the viscosity can increase significantly. Hence, it can be expected that at high conversions reactants diffuse slower towards each other before the actual reaction step takes place. In other words, apparent rate coefficients have to be used in the kinetic model instead of intrinsic chemical rate coefficients.[21,52-57,66]

For the major part of this PhD thesis, diffusional limitations can be neglected. Most simulations are related to solution polymerizations in which only a small amount of polymer is formed, i.e. the viscosity is low. The initial (pre)monomer are of the order of 0.1 M, whereas typical initial monomer concentrations for FRP and CRP, in which diffusional limitations can become important at sufficiently high conversions and chain lengths, are of the order of 10 M. The latter can also be understood by comparing time scales. Taking into account a typical average diffusion coefficient of 10^{-10} m^{-2} s^{-1} in low viscosity media,[21] a time scale of 10^{-5} s results for a macroradical, which is too low to obtain a diffusion controlled regime.

Similar to the diffusion of reactants toward each other on the molecular scale, fluid particles must mix on the meso- and on the macro- or reactor scale to allow reaction.[67-69] Mostly in modeling studies spatial homogeneity, i.e. perfect mixing, in one or more spatial directions is however assumed, leading to relatively simple continuity equations for the reaction components.

The simplest way to describe imperfect mixing on macroscale consists of representing the reactor with two (or more) perfectly mixed zones, accompanied with exchange (or recycle) flows between the zones.[70-73] In most mixing models, the zones are easily interpreted (e.g. around an impeller or around an inlet point in the reactor, or based on a cold-flow

computational fluid dynamics (CFD) simulations). More advanced models use zones with variable boundaries and volumes for moving reaction zones, using empirical correlations to define the growth and shrinkage of the zones.[74] Finally, the most fundamental descriptions are obtained using CFD, which integrate so-called Navier-Stokes equations on the discretized physical space.[75-80] However, since all reactant concentrations become function of the spatial coordinate, current CFD methods require the use of limited reaction schemes.

For simplicity, concentrations are also considered uniform in this PhD thesis, i.e. perfect mixing is assumed on scales larger than the molecular scale.

1.3.3. Numerical methods

The numerical methods to describe the polymerization rate and polymer microstructure characteristics may be divided into deterministic and stochastic methods. In the deterministic approach, the time evolution of chemical reactions is seen as a continuous predictable process. In such approach, differential equations are applied and integrated using either numerical methods or Monte Carlo integration. The latter deterministic integration method is profitable if the differential equations contain many independent variables, hence it is not useful if independent variables (concentrations) are assumed spatially uniform. In contrast to deterministic descriptions, stochastic descriptions sample reaction events from probabilities based on reaction kinetics, without resorting to differential equations. Hence, in such approach a random-walk character of the chemical reactions is obtained, with a unique, random solution for every simulation. Since the latter approach is most suitable to simulate detailed polymer microstructure characteristics, most attention is paid to the latter.

1.3.3.1. Deterministic methods

The most commonly used and fastest deterministic method is the method of moments in which only the above mentioned averages of the CLD are calculated.[16,24-49] In this method, the continuity equations for all macrospecies (typically 1000-10000) are reduced to moment equations (typically 3 per distribution type) using substitution of variables. These moment equations are integrated by linear multistep methods (e.g. the Adams and backward differentiation method).[81-83] However, during this integration mostly all population weighted apparent rate coefficients are kept constant as a function of the polymerization time, which is a rough assumption in case chain length dependent kinetics are important.[21,54-56,84-85] In principle, updated population weighted apparent rate coefficients can be obtained during the integration by a coarse description of the macroradical population, i.e. an approximated

macroradical distribution is calculated based on a distinction into coarse grains for which reactivity can be assumed equal.[21,54-56] Alternatively, correlations can be used to calculate these rate coefficients.[47]

Deterministic methods simulating the CLD differ in the technique used to discretize the chain length domain. As before, linear multistep methods are used to integrate the continuity equations corresponding to the discretized chain length domain. A discretization of the chain length domain is necessary to limit the number of continuity equations to be integrated. The most important methods are the fixed pivot method,[86-89] the orthogonal collocation on finite elements[90-92], the discrete weighted Galerkin formulation[93-95] and the extended methods of moments, e.g. the probability generating function (pgf) method.[96-98] The success of each of these methods depends on how well their chain length domain discretization can describe the different shapes of CLDs resulting from the reaction kinetics. If the shape of the CLD changes significantly throughout the polymerization, the discretization of the chain length domain must be either dynamically adaptive, which is a cumbersome task rarely performed, or include a large number of grid points. The same principle applies for the simulation of particle size distributions (PSDs), which are analogously affected by particle nucleation, growth, breakage or aggregation.[2]

1.3.3.2. Stochastic methods

For modeling of chemical kinetics stochastic or so-called kinetic Monte Carlo (kMC) approaches have been developed, which differ in the algorithm followed. The first kMC algorithms, the ”direct” and “first reaction” methods were proposed by Gillespie.[99] They are exact procedures for numerically simulating the time evolution of a uniform chemically reacting mixture and involve a linear search on the reaction probabilities. They differ in their usage of random generated numbers but both yield correct reaction event sampling. Later, modified algorithms were proposed in which the searching strategy and representation and storing of the reaction probabilities were altered.[100-101] One example is the “logarithmic direct method” discussed later.

The most important advantages of the kinetic Monte Carlo technique are its ease of implementation and its almost assumption-free nature, i.e. the method allows the description of any set of chemical reactions without QSSA application for the macroradicals or a priori information of the CLD shape. Stiffness of continuity equations implies a large difference in

magnitude of the integration variables and can thus lead to accuracy issues. In a kMC framework, the only penalty for highly stiff systems is computational time, due to the brute-force nature of the kMC method. Moreover, it is possible to implement the description of a wide range of polymer characteristics, going from calculating only average properties to tracking monomer sequences of individual chains and their topology, which cannot be performed by deterministic methods.

Practically, in Monte Carlo at certain time values one reaction is selected using search methods of logarithmic complexity based on a criterion which favors reactions with a high reaction probability via randomly generated numbers followed by an adjustment of the numbers of the reactant types. The time values result from a second criterion also based on a randomly generated number and are related to the above mentioned reaction probabilities. In particular, the selected algorithm allows an efficient simulation of the CLD. More in detail, to perform the logarithmic search on the reaction probabilities, the method uses a binary tree data structure from which array can be defined as illustrated in Figure 14. This array contains $2^4 - 1 = 15$ elements (so-called “nodes”) and the “tree” height is 4. The numbers in the circles must be considered array labels or function arguments (here 1 to 15). The bottom (green) nodes are also referred to as leafs.

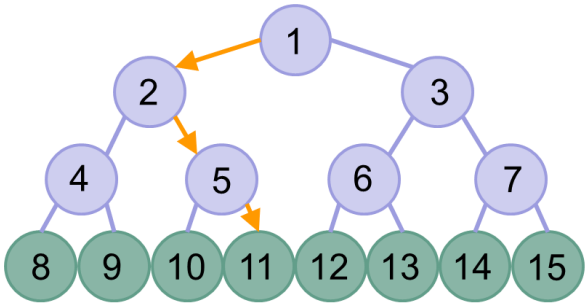

Figure 14: Arrangement of a binary tree in an array; each circle is a node with a label between 1 and 15; in each node, a value can be stored (e.g. Figure 15: in the 11th node, 5 is stored)

For each node of the above tree, function values may be stored (Figure 15). Here these values represent reaction probabilities of the various reaction channels in the model. The purple leafs contain sums of the underlying leafs. The only use of the purple leafs is to traverse down the tree to find a green leaf. Note that the algorithm, which starts from the root node (the top

node) needs to choose three times between left and right to traverse down the tree. An example path is shown with orange arrows (Figure 14 and 15).

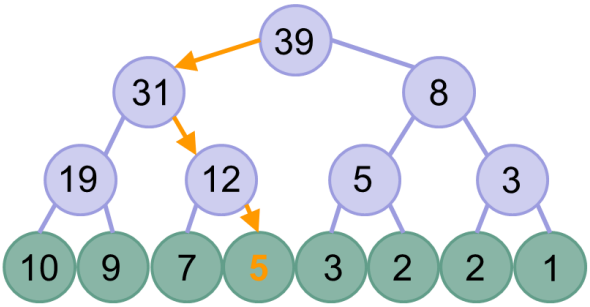

Figure 15: Reaction probabilities contained in a binary tree data structure; corresponding array labels: Figure 14; arrows relate to exemplary search pathway

Contrary in the "direct reaction method", only the leafs from the binary tree are used. Using a conventional linear search as illustrated in Figure 16, this means that on average 4 searches are necessary to fire a reaction event. Although the difference between three searches (Figure 15) and four searches (Figure 16) is not appreciable, this difference quickly increases for large numbers of reaction channels. For example, for FRP with a maximum chain length of 8191 the "direct" method needs over 4000 searches to select a propagation, while the "logarithmic direct" method traverses down the height of the tree in a mere $\log_2(8192) = 13$ "left" or "right" instructions. Such algorithmic adjustments improve CLD calculation time by orders of magnitude. In this PhD thesis, the powerful "logarithmic direct method"[98-99] is therefore used for reactions of distributed species in conjunction with the direct method for the reaction families. Both methods are discussed in detail in Appendix A.

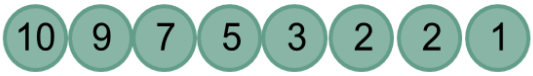

Figure 16: Reaction probabilities contained in a linear data structure

Finally, it should be stressed that the sample size, i.e. the initial number of molecules considered, has to be carefully selected. Although simulations of small samples are conducted very fast, it can be necessary to perform several simulations in order to obtain less noisy simulation results for all polymerization properties (e.g. CLD). Typically, radical concentrations in controlled polymerizations cannot be calculated due to their very small numbers. Alternatively, a single simulation of a large sample may yield less noisy polymer properties. In such a case, the radical concentration, or any other compound present in very

low numbers, may be accessible. Hence, in both cases, a high computational cost might be necessary to obtain a high accuracy for all tracked species.

1.4. Objectives and outline of the PhD thesis

The objective of this PhD is the development of a stochastic kinetic model which allows the optimization of radical (co)polymerizations and the polymer microstructure. In what follows two radical polymerization processes are optimized using kMC simulations.

In Chapter 2, focus is on the importance of reaction conditions for the synthesis of poly(p-phenylene vinylene)s (PPV) via the sulfinyl precursor route starting from 1-(chloromethyl)-4-[(n-octylsulfinyl)methyl]benzene as premonomer. This conjugated polymer is used in opto-electronic applications of which the device efficiency is greatly affected by polymer properties such as the CLD, the average chain length and structural defects. In this chapter, the kinetics and microstructure of conjugated polymers formed via the versatile sulfinyl route are modeled for the first time. The presented kinetic model is in agreement with GC and GPC data and allows not only to obtain insight in the effect of reaction conditions on the polymer properties but also to optimize the yield or average chain length.

In Chapter 3, the sulfinyl route for the synthesis of PPV derivatives is further studied. The effect of the molecular structure (aromatic moiety, polarizer, leaving group and substituents on the aromatic moiety) on the polymer yield and properties is studied. In particular, for the effect of substituents (on the aromatic moiety) on the properties of the PPVs, structure-reactivity relations are determined based on reported ab initio data and rate data obtained via UV-vis spectroscopy. Such structure-reactivity relations allow to further optimize the yield or the average chain length of the various PPV derivatives.

In Chapter 4, focus is on the synthesis of poly(p-phenylene vinylene)s (PPVs) via the dithiocarbamate precursor route. The resulting polymers possess regioregularity depending on the base used during synthesis. Regioregularity is beneficial for device performance and hence a clear insight in the origin of regioregularity is necessary to optimize the use of regioregular polymers in opto-electronic devices. Such regioregularity is affected by the reaction conditions and in particular the base type used for the synthesis, but has not yet been modeled in literature. The presented kinetic model is able, for the first time, to describe the regioregularity using a monomer sequence distribution of length three, the so-called triad

distribution, which is accessible via ^{1}H NMR. For the first time, the microstructure of conjugated polymers is described using a kinetic model in agreement with GC, GPC and NMR data.

In Chapter 5, the copolymerization of acrylates and methacrylates via ATRP is studied allowing the controlled synthesis of linear gradient copolymers. The models available in literature to describe the synthesis of gradient copolymers are able to accurately describe the kinetics but provide limited information on the polymer microstructure. The model developed in this PhD is based on detailed reaction kinetics combined with a novel method to not only track but also to assess the linear gradient quality. It must be stressed that the linear gradient quality is not experimentally accessible, although it is an important molecular property. E.g. for damping and shock absorbing materials, gradient copolymers perform better than block-like copolymers. In the model, the linear gradient quality is considered a microstructural deviation of each copolymer chain from an ideal gradient profile. In this way, objective criteria are used to determine the effect of reaction conditions on the microstructure of the linear gradient copolymer. For the first time, a negative correlation between the PDI and the gradient quality is demonstrated.

Finally, in Chapter 6 the main conclusions from the previous chapters are summarized and prospects for future research are presented.

References

1. Sperling, L. H., editor. *Introduction to physical polymer science.* New York: Wiley-Interscience; 2001.
2. Asua, J., editor. *Polymer Reaction Engineering*. Oxford: Blackwell publishing; 2007.
3. Aggarwal, S. L.; Sweeting, O. J. *Chem. Rev.* **1957**, 57, 665-742.
4. White, J. L.; Dharod, K. C.; Clark, E. S. *J. Appl. Polym. Sci.***1974**, 18, 2539-2568.
5. Mozer, A.J.; Denk, P.; Scharber, M.C.; Neugebauer, H.; Sariciftci, N.S.; Wagner, P.; Lutsen, L.; Vanderzande, D. *J. Phys. Chem. B* **2004**, 108, 5235-5242.
6. Vandenbergh, J.; Wouters, J. ; Adriaensens, P.J.; Mens, R. ; Cleij, T.J. ; Lutsen, L.; Vanderzande, D.J.M. *Macromolecules* **2009**, 42, 11, 3661-3668.
7. Beginn, U. *Colloid and Polymer Science* **2008**, 286, 13, 1465-1474.
8. Dervaux, B.; Junkers, T.; Barner-Kowollik, C.; Du Prez, F.; *Macromol. React. Eng.* **2009**, 3, 9, 529-538.

9. Wang, L. and Broadbelt, L. *Macromolecules* **2009**, 42, 7961-7968.
10. Wang, L. and Broadbelt, L. *Macromolecules* **2009**, 42, 8118-8128.
11. Wang, L. and Broadbelt, L. *Macromolecules* **2010**, 43, 2228-2235.
12. Winston, A.; Wichacheewa, P. *Macromolecules* **1973**, 6, 200-205.
13. Wang, L. and Broadbelt, *Macromol. Theory Simul.* **2011**, 20, 191-204.
14. Zhang, C.; Sun, J.; Li, R.; Sun S.-S.; Lafalce, E.; Jiang, X. *Macromolecules* **2011**, 44, 6389-6396.
15. Mozer, A. J.; Denk, P.; Scharber, M. C.; Neugebauer, H.; Sariciftci, N. S.; Wagner, P.; Lutsen, L.; Vanderzande, D.; Kadashchuk, A.; Staneva, R.; Resel, R. *Synth. Met.* **2005**, 153, 81-84.
16. J. Wieme, M.-F. Reyniers, G. B. Marin, *Macromolecules* **2009**, 42, 7797.
17. K. Matyjaszewski, *Macromolecules* **2012**, 45, 10, 4015-4039.
18. Al-Harthi, M.; Khan, M.J.; Abbasi, S.H.; Soares, J.B.P., *Macromol. React. Eng.* **2009**, 3, 148-159.
19. Junkers, T.; Vandenbergh, J.; Adriaensens, P.J.; Lutsen, L.; Vanderzande, D. *Polym. Chem.* **2011**, 3, 2, 275-285.
20. Schwalm, T.; Wiesecke, J.; Immel, S.; Rehahn, M. *Macromol. Rapid Commun.* **2009**, 30, 1295-1322.
21. D'hooge, D. R.; Reyniers, M.-F.; Marin, G. B. *Macromol. React. Eng.* **2009**, 3, 181-209.
22. Zhang, Y.; Wang, Y.; Peng, C.-H.; Zhong, M.; Zhy, W.; Konkolewicz, D.; Matyjaszewski, K. *Macromolecules* **2012**, 45, 78-86.
23. Percec, V.; Guliashvili, T.; Ladislaw, J. S.; Wistrand, A.; Sterjdahl, A.; Sienkowska, A.; Monteiro, M. J.; Sahoo S. *J. Am. Chem. Soc.* **2006**, 128, 14156-14165.
24. Louie, B. M.; Carratt, G. M.; Soong, D. S . J. *J. Appl. Polym. Sci.* **1985**, 30, 3985-4012.
25. Mikos, A. G.; Takoudis, C. G.; Peppas, N. A. *Macromolecules* **1986**, 19, 2174-2182.
26. Zhu, S.; Hamielec, A. *Macromolecules* **1989**, 22, 3093-3098.
27. Achillias, D. S.; Kiparissides, C. *Macromolecules* **1992**, 25, 14, 3739-3750.
28. Zhu, S.; Hamielec, A. E. *J. Polym. Sci. Part B: Polym. Phys.* **1994**, 32, 929-943.
29. Scheren, P. A. G. M.; Russell, G. T.; Sangster, D. F.; Gilbert, R. G.; German, A. L. *Macromolecules* **1995**, 28, 3637-3649.
30. Greszta, D.; Matyjaszewski, K. *Macromolecules* **1996**, 29, 7661-7670.

31. Baltsas, A.; Achilias, D. S.; Kiparissides, C. *Macromol. Theory Simul.* **1996**, 5, 3, 477-497.
32. Pladis, P.; Kiparissides, C. *Chem. Eng. Sci.* **1998**, 53, 18, 3315- 3333.
33. Zhu, S. *Macromol. Theory Simul.* **1999**, 8, 29-37.
34. Zhu, S. *J. Polym. Sci. Part B: Polym. Phys.* **1999**, 37, 2692-2704.
35. Monteiro, M. J.; Subramaniam, M.; Taylor, J. R.; Pham, B. T. T.; Tonge, M. T.; Gilbert, R. G. *Polymer* **2001**, 42, 2403-2411.
36. Kruse, T. M.; Woo, O. S.; Wong, H.-W.; Kahn, S. S.; Broadbelt, L. J. *Macromolecules* **2002**, 35, 7830-7844.
37. Delgadillo-Velazquez, O.; Vivaldo-Lima, E.; Quintero-Ortega, I. A.; Zhu, S. *AIChE J.* **2002**, 18, 2597-2608.
38. Butté, A.; Storti, G.; Morbidelli, M. *Macromol. Theory Simul.* **2002**, 11, 22-36.
39. Kruse, T. M.; Souleimonova, R.; Cho, A.; Gray, M. K.; Torkelson, J. M.; Broadbelt, L. J. *Macromolecules* **2003**, 36, 7812-7823.
40. Kruse, T. M.; Wong, W.; Broadbelt, L. J. *Macromolecules* **2003**, 36, 9594-9607.
41. Quintero-Ortega, I. A.; Vivaldo-Lima, E.; Luna-Barcenas, G.; Alvarado, J. F. J.; Louvier-Hernandez, J. F.; Sanchez, I. C. *Ind. Eng. Chem. Res.* **2005**, 44, 2823-2844.
42. Al-Harthi, M.; Soares, J. B. P; Simon, L. C. *Macromol. React. Eng.* **2007**, 1, 468-479.
43. Johnston-Hall, G.; Monteiro, M. J. *Macromolecules* **2007**, 40, 7171-7179.
44. Al-Harthi, M.; Cheng, L. S.; Soares, J. B. P; Simon, L. C. *J. Polym. Sci. Part A: Polym. Chem.* **2007**, 45, 2212-2224.
45. Wieme, J.; De Roo, T.; Marin, G. B.; Heynderickx, G. J. *Ind. Eng. Chem. Res.* **2007**, 46, 1179-1196.
46. Roa-Luna, M.; Diaz-Barber, M. P.; Vivaldo-Lima, E.; Lona, L. M. F.; Mc-Manus, N. T.; Penlidis, A. *J. Macromol. Sci. A* **2007**, 44, 193-203.
47. Fu, Y.; Cunningham, M. F.; Hutchinson, R. A. *Macromol. React. Eng.* **2007**, 1, 243-252.
48. Fu, Y.; Mirzaei, A.; Cunningham, M. F.; Hutchinson, R. A. *Macromol. React. Eng*. **2007**, 1, 425-439.
49. Zargar, A.; Schork, F. J. *Macromol. React. Eng.* **2009**, 3, 118-130.
50. Van Krevelen, D. W., editor. *Properties of Polymers.* Amsterdam: Elsevier; 1997.
51. Müller, R.-J.; Klein, J. *Makromol. Chem.* **1988**, 189, 2341-2355.
52. Saliakas, V.; Chatzidoukas, C.; Krallis, A.; Meimaroglou, D.; Kiparissides, C. *Macromol. React. Eng.* **2007**, 1, 119-136.

53. Johnston-Hall, G.; Monteiro, M. J. *J. Polym. Sci. Polym. Chem*. **2008**, 46, 3155-3173.
54. Barner-Kowollik, C.; Russell, G. T. *Prog. Polym. Sci.* **2009**, 34, 1211-1259.
55. D'hooge, D. R.; Reyniers, M.-F.; Stadler, F. J.; Dervaux, B.; Bailly, C.; Du Prez, F. E.; Marin, G. B. *Macromolecules* **2010**, 43, 8766-8781.
56. Bentein, L.; D'hooge, D. R.; Reyniers, M.-F.; Marin, G. B. *Macromol. Theory Sim.* **2011**, 20, 238-265.
57. He, J.; Zhang, H.; Chen, J.; Yang, Y. *Macromolecules* **1997**, 30, 8010-8018.
58. Matyjaszewski, K.; Ziegler, M. J.; Arehart, S.V. Greszta D., Pakula, T. *J. Phys. Org. Chem*. **2000**, 13, 12, 775-786.
59. Ziegler, M. J.; Matyjaszewski, K. *Macromolecules* **2001**, 34, 415-424.
60. Wang, W.; Hutchinson, R.A. *AIChE J.* **2011**, 75, 227-238.
61. Konkolewicz, D.; Sosnowski, S.; D'hooge, D. R.; Szymanski, R.; Reyniers, M.-F.; Marin, G. B; Matyjaszewski, K. *Macromolecules* **2011**, 44, 8361-8373.
62. Krallis, A.; Kiparissides, C. *Chem. Eng. Sci.* **2007**, 62, 5304-5311.
63. Szymanski, R.; *E-polymers* **2009**, 044.
64. Krallis, A.; Meimaroglou, D.; Kiparissides, C. *Chem. Eng. Sci.* **2008**,63, 4342-4360.
65. Meimaroglou, D.; Pladis, P.; Baltsas, A.; Kiparissides, C. *Chem. Eng. Sci.* **2011**, 66, 1685-1696.
66. De Roo, T.; Wieme, J.; Heynderickx, G. J., Marin, G. B *Polymer* **2005**, 46, 19, 8340-8354.
67. Baldyga, J.; Born, J. R. *Chem. Eng. Sci.* **1992**, 47, 1839-1848.
68. Zhang, S. X.; Ray, W. H. *AIChE J.* **1997**, 43, 1265-1277.
69. Kolhapure, N. H.; Fox, R. O. *Chem. Eng. Sci.* **1999**, 54, 3233-3242.
70. Alvarez, J.; Alvarez, J.; Hernandez, M. *Chem. Eng. Sci.* **1994**, 49, 99-113.
71. Villa, C.; Dihora, J.; Ray, W. *AIChE J.* **1998**, 44, 5127-5140.
72. Alexopoulos, A. H.; Maggioris, D.; Kiparissides, C. *Chem. Eng. Sci.* **2002**, 57, 1735-1752.
73. Ghiass, M.; Hutchinson, R. A. *Macromol. Symp.* **2004**, 206, 443-456.
74. Villermaux, J.; Falk, L. *Chem. Eng. Sci.* **1994**, 49 (24B): 5127-5140.
75. Fox, R. O. *Rev. I. Fr. Petrol* **1996**, 2, 215-243.
76. Fox, R.O., editor. *Computational Models for Turbulent Reacting Flows*. New York: Cambridge University Press; 2003.
77. Read, N. K.; Zhang, S. X.; Ray, W. H. *AIChE J.* **1997**, 43, 1, 104-117.
78. Zhou, W.; Marshall, E.; Oshinowo, L. *Ind. Eng.Chem. Res.* **2001**, 40, 5533-5542.

79. Kolhapure, N. H.; Fox, R. O. *AIChE J.* **2005**, 51, 2, 585-606.
80. Tsai, K.; Fox, R. O. *AIChE J.* **1996**, 42, 10, 2926-2940.
81. Gear, C. W. *Commun. ACM* **1971**, 14, 176-179.
82. Petzold, L. R. *SIAM J. Sci. Stat. Comp.* **1983**, 4, 136-148.
83. Sandu, A. ; Constantinescu, E. M. *J. Sci. Comput*. **2009**, 38, 229-249.
84. Russell, G. T. ; Gilbert, R. G.; Napper, D. H. *Macromolecules* **1992**, 25, 2459-2469.
85. Russell, G. T. *Aust. J. Chem.* **2002**, 55, 399-414.
86. Butté, A.; Storti, G.; Morbidelli, M. *Macromol. Theory Simul.* **2002**, 11, 22-36.
87. Mueller, P. A.; Storti, G.; Morbidelli, M. *Chem. Eng. Sci.* **2005**, 60, 1911-1925.
88. Butté, A.; Ghielmi, A.; Storti, G.; Morbidelli, M. *Macromol. Theory Simul.* **1999**, 8, 498-512.
89. Kumar, S.; Ramkrishna, D. *Chem. Eng. Sci.* **1996**, 51, 1311-1332.
90. Kiparissides, C.; Seferlis, P.; Mourikas, G.; Morris, A. J. *Ind. Eng. Chem. Res.* **2002**, 41, 6120-6131.
91. Carey, G. F.; Finlayson, B. A. *Chem. Eng. Sci.* **1975**, 51, 587-596.
92. Nele, N.; Sayer, S.; Pinto, C. *Macromol. Theory Simul.* **1999**, 8, 199-213.
93. Budde, U.; Wulkow, M. *Chem. Eng. Sci.* **1991**, 46, 497-508.
94. Wulkow, M. *Macromol. React. Eng.* **2008**, 2, 461-494.
95. Wulkow, M. *Macromol. Theory Simul.* **1996**, 5, 393-416.
96. Asteasuain, M.; Sarmoria, C.; Brandolin, A. *Polymer* **2002**, 43, 2513-2527.
97. Asteasuain, M.; Sarmoria, C.; Brandolin, A. *Polymer* **2002**, 43, 2529-2541.
98. Arzamendi, G.; Plessis, C.; Leiza, J. R.; Asua, J. M. *Macromol. Theory Simul.* **2003**, 12, 315-324.
99. Gillespie, D. T. *J. Phys. Chem.* **1977**, 81, 25, 2340-2361.
100. Gibson, M. A.; Bruck, J. *J. Phys. Chem. A* **2000**, 104, 9, 1876-1889.
101. Chaffey-Millar, H.; Stewart, D.; Chakravarty, M. M. T; Keller, G.; Barner-Kowollik, C. *Macromol. Theor. Simul.* **2007**, 16, 6, 575-592.

Chapter 2: Kinetic Monte Carlo modeling of the sulfinyl precursor route for poly(para-phenylene vinylene) synthesis

Summary

A kinetic Monte Carlo modeling study is presented for precursor polymer formation via the sulfinyl precursor route. The premonomer, 1-(chloromethyl)-4-[(n-octylsulfinyl)methyl]-benzene, is subjected to a Na*t*BuO induced 1,6-elimination in sBuOH yielding the actual para-quinodimethane monomer that leads, via a radical polymerization, to the precursor polymer. The kinetic Monte Carlo model is able to predict the experimental trends in yield, mass averaged molar mass and structural defect content. The effect of radical recombination and cyclization is modeled and found to be negligible. The effect of the initial base and premonomer concentration on the polymer properties is investigated. Simulation results indicate a maximum in the polymer yield and chain length for initial [base]/[premonomer] = 1 and that the molecular properties of the precursor polymers can be varied by as much as 50% of their initial values by the appropriate choice of initial [base]/[premonomer]. The kinetic Monte Carlo model is used to determine reaction conditions to achieve targeted polymer yields, chain lengths and structural defect contents. This work has been published in *Macromolecules* **2011**, 44, 8716-8726.

2.1. Introduction

Since the discovery[1] of the luminescence of poly(para-phenylene vinylene) (PPV) and the subsequent device fabrication[2] of Light Emitting Diodes (LEDs) using PPV layers, this type of conjugated polymers have drawn significant interest. PPVs are currently used in solar cells, LEDs, Thin Film Transistors (TFT), Field Effect Transistors (FET), chemical and biosensors, laser-dyes[3-5], scintillators[3], piezoelectric and pyroelectric materials[6], photoconductors[7] to switch elements and data processors.[6,8,9] The major advantages of using PPVs as the active layer in semi-conductor devices are their low-cost solution processing into large surface area coatings and the possibility of designing new materials by modification of their molecular structure. The microstructure of the PPV is a key parameter for opto-electronic applications since it strongly influences the chain packing and morphology in the final polymer films. Low molar mass

polymers are less suited because the produced films are fragile and less stable.[10] For LED fabrication, high molar mass polymers favor the formation of lamellar structures and correspondingly higher charge mobility.[11,12]

PPVs can be synthesized in various ways[13-21] but most frequently a precursor route is used to obtain a soluble, high molar mass precursor polymer. As illustrated in Figure 1, various precursor routes have been developed. Common to all these precursor routes is that a α,α'-disubstituted para-xylene premonomer is subjected to a base induced 1,6-elimination yielding the active p-quinodimethane monomer that leads to a precursor polymer via radical and/or anionic quinoid polymerization. The conjugated PPV is formed from the precursor polymer through a series of intramolecular thermally, base or, in some specific cases, acid[22] induced eliminations.

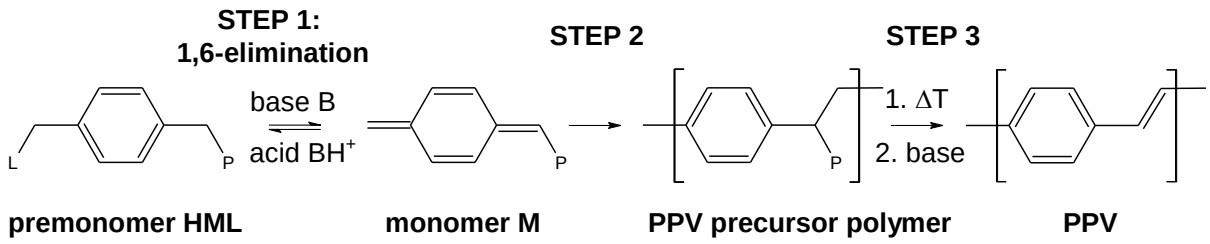

Gilch route: L = P = Cl or Br;
Wessling-Zimmermann/Sulfonium route: L = P = R_2S;
Sulfinyl route: L = Cl or Br; P = RS(O);
Xanthate route: L = P = RO-C(S)-S;
Dithiocarbamate route: L = P = R_2N-C(S)-S

Figure 1: Precursor routes toward poly(para-phenylene vinylene) (PPV) derivatives

To obtain high performance materials, a pure, soluble and thermally stable precursor polymer must be obtained that undergoes a clean thermal elimination reaction toward the conjugated structure. Also, tuning of the conjugation length[23-29] and control of the defect content[30-41] are key factors to obtain PPVs with the desired electroluminescence and photoluminescence properties. Control of the molar mass of the polymer and optimization of the number of critical defects in the synthesized PPVs requires a detailed knowledge of the reaction kinetics. Several studies have

investigated the reaction mechanism that governs polymer formation via the various precursor routes. Although each precursor route has its own characteristics, some mechanistic analogy exists between the various precursor routes. In particular, for the Gilch[42], the sulfinyl and the dithiocarbamate route, a series of detailed studies performed by the groups of Rehahn[33,34,36-39,41,43] and Vanderzande[31,35,44-59] has revealed mechanistic similarities in precursor polymer formation. There are convincing indications[31,44,48,50,52,55,60,61] that in polar aprotic solvents, radical and anionic quinoid polymerization can proceed in parallel; higher molar mass polymer is thought to originate form a radical chain mechanism while a parallel anionic polymerization mechanism produces lower molar masses leading to a precursor polymer that displays a bimodal molar mass distribution.[31,44,48,50,52,55,60,61] In protic solvents, the anionic mechanism seems to be suppressed effectively and high molar mass precursor polymer is produced mainly via a free radical polymerization[33,44,46,48,50,52,53,55,60,62-64] that is initiated by spontaneous dimerization of the active p-paraquinodimethane monomer to dimer diradicals. Experimental and theoretical studies[33,34,36-38,49,53,60,64,65,66,67,68] indicate that the preferred mode of initiation involves formation of the diradical which has both radicals located at terminal CHP-groups, see Figure 2.

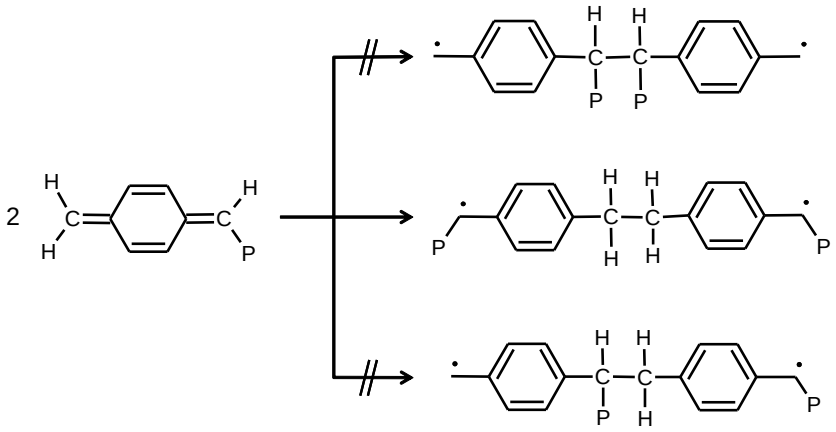

Figure 2: Initiator radicals produced by dimerization of the monomer

Two reasons have been put forward to explain the dominance of this initiation path. Firstly, C-C-bond formation between the two CH_2 groups is least sterically hindered and, secondly, both radicals centers are stabilized by the presence of the polarizer P in the terminal CHP-group. Next to chain initiation, the diradical can undergo intramolecular radical recombination leading to the

formation of [2.2]paracyclophane sideproducts[37-39,69]. It has been suggested[37-39,44,65,66,69,70] that radical chain propagation is not merely a conventional free radical polymerization but that a more complex binary mechanism is operative in which, next to the "conventional" 1,6-type addition to the radical chain ends, recombination of growing α,ω-macro-diradicals can contribute to chain growth too. In contrast to conventional free radical polymerization, recombination of two α,ω-macro-diradicals does not lead to dead polymer but to another α,ω-macro-diradical which can grow further by addition of monomer.

As can be seen in Figure 1, the various precursor routes differ in the chemical structure of the leaving group (L) and the polarizer (P). Precursor routes in which the polarizer and leaving group are identical, such as the Gilch,[42] the Wessling-Zimmermann/Sulfonium,[63] the xanthate[28,71,72] and the dithiocarbamate[59,31] routes, offer less synthetic possibilities to improve the quality of the polymer properties than the sulfinyl route which features a differentiation between the alkyl sulfinyl polarizer and the halogen (mostly Cl or Br) leaving group. This differentiation between leaving group and polarizer in the sulfinyl route opens up synthetic possibilities unseen in any other precursor route, such as (i) improved solubility via structural variation of the alkylsulfinyl group, (ii) improved viscosity characteristics, (iii) reduction of the number of defects due to irregular chain growth (iv) the use of extended aromatic moieties, all of which enable the synthesis of conjugated polymers with emission wavelengths tuned by molecular structure.

The attractiveness of the sulfinyl precursor route to synthesize high performance PPVs mainly stems from the fact that the sulfinyl group is not prone to basic elimination and its thermal elimination typically requires mild heating. Combined with the excellent leaving capacity of the halogen that ensures quantitative para-quinodimethane formation, the sulfinyl route allows synthesizing pure and thermally stable precursor polymer at low temperatures (Figure 1, STEP 2). In contrast, in the Gilch route, the quinoid polymerization (Figure 1, STEP 2) is accompanied by intramolecular elimination (Figure 1, STEP 3) because the chlorine polarizer in the precursor polymer is prone to basic elimination. This typical elimination behavior of the sulfinyl group has also been exploited to obtain modified PPV derivatives with restricted conjugation length.[73] Controlled oxidation of the sulfinyl precursor polymer produces a polymer that possesses both sulfinyl and sulfonyl groups. Selective elimination of the sulfinyl group is then possible because

it can be eliminated at temperatures as low as 140° C, whereas elimination of the sulfonyl group requires temperatures above 400° C. A similar tuning of the conjugation length was performed for the Wessling route.[24] By precisely controlling the molar fraction of the sulfonyl group, which functions as the defect restricting the conjugation length, the physical properties of the materials can be optimized.

The differentiation between leaving group and polarizer in the sulfinyl route also leads to materials with very low structural defect contents, as shown in a ^{13}C NMR study on labeled polymers[35]: the measured content of defects fell below the detection limit of 0.1%. The formation of very "regular" polymer chains with low amounts of defects is attributed to the dominant occurrence of head-to-tail addition during chain growth (Figure 3). Defects in the "regular" polymer chain such as CH_2-CH_2 bonds can be introduced via tail-to-tail addition while CHS(O)R-CHS(O)R bonds can be formed via head-to-head addition and/or recombination of α,ω-macro-diradicals. The only defects formed during the sulfinyl polymerization are believed to be related to initiation (Figure 2 and 4) and recombination. In contrast to the low-defect sulfinyl polymers, the Gilch route was shown[35] to produce higher amounts of structural defects, which were proposed to result from head-to-head and tail-to-tail addition and the occurrence of α,ω-macro-diradical recombination. According to Schwalm et al.[38], the occurrence of α,ω-macro-diradical recombination in the Gilch route could explain the tremendously high molar masses (up to one million g/mol) obtained via this PPV precursor route.

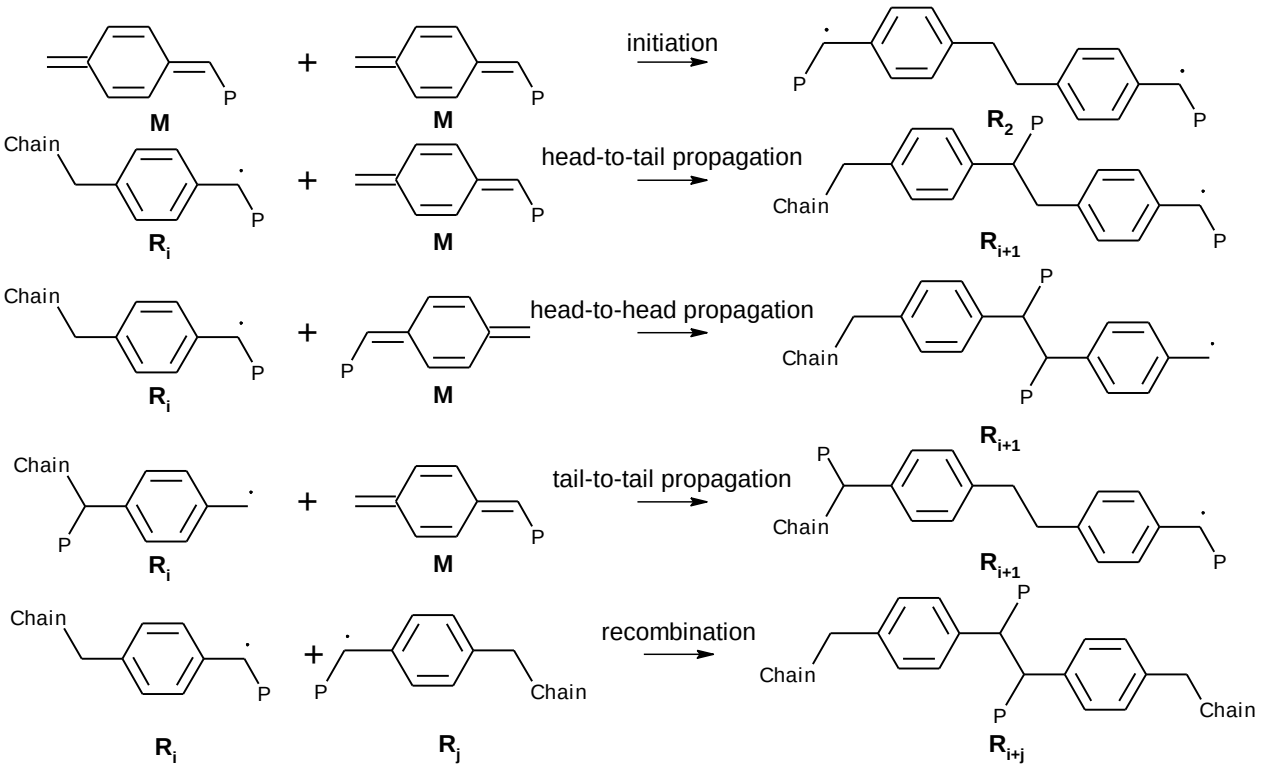

Figure 3: Structural defects resulting from initiation and recombination in precursor routes. Head-to-tail propagation does not lead to structural defects, whereas head-to-head and tail-to-tail propagation are known to be negligible in the sulfinyl route

Currently, the nature of the termination steps in quinoid polymerization and their influence on the polymer yield, the structural defect content and the molar mass distribution remain unclear. As mentioned above, conventional recombination of radicals does not completely terminate chain growth due to the diradical nature of the propagating species. Also, no obvious reaction path is available for chain termination by disproportionation since the absence of a β hydrogen at the chain ends prevents β hydrogen abstraction and double bond formation.[37,38,65] Transfer to solvent or to other transfer agents is largely ineffective to limit the chain length because of the very high propagation rates.[37,65,68,69,74] Concerning transfer to polymer, strong indications for the absence of transfer to polymer have been reported by Rehahn's group.[43] According to Schwalm et al.[37-39], this type of polymerization would therefore lead to essentially infinite chain lengths. However, in practice, termination reaction can occur due to the presence of oxygen[35,44,48,64,65] or other impurities[35,37-39,48,65] in the reaction mixture or by cyclization[68] of the α,ω-macro-diradical.

In p-xylylene free radical polymerization, Errede et al. found[69] that termination does not occur by interaction with atmospheric oxygen and that polymerization proceeds until all monomer is consumed or the radical ends of the linear polymer chains become entrapped in the polymer chain mesh. In diluted solution, the decrease of the radical concentration displayed a 2nd order dependence on the total radical concentration, excluding cyclization as the main termination mechanism for the larger radicals. The formation of cyclic low molar mass products was attributed to cyclization of small α,ω-diradicals.

Despite the immense potential of conjugated polymers, kinetic modeling studies for precursor routes toward PPV synthesis are scarce.[51,67,75-77] For the Wessling route, Cho et al.[67,76] have extensively studied the kinetics of monomer formation and polymerization. For the p-quinodimethane formation, these authors suggested a reversible E1cb mechanism, in which the deprotonation to the carbanion is reversible and the expulsion of the leaving group is the rate determining step in the elimination reaction. A kinetic model was developed that allowed a good prediction of the polymer yield. However, no attention was given to the modeling of the molecular polymer properties such as average molar mass, defect content and chain length distribution and the occurrence of recombination and cyclization reactions was not considered. For the sulfinyl route, Pyun et al.[77] reported observed rate coefficients for monomer formation from 4-[(n-butylsulfinyl)methyl]-4'-(chloromethyl)benzene with Na*t*BuO in dichloromethane/N-monomethyl formamide and the subsequent polymerization. Recently, Hermosilla et al.[51] studied the kinetics of monomer formation in the sulfinyl precursor route using stop-flow UV-vis spectroscopy and theoretical calculations. Kinetic measurements were performed for various premonomers with Na*t*BuO in pseudo-first-order reaction conditions in sBuOH. At these conditions, polymer formation is effectively suppressed while conjugated nucleophilic addition is the only monomer consuming reaction (see Figure 4). Based on the experimental results and the theoretical calculations, these authors proposed an E2 mechanism for the based induced 1,6-elimination. Rate coefficients were reported for the E2 elimination step only. A kinetic model for formation of the p-quinodimethane monomer and its polymerization via the sulfinyl route is still lacking.

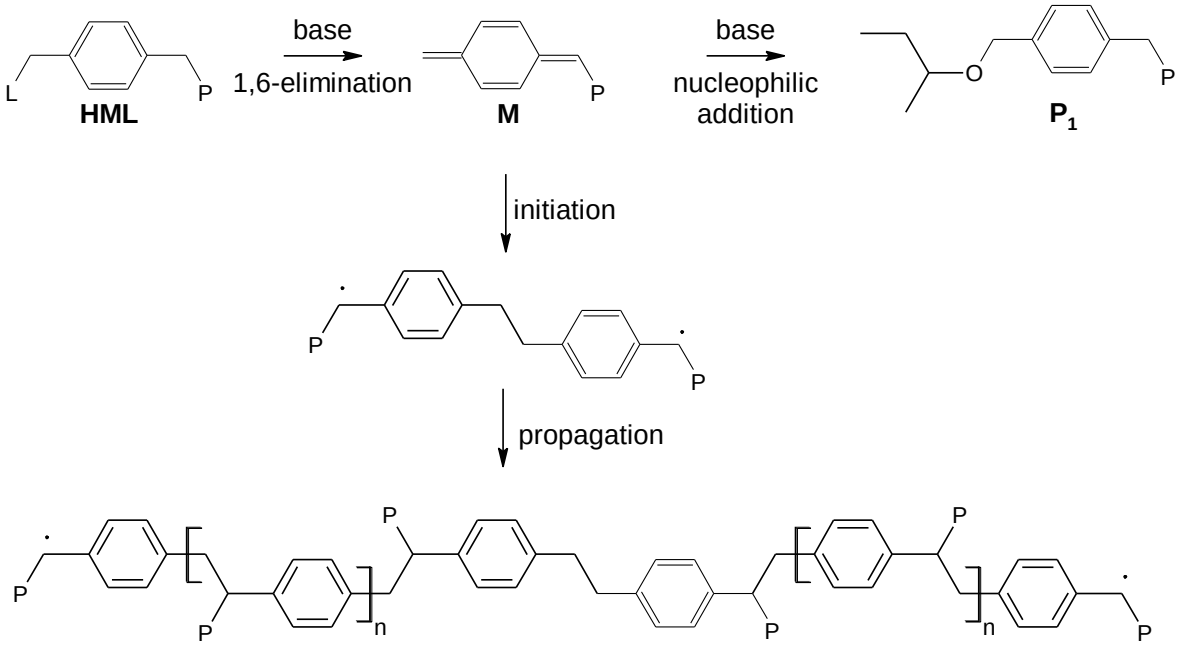

Figure 4: General reaction scheme for p-quinodimethane formation and its consumption by conjugate nucleophilic addition and polymerization via the sulfinyl route; HML: premonomer, L: Leaving group, P: Polarizer, M: monomer, P_1: ether byproduct; Recombination and cyclization reactions are not shown

Clearly, the availability of a kinetic model enabling to tune the reaction conditions in order to obtain optimal precursor polymer yield, structural defect content and molar mass distribution can contribute to realize the tremendous potential of the sulfinyl route to synthesize PPVs with controlled properties. In this work, a kinetic Monte Carlo model for precursor polymer formation via the sulfinyl precursor route from 1-(chloromethyl)-4-[(n-octylsulfinyl)methyl]-benzene (see Figure 5) with Na*t*BuO in sBuOH is presented.

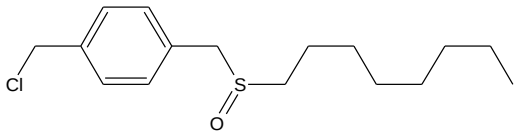

Figure 5: Structure of 1-(chloromethyl)-4-[(n-octylsulfinyl)methyl]-benzene

To model monomer formation, the rate coefficients for E2 elimination and conjugate nucleophilic addition are determined from in situ stop-flow UV-vis measurements using low initial premonomer concentrations and a large excess of Na*t*BuO to suppress polymerization. To model precursor polymer formation, rate coefficients for radical polymerization of the p-quinodimethane are obtained from data reported in literature. The kinetic Monte Carlo method is used to calculate the entire molar mass distribution. This method is easy to implement and does not rely on assumptions such as the quasi steady state approximation for reactive species. Unlike other numerical methods, no manual fine-tuning of numerical integration parameters is necessary, due to the brute-force nature of the method. Then, the kinetic Monte Carlo simulations are benchmarked by comparison with simulations using the PREDICI© software[78,79] and used to evaluate the importance of termination by recombination of all α,ω-macrodiradicals and cyclization of small (i = 2, 3 and 4) α,ω-diradicals. Their effect on the simulated yields and polymer properties is discussed. Finally, the kinetic Monte Carlo model is used to study the effect of the reaction conditions on the polymer yield and properties.

2.2. Experimental procedures

Chemicals were purchased from Aldrich or Acros and used without further purification. The synthesis procedure of 1-(chloromethyl)-4-[(n-octylsulfinyl)methyl]-benzene (Figure 5) has been reported elsewhere.[80,81] In-situ UV-vis experiments were performed using a Cary 500 UV-Vis-NIR spectrophotometer equipped with a stop-flow module (Hi-Tech Limited) according to the procedure described by Hermosilla et al.[51] The optic path length of the sample cell was 10 mm. All spectroscopic and kinetic data were obtained using the ”Scanning kinetics” and ”Kinetics” software module supplied by Varian. Solutions of 10^{-4} mol L^{-1} of the premonomer 1-(chloromethyl)-4-[(n-octylsulfinyl)methyl]-benzene in sBuOH were used while base solutions were prepared by dilution of 0.1 mol L^{-1} sodium-butoxide solution in sBuOH. All solutions were degassed with nitrogen prior to the kinetic UV-vis experiment. The temperature of the reacting solutions was maintained at 298 K. To determine the rate coefficients related to the monomer formation, Na*t*BuO was added in excess, creating pseudo-first order conditions.

In accordance with the observations reported by Hermosilla et al.,[51] no indication for polymerization was found during the kinetic runs in this work and the only products absorbing in the UV-vis spectrum are the premonomer (HML), the para-quinodimethane monomer (M) and

the ether byproduct (P_1). The maximum of the UV-VIS absorbance of the para-quinodimethane is situated around a wavelength of 313 nm[51,77], which is also the wavelength used in the UV-vis experiments in this study to monitor the para-quinodimethane. As indicated by Hermosilla et al.[51], the contributions to the absorbance at 313 nm of the premonomer and the substitution product P_1 can be neglected. The para-quinodimethane concentration is thus directly proportional to the total absorbance at 313 nm.

2.3. Kinetic model

A kinetic Monte Carlo (kMC) model was developed on the basis of the stochastic simulation algorithm developed by Gillespie.[82] Details of this method and the reasons for its use are given in Appendix A.

2.4. Results and discussion

2.4.1. Kinetic modeling of monomer formation

In the in situ UV-vis experiments, the kinetics of monomer formation were separated from the polymerization kinetics by adding N*a*tBuO in excess and creating pseudo-first order conditions. The absorbance of the reaction mixture at 313 nm was measured as a function of the reaction time. The Guggenheim method[86,87] was applied to extract kinetic information on the formation of the monomer by 1,6-elimination (k_{E2}, see Figure 4) and its disappearance to the ether byproduct, P_1, by conjugate nucleophilic addition (k_{NA}, see Figure 4). In all cases, the absorbance at 313 nm first increased to a maximum value and then decreased with time, indicating that the p-quinodimethane monomer accumulated before undergoing nucleophilic addition.

The value for the rate coefficient of the 1,6-elimination is determined from the absorbance at low reaction times, i.e. the region where the 1,6-elimination proceeds much faster than the nucleophilic addition (see Appendix B). Figure 6 shows the plots of $-\ln(A_{t+\Delta t} - A_t)$ versus time for the reaction between 1-(chloromethyl)-4-[(n-octylsulfinyl)methyl]-benzene and N*a*tBuO in sec-butanol. For all 5 base concentrations, pseudo-first order plots are obtained over multiple half-lives of the reaction. The observed rate coefficients, k_{obs} (s^{-1}), and their corresponding

Na*t*BuO concentrations (mol L^{-1}) are presented in Table 1. Within this concentration range, the 1,6-elimination rate clearly shows pseudo-first order dependence on the Na*t*BuO concentration, which was also observed by Hermosilla et al.[51] Linear regression (see Appendix C) yields the intrinsic, bimolecular rate coefficient k_{E2} (L mol^{-1} s^{-1}) for the 1,6-elimination as k_{E2} = 1.2 L mol^{-1} s^{-1} at 298 K. Hermosilla et al.[51] reported a value of 14 L mol^{-1} s^{-1} at 298 K for k_{E2}. Using a similar approach as the one used in this work, Pyun et al.[77] reported a value of 0.44 L mol^{-1} s^{-1} for the rate coefficient of the 1,6-elimination of 1-(chloromethyl)-4-[(n-octylsulfinyl)methyl]-benzene with Na*t*BuO in CH_2Cl_2/MMF (4/6) at 298 K. The value determined in this work is situated between Pyun's and Hermosilla's values and gives reasonable agreement with experimental data in combination with literature values for the polymerization kinetics (vide infra).

Table 1: Observed rate coefficients for monomer formation. Reaction conditions: 298 K, $[HML]_0 = 10^{-4}$ mol L^{-1}, $[RO^-]_0 = 10^{-3}$ mol L^{-1}, 4 10^{-3} mol L^{-1}, 10^{-2} mol L^{-1}, 4 10^{-2} mol L^{-1}, 10^{-1} mol L^{-1}.

$[RO^-]_0$ (mol L^{-1})	1,6-elimination (s^{-1})	Nucleophilic addition (s^{-1})
0.1	0.1214	0.0206
0.04	0.0297	0.0059
0.01	0.0172	0.0047
0.004	0.0072	N/A
0.001	0.0026	N/A

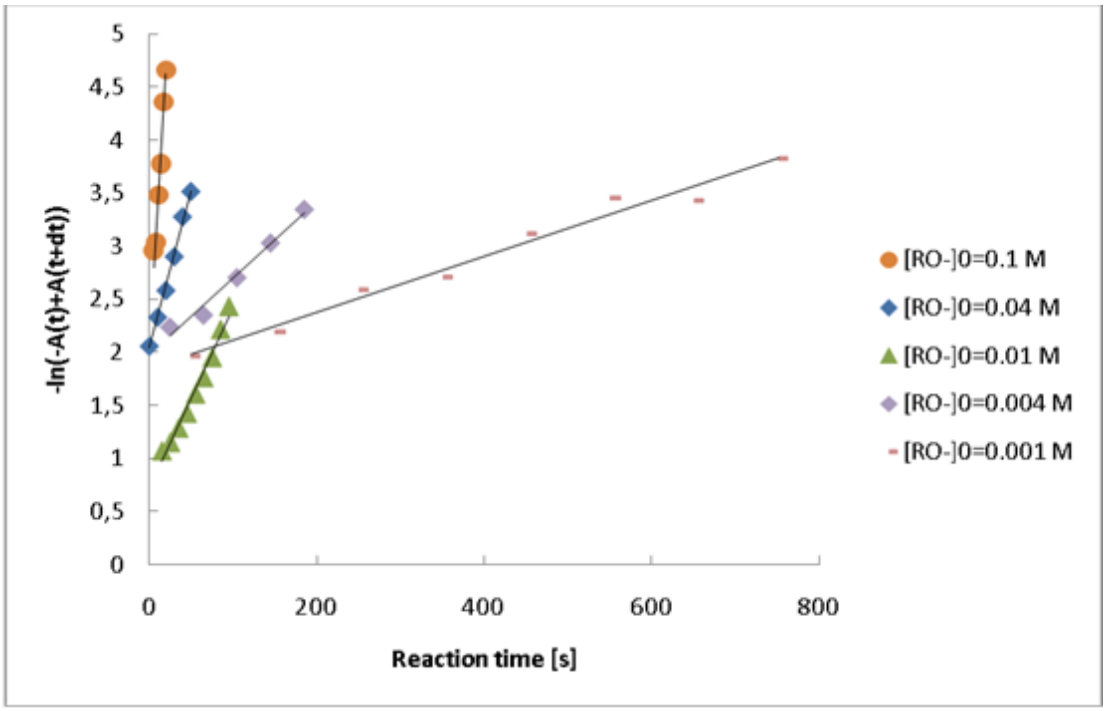

Figure 6: Plot of absorbance as a function of reaction time and base concentration; Reaction conditions: 298 K, $[HML]_0 = 10^{-4}$ mol L^{-1}, $[RO^-]_0 = 10^{-3}$ mol L^{-1}, 4 10^{-3} mol L^{-1},10^{-2} mol L^{-1}, 4 10^{-2} mol L^{-1}, 10^{-1} mol L^{-1}; Symbols: experimental data from the Guggenheim method. Full line: linear regression; The slope of the straight lines is the observed rate coefficient for the 1,6-elimination as a function of the base concentration

The Guggenheim method can also be used to determine the value for the rate coefficient of the nucleophilic addition from the absorbance at high reaction times, i.e. the region where the nucleophilic addition is proceeding much faster than the 1,6-elimination. Figure 7 shows the plots of $-\ln(A_t - A_\infty)$ for the three highest base concentrations 0.01 mol L^{-1}, 0.04 mol L^{-1} and 0.1 mol L^{-1}.

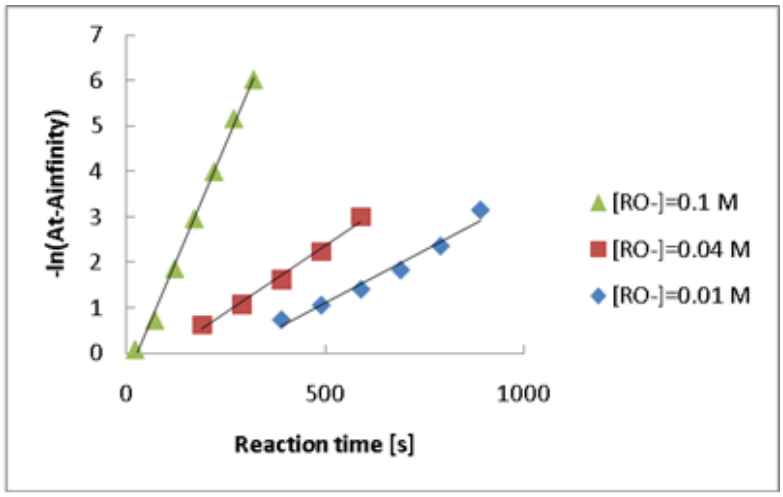

Figure 7: Absorbance as a function of reaction time; Reaction conditions: 298 K, $[HML]_0$ = 10^{-4} mol L^{-1}, $[RO^-]_0$ = 10^{-2} mol L^{-1}, 4 10^{-2} mol L^{-1}, 10^{-1} mol L^{-1}; Symbols: experimental data from the Guggenheim method; Full line: linear regression; The slope of the straight lines is the observed rate coefficient for the nucleophilic addition

Only the pseudo-first order rate coefficient for the highest base concentration is used for the calculation of the value for the rate coefficient of the nucleophilic addition, the reasoning being that potential polymerization is suppressed most effectively when the nucleophilic addition is proceeding fastest. From the slope obtained for the $\ln(A_t - A_\infty)$ plot for $[NatBuO]_0$ = 0.1 mol L^{-1}, it is clear that the observed rate coefficient for the nucleophilic addition is 0.02 s^{-1}. As mentioned above, the only reactant consuming the para-quinodimethane is the base in the nucleophilic addition. Therefore, by definition, $k_{obs} = k_{NA}\,[NatBuO]_0$. Solving for k_{NA} yields k_{NA} = 0.2 L mol^{-1} s^{-1}. Using all 3 observed rate coefficients results in the same value of k_{NA} = 0.2 L mol^{-1} s^{-1} (see Appendix C). A value for the rate coefficient for the nucleophilic addition of the base was not reported in the kinetic studies by Hermosilla et al.[51] or Pyun et al.[77] The final value of k_{NA} = 0.2 L mol^{-1} s^{-1} for the rate coefficient for the nucleophilic addition is used as input in the kinetic Monte Carlo modeling, together with the earlier determined value of k_{E2} = 1.2 L mol^{-1} s^{-1} for the rate coefficient for the 1,6-elimination.

To relate the absorbance of the p-quinodimethane monomer at 313 nm to its concentration, its extinction coefficient, ε, in sBuOH is required. However, this extinction coefficient cannot be

measured directly because the monomer is not stable and, hence, it must be determined by matching[76] the simulated para-quinodimethane concentration with the normalized UV-vis absorbance. Therefore, the extinction coefficient was fitted to the UV-vis data using the kinetic parameters for k_{E2} and k_{NA} determined above until a best fit between the experimental and calculated data was obtained. A value of $\varepsilon = 1.48\ 10^6$ L mol^{-1} m^{-1} was obtained. The approximated value for the extinction coefficient determined[76] by Cho et al. amounts to $2.9\ 10^6$ L mol^{-1} m^{-1} for sulfonium substituted para-quinodimethanes in water. For more stable compounds[76] values of ε are in the range $1.65 - 6.36\ 10^6$ L mol^{-1} m^{-1}. Also reported[80] in literature is the extinction coefficient for the repeating unit in a conjugated PPV chain, i.e. $2\ 10^6$ L mol^{-1} m^{-1}. This must be considered an upper limit for the monomer itself because the polymer chain possesses more π-conjugation. Finally, Denton et al. report[88] $1.2\ 10^6$ L mol^{-1} m^{-1} for sulfonium substituted para-quinodimethanes in water, which differs more than a factor 2 from Cho's value. Denton et al. also refer to a value of $1.27\ 10^6$ L mol^{-1} m^{-1} for the stable tetracyanobenzoquinodimethane in MeOH.[88]

Figure 8 illustrates the agreement between simulated and experimental UV-vis absorbance for a representative initial base concentration $[Na\textit{t}BuO]_0 = 0.01$ mol L^{-1}. Clearly, the kinetic model succeeds in describing the exponential regions of the para-quinodimethane intermediate reasonably well.

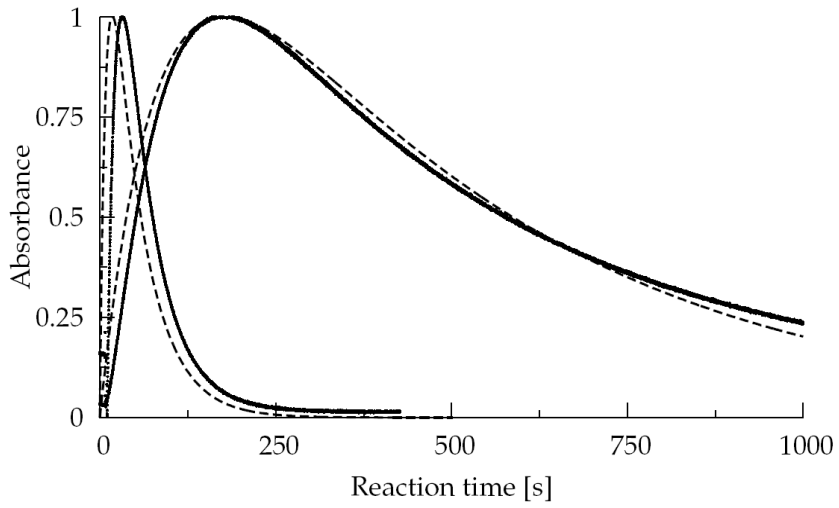

Figure 8: normalized UV-vis absorbance at 313 nm as a function of reaction time; Reaction conditions: 298 K, $[HML]_0 = 10^{-4}$ mol L^{-1}, $[RO^-]_0 = 10^{-1}$, 10^{-2} mol L^{-1}; Full line: experimental data; Dotted line: simulated data; Fitted extinction coefficient = 1482000 L mol^{-1} m^{-1}

2.4.2. Kinetic modeling of precursor polymer formation

2.4.2.1. Radical p-quinodimethane polymerization

Precursor polymer formation via the sulfinyl route from 1-(chloromethyl)-4-[(n-octylsulfinyl)methyl]-benzene with Na*t*BuO in sBuOH has been reported by van Breemen et al.[55] Table 2 summarizes the reported polymerization conditions, product yields and precursor polymer properties. Using a premonomer concentration $[HML]_0 = 0.1$ mol L^{-1} and sodium tert-butoxide concentrations of $[Na tBuO]_0 = 0.05$, 0.13 and 0.2 mol L^{-1} in sBuOH at 308 K, a mixture of the reactant premonomer, ether byproduct and polymer results in each case. Precursor polymer yields range from 42% to 88% and display a maximum as a function of the initial base concentration. The mass averaged molar masses ranges from 236 – 249 kg/mol and are only slightly influenced by the initial base concentration while the initiator and recombination defect content remained very low in all cases. Clearly, the occurrence of recombination between α,ω-macro-diradicals contributes only marginally to chain growth in the sulfinyl route. Therefore, in a first step, recombination between α,ω-macro-diradicals is not considered in the kinetic scheme used to model precursor polymerization in the sulfinyl route. Also, since no experimental data is

available on the formation of oligomeric cyclic species produced by intramolecular cyclization of small α,ω-macro-diradicals, this reaction was not considered in the kinetic model in a first step.

Values for the rate coefficients for the radical initiation and propagation reactions (see Table 3), based on data available in literature, were used to describe the experimental data of Van Breemen et al. presented in Table 2. Beach[89] described chemical vapor deposition of para-quinodimethanes and subsequent polymerization using rate coefficients derived from the work of Errede and Gregorian.[69] Based on Errede and Gregorian's activation energy of E_a = 36.4 kJ mol^{-1} for the propagation step, Beach[89] calculated a termolecular initiation rate coefficient $k_{ini,3}$ = 7 L^2 mol^{-2} s^{-1} for the CVD process. However, when the polymerization occurs in solution, the initiation reaction is bimolecular. Hence, the value for the initiation rate coefficient reported by Beach was corrected with the value for the propagation coefficient at 308 K (see below) to yield a crude estimate for the value of the bimolecular initiation rate coefficient: k_{ini} = 5 10^{-3} L mol^{-1} s^{-1}. The value for the rate coefficient for the initiation reaction was further tuned based on the available experimental data to yield k_{ini} = 3 10^{-3} L mol^{-1} s^{-1}, i.e. close to the value based on the data reported by Beach.[89]

Table 2: Simulated polymer properties as a function of the base concentration and reaction system at t = 3600s. Reaction conditions: 308 K, $[HML]_0$ = 0.1 mol L^{-1}, $[RO^-]_0$ = 0.05, 0.13, 0.20 mol L^{-1}.

$[RO^-]_0$ (mol L^{-1})	0.05 mol L^{-1}		0.13 mol L^{-1}			0.20 mol L^{-1}	
	exp.	**sim.**	**exp.**	**exp.**	**sim.**	**exp.**	**sim.**
Polymer yield (mol%)	42.0	47.7	88.0	88.0	86.9	80.0	77.0
P_1 yield (mol%)	3.5	2.3	12.0	12.0	13.1	20.0	23.0
Residual premonomer yield (mol%)	54.5	50.0	≈0	≈0	0	≈0	0
Mass averaged molar mass (kg/mol)	236	241 [b]	249	238	263 [b]	244	226 [b]
Initiator defect (mol%)	-	0.13 [c]	<0.10[a]	<0.10[a]	0.11 [c]	-	0.14 [c]
Recombination defect (mol%)	-	0	<0.10[a]	<0.10[a]	0	-	0

[a] ^{13}C NMR detection limit

[b] The reported simulated molar masses were obtained by multiplying the molar mass of a precursor PPV unit (264 g/mol) and the mass averaged chain length of the simulated chain length distributions (CLDs).

[c] The reported simulated structural defect content is obtained from the ratio of the number of defects and the total number of propagation, initiation and recombination events.

For the propagation rate coefficient at 308 K, Szwarc[68] extrapolated the data reported by Errede and Gregorian[69] and obtained A = 2 10^9 L mol^{-1} s^{-1} and E_a = 36.4 kJ mol^{-1}, yielding k_p = 1.34 10^3 L mol^{-1} s^{-1} at 308 K. It was reported[65] by Errede and Szwarc that the propagation rate coefficient of a polystyryl radical should be much smaller than the propagation rate coefficient of a poly-p-xylyl radical. The value at 308 K for the propagation coefficient for styrene is about 2 L mol^{-1} s^{-1}, much smaller than 1.34 10^3 L mol^{-1} s^{-1}. The rate coefficients for initiation and propagation were taken as indicated above: k_{ini} = 3 10^{-3} L mol^{-1} s^{-1} and k_p = 1.34 10^3 L mol^{-1} s^{-1}. Table 3 summarizes the rate coefficients used in this work. Note that the rate coefficients for the monomer formation (k_{E2} and k_{NA}) are determined at 298 K while the polymerization kinetics (k_p and k_{ini}) are determined at 308 K. The temperature dependence of the acid-base and nucleophilic addition reaction is not expected to be large over a temperature interval of 10 K.

Table 3: Values for the rate coefficients at 308 K for the reactions shown in Figure 4.

	k (L mol^{-1} s^{-1})
1,6-elimination (E2)	
$RO^- + HML \rightarrow M + ROH + L^-$	1.2
nucleophilic addition (NA)	
$RO^- + M \rightarrow P_1$	2 10^{-1}
radical initiation (ini)	
$M + M \rightarrow R_{ini}$	3 10^{-3}
radical propagation (p)	
$R_i + M \rightarrow R_{i+1}$	1.34 10^3

Table 2 shows, for 3 polymerization conditions, the simulated polymer, ether byproduct and premonomer yield, simulated average molar mass and simulated structural defect content at a polymerization time t = 3600 s using the rate coefficients from Table 3. It can be seen from these data that the simulated polymer yield displays a maximum value as a function of the base concentration. The simulated average molar masses follow the trend of the yields and reach a

maximum value for an intermediate base concentration $[RO^-]_0$ = 0.13 mol L^{-1}, in close agreement with the trends observed experimentally. The corresponding simulated mass chain length distributions are given in Appendix D. Although the simulated structural defect contents are somewhat above the ^{13}C NMR detection limit, they remain in the same (low) order of magnitude in all 3 reaction conditions in accordance with the trend observed experimentally. Also, using the kinetic parameters in Table 3, the suppression of the polymerization at the UV-vis conditions (vide supra) could be simulated: the simulated polymer yields in these conditions varied from 0.0031 mol% to 0.1189 mol% depending on the initial base concentration. Clearly, the kinetic Monte Carlo model is able to capture the experimentally observed trends quite well.

2.4.2.2. Evaluation of the importance of α,ω-macro-diradical recombination

As mentioned above, in the sulfinyl route, α,ω-macro-diradical recombination is not expected to have an important contribution to chain growth. However, the recombination of α,ω-macro-diradicals is often suggested, but was never incorporated in a kinetic model. Therefore, recombination of α,ω-macro-diradicals has been implemented in the kinetic Monte Carlo model to evaluate its possible influence on the precursor polymer properties. Kinetic Monte Carlo simulations, with and without recombination, are again compared with simulations performed using the PREDICI© software.[78,79] The polymerization conditions used in both simulations are $[HML]_0$ = 0.1 mol L^{-1}, $[RO^-]_0$ = 0.13 mol L^{-1} at 308 K (see Table 2). Recombination of α,ω-macro-diradicals is absent in the first simulation; in the second simulation, this recombination reaction is added using an arbitrary value for the rate coefficient (k_{rc} = 5 L mol^{-1} s^{-1}) and the effect on the polymer yield and properties is interpreted. Table 4 compares the results for both simulations.

Table 4: Simulated yields and polymer properties at t = 3600s for the reaction scheme in Figure 4 and a reaction scheme with recombination of α,ω–macrodiradicals. Reaction conditions: 308 K, $[HML]_0$ = 0.1 mol L^{-1}, $[RO^-]_0$ = 0.13 mol L^{-1}.

$[RO^-]_0$	0.13 mol L^{-1}	
Recombination rate coefficient (L mol^{-1} s^{-1})	**0**	**5**
Polymer yield (mol%)	86.9	86.9
P_1 yield (mol%)	13.1	13.1
Residual premonomer yield (mol%)	0	0
Mass averaged molar mass (kg/mol)	263	1082
Initiator defect (mol%)	0.11	0.11
Recombination defect (mol%)	0	0.07 [a]

[a] The reported simulated initiator defect content is obtained as $\frac{n_{ini}}{n_{ini}+n_p+n_{rc}}\times 100\%$ in which n_{ini}, n_p and n_{rc} are the number of initiation, propagation and recombination events respectively. The simulated recombination defect content is obtained as $\frac{n_{rc}}{n_{ini}+n_p+n_{rc}}\times 100\%$.

Considering recombination results in an increase of the mass averaged molar mass by a factor 5 without affecting the yields. This implies that recombination becomes important after the monomer has been consumed and agrees with the findings of Errede and Szwarc[65] that dead polymer cannot be produced by recombination of the growing diradicals because this merely doubles the molar mass of the growing species. Table 4 also indicates that the defect content due to recombination remains below the detection limit of ^{13}C NMR. On average, each α,ω-macro-diradical has recombined twice at t = 3600 s; since the ratio of recombination defects (0.07) to initiation defects (0.11) is about 0.66, the average chain contains 2 recombination defects and 3 initiator defects. This implies that recombination events could contribute to polymer growth while the resulting structural defects remain unnoticed in NMR characterization of ^{13}C labeled precursor PPV polymers. However, a clear influence of recombination can be seen in the simulated chain length distributions (CLDs).

Figure 9 shows the simulated CLDs with and without recombination at t = 60, 600 and 3600 s ($[HML]_0$ = 0.1 mol L^{-1} and $[RO\text{-}]_0$ = 0.13 mol L^{-1}) together with the results obtained from the PREDICI© software.[78,79]

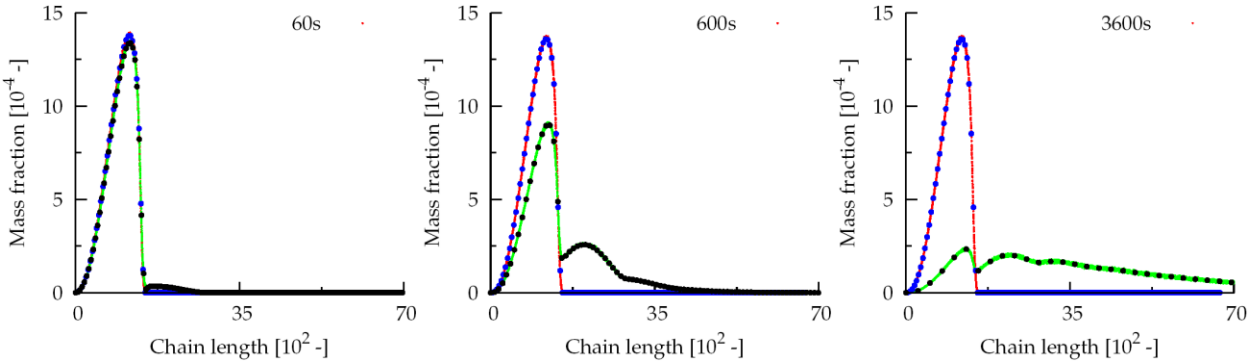

Figure 9: Simulated chain length distributions as a function of the recombination rate coefficient and the polymerization time; Reaction conditions: 308 K, $[HML]_0$ = 0.1 mol L^{-1}, $[RO^-]_0$ = 0.13 mol L^{-1}; Red line: k_{rc} = 0 L mol^{-1} s^{-1}; Green line: k_{rc} = 5 L mol^{-1} s^{-1}; Blue symbols: PREDICI (k_{rc} = 0 L mol^{-1} s^{-1}); Black symbols: PREDICI (k_{rc} = 5 L mol^{-1} s^{-1})

Clearly, kinetic Monte Carlo and PREDICI© yield identical results. From the mass CLD at t = 60 s, when most of the monomer is consumed, it can be seen that a 2nd peak emerges in the CLD indicating that a small number of recombination events have occurred. At t = 600 s, more recombination events have occurred: the 2nd peak is more pronounced and the emergence of a 3rd peak (shoulder) at high chain lengths can be observed. At t = 3600 s, chain lengths up to 4000 repeating units (higher than 10^6 g/mol para-quinodimethane) are formed. Even for the relatively low value of the recombination rate coefficient, the maximum change lengths produced, within the Monte Carlo sample size, are excessively large (up to chain lengths of 32.000 monomer units), while the experimentally observed range of molar masses is 236 – 249 kg/mol (see Table 2). This again indicates again that intermolecular recombination can be safely neglected in the sulfinyl route.

For the same polymerization conditions, Adriaensens et al.[50] reported a Size Exclusion Chromatography (SEC) elugram obtained at the end of the polymerization process. The reported

SEC elugram is monomodal and shows fronting, akin to the simulated CLDs in the absence of recombination. SEC elugrams showing a 2nd peak have not been reported in any precursor route for PPV synthesis in a protic solvent. The only exception was reported by Vanderzande[61], who found a bimodal distribution in the co-solvent tetrahydrofuran/sBuOH. A polymeric and an oligomeric fraction was found, suggesting an anionic mechanism.[48,55] In aprotic solvents, in the sulfinyl route, often oligomeric fractions are found to be the result of an anionic propagation mechanism coexisting with the radical branch which produces much longer chains. However, in protic solvents such as sBuOH, this is unusual. Moreover, the additional peak in the simulated bimodal CLD is a high molar mass peak, which does not represent the typical oligomeric fraction originating from an anionic mechanism. The simulation data clearly indicate that recombination is negligible during the synthesis of the precursor PPV. One reason for the absence of intermolecular recombination in the sulfinyl route could be steric hindrance of the recombining CHP-groups. For the cyclization, which will be discussed in the next paragraph, the same steric hindrance of the recombining CHP-groups could prevent the formation of a [2.2]paracyclophane. So far, the formation of [2.2]paracyclophanes has not yet been reported in the sulfinyl route, confirming the point made above.

It can thus be concluded that, for the sulfinyl route, chain growth by recombination of α,ω-macro-diradicals is limited and cannot be detected in ^{13}C NMR spectra of labeled PPV polymers, nor in polymer yields. Kinetic modeling indicates that the effect is strongly pronounced on the mass averaged molar masses and the related mass CLDs. Even if recombination would occur at low rates (k_{rc} = 5 L mol^{-1} s^{-1}), a 2nd or 3rd peak should be clearly visible in SEC elugrams.

2.4.2.3. Evaluation of the importance of cyclization of α,ω-diradical oligomers

Termination in the sulfinyl route may occur by cyclization of α,ω-diradicals similar to the Gilch[65] route. In the latter route, the isolated cyclic products are limited to very small chain lengths and [2.2]-paracyclophane-type cyclic products have been identified as the main side products. It was suggested by Errede[65,69] that cyclization becomes unlikely at higher chain lengths, especially at the typically diluted conditions of the precursor routes. Errede[69] observed that termination is second order in the total radical concentration, suggesting that the main

termination mechanism cannot be cyclization for every chain length and that cyclization mainly occurred for oligomeric (chain lengths i = 2, 3, 4) diradicals.

According to Schwalm et al.,[36] the formation of cyclic oligomers may go unnoticed as they do not precipitate with the polymer and, therefore, cannot be detected by ^{13}C NMR[35] of precipitated polymer samples produced via the sulfinyl route.[35] To evaluate the effect of intramolecular cyclization of oligomeric (chain lengths i = 2, 3, 4) α,ω-diradicals on the yields and polymer properties, simulations with and without cyclization are compared. The same polymerization conditions as above are used, i.e. $[HML]_0$ = 0.1 mol L^{-1} and $[RO^-]_0$ = 0.13 mol L^{-1}. Since literature data on cyclization in the sulfinyl route are not available, the value for the rate coefficient for cyclization is set at an arbitrary value of 10 s^{-1} resulting in a yield of cyclic products of 0.2 mol% (see Table 5).

Table 5: Simulated polymerization outcome for the reaction scheme in Figure 4 and a reaction scheme including intramolecular cyclization of oligomeric (i = 2, 3, 4) α,ω-diradicals. Reaction conditions: 308 K, $[HML]_0$= 0.1 mol L^{-1}, $[RO^-]_0$ = 0.13 mol L^{-1}.

$[RO^-]_0$ (mol L^{-1})	**0.13 mol L^{-1}**	
Cyclization rate coefficient (s^{-1})	**0**	**10**
Polymer yield (mol%)	86.9	84.6
P_1 yield (mol%)	13.1	15.2
Residual premonomer yield (mol%)	0	0
Cyclic product yield (mol%)	0	0.2
Mass averaged molar mass (kg/mol)	263	767
Initiator defect (mol%)	0.11	0.09

For para-xylylene polymerization, Errede[69] reports cyclic oligomer yields in the order of 1 mol% indicating that in the absence of a polarizer, P, the tendency for intramolecular recombination of the unsubstituted α,ω-diradicals (i = 2, 3 and 4) is higher than that of their sulfinyl counterparts

due to the absence of steric hindrance exerted by the CHP-group. As mentioned, the yield of cyclic products is distributed with respect to the chain length i, i ranging from 2 to 4. The CLD of the cyclic products is given in Table 6; the yield of the cyclic products in this CLD is 0.2 mol% and hence very small compared to the CLD of the α,ω-macroradicals which represents 84.6 mol%. The total mass CLD is essentially the mass CLD of the α,ω-macrobiradicals.

Table 6: Chain length distribution for the cyclic products formed via cyclization. Reaction conditions: 308 K, $[HML]_0$ = 0.1 mol L^{-1}, $[RO^-]_0$ = 0.13 mol L^{-1}.

chain length	2	3	4
number fraction	0.40	0.33	0.27
mass fraction	0.28	0.34	0.38

Considering cyclization of small oligomeric α,ω-diradicals results in a large increase in mass averaged molar mass of the macroradicals because the cyclization of the oligomeric α,ω-diradicals leads to a lower total radical concentration. Schwalm et al. observed[36,37] up to 30% yields of [2.2]-paracyclophane (the internally recombined dimer diradical) in the Gilch route while the produced polymers exhibited mass averaged molar masses up to 10^6 g/mol. In our view, it is highly likely that these high chain lengths not only result from chain growth by recombination of α,ω-macro-diradicals, as suggested by Schwalm et al.[37], but can, at least partly, also be attributed to the large cyclization rates and the concomitant increase in chain length.

In the presence of cyclization, the fraction of initiation defects at the end of the process is 0.1 mol%, which is lower than in case cyclizations are absent. This can be explained by the fact that the initiation defects of the cyclic oligomers are not taken into account for the calculation of the initiation defects in Table 5, as explained in Appendix E. For the calculation of polymer properties and structural defects, the high molar mass fraction, i.e. the α,ω-macro-diradicals, is considered.

Our simulations indicate that even very low yields of cyclic oligomers would lead to an important increase of the chain length. In contrast, to the Gilch route, the isolation of cyclic

products has not been reported for the sulfinyl route, most likely due to their very low yields and increased sterical hindrance of the sulfinyl groups (P = S(O)C_8) compared to the Gilch (P = Cl) and p-xylylene polymerizations (P = H). Apparently, the cyclization of small oligomeric α,ω-diradicals can be safely neglected for the sulfinyl route.

2.4.3. Effect of reaction conditions on monomer and polymer formation

After ensuring that termination reactions can be neglected, the effect of the reaction conditions on the PPV process can be investigated over a broad range of concentrations. This illustrated in Appendix F and allows to conclude that the final polymer properties and yields are only influenced by the ratio $[RO^-]_0/[HML]_0$. This can be understood by the bimolecular nature of all involved reactions and, hence, the independence of the relative reaction rates on the absolute values of the concentrations. It must be stressed that there is no dilution effect on the *final* yields and properties because unimolecular reactions are absent in the model. The direct consequence of the above observation is that a single independent variable, i.e. $[RO^-]/[HML]_0$, can be used to visualize the results.

Focusing on the regime of interest, i.e. where high polymer yields are obtained, the reactant concentrations are varied over a more narrow range to see how chain length and structural defects of the precursor polymer can be influenced. The simulation results are displayed in Figure 10 which shows the final yields and properties as a function of the initial reactant ratio $[RO^-]_0/[HML]_0$ for two values of $[HML]_0$ (0.1 mol L^{-1} and 0.01 mol L^{-1}). Again, it is clear that the *final* yields and properties depend only on $[RO^-]_0/[HML]_0$. The absolute values of the reactant concentrations only influence the rate at which the reaction system approaches the final values. As noted before, the polymer yield for $[RO^-]_0/[HML]_0 = 1.3$ is higher than for $[RO^-]_0/[HML]_0 = 0.5$ and $[RO^-]_0/[HML]_0 = 2.0$. However, an even higher polymer yield can be achieved for $[RO^-]_0/[HML]_0$ equal to unity. The occurrence of this maximum can be understood from the behavior of the substitution product yield Y_{P1} as a function of $[RO^-]_0/[HML]_0$: as the base excess increases, more and more substitution product is formed at the cost of polymer formation, as their sum equals 100 mol% yield. However, for $[RO^-]_0/[HML]_0$ lower than unity, not enough base is present to convert all of the premonomer to monomer, lowering both polymer

and byproduct yield and increasing the amount of unreacted premonomer. Hence, neither too low nor too high base concentrations are suitable for obtaining high polymer yields.

Figure 10 also shows the corresponding mass averaged molar mass as a function of $[RO^-]_0/[HML]_0$: it can be seen that the mass averaged molar mass follows the trend of the polymer yield, for the same reasons as mentioned before. The actual value of the mass averaged molar mass varies between 200 kg/mol and 300 kg/mol, depending on the reaction condition.

As shown above, termination can be neglected in the sulfinyl route and, hence, every precursor polymer chain contains only 1 structural defect due to initiation. This means that the lowest initiation defect fraction will always correspond to the highest average chain lengths (compare the upper and lower right hand graphs in Figure 10). Figure 10 also illustrates that the defect content can be changed by no less than 50% (from 0.1 mol% to 0.15 mol% depending on the reaction condition).

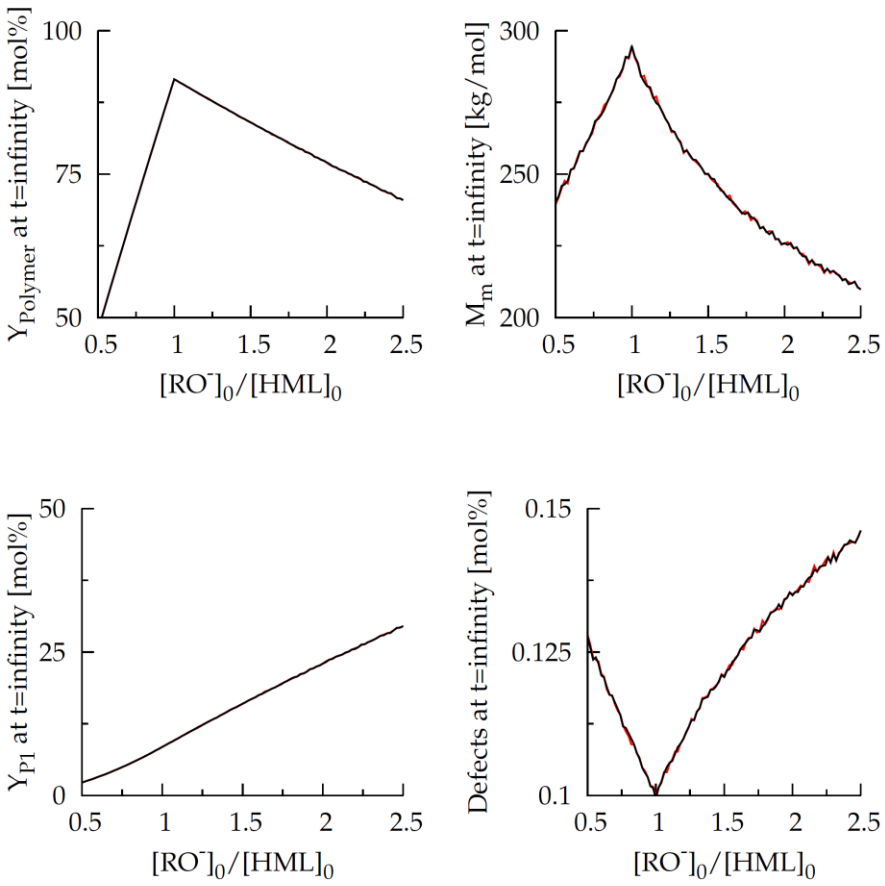

Figure 10: Influence of the ratio of initial base to premonomer concentration on the simulated final yields of substitution product P_1 and polymer, the mass averaged molar mass and the structural defect content; Reaction conditions: $[HML]_0 = 10^{-1}$ mol L^{-1} (red line), 10^{-2} mol L^{-1} (black line), 308 K

In addition, the mass averaged molar mass (see Figure 10) yields an estimate of the potential conjugated chain length of the precursor polymer chains. Neglecting the Gaussian nature of propagation steps (at both ends of the initiator defect) and assuming a perfect thermal elimination of the precursor polymer, the simulated *mass averaged* conjugated chain length corresponds to exactly half of the mass averaged molar mass. However, it must be mentioned that experimentally measured conjugation lengths are strong functions of the measurement technique itself, and by no means they lead to a unique value of the conjugated chain length. In any case, the value of the conjugation length simulated must be considered an upper limit of the real value.

The simulation results clearly show that, for a given combination of premonomer and base with its inherent kinetics, there is a unique reaction condition which will result in the highest polymer yield and the highest chain lengths with the lowest amounts of defects. Moreover, the structural defect content and chain (and conjugation) length can be varied by as much as 50% by proper choice of $[RO^-]_0/[HML]_0$.

2.5. Conclusions

A kinetic model for the base inducted polymerization reaction of 1-(chloromethyl)-4-[(n-octylsulfinyl)methyl]benzene in sBuOH was developed to investigate the effect of reaction conditions on PPV polymer properties. Experiments were designed to determine values for rate coefficients for the monomer formation and ether byproduct formation. Experimental and simulated reaction conditions span a product range from 95% polymer yield to 100% ether byproduct yield. The kinetic Monte Carlo model succeeds in predicting the experimentally observed trends over a broad range of experimental conditions, such as the suppression of polymerization and the competition between the anionic formation of the ether byproduct and precursor polymer formation via a radical mechanism. The effect of intramolecular and intermolecular recombination during precursor PPV synthesis was modeled and found to be negligible upon comparison with experimental data.

It was shown that the final polymer yield and properties are only determined by the ratio $[RO^-]_0/[HML]_0$, while the absolute concentration values determine the rate at which the final yields and properties are approached. Simulations allowed determination of reaction conditions yielding targeted polymer yields and mass averaged molar masses with targeted amount of structural defects, which can serve as a guideline for precursor synthesis of conjugated polymers.

References

1. Burroughes, J.; Bradley, D.; Brown, A.; Marks, R.; Friend, R.; Holmes A. *Nature* **1990**, 347, 539-541.
2. Friend, R. ; Gymer, R.; Holmes, A.; Burroughes, J.; Marks, R.; Taliani, C.; Bradley, D.; Dos Santos, D.; Bredas, J.; Logdlund, M.; Salaneck W. *Nature* **1999**, 397, 121-128.
3. Meier, H. *Angew. Chem., Int. Ed.* **1992**, 104, 1425-46.

4. Hide, F.; Diaz-Garcia, M. A.; Schwartz, B. J.; Heeger, A. J. *Acc. Chem. Res.* **1997**, 30, 430-436.
5. McGehee, M. D.; Heeger, A. J. *Adv. Mater.* **2000**, 12, 1655-1668.
6. Petty, M. C.; Bryce, M. R.; Bloor, D., editors. *Introduction to molecular electronics.* London: Edward Arnold; 1995.
7. Loutfy, R. O.; Hor, A. M.; Hsiao C. K.; Baranyi, G.; Kazmaier, P. *Pure Appl. Chem.* **1988**, 60, 1047-1054.
8. Nalwa, H.S., editor. *Nonlinear optics of organic molecules and polymers*. New York, NY: CRC; 1997.
9. Feringa, L.; Jager, W. F.; de Lange B. *Tetrahedron*, **1993**, 49, 8267-8310.
10. Pan, J.-Q.; Chen, Z.-K.; Xiao, Y.; Huang, W. *Chinese Journal of Polymer Science* **2000**, 18, 6, 541-549.
11. Sirringhaus, H.; Brown, P. J.; Friend, R. H.; Nielsen, M. M.; Bechgaard, K.; Langeveld-Voss, B. M. W.; Spiering, A. J. H.; Janssen, R. A. J.; Meijer, E. W.; Herwig, P.; de Leeuw, D. M. *Nature* **1999**, 401, 685-688.
12. Erb, T.; Raleva, S.; Zhokhavets, U.; Gobsch, G.; Stühn, B.; Spode, M.; Ambacher, O. *Thin Solid Films* **2004**, 450, 97-100.
13. Greiner, A.; Martelock, H.; Heitz, W. *Synth. Met.* **1991**, 41-43, 881-884.
14. Heitz, W.; Brugging, W.; Freund, L.; Gailberger, M.; Greiner, A.; Jung, H.; Kampschulte, I.; Niesner, N.; Osan, F.; Schmidt, H. W.; Wicker, M. *Makromol. Chem.* **1988**, 189, 119-127.
15. Greiner, A.; Heitz, W. *Makromol. Chem. Rapid Commun.* **1988**, 9, 581-588.
16. Brenda, M.; Greiner, A.; Heitz, W. *Makromol. Chem.* **1990**, 191, 1083-1100.
17. Wayne Cooke A.; Wagener, K. B. *Macromolecules* **1991**, 24, 1404-1407.
18. Wang, D.; Wei, P.; Wu, Z. *Macromolecules* **2000**, 33, 6896-6898.
19. Conticello, V. P.; Gin, D. L.; Grubbs, R. H. *J. Am. Chem. Soc.* **1992**, 114, 9708-9710.
20. Staring, E. G.; Braun, D.; Rikken, G. L. J. A.; Demandt, R. J. C. E.; Kessener, Y. A. R. R.; Bouwmans, M.; Broer, D. *Synth. Met.* **1994**, 67, 71-75.
21. Chang, W.-P.; Whang W.-T.; Lin P.-W. *Polymer* **1996**, 37, 1513-1518.
22. Diliën, H.; Vandenbergh, J.; Banishoeb, F.; Adriaensens, P.; Cleij, T. J.; Lutsen, L.; Vanderzande, D. J. M. *Macromolecules* **2011**, 44, 711-718.

23. de Kok, M. M.; van Breemen, A. J. J. M.; Adriaensens, P. J.; van Dixhoorn, A.; Gelan J. M.; Vanderzande, D. J. *Acta Polym.* **1998**, 49, 510-513.
24. Gowri, R.; Padmanaban, G.; Ramakrishnan, S. *Synth. Met.* **1999**, 101, 166-169.
25. Chen, Z. K.; Pan, J. Q.; Lee, N. H. S.; Chua, S. J.; Huang, W. *Thin Solid Films* **2000**, 363, 1-2, 98-101.
26. Kesters, E.; de Kok, M. M.; Carleer, R. A. A.; Czech, J. H. P. B.; Adriaensens, P. J.; Gelan, J. M.; Vanderzande, D. J. *Polymer* **2002**, 43, 5749-5755.
27. Kesters, E.; Vanderzande, D.; Lutsen, L.; Penxten, H.; Carleer, R. *Macromolecules* **2005**, 38, *4*, 1141-1147.
28. Kesters, E.; Gillissen, S.; Motmans, F.; Lutsen, L.; Vanderzande D. *Macromolecules* **2002**, 35, 7902-7910.
29. Henckens, A.; Colladet, K.; Fourier, S.; Cleij, T.J.; Lutsen, L.; Gelan, J.; Vanderzande, D. *Macromolecules* **2005**, 38, 1, 19-26.
30. de Kok, M. M.; Nguyen, T. P.; Molinie, P.; van Breemen, A. J. J. M.; Vanderzande, D. J.; Gelan, J. M. *Synth. Met.* **1999**, 102, 1-3, 949-950.
31. Henckens, A.; Duyssens, I.; Lutsen, L.; Vanderzande, D.; Cleij, T. J.; *Polymer* **2000**, 47, 123-131.
32. Adriaensens, P.; Roex, H.; Vanderzande, D.; Gelan, J. *Polymer* **2005**, 46, 6, 1759-1765.
33. Wiesecke, J.; Rehan, M. *Macromol. Rapid Commun.* **2007**, 28, 188-193.
34. Wiesecke, J.; Rehahn, M. *Angew. Chem., Int. Ed.* **2003**, 42, 5, 567.
35. Roex, H.; Adriaensens, P.; Vanderzande, D.; Gelan, J. *Macromolecules* **2003**, 36, 5613-5622.
36. Schwalm, T.; Rehahn, M.; *Macromolecules* **2007**, 40, 3921-3928.
37. Schwalm, T.; Wiesecke, J.; Immel, S.; Rehahn, M. *Macromol. Rapid Commun.* **2009**, 30, 1295-1322.
38. Schwalm, T.; Wiesecke, J.; Immel, S.; Rehahn, M. *Macromolecules* **2007**, 40, 8842-8854.
39. Schwalm, T.; Rehahn, M.; *Macromol Rapid Commun.* **2008**, 29, 207-213.
40. Becker, H.; Spreitzer, H.; Ibrom, K.; Kreuder, W. *Macromolecules* **1999**, 32, 15, 4925-4932.
41. Wiesecke, J.; Rehahn , M. *Macromol. Rapid Commun.* **2007**, 28, 1, 78-83.

42. Gilch, H. G.; Wheelwright, W. L. *J. Pol. Sci. Part A-1* **1966**, 4, 1337-1349.
43. Schwalm, T.; Rehahn, M.; *Macromol. Rapid Commun.* **2008**, 29, 33-38.
44. Vanderzande, D. J. M.; Hontis, L.; Palmaerts, A.; Van Den Bergh, D.; Wouters, J.; Lutsen, L.; Cleij, T. *Proc. Of SPIE* **2005**, 5937, 59370Q-1.
45. Louwet, F.; Vanderzande D.; Gelan J. *Synth. Met.* **1992**, 52, 1, 125-130.
46. Hontis, L.; Lutsen, L.; Vanderzande, D.; Gelan J. *Synth. Met.* **2001**, 119, 1-3, 135-136.
47. Louwet, F.; Vanderzande, D.; Gelan, J.; Mullens, J. *Macromolecules* **1995**, 28, 4, 1330-1331.
48. Hontis, L.; Vrindts, V.; Vanderzande, D.; Lutsen, L. *Macromolecules* **2003**, 36, 3035-3044.
49. Issaris, A.; Vanderzande, D.; Adriaensens, P.; Gelan, J. *Macromolecules* **1998**, 31, 14, 4426-4431.
50. Adriaensens, P.; Van der Borght, M.; Hontis, L.; Issaris, A.; van Breemen, A.; de Kok, M.; Vanderzande, D.; Gelan, J. *Polymer* **2000**, 41, 19, 7003-7009.
51. Hermosilla, L.; Catak, S.; Van Speybroeck, V.; Waroquier, M.; Vandenbergh, J.; Motmans, F.; Adriaensens, P.; Lutsen, L.; Cleij, T.; Vanderzande, D. *Macromolecules* **2010**, 43, 18, 7424-7433.
52. Hontis, L.; Van der Borght, M.; Vanderzande, D.; Gelan J. *Polymer* **1999**, 40, 23, 6615-6617.
53. Issaris, A.; Vanderzande, D.; Gelan, J. *Polymer* **1997**, 38, 10, 2571-2574.
54. Louwet, F.; Vanderzande, D.; Gelan, J. *Synth. Met.* **2005**, 69, 1-3, 509-510.
55. van Breemen, A. J. J. M.; Issaris, A. C. J.; de Kok, M. M.; Van der Borght, M. J. A. N.; Adriaensens, P. J.; Gelan, J. M. J. V.; Vanderzande, D. J. M. *Macromolecules* **1999**, 32, 18, 5728-5735.
56. Van der Borght, M.; Adriaensens, P.; Vanderzande, D.; Gelan, J. *Polymer* **2000**, 41, 8, 2743-2753.
57. Hontis, L.; Vrindts, V.; Lutsen, L.; Vanderzande, D.; Gelan, J. *Polymer* **2001**, 42, 13, 5793-5796.
58. Lutsen, L.; Adriaensens, P.; Becker, H.; van Breemen, A. J.; Vanderzande, D.; Gelan, J. *Macromolecules* **1999**, 32, 20, 6517-6525.

59. Vandenbergh, J.; Wouters, J.; Adriaensens, P.; Mensa, R.; Cleij, T.; Lutsen, L.; Vanderzande, D. *Macromolecules* **2009**, 30, 1295-1322.
60. Cho, B.R. *Prog. Pol. Sci.* **2002**, 27, 2, 307-355.
61. Gillissen, S.; Lutsen, L.; Vanderzande, D.; Gelan, J. *Synth. Met.* **2001**, 119, 1-3, 137-138.
62. Cho, B. R.; Kim, T. H.; Son, K. H.; Kim, Y. K.; Lee, Y. K.; Jeon, S. J. *Macromolecules* **2000**, 33, 22, 8167-8172.
63. Wessling, R. A. *J. Pol. Sci. Pol. Symp.* **1985**, 72, 55-66.
64. Denton, F. R.; Lahti, P. M.; Karasz, F. E. *J. Pol. Sci. Part A Pol. Chem.* **1992**, *30, 10,* 2223-2231.
65. Errede, L.A.; Szwarc, M. *Quarterly Reviews* **1958**, 12, 4, 301-320.
66. Schafer, O.; Brink-Spalink, F.; Greiner, A. *Macromol. Rapid Commun.* **1999**, 20, 4, 190-193.
67. Cho, B. R.; Kim, Y. K.; Han, M. S. *Macromolecules* **1998**, 31, 2098-2016.
68. Szwarc, M.; *Polymer Engineering and Science* **1976**, 16, 7, 473-479.
69. Errede, L.; Gregorian, R.; Hoyt, J. *J. Am. Chem. Soc.* **1960**, 82, 5218-5223.
70. Itoh, T.; Nakanishi, E.; Okayama, M.; Kubo, M. *Macromolecules* **2000**, 33, 2, 269-277.
71. Son, S.; Lovinger, A.J.; Galvin, M.E. *Science* **1995**, 269, 376-378.
72. Son, S.; Lovinger, A.J.; Galvin, M.E. *Polym. Mat. Sci. Engng.* **1995**, 72, 567-568.
73. de Kok, M.M.; van Breemen A. J. J. M.; Adriaensens, P. J.; van Dixhoorn, A.; Gelan J. M.; Vanderzande, D. J. *Acta Polym.* **1998**, 49, 510-513.
74. Errede, L.A.; Hoyt, J. M. *J. Am. Chem. Soc.* **1960**, 82, 2, 436-439.
75. Yin, C.; Yang, C.-Z. *Synth. Met.* **2001**, 118, 75-79.
76. Cho, B. R.; Han, M. S.; Suh, Y. S.; Oh, K. J.; Jeon, S. J. *J. Chem. Soc., Chem. Commun.* **1993**, 6, 564-566.
77. Pyun, S. Y.; Kim, W. G.; Jeong, J.-H.; Cho, B. R. *Bull. Korean Chem. Soc.* **2008**, 29, 2453-2458.
78. Wulkow, M. *Macromol. React. Eng.* **2008**, 2, 6, 461-494.
79. Wulkow, M. *Macromol. Theor. Simul.* **1996**, 5, 3, 393-416.
80. Bianchi, C.; Grassl, B.; Francois, B.; Dagron-Lartigau, C. *J. Pol. Sci. Part A* **2005**, 43, 19, 4337-4350.
81. Kim, T. H.; Park, S. M. *Electrochimica Acta* **2005**, 50, 7-8, 1461-1467.

82. Gillespie, D. T. *J. Phys. Chem.* **1977**, 81, 25, 2340-2361.

83. Szymanski, R. *e-polymers* **2009**, 044.

84. Gibson, M. A.; Bruck, J. *J. Phys. Chem. A* **2000**, 104, 9, 1876-1889.

85. Chaffey-Millar, H.; Stewart D.; Chakravarty, M. M. T; Keller, G.; Barner-Kowollik, C. *Macromol. Theor. Simul.* **2007**, 16, 6, 575-592.

86. Frost, A. A.; Pearson, R. G., editors. *Kinetics and Mechanism*. Tokyo: Wiley; 1961.

87. Fleck, G., editor. *Chemical Reactions and Mechanisms*. New York: Holt, Rinehart and Winston, Inc.; 1971.

88. Denton III, F.; Sarker, A.; Lahti, P. M.; Garay, R. O.; Karasz, F. E. *J. Pol. Sci.* **1992**, 30, 2233-2240.

89. Beach, W. F. *Macromolecules* **1978**, 11, 1, 72-76.

Chapter 3: Kinetic modeling of conjugated copolymer synthesis using structure-reactivity relations for the sulfinyl route

Summary

The performance of organic opto-electronic applications, such as polymeric solar cells and polymeric light emitting diodes, depends on the copolymer microstructure. In this work, a kinetic Monte Carlo model is used to describe the effect of the monomer structure on the microstructure of poly(*p*-phenylene vinylene) (PPV) based copolymers synthesized via the sulfinyl precursor route. The premonomers, 1-(halomethyl)-4-[(n-octylsulfi(o)nyl)methyl]-aryls, with various electron donating and withdrawing substituents on the aromatic moiety, are subjected to a Na*t*BuO induced 1,6-eliminationin sBuOH yielding the actual monomer *p*-quinodimethane derivative which leads, via a radical polymerization, to the precursor polymers. Rate coefficients for these reactions are based on reported theoretical modeling, UV-vis spectroscopy and earlier work on structure-reactivity of *p*-quinodimethane chemistry. The kinetic model predicts correctly that electron-poor PPVs possess low chain lengths, while electron-rich PPVs (such as the industrially used MDMO-PPV) possess high chain lengths. For the first time, a consistent picture of the interplay between molecular structure, polymer yield, chain length and initiator defects is presented. Finally, the found structure-reactivity relations for homopolymerizations are used to describe copolymerizations, which allow tailored synthesis of conjugated materials for photovoltaic devices through optimized regioregularity and solubility.

3.1. Introduction

Conjugated polymers couple the mechanical properties and inherent processing ease of polymers with the electrical, electronic, magnetic and optical properties of metals and semiconductors. They are mostly suitable for high tech applications such as organic photovoltaic cells (OPVs),[1-10]organic light emitting diodes (OLEDs),[6,11-18] organic field effect transistors (OFETs),[19-26] sensor devices,[27-32] thin film transistors (TFT), laser-dyes,[33-35]

scintillators,[33] piezoelectric and pyro electric materials,[36] photoconductors[37] to switch elements, data processors,[36,38,39] printable electronics[40] and a lot of other devices.[41-51]

Polymeric solar cells are of particular interest due to the increasing need of energy. Best performance is obtained for the bulk hetero-junction type, in which the electron donor (a p-type material) is a conjugated polymer and the electron acceptor (an n-type material) is phenyl-C_{61}-butyric acid methyl ester (PCBM). The p-type material (usually MDMO-PPV, absorbing between 400-600 nm.) can be optimized by narrowing its band gap, leading to a shifted absorbance spectrum which matches the emission spectrum (400-800 nm.) of the sun better, ultimately resulting in a greater collection of solar energy. Electron donating groups (EDGs) generally raise the HOMO whilst electron withdrawing groups (EWGs) lower the LUMO, both reducing the band gap. The band gap may be further reduced by increasing the conjugation length, which can be accomplished by providing a sufficiently long chain length and reducing structural defect formation. The beneficial effect of decreased defect content on photovoltaic device performance using sulfinyl PPVs has recently been reported.[52] Control of the chain length is also important to obtain film-forming properties and ensure solubility for processing. The solubility is further affected by the regioregularity of the polymer: regioregular polymers are more difficult to spin coat from solution. Not many reports exist on regioregularity control.[53,54] The group of Vanderzande prepared[55] two isomers of asymmetric monosulfinyl chloromethylbenzenes in 50:50 ratio and demonstrated their polymerization toward regiorandom high chain length MDMO-PPV.[56] Using only one of the two isomers, they could synthesize fully regioregular MDMO-PPV, albeit with poor solubility in common solvents, inhibiting further characterization. Joint work of the Vanderzande group and Mozer et al.[57,58] resulted in MDMO-PPV with a 30:70 composition of isomeric comonomers, displaying a 3.5-fold higher hole mobility than its regiorandom (50:50) counterpart. The latter result is of particular importance toward device optimization because the hole mobility in MDMO-PPV films is currently the bottleneck of the performance of photovoltaic devices (the electron mobility in PCBM films is an order of 2 to 4 times larger). The 30:70 MDMO-PPV was used to fabricate a bulk hetero-junction solar cell with a very high fill factor. Thus, copolymerizations allow tuned regioregularity and better device performance but the solubility issue needs to be resolved. Also, no reports exist of a quantitative method to measure the regioregularity, which is necessary to relate the regioregularity to the device performance. The need for this is illustrated by certain classes of conjugated polymers whose regioregularity is not strongly affecting the opto-electronic properties and thus, variable

regioregularity can be used to improve their solubility. This concept is illustrated for the statistical copolymers of 3-butylthiophene and 3-octyltiophene of several compositions, which turned out to be remarkably crystalline in spite of the statistical arrangement of the side chains with different size for a 50:50 initial monomer composition. Power conversion efficiencies up to 3.0% were obtained in photovoltaic devices, which is significantly higher than for the respective homopolymers and their blends. The copolymer avoids the disadvantages of the poorly processable poly(3-butylthiophene) (P3BT) and the long alkyl side chains of poly(3-octylthiophene) (P3OT).[59]A similar idea to improve processability using copolymers is reported[60] for the synthesis of poly(3-dodecylthienylenevinylene)s, in which also isomeric comonomers are used to introduce regiorandomness to improve solubility, while not affecting the crystallinity and photovoltaic performance strongly. The result is attributed to the long separation between the side chains, allowing all side chains to be stacked in the polymer backbone plane irrespective of the degree of regioregularity. The best solar cell device efficiencies were obtained for the poly(3-dodecylthienylenevinylene) with a 30:70 initial monomer ratio, coincidentally the same initial (pre)monomer composition as demonstrated[57,58] best for MDMO-PPV.

As opposed to research being done on the optimization of the p-type material via copolymers with targeted chemical composition (as illustrated above), much less research has been conducted toward optimization of the n-type material. Currently, almost exclusively PCBM is used because of its excellent solubility, electron-accepting and transporting properties. However, PCBM absorbs weakly in the visible and near-infrared region. Absorbance can be improved by using a conjugated polymer as the n-type material, which has a number of advantages.[61] Poly(2,5,2',5'-tetrahexyloxy-7,8'-dicyano di-*p*-phenylene vinylene) (CN-PPV) or poly(p-pyridyl vinylene) (PPyV), based on pyridine units instead of phenylene units, displays electron transport properties instead of hole transporting properties and hence may serve as n-type material. Additionally, the phase separation between two conjugated polymers is less severe than when using PCBM.

As opposed to the currently superior bulk hetero-junction architecture of photovoltaic devices, in which the p-n junction is formed on the nanoscale, research is also being performed on so-called molecular hetero-junctions, in which the p-type (with EDGs) and n-type (with EWGs) material reside on the same block copolymer molecule. It was shown that these block

copolymers phase separate and form ordered domains, and hence may serve as active layers in photovoltaic devices.[62]

For LED devices, the main interest is controlling the absorption maximum of the absorption spectra, which determines the emission color of the LED. The absorption maximum is determined by the conjugation length: a short conjugation length yields a blue shifted emission, while a long conjugation length yields a red shifted emission. The conjugation length is modified by adding different alkoxy and alkyl substituents on the monomer, imposing steric torsions on the polymer chain. Hence, more voluminous substituents cause larger dihedral angles between the aromatic rings, leading to a short effective conjugation along the polymer backbone, i.e. a blueshift. In such way, colors ranging from blue, green, orange to red are obtainable for PTVs. Similar as for photovoltaic devices, lower defect content is beneficial for LED devices.[63]

Although only two applications of conjugated polymers have been discussed above, it is clear that the ability to synthesize PPVs via copolymerizations allows to tailor the opto-electronic properties of the active material.[64] To synthesize conjugated polymers, two distinct approaches exist: (i) the precursor routes, consisting of chain-type polymerizations of *p*-quinodimethanes, which readily offer high chain length polymer and (ii) the direct routes, involving either polycondensations, transition-metal catalyzed coupling or electrochemical polymerization, which yield significantly lower chain lengths than the precursor routes. In addition, the direct routes are very sensitive to the reaction condition and consequently not easy to control, which is problematic if the desired polymers possess complex functionalization. It is clear that precursor routes offer the possibility to obtain soluble functionalized high chain length polymers. Moreover, the chain type polymerization of the precursor routes is fast and cost effective, suitable for industrial production. Figure 1 depicts the most frequently employed precursor routes for the synthesis of PPV (and PPyV) based homopolymers.[65] For copolymers, the reaction scheme is similar.

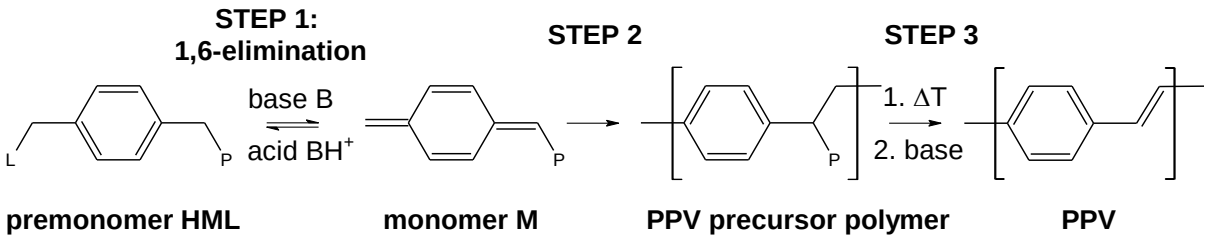

Gilch route: L = P = Cl or Br;
Wessling-Zimmermann/Sulfonium route: L = P = R_2S;
Sulfinyl route: L = Cl or Br; P = RS(O);
Xanthate route: L = P = RO-C(S)-S;
Dithiocarbamate route: L = P =R_2N-C(S)-S

Figure 1: Precursor routes toward poly(p-phenylene vinylene) (PPV)

The premonomer HML is subjected to a base induced 1,6-elimination, forming the highly reactive *p*-quinodimethane monomer. At ambient temperature, the *p*-quinodimethane monomer auto-initiates a radical or anionic polymerization, leading to a precursor polymer. In a final step, a (preferably complete) macromolecular elimination (thermal, basic or acidic) leads to the conjugated material. As shown in Figure 1, the precursor routes differ by the chemical structure of the premonomer. The precursor routes characterized by identical polarizer and leaving group (such as the Gilch, the Wessling-Zimmermann/Sulfonium, the xanthate and the dithiocarbamate routes) offer a straightforward synthesis of the premonomer, while the sulfinyl route differentiates between the leaving group and the polarizer. This allows to form the *p*-quinodimethane quantitatively due to the excellent leaving properties of the halide, while the precursor polymer is stable because the sulfinyl group is a bad leaving group in basic conditions, not prone to substitution or other side reactions during polymerization. Mild heating is required to eliminate the polarizer in a controlled fashion (STEP 3 in Figure 1), leading to PPVs of extreme constitutional purity. Contrary to e.g. the Wessling route, the sulfinyl route also allows to synthesize electron-poor PPVs and PPVs with extended aromatic moieties.

As illustrated above, the premonomer structure affects the microstructure of the (co)polymers. A wide range of sulfinyl premonomers has been considered experimentally.[66] The effect of the structure of the premonomer by measuring polymer yield, byproduct yield and chain length was investigated.[66] The authors observe that electron donating groups (EDGs) on the aromatic

moiety lead to high chain lengths. Assuming that a high monomer concentration is responsible for these high chain lengths, it was proposed[66] that "Electron donor substituents seem to enhance the rate of formation of the *p*-quinodimethane system probably because they facilitate the expulsion of the leaving group in the transition state.". Such statement can only be ascertained by monitoring the *p*-quinodimethane directly, which has been reported very recently.[67] In this second work, the 1,6-elimination is decoupled from the polymerization reactions by lowering the premonomer concentration and using a large base excess, effectively suppressing the bimolecular initiation reaction (Figure 2). This approach was followed to investigate the kinetics of 8 premonomers: **1**, **2** and **4** in Figure 3, **9** in Figure 4 and **10**-**13** in Figure 5. It is found that a better leaving group effect (**10** in Figure 5) only slightly accelerates the 1,6-elimination, whereas replacing the sulfinyl polarizer (**1** in Figure 3) with a sulfonyl polarizer (**13** in Figure 5) accelerates the1,6-elimination much more. This suggests an E2 mechanism with a carbanion-like transition state for the 1,6-elimination, as opposed to the suggestion[66] that the leaving group expulsion may be the rate-determining step in the *p*-quinodimethane formation. The 1,6-elimination also accelerates when EWGs (**9** in Figure 4) are present on the aromatic moiety. The same authors report[67] theoretical calculations of the deprotonation energies of the 1,6-eliminations, which are excellently correlated with the reported UV-vis data. Hence, strong indications are found that the 1,6-elimination does not accelerate with EDGs, as was originally[66] supposed, but rather the 1,6-elimination accelerates with EWGs. The same work reports[67] kinetic data on the formation of P_1 (Figure 2), which is discussed in the next paragraph.

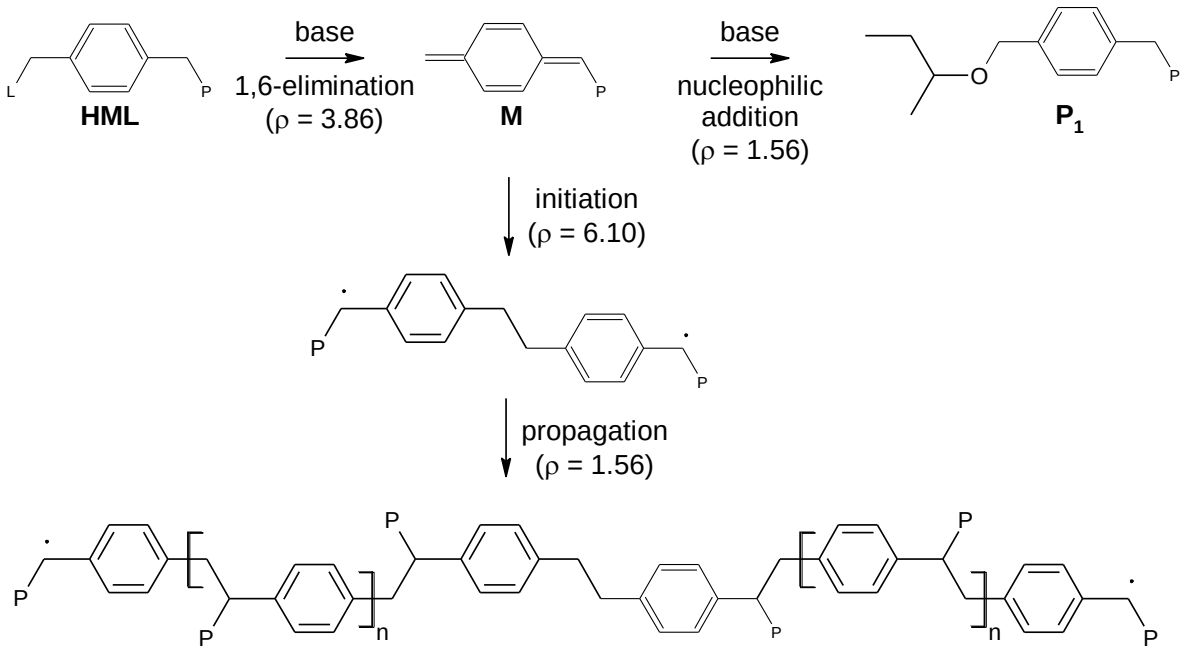

Figure 2: Reaction scheme for p-quinodimethane formation and its consumption by conjugate nucleophilic addition and polymerization via the sulfinyl route in solvent sBuOH; HML: premonomer, L: leaving group, P: polarizer, M: monomer, P_1: ether byproduct

It can be seen in Figure 2 that the polymerization is complicated by the occurrence of an anionic side reaction of the monomer, and thus competes in parallel with the radical polymerization. The rate of this conjugate nucleophilic addition reaction depends, in principle, on the molecular structure of the premonomer, and hence it stands to reason that the microstructure of the polymer can only be modeled if kinetic data on this monomer consuming side reaction are available for various types of premonomers. Such information has been reported[67] by Hermosilla et al., who report times of maximum UV-vis absorbance for 8 different premonomers (designated **1**, **2** and **4** in Figure 3, **9** in Figure 4 and **10**-**13** in Figure 5) in conditions where polymerization is suppressed. Although these authors did interpret the data, they did not link the times of maximum UV-vis absorbance of **M** to the kinetics of the conjugate nucleophilic addition. It will be demonstrated that these time values can be used to characterize the structure-effect on the conjugate nucleophilic addition, allowing to correctly model the effect of the side reaction on the (co)polymer microstructure.

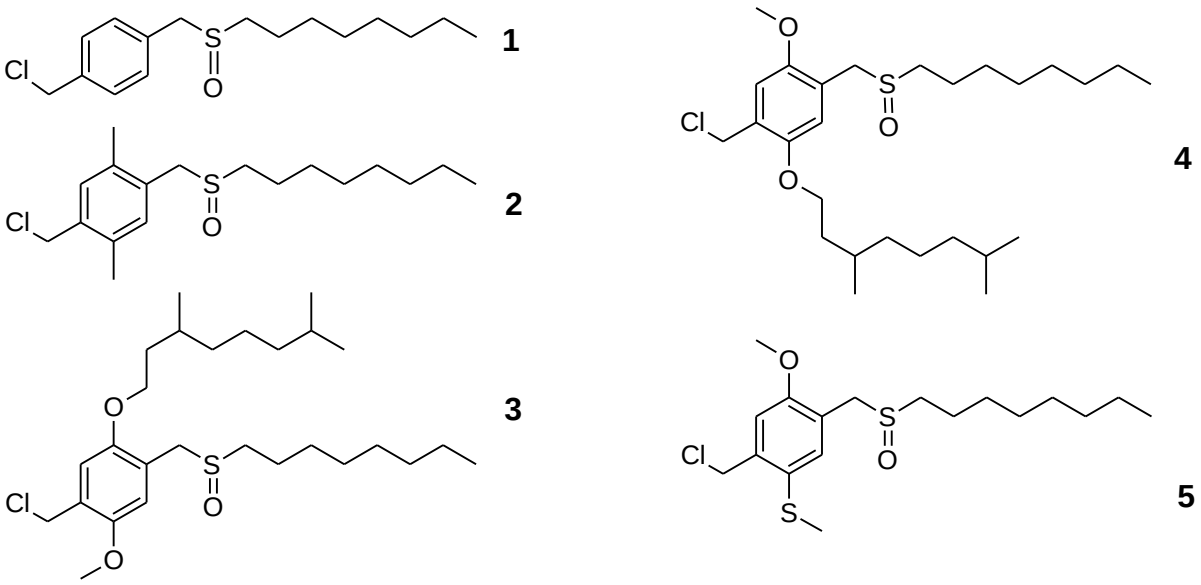

Figure 3: 1-(chloromethyl)-4-[(n-octylsulfinyl)methyl]-benzene 1 and derivatives with electron donating groups 2-5 on the aromatic moiety

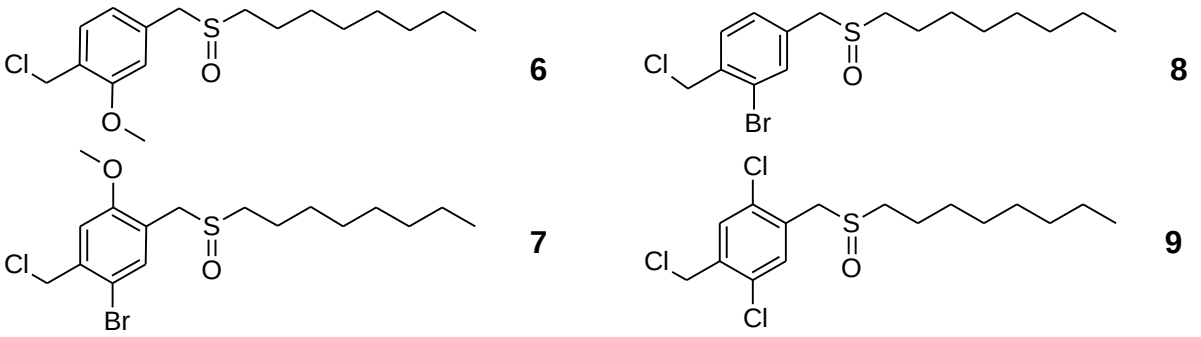

Figure 4: Premonomers with electron withdrawing groups 6-9 on the aromatic moiety

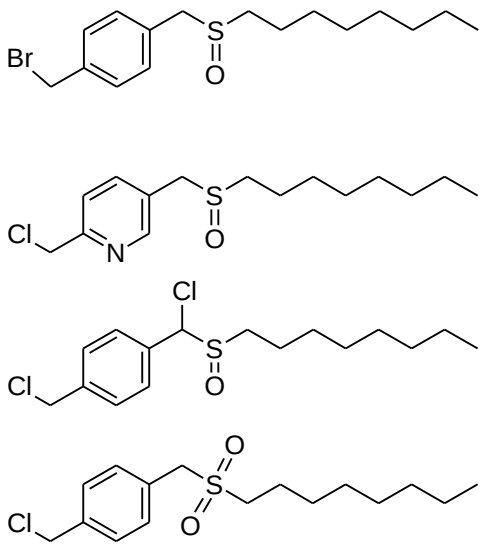

10 Different leaving group

11 Different aromatic moiety

12 Different polarizer

13 Different polarizer

Figure 5: Premonomers with different leaving group (10), aromatic moiety (11) and polarizers (12 and 13)

As mentioned earlier, it is observed[66] that electron donating groups (EDGs) on the aromatic moiety lead to high chain lengths. This effect could, in principle, be attributed to an increase in propagation reactivity. For the sulfinyl route this has not been investigated, but for the Wessling route a kinetic study is reported[68,69] indicating that the propagation obeys a Hammett free energy relation, based on kinetic UV-vis data for 5 different substituents (**1** and **5** in Figure 3 and **6**, **7** and **8** in Figure 4) on the aromatic moiety. However, the corresponding Hammett reaction constant is positive, implying that the propagation is retarded with EDGs in the Wessling route. Assuming mechanistic similarity between the Wessling and sulfinyl route, as recently proposed by the group of Rehahn,[70] it is reasonable to state that the sulfinyl propagation follows Hammett's relation with a similar positive Hammett reaction constant. Because the latter implies a slower propagation in the presence of EDGs, it cannot explain high chain lengths for electron-rich PPVs in the sulfinyl route by itself.[66] However, it will be demonstrated in the remainder of this work that, based on previous[67,68,69] work on *p*-quinodimethane chemistry, it is possible to simulate the experimental trends observed.[66]

Nothing has been said about the remaining reaction in Figure 2, the radical chain initiation. Unlike the 1,6-elimination and conjugate nucleophilic addition, the initiation reaction cannot be isolated. Hence, the structure effect on the initiation can be expected to be difficult to determine. To the best of the authors' knowledge, the only indication is reported for the so-called Gorham route toward poly(p-xylylene)s (PPX).[71] The Gorham route is not considered a

precursor route toward PPVs, as PPX is formed. Also, the monomer is not formed via basic elimination of the premonomer, but rather via fast pyrolysis. Hence, the Gorham route is not mentioned in Figure 1. However, the Gorham mechanism bears some mechanistic similarity: after pyrolysis of p-xylenes, a chain type polymerization of p-xylylenes takes place. In said work, strong indications for the formation of the dimer diradical are reported and a small difference in dimerization reactivity between p-xylylene and 2,6-dimethyl-p-xylylene is briefly mentioned. However, because the work is not focusing on the kinetics, no tangible, quantitative data about the structure effect on the initiation reaction is reported.

Everything introduced thus far is well-known but has not been modeled. In this kinetic modeling study, the previously described structure effects on the various reaction steps (Figure 2) have been incorporated: the structure-reactivity relation for the propagation reaction for the kinetic model is adopted from Cho et al.[68,69] and structure-reactivity relations for the 1,6-elimination and conjugate nucleophilic addition are determined from reported[67] kinetic data for the sulfinyl route. For the unknown structure effect on the initiation reaction, it is assumed that the presence of EDGs decelerates the initiation more than the propagation: the Hammett reaction constant for initiation is larger than the one for propagation (Figure 2). This is in accordance with the kinetic model for the dithiocarbamate precursor route presented in Chapter 4. It will be demonstrated that these four structure-reactivity relations allow to computer-simulate the observed[66] trends in the sulfinyl precursor route: PPVs with EWGs possess low chain lengths and PPVs with EDGs possess high chain lengths. The structure-reactivity relations determined in this work are then used to simulate the sulfinyl precursor synthesis of PPV based copolymers.

3.2. Kinetic model

Recently, Van Steenberge et al. developed[72] a kinetic Monte Carlo model to describe the reactions of the sulfinyl precursor route, in which substituents on the aromatic moiety are absent as shown in Figures 1 and 2. In this work, the same model is used for substituted premonomers, but the rate coefficients are different. Rate coefficients are based on UV-vis data reported[67] for the 1,6-elimination and conjugate nucleophilic addition of **1**, **2** and **4** and **9-13**. From these values, a Hammett[73] relation (see Appendix G) is constructed. The kinetics of the 1,6-elimination and conjugate nucleophilic addition of the remaining premonomers with substituents on the aromatic moiety, namely **3** and **5-8**, have been calculated from the Hammett relation. The propagation kinetics of all premonomers with substituents on the

aromatic moiety, namely **1**-**9**, have been calculated from Hammett relations in agreement with the findings of Cho et al.[68,69] for the Wessling route. The propagation rate coefficients of the remaining premonomers **10**-**13** are assumed to be equal to the reported value.[72] For the initiation kinetics of the premonomers **1**-**9**, the Hammett relation is used on empiric basis. The initiation rate coefficients of the premonomers **10**-**13** are assumed to be equal to the reported values.[72] The reference rate coefficients for the Hammett relations are reported[72] and used here for **1**. The rate coefficients used in the simulations are presented in Appendix H (Table H1) together with a detailed description of how these rate coefficients are obtained.

3.3. Results and discussion

First, the effect of the premonomer structure on the 1,6-elimination and conjugate nucleophilic addition in conditions for the monomer formation is demonstrated to be in good agreement with reported[67] UV-vis data for **1-2**, **4** and **9-13** and the effect of the leaving group, polarizer, aromatic moiety, EDGs and EWGs on the 1,6-elimination and conjugate nucleophilic addition is discussed in diluted (i.e. no polymerization) conditions. Next, the effect of the leaving group, polarizer, aromatic moiety, EDGs and EWGs on the polymerization is discussed. In particular, the Hammett relations describing the effect of EDGs and EWGs explain experimentally observed trends.[66] Finally, these Hammett relations are used to describe copolymerizations of premonomers with different substituents on the aromatic moiety.

3.3.1. Effect of premonomer structure on the monomer formation

Figure 6 shows a parity plot of the times of maximum absorbance, t_{max}, for **1-2**, **4** and **9-13**. Reaction conditions and experimental t_{max} are taken from (67). Simulation and experimental data agree using the rate coefficients in Appendix H.

Figures 7, 8 and 9 show the simulated yields of premonomer HML, monomer M and ether byproduct $\mathbf{P_1}$ for **1-13**. The simulated times of maximum monomer yield of **1-2**, **4** and **9-13** are equal to the simulated t_{max} values in Figure 6. No UV-vis data has been reported for **3** and **5-8**, but the corresponding rate coefficients for 1,6-elimination and conjugate nucleophilic addition obey Hammett relations constructed from the known rate coefficients for **1-2**, **4** and **9**, as explained in Appendix H.

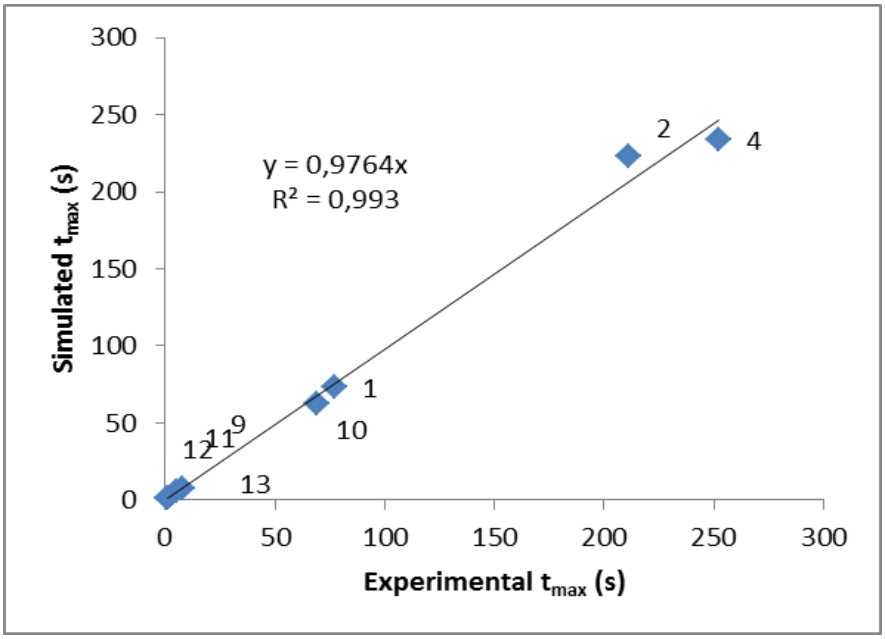

Figure 6: Parity plot of the t_{max} of premonomers 1-2, 4 and 9-13; Reaction conditions[67]: $[HML]_0 = 10^{-4}$ mol L^{-1}, $[RO^-]_0 = 25\ 10^{-3}$ mol L^{-1}, 298 K, solvent sBuOH. Experimental data taken from (67)

Figure 7 shows that the 1,6-elimination retards if EDGs ($\sigma < 0$) are present on the aromatic moiety because the transition state is negatively charged ($\rho_{E2} > 0$, Figure 2). Also, the peak monomer yield shifts right and downward for an increasing electron donating effect of the substituents on the aromatic moiety. Finally, the byproduct is formed slower if EDGs are present.

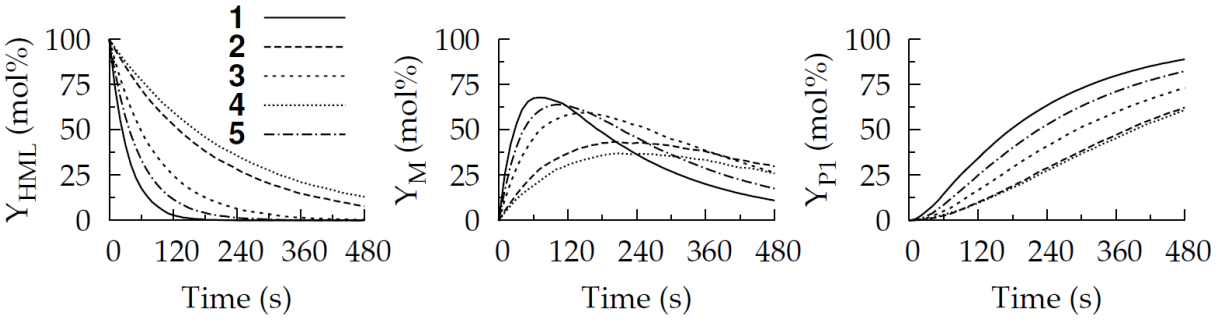

Figure 7: Effect of electron donating groups on the (pre)monomer and byproduct yield as a function of time; Reaction conditions: $[HML]_0 = 10^{-4}$ mol L^{-1}, $[RO^-]_0 = 25\ 10^{-3}$ mol L^{-1}, 298 K, solvent sBuOH. P = SOR, L = Cl, Ar = Phenylene

In contrast to Figure 7, Figure 8 shows that the 1,6-elimination accelerates if EWGs ($\sigma > 0$) are present on the aromatic moiety because the transition state is negatively charged ($\rho_{E2} > 0$, Figure 2). The peak monomer yield shifts left and upward for an increasing electron withdrawing effect of the substituents. Also, byproduct is formed faster if EWGs are present. Note that for premonomers **8** and **9**, which possesses highly electron withdrawing groups such as chlorine and bromine, less than 100% byproduct yield is simulated. The remainder is polymer product, which is related to the high initiation rate coefficients of these *p*-quinodimethanes, as explained in Appendix H and in the remainder of this chapter. The other premonomers, whose *p*-quinodimethanes are less reactive toward dimerization, yield exclusively the byproduct under diluted conditions. Because no indication of polymerization for **9** has been reported[67] under diluted conditions, this simulation result may indicate that the Hammett reaction constant for the initiation reaction, ρ_{ini} (Appendix H), is slightly overestimated.

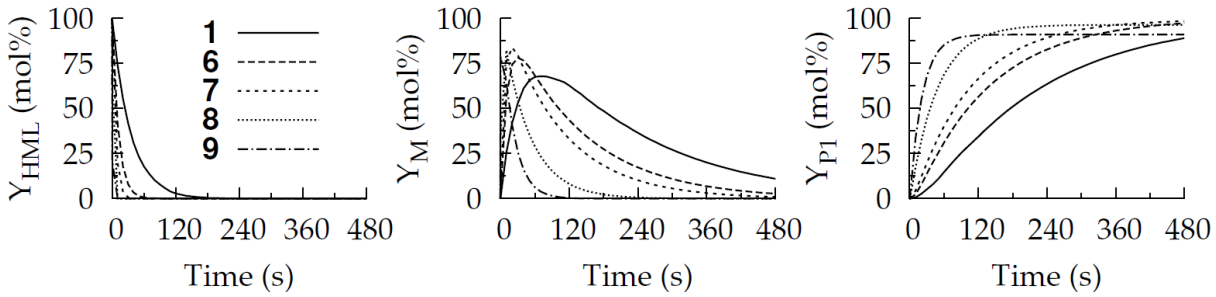

Figure 8: Effect of electron withdrawing groups on the (pre)monomer and byproduct yield as a function of time; Reaction conditions: $[HML]_0 = 10^{-4}$ mol L^{-1}, $[RO^-]_0 = 25\ 10^{-3}$ mol L^{-1}, 298 K, solvent sBuOH. P = SOR, L = Cl, Ar = Phenylene

Figure 9 (top row) shows that the leaving group influences the 1,6-elimination rate very little. This is in accordance with reported[67] data in which the leaving group effect on the 1,6-elimination is studied. It is found[67] that $k_{E2,Br}/k_{E2,Cl}$ is greater than unity in the solvent sBuOH and an E2 mechanism for the 1,6-elimination is proposed. The leaving group effect in the sulfinyl route was also studied[74] in the solvent dichloromethane/N-monomethylformamide (DCM:MMF 4:6), in which $k_{E2,Br}/k_{E2,Cl}$ was smaller than unity. The explanation offered is that Cl is stabilizing the negative charge of the intermediate carbanion better than Br and hence an E1cb(irr) mechanism is proposed. It is unclear whether the change in mechanism can be attributed in experimental error or the change in solvent. Changing the aromatic moiety to

pyridine (Figure 9, center row) leads to faster 1,6-elimination rates, with the monomer concentration peak shifting left and upward, similar to the effect of EWGs (Figure 8). In contrast to the leaving group effect, the polarizer has a large effect on the 1,6-elimination reactivity (Figure 9, bottom row). However, using stronger polarizers also leads to a much faster byproduct formation.

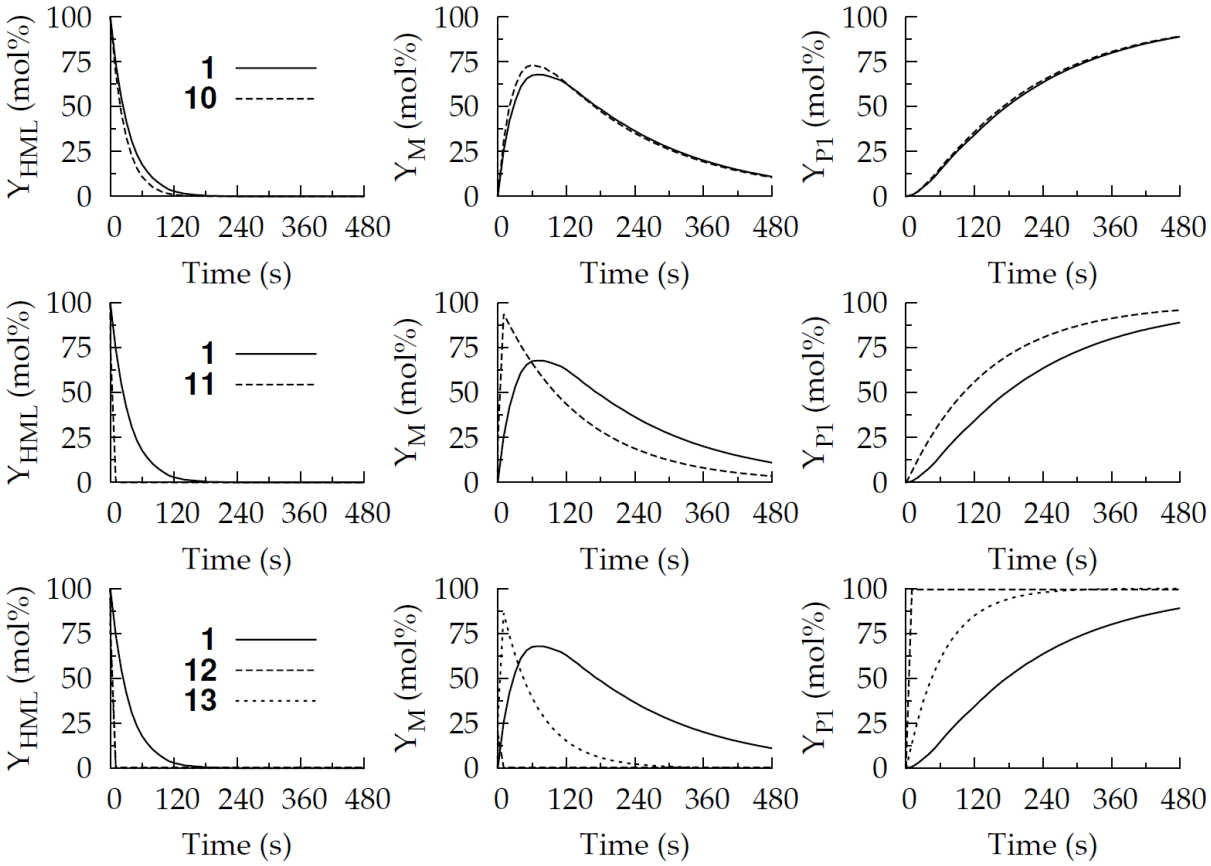

Figure 9: Effect of leaving group (top row), aromatic moiety (center row) and polarizer (bottom row) on the (pre)monomer and byproduct yield as a function of time; Reaction conditions: $[HML]_0 = 10^{-4}$ mol L^{-1}, $[RO^-]_0 = 25\ 10^{-3}$ mol L^{-1}, 298 K, solvent sBuOH; X = Y = H

It can be concluded that a wide range exists in reactivity of the (pre)monomers. The premonomer is consumed within seconds or minutes, depending on its molecular structure. The corresponding peak monomer yields range from under 50 mol% to as high as 100 mol%. Due to the bimolecular nature of the dimerization reaction, this concentration effect implies that the fastest initiation reaction (**9**) is roughly 4 times faster than the slowest initiation (**4**), provided that changes in initiation rate coefficients are not considered. In diluted conditions,

this effect remains rather unimportant as demonstrated in Figures 7, 8 and 9, but in polymerization conditions, this effect allows to rationalize, at least partly, the dependency of the chain length on the electronic nature of the substituents on the aromatic moiety.

3.3.2. Effect of premonomer structure on the polymerization

Figure 10 shows increasing chain length and byproduct yields for increasing electron donating character of the substituents on the aromatic moiety, irrespective of the initial base concentration used. In contrast, polymer yield and initiator defect content decrease for increasing electron donating character of the substituents. The increase in chain length for increasing electron donating character of the substituents is in line with reported[66] trends. Number averaged chain lengths range from 700 to 2800 repeating units in the range of 0.5 to 2.5 equivalents base. Extreme values of the polymer yield, the average chain length and initiator defect are obtained when $[RO^-]_0/[HML]_0 = 1$.

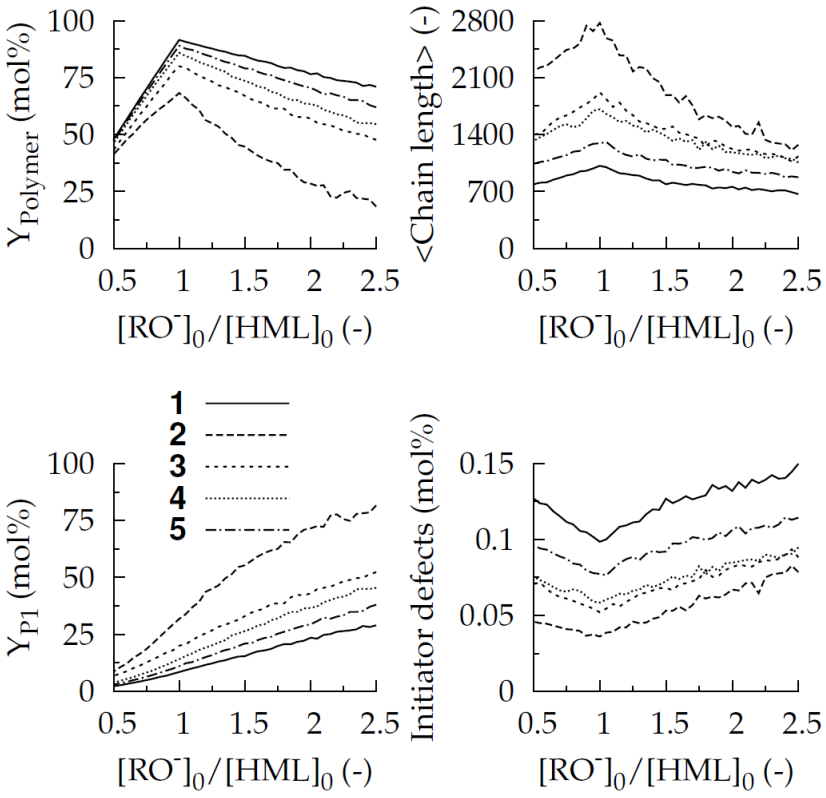

Figure 10: Effect of electron donating groups on the yields and polymer properties as a function of time; Reaction conditions: $[HML]_0 = 10^{-1}$ mol L^{-1}, 308 K, solvent sBuOH. P = SOR, L = Cl, Ar = Phenylene

Figure 11 shows decreasing chain length and byproduct yields for increasing electron withdrawing character of the substituents, irrespective of the initial base concentration used. In contrast, polymer yield and initiator defect content increase for increasing electron withdrawing character of the substituents on the aromatic moiety. The increase in polymer yield is in agreement with a theoretical study recommending EWGs such as CN groups to obtain higher yields.[75] The decrease in chain length for increasing electron withdrawing character of the substituents is in line with reported[66] trends. Number averaged chain lengths range from 50 to 1000 repeating units in the range of 0.5 to 2.5 equivalents base. Extreme values of the polymer yield, the average chain length and initiator defect are obtained when $[RO^-]_0/[HML]_0 = 1$.

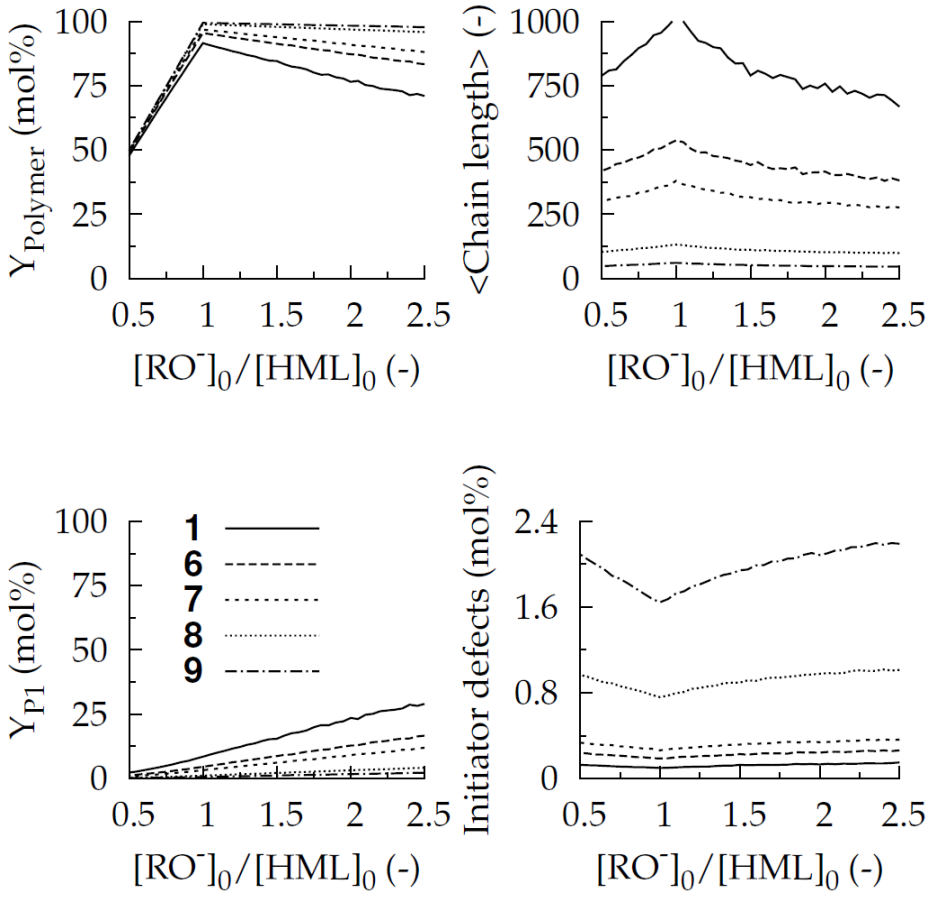

Figure 11: Effect of electron withdrawing groups on the yields and polymer properties as a function of time; Reaction conditions: $[HML]_0 = 10^{-1}$ mol L^{-1}, 308 K, solvent sBuOH. P = SOR, L = Cl, Ar = Phenylene

The chain length dependency on the electronic nature of the substituents, seen in Figures 10 and 11, can be explained as follows. It has already been demonstrated that the presence of

EDGs results in lower peak monomer concentrations and that slower dimerization (initiation) rates can be expected, all other factors remaining equal. Because the total monomer available for polymerization remains approximately constant but fewer chains are initiated, the chain length increases. In addition, a second effect causes the chain length to increase further. The rate coefficients for initiation and propagation vary over 5 orders of magnitude, while the propagation rate coefficients vary over only 1 order of magnitude when changing the electronic character of the substituents on the aromatic moiety (see Appendix H). This can be understood better when considering the initiation rates of **4** and **9**, displaying resp. the lowest and highest peak monomer yield in diluted conditions. These rates are shown in Figure 12 under typical polymerization conditions. It can be seen that **9** initiates faster and more than **4** does.

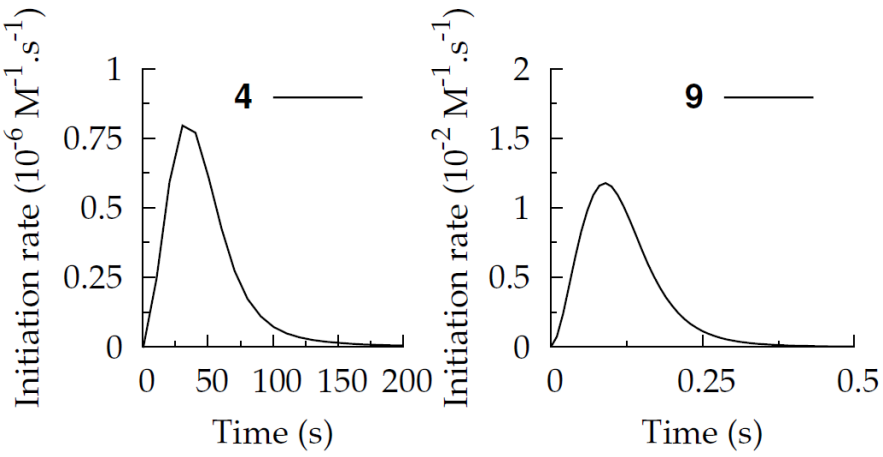

Figure 12: Initiation rates of 4 and 9 as a function of time; Reaction conditions: $[HML]_0 = [RO^-]_0 = 10^{-1}$ mol L^{-1}, 308 K, solvent sBuOH; P = SOR, L = Cl, Ar = Phenylene

The structure-reactivity relations and corresponding Hammett reaction constants (Figure 2) lead to the counter-intuitive conclusion that longer chains are achieved when the *p*-quinodimethane is formed slower, because they initiate slower yet approximately the same monomer amount is available for polymerization. Such behavior contrasts with free radical vinyl polymerizations, in which the opposite is known, i.e. higher monomer concentrations lead to higher chain lengths. This conclusion is important for the behavior of copolymerizations, as will be illustrated later.

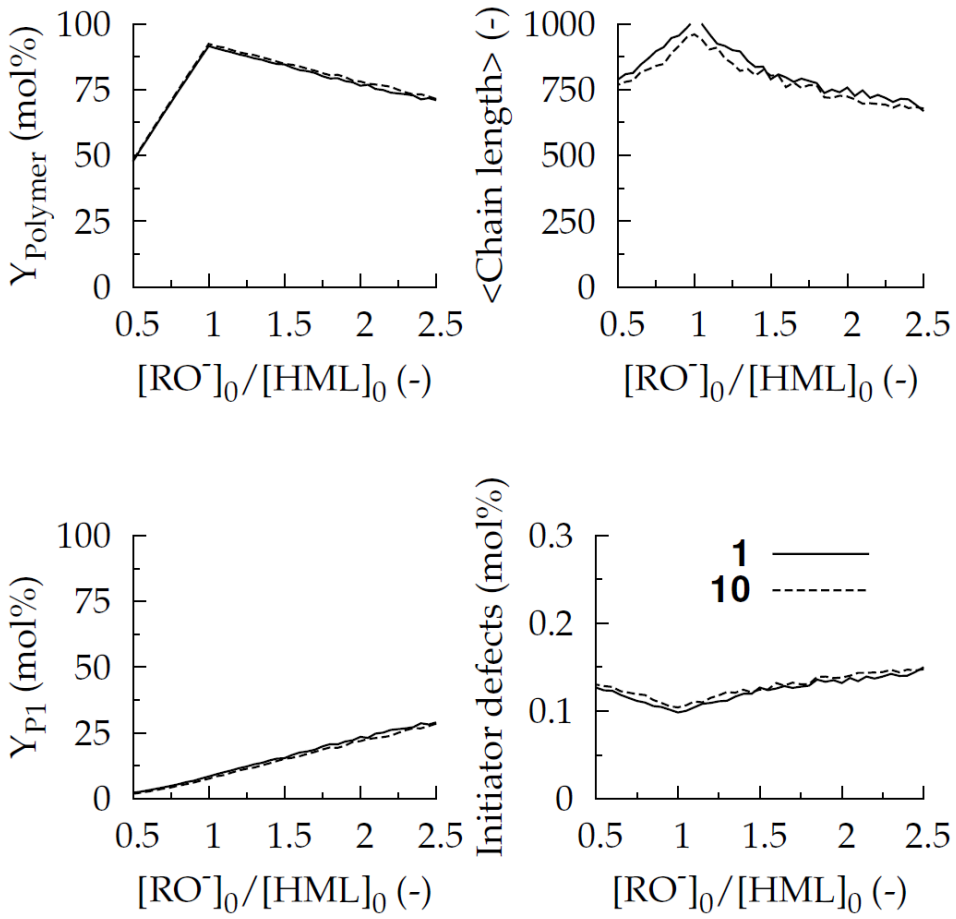

Figure 13: Effect of the leaving group on the yields and polymer properties as a function of $[HML]_0/[RO^-]_0$; Reaction conditions: $[HML]_0 = 10^{-1}$ mol L^{-1}, 308 K, solvent sBuOH; P = SOR, Ar = Phenylene, X = Y = H

Figure 13 shows that the effect of the leaving group can be neglected. As mentioned in the introduction, the 1,6-elimination is proposed[67] to follow an E2 type mechanism with a carbanion-like transition state, for which the C-X bond is much less elongated than the C-H bond. In such case, the identity of the halide does not play a major role.

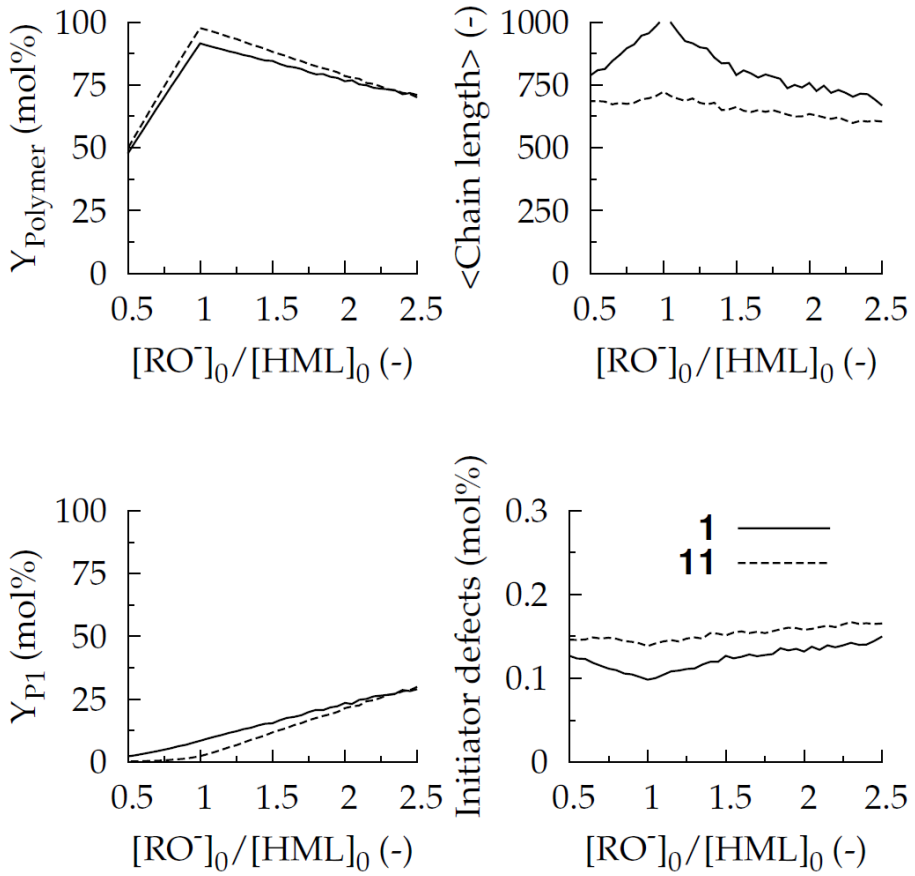

Figure 14: Effect of the aromatic moiety on the yields and polymer properties as a function of $[HML]_0/[RO^-]_0$; Reaction conditions: $[HML]_0 = 10^{-1}$ mol L^{-1}, 308 K, solvent sBuOH; P = SOR, L = Cl, X = Y = H

Figure 14 shows the effect of the aromatic moiety, exchanging the phenylene by a pyridine. As in diluted conditions, the effect of the aromatic moiety is similar to the presence of an EWG on the aromatic moiety. However, it must be noted that the effect of the aromatic moiety has not been accounted for on the polymerization reactions, as explained in Appendix H. Hence, the observed chain length difference (700 for PPyV as opposed to 1000 for PPV) stems from a difference in monomer concentration profiles, not from a difference in initiation/propagation rate coefficients. As mentioned in the introduction, PPyVs are important candidates for n-type materials. Synthesized via the sulfinyl route, the photoluminescence efficiency of the PPyV was shown to be as high as 14%.[76]

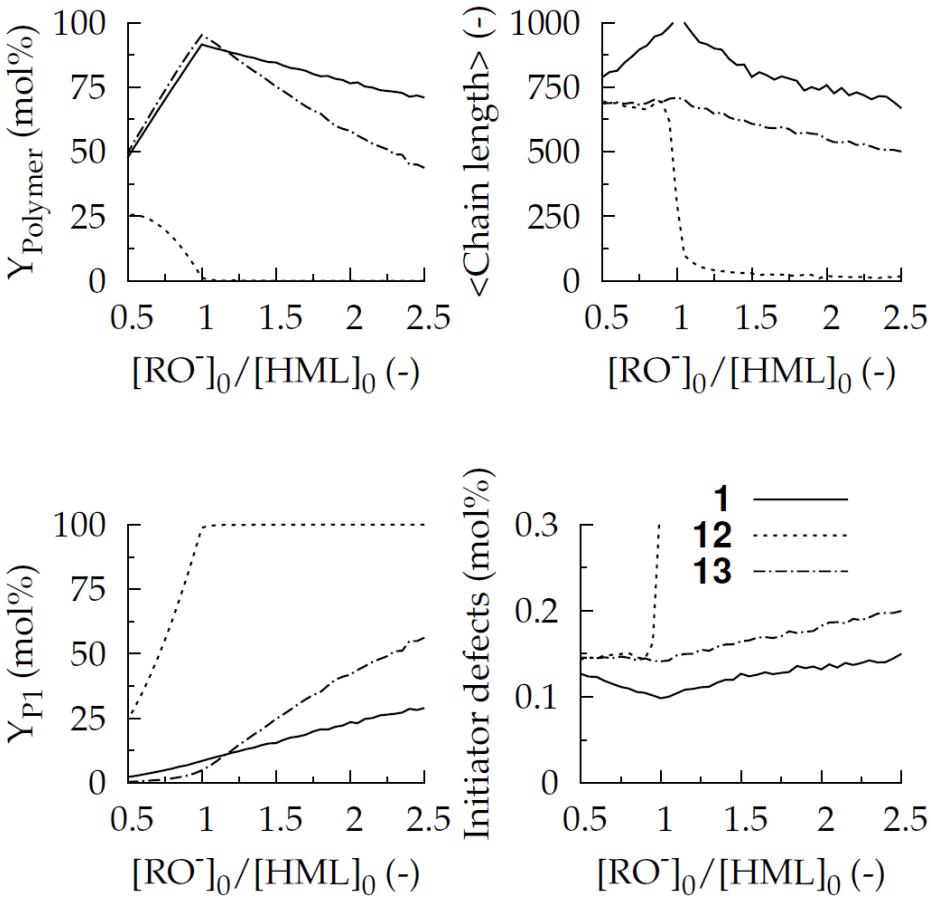

Figure 15: Effect of the polarizer on the yields and polymer properties as a function of $[HML]_0/[RO^-]_0$; Reaction conditions: $[HML]_0 = 10^{-1}$ mol L^{-1}, 308 K, solvent sBuOH; L = Cl, Ar = Phenylene, X = Y = H

Figure 15 shows the effect of the polarizer. If the sulfinyl polarizer is replaced by a sulfonyl polarizer (**13**), it can be seen that polymer yield decreases and byproduct yield increases if the base is in excess. This is explained by the high reactivity toward nucleophilic addition and the necessity of a base molecule to form the byproduct. Lower chain lengths and higher initiation defect content are seen irrespective of the base concentration. This is explained by the faster 1,6-elimination of **13**, leading to high monomer concentration and initiation rates. Possible reactivity differences for the initiation/propagation are not accounted for, as explained in Appendix H. If an additional chloride is present in the polarizer position (**12**), nucleophilic addition is accelerated even more, leading to oligomers in very low yield as soon as $[HML]_0/[RO^-]_0$ exceeds unity. The importance of being able to vary the polarizer has been outlined in a number of reports synthesizing statistical copolymers of premonomers differing

in polarizer: the difference in elimination behavior of the polarizer allowed to tune the conjugation length.[77-80]

3.3.3. Supporting maps for the effect of EWGs and EDGs on the polymerization

Figure 16 shows the polymer yield, byproduct yield, chain length and initiator defect contents as a function of the Hammett substituent constant, for a range containing most substituents of interest (e.g. $\sigma(CF_3,CF_3) = \sigma_m(CF_3) + \sigma_o(CF_3) = 0.43 + 0.54*0.75 = 0.83$ and $\sigma(CN,CN) = \sigma_m(CN) + \sigma_o(CN) = 0.56 + 0.75*0.66 = 1.06$). In Figure 16, the rate coefficients k_{E2} and k_{NA} are not taken from Table H1 in Appendix H, but are calculated from Hammett relations as explained in Appendix H:

$$\log\left(\frac{k_{E2,X}}{k_{E2,H}}\right) = \rho_{E2}\sigma_X$$

$$\log\left(\frac{k_{NA,X}}{k_{NA,H}}\right) = \rho_{NA}\sigma_X$$

This is explained in more detail in the section about copolymerizations. It can be seen from Figure 16 that polymer yield and initiation defects increase with the electron withdrawing effect of the substituent on the aromatic moiety. Also, byproduct yield and chain length decrease with the electronic withdrawing effect. Note that for $\sigma = 0.4$, an average chain length of 100 is obtained and an initiator defect content of 1 mol%: the average chain contains 100 units and 1 initiator defect. It can be concluded that, due to the formation of the byproduct, a large ρ_{ini} is necessary to obtain high polymer yield lengths. However, the latter also implies a low chain length. To obtain simultaneously high polymer yield and chain length, a low ρ_{NA} value is necessary to suppress byproduct formation in the region of slow initiation kinetics. However, as it appears, the found ρ_{NA} value is too large to achieve both high yield and chain length.

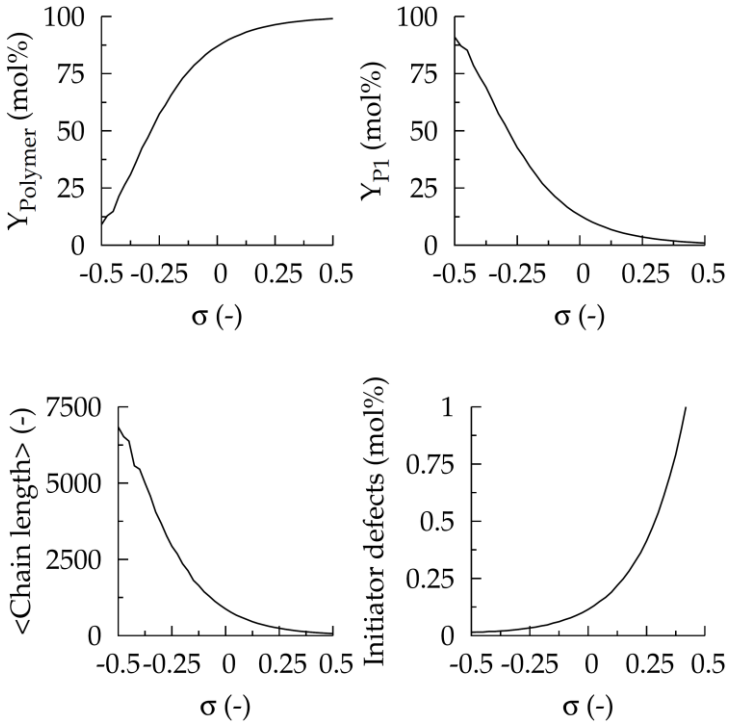

Figure 16: Yields and polymer properties as a function of the Hammett substituent constant; Reaction conditions: $[HML]_0 = 10^{-1}$ mol L^{-1},$[RO^-]_0 = 0.13$ mol L^{-1}, 308 K, solvent sBuOH; P = SOR, L = Cl, Ar = Phenylene

Figures 17 and 18 show the same as Figure 16 but as a function of the initial base concentration. It can be seen that the properties and yield reach extreme values for $[RO^-]_0/[HML]_0 = 1$, as before. The premonomer yield varies linearly with the base concentration if $[RO^-]_0/[HML]_0 < 1$, because the base is the limiting reactant. As in Figure 16, it can be seen that no region exists where both chain length and polymer yield are high. The byproduct formation can be avoided by limiting the base concentration and using EWGs, as these increase the polymerization rate. Polymer yield can be increased by using equimolar amounts of base and premonomer, and by using EWGs. However, with increasingly electron withdrawing character of the substituents on the aromatic moiety, chain length decreases. The chain length is highest for equimolar base and premonomer amounts.

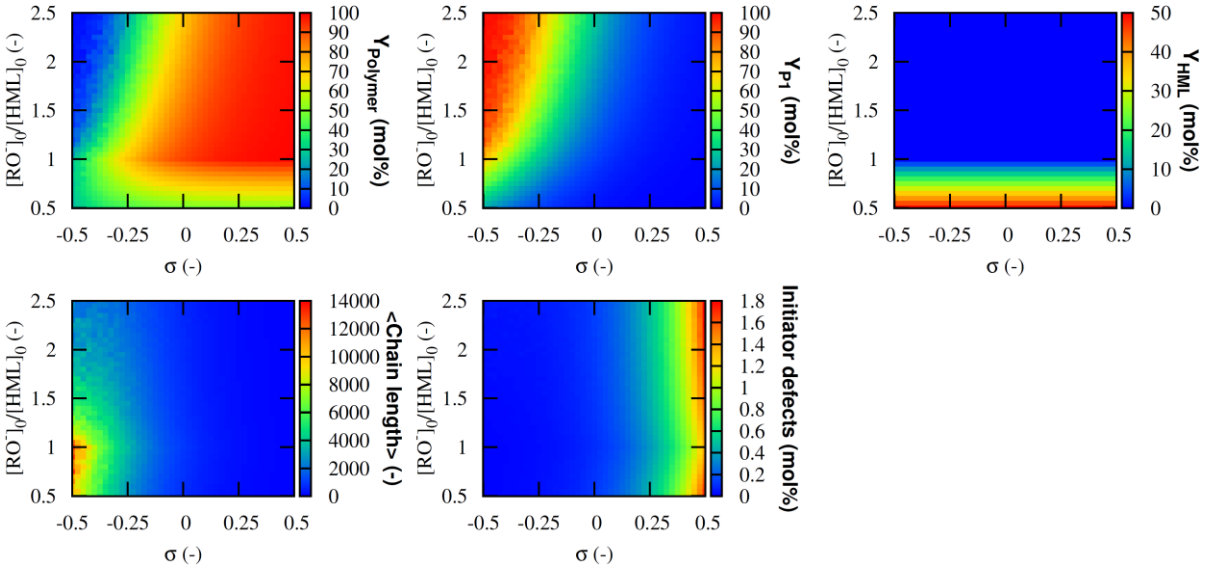

Figure 17: Yields and polymer properties as a function of the Hammett substituent constant and $[RO^-]_0/[HML]_0$; Reaction conditions: $[HML]_0 = 10^{-1}$ mol L^{-1}, 308 K, solvent sBuOH; P = SOR, L = Cl, Ar = Phenylene

Concluding, the synthetic limitations of the sulfinyl route toward homopolymers outlined in this section do not strongly depend on the values of the rate coefficients nor on the initial concentrations. They are inherent to the reaction scheme (Figure 2), which is well-accepted, and the four Hammett reaction constants ρ, which are all literature[67-69] based except for the initiation reaction constant. When choosing $\rho_{ini} > \rho_p$, short chain lengths are predicted for electron-poor PPV and long chain lengths for electron-rich PPV, as observed experimentally.[66] The characteristics of homopolymerizations illustrated in this section are extended to copolymerizations in the next paragraph. The rate coefficients for the homoreaction steps in the copolymerizations are taken from their respective homopolymerizations, while the cross-reaction steps in the copolymerizations are assigned values calculated from the geometric mean of their respective homopolymerizations.

3.3.4. Effect of premonomer structure on the copolymerization

Copolymerizations of premonomers **3** and **9** with **1-9** are considered. $[RO^-]_0/([HML,A]_0+[HML,B]_0)$ is equal to unity. The x-axis shows the initial premonomer composition, where A is the first premonomer given in the legend, either **3** or **9**, and B the second premonomer given in the legend. The y-axis is either a yield, chain length, initiator defect content or the conjugated triad fraction of the AAA+BBB type. The conjugated triad

fraction is used as an indicator of the random character (a value of 25%) or block character (a value of 100%) of the copolymer.

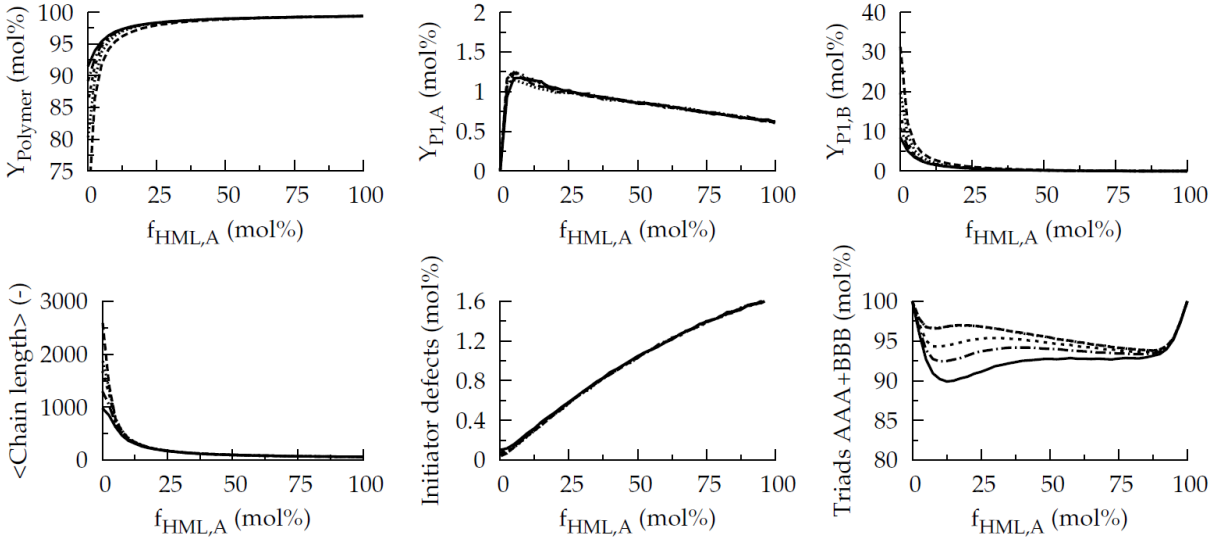

Figure 18: Effect of initial premonomer composition on the yields and properties for the copolymerizations of 9 (possessing Cl groups) with 1-5 (possessing EDGs) (see Figures 3, 4 and 5); Reaction conditions: $[RO^-]_0/[HML]_0$=1, 308 K; $f_{HML,A}$ is defined as $[HML,A]_0/([HML,A]_0+[HML,B]_0)$; HML,A = 9 and HML,B: ——— : 9 with 1; - - - - - : 9 with 2; . . . . . : 9 with 3; ····· : 9 with 4; —·—·— : 9 with 5

Figure 18 shows that the copolymerization of **9** with a premonomer possessing EDGs (such as **1**-**5**) leads to lower polymer yields (and higher chain lengths) if the initial fraction of premonomer **9** decreases. The yield decrease (and the chain length increase) is more pronounced if premonomer B possesses more electron donating groups. The byproduct formation corresponding to **9** is insensitive to the molecular structure of premonomer B, while both byproduct yields depend on the initial premonomer composition. Initiator defects are insensitive to the structure of premonomer B, while a lower initial fraction of **9** leads to a decrease in defects. This indicates that **9** is responsible for chain initiation. The results show that **9** is polymerizing first, before any byproduct formation can occur. In a next phase of the polymerization, premonomer B starts polymerizing as well. Due to the slower polymerization of premonomer B, byproduct formation may be as high as 40 mol%, compared to 1.5 mol% at most for the byproduct of **9**. This block-type copolymerization is also reflected in the

conjugated triad fraction being always higher than 90%, again confirming the large reactivity difference between **9** (electron withdrawing groups) and premonomer B (electron donating groups).

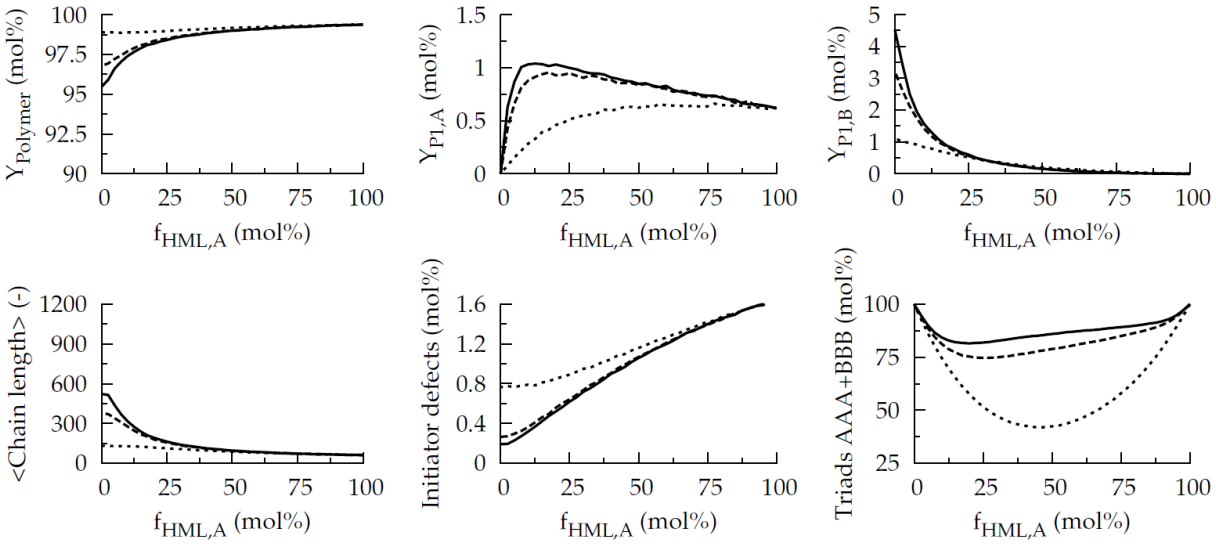

Figure 19: Effect of initial premonomer composition on the yields and properties for the copolymerizations of 9 (possessing Cl groups) with 6-8 (possessing EWGs) (see Figures 3, 4 and 5); Reaction conditions: $[RO^-]_0/[HML]_0$=1, 308 K; $f_{HML,A}$ is defined as $[HML,A]_0/([HML,A]_0+[HML,B]_0)$; HML,A = 9 and HML,B: ——— : 9 with 6; - - - - - - : 9 with 7; . . . . . : 9 with 8

Figure 19 shows that a copolymerization of **9** with a premonomer possessing EWGs (such as **6**-**8**) leads to lower polymer yields (and higher chain lengths) with the decrease of the initial fraction of premonomer **9**. This yield decrease (and chain length increase) is more pronounced if premonomer B possesses less electron withdrawing groups. Contrary to Figure 18, in Figure 19 both byproduct yields depend on the molecular structure of premonomer B, although both yields are very low (lower than 5 mol%), indicating a fast polymerization without much byproduct formation. Whereas in Figure 18 low initiation defect content is obtained for low initial fractions of **9**, the initiation defect content for low initial fractions of **9** is rather high in Figure 19. This is explained by the faster dimerization of premonomer B when it possesses EWGs instead of EDGs (as in Figure 18). The conjugated triad fraction shows a range of approximately random to block-like copolymers, depending on the molecular structure of **9** and premonomer B. For very similar electron withdrawing effects (e.g. B = **8**), both monomers will incorporate at the same rate and an approximately random copolymer results.

For different electronic effects of the EWGs (e.g. B = **6**), a block-like copolymer results, similar to Figure 18 in which a premonomers with EWGs is polymerized with a premonomer with EDGs.

Figures 18 and 19 allow to conclude that, when the initial premonomer fraction of **9** exceeds 25 mol%, yields and defects are not affected appreciably by the presence of the second premonomer B, irrespective of its substituents. This is caused by the fast initiation and propagation of premonomer **9** compared to the slower kinetics of the second premonomer B, which possesses EDGs or less EWGs than Cl, as illustrated in the section on homopolymerization. When the initial premonomer fraction of **9** does not exceed 25 mol%, a large impact on the chain length of electron-rich PPVs (based on premonomer such as **2** and **3**) is seen, as can be expected from the reactivity difference in the dimerization reactions of premonomers with EDGs and EWGs. The copolymerizations of **9** are thus dominated by **9** alone over a large initial premonomer composition range. Adding small amounts of **9** to synthesize shorter chains of PPVs based on premonomers **1-5** may be interesting, because it is known that increasing the chain length attenuates the substituent effect on the supramolecular level, one example being a reduction of the bathochromic shift (i.e. the shift in the emission spectrum toward longer wavelengths). At the same time, defect content will increase, which is known to be advantageous for photoluminescence efficiency. The block character of the copolymer is not affected appreciably as only minor amounts of **9** are added, hence the copolymer contains large blocks of **1**-**5**, with infrequent incorporations of **9**. An entirely different picture is seen in Figures 20 and 21, which shows the copolymerizations of **3** with premonomers possessing EDGs and EWGs respectively.

Figure 20 shows a much larger effect of the presence of premonomer B on the copolymer yields and properties, due to **3** possessing EDGs. Consequently (and contrary to Figures 18 and 19) premonomer **3** initiates a lot slower and thus does not dominate the kinetics over a large composition range like **9** does, because **9** possesses EWGs. Instead, the copolymerizations of **3** are slower and byproduct yields are much higher than in Figures 18 and 19. Figure 20 shows that polymer yields increase when premonomer B possesses the electron donating groups **1** and **5** and, conversely, that the polymer yield decreases when premonomer B possesses the electron donating groups **2** and **4**. The effect becomes stronger as more premonomer B is added, because then the homopolymer limit of B is approached more. As before, the effects seen on the chain length are reversed compared with the polymer yield, the longest chains being obtained for the homopolymer of **2**. This is explained by the

fact that higher polymer yields originate from faster initiation rates, which automatically imply shorter chain lengths. Note that the defect content varies almost linearly over the entire composition range, which may allow easy tuning of the electro- and photoluminescence (this is explained in the next paragraph). Contrary to Figure 19, the conjugated triad fraction only varies between 25% (purely random copolymer) and 30% (random-like).

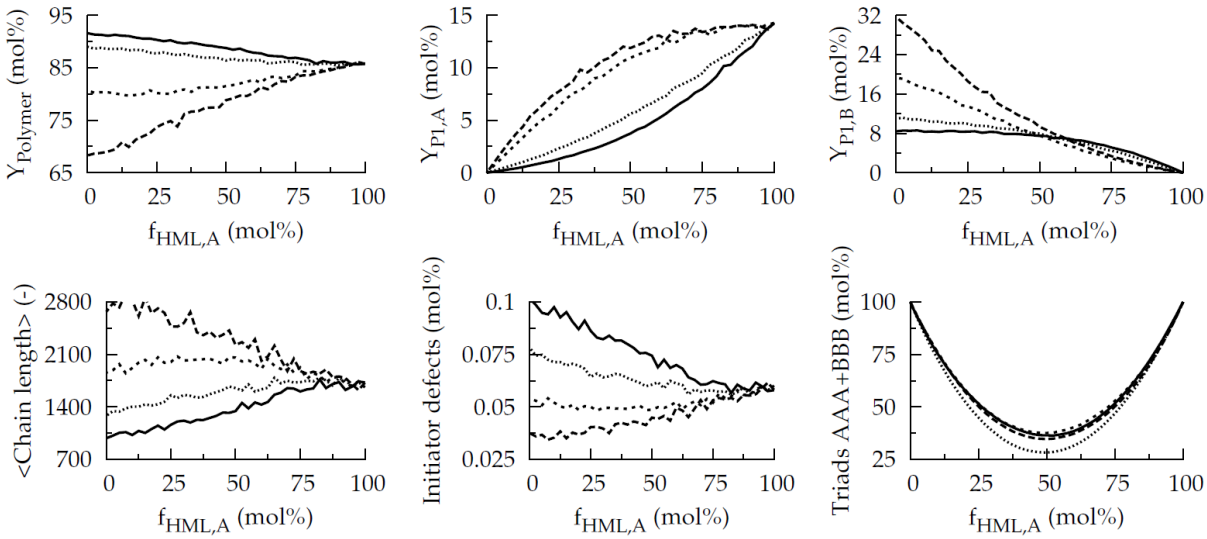

Figure 20: Effect of initial premonomer composition on the yields and properties for the copolymerizations of 3 (possessing methoxy and 3,7-dimethyl octyloxy groups) with 1-5 (possessing EDGs) (see Figures 3, 4 and 5); Reaction conditions: $[RO^-]_0/[HML]_0$=1, 308 K; $f_{HML,A}$ is defined as $[HML,A]_0/([HML,A]_0+[HML,B]_0)$; HML,A = 3 and HML,B: ——— : 3 with 1; - - - - - : 3 with 2; . . . . . : 3 with 4; ····· : 3 with 5

Note that the copolymerization of **3** and **4** is simulated in Figure 20. Although these have been treated as pure compounds in the section on monomer formation and homopolymerization, usually a 50:50 mixture of **3** and **4** is polymerized. The resulting copolymer is reported to be regiorandom for the Gilch and sulfinyl route, although it is not clear on which data this is based.[55,56,65] For the dithiocarbamate route, strong indications of regiorandom character have been obtained from ^{1}H NMR.[33] Comparisons of regioregular MDMO-PPVs with regiorandom MDMO-PPVs have been performed using regiorandom PPV purchased from Covion GmbH.[65,57,58] Hence, it is not clear if the MDMO-PPVs starting from a 50:50 initial

premonomer mixture are truly random. The simulation data indicates a conjugated triad fraction of 30% for a 50:50 mixture of **3** and **4**, which is expected for the regiorandom MDMO-PPV. The modeling of these copolymers is important as recently demonstrated.[57,58] MDMO-PPV with a composition of **3**:**4** = 30:70 showed a hole mobility approximately 3.5 times larger than the regiorandom MDMO-PPV, at all measured electric fields.

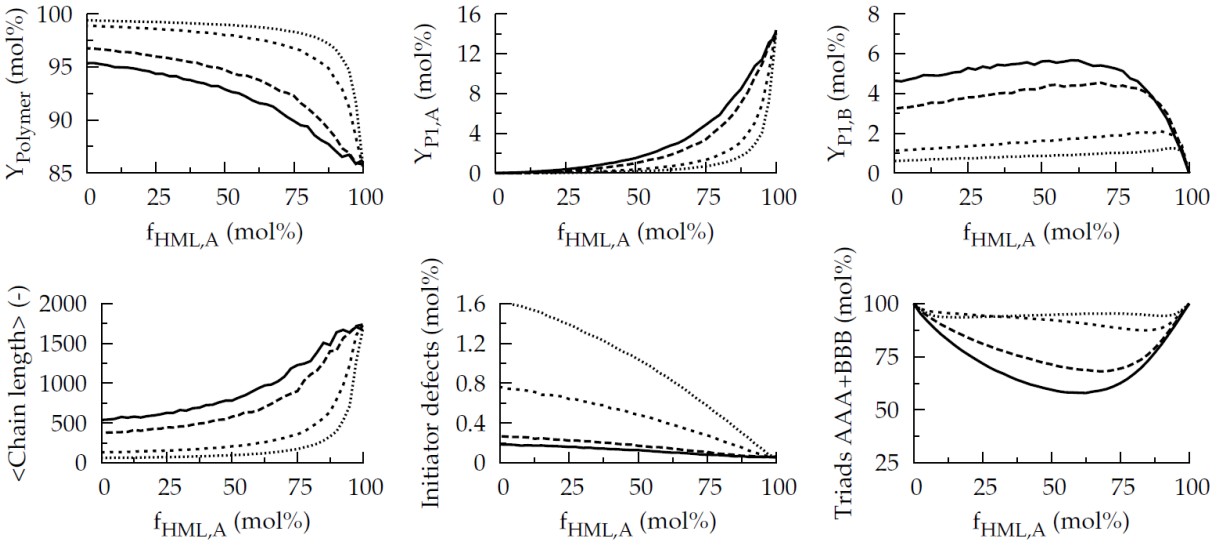

Figure 21: Effect of initial premonomer composition on the yields and properties for the copolymerizations of 3 (possessing methoxy and 3,7-dimethyl octyloxy groups) with 6-9 (possessing EWGs) (see Figures 3, 4 and 5); Reaction conditions: $[RO^-]_0/[HML]_0$=1, 308 K; $f_{HML,A}$ is defined as $[HML,A]_0/([HML,A]_0+[HML,B]_0)$; HML,A = 3 and HML,B: ——— : 3 with 6; - - - - - : 3 with 7; . . . . . : 3 with 8; ····· : 3 with 9

Similar to Figure 20, Figure 21 also shows a large effect of the presence of premonomer B on the copolymer yields and properties, although here premonomer B possesses EWGs. Hence, small initial fractions of the reactive premonomer B are sufficient to achieve large effects on the yields and properties. It follows in particular that low initial fractions of **9**, which possesses Cl groups, combined with a large initial fraction of **3** (which leads to regioregular MDMO-PPV if homopolymerized), allow to strongly increase the yield, but at the cost of a reduced chain length. As in Figure 20, the initiator defect content varies almost linearly over the entire composition range, with the strongest effect being realized when adding **9**.

It can be concluded from Figures 20 and 21 that the effect of the initial premonomer composition is much more dependent on the premonomer structure of the second premonomer B than in Figures 18 and 19, due to the difference in electron withdrawing/donating nature of the substituents of premonomer A (either **3** or **9**). As mentioned before, the broader property region attainable is related to the comparatively slow reaction kinetics of the electron donating premonomer **3**, whereas in Figures 20 and 21, the initiation and propagation kinetics of premonomer **9** are so fast they dominate the global reaction kinetics. Hence, chain length, yield and defects of MDMO-PPV can be varied by adding premonomers with EWGs. In particular **9** is suitable for this purpose due to the large variations in chain length and defect variations for very low addition amounts, retaining largely the MDMO-PPV character of the polymer product, but with variable initiator defect level. Note that the chain length variation is much stronger than demonstrated for the variation of the reaction conditions for the homopolymerizations in the previous section.

By controlling the initiator defect content, which is restricting the conjugation length, the opto-electronic properties of MDMO-PPV can be optimized: by confinement of an exciton in shorter conjugated units, the radiative decay is favored at the expense of the non-radiative decay at quenching sites in the polymer.[81] Hence, when conjugation lengths are shorter, mobility of excitons is reduced and photoluminescence efficiency is increased.[82] Indeed, a linear relationship between photoluminescence efficiency and introduced sulfonyl sp^3 defects was recently demonstrated by the group of Vanderzande for the sulfinyl precursor route,[83] in the range of 5% – 60% photoluminescence efficiency and a range 0 to 0.8 mol% of introduced sulfonyl sp^3 defects. In this kinetic model, the sp^3 defect interrupting the conjugation is not an intentionally introduced sulfonyl defect but rather consists of the inevitable initiator sp^3 defect. As seen in Figures 20 and 21, the sp^3 initiator defect varies between 0 and 1.6 mol%. Because both types sp^3 defects interrupt the conjugation length, it can be expected that a similarly large, linear, effect on the photoluminescence efficiency is present for these MDMO-PPVs with a small number of incorporated units of chlorinated premonomer **9**.

Concluding, there are grounds to believe that small amounts of **9** can increase the photoluminescence efficiency of MDMO-PPV synthesized via the sulfinyl route. The effect of a small amount of **9** (e.g. 1 mol%, to reduce chain length by a factor two and increase defect level by a factor two) on the regioregularity and hence the morphology in films is expected to be very small, as it can be seen that the conjugated triad fraction remains around 99% (i.e. highly block-like). If a large effect on the regioregularity is desired to improve

solubility, it is better to copolymerize **3** with either **1**, **2**, **4** or **5**, as these possess also EDGs and hence will randomly incorporate. This is evidenced in Figure 20 in the steep decline in the conjugated triad fraction at high content of **3** and in the experimental work of Mozer et al.[57,58]

In this paragraph, the effect of the initial premonomer composition on the copolymerizations of **3** and **9** is illustrated. The effect of the initial premonomer composition on the copolymerizations of **1**, **2**, **4**-**8** shows intermediate behavior, simulation data are given in Appendix I.

3.3.5. Effect of the base on the copolymerization

Figure 22 shows the copolymerization of premonomer **3** with **4**, both possessing electron donating groups and leading to MDMO-PPV.

It can be seen that unconverted premonomer is obtained only when the base is the limiting reactant. When the premonomer is the limiting reactant, large yields of byproducts are obtained, which reflect the initial premonomer composition. For base concentrations which are approximately equimolar with respect to the premonomer concentration, polymer yields ranging from 80 mol% to 90 mol% are obtained and number average chain lengths ranging from 1800 to 2800, while these values drop to 30 mol% and 800 when the base is added in too large excess. Initiator defect content is generally low, the highest values being obtained when the chain length is lowest. The conjugated triad fraction of the AAA and BBB types are approximately symmetric due to the similar reactivity of **3** and **4** toward propagation.

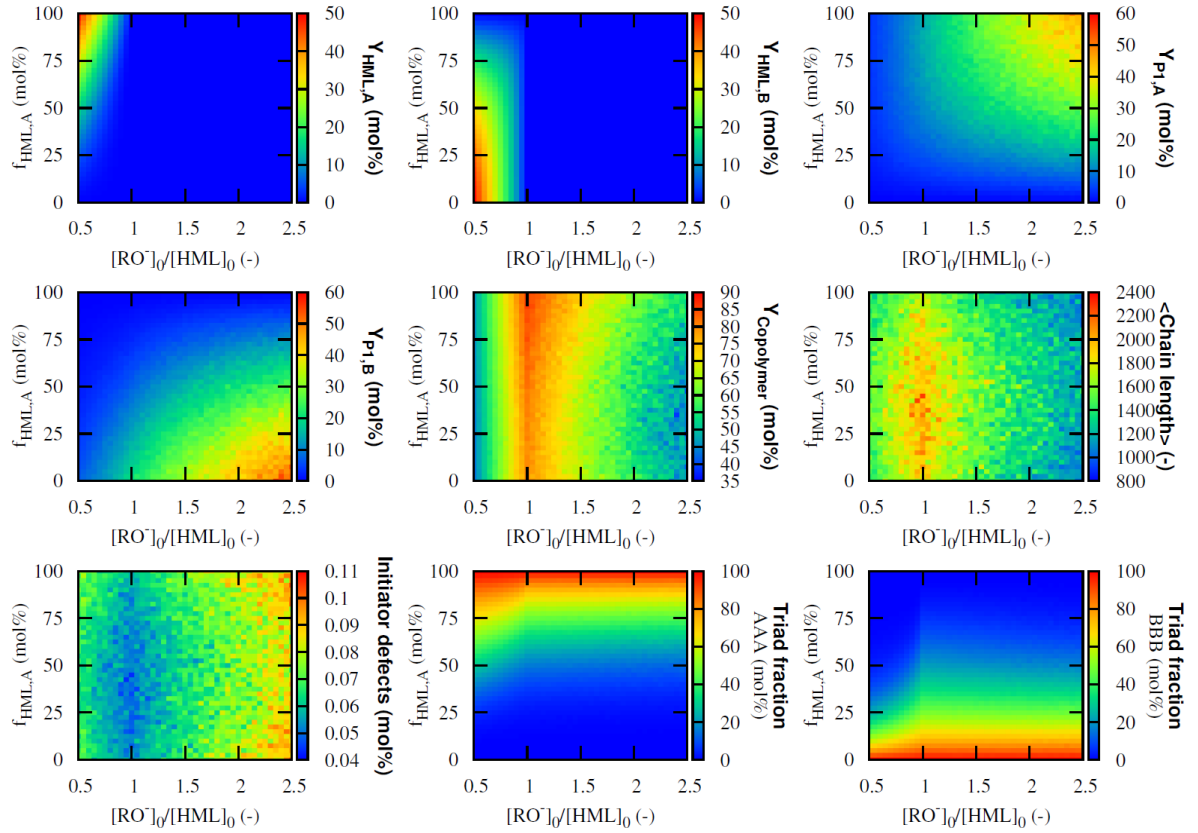

Figure 22: Effect of the base and the initial premonomer composition on the yields and properties for the copolymerization of 3 with 4 (see Figures 3, 4 and 5); Reaction conditions: 308 K; $f_{HML,A}$ is defined as $[HML,A]_0/([HML,A]_0+[HML,B]_0)$

Figure 23 shows the copolymerization of premonomers **3** and **9**, possessing electron donating groups and electron withdrawing groups respectively. In contrast to Figure 22, only very little byproduct is formed originating from **9**: due the electron withdrawing substituent, polymerization reactions of **9** are favored more than the side-reaction of **9**. This is reflected in the copolymer yield, which shows yields higher than 90 mol% over nearly the entire range of reaction conditions: Only when the base is the limiting reactant or when very high initial amounts of **3** are used, low copolymer yields are obtained. Again, this can be explained by the faster initiation and propagation kinetics of **9** compared to **3**. However, in the same region of high polymer yield, chain lengths will be low due to fast radical initiation. Hence, the chain length and the initiator defect content do not strongly depend on the base concentration when a premonomer with EDGs is copolymerized with a premonomer containing EWGs. This contrasts with Figure 22, in which both premonomers possessed EDGs and where the copolymer properties were codetermined by the base concentration and the initial

premonomer composition. In Figure 23, the initial premonomer composition determines strongly the properties. Note also the difference with Figure 22 when comparing the conjugated triad fractions of the AAA and BBB type: these are much higher in Figure 23. This again indicates that **9** is copolymerizing much faster than **3**, yielding block-like copolymers.

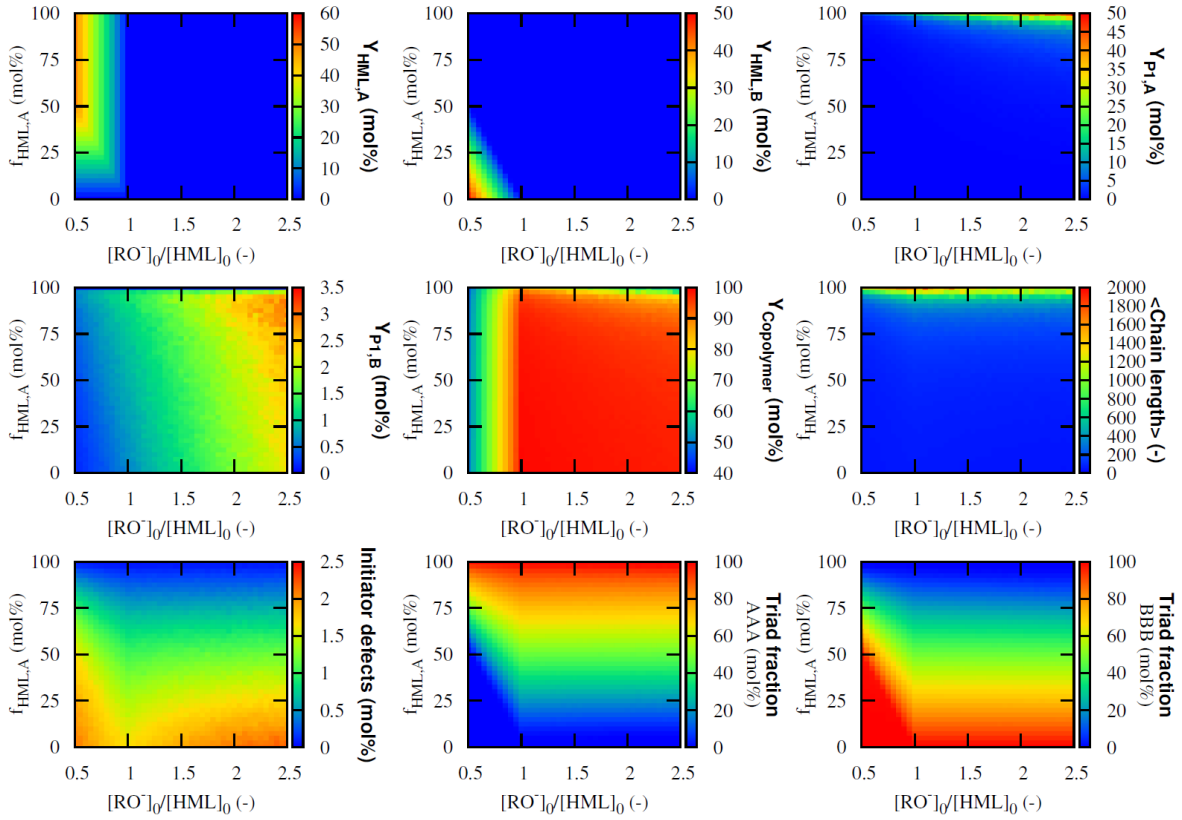

Figure 23: Effect of the base and the initial premonomer composition on the yields and properties for the copolymerizations of 3 with 9 (see Figures 3, 4 and 5); Reaction conditions: 308 K; $f_{HML,A}$ is defined as $[HML,A]_0/([HML,A]_0+[HML,B]_0)$

Figure 24 shows the copolymerization of premonomers **8** and **9**, both possessing electron withdrawing groups. In this case, both byproducts are formed in very low amount, again due to the fast polymerization kinetics, as indicated in Figure 23 for the premonomer with the EWGs. The copolymer yield is similar to the one shown in Figure 23, except when high initial content of premonomer A is used, because premonomer A possesses EDGs in Figure 23 and EWGs in Figure 24. Hence, in this region, also high copolymer yield is obtained. Similar to Figure 23, the presence of two premonomers with EWGs in Figure 24 determines the copolymer properties much stronger than the base concentration does. However, due to the

similarity in reactivity of **8** and **9**, they incorporate randomly and hence the conjugated triad fraction of the AAA and BBB type indicates random copolymers when a 50:50 mixture of **8**:**9** is copolymerized. The latter contrasts with Figure 23.

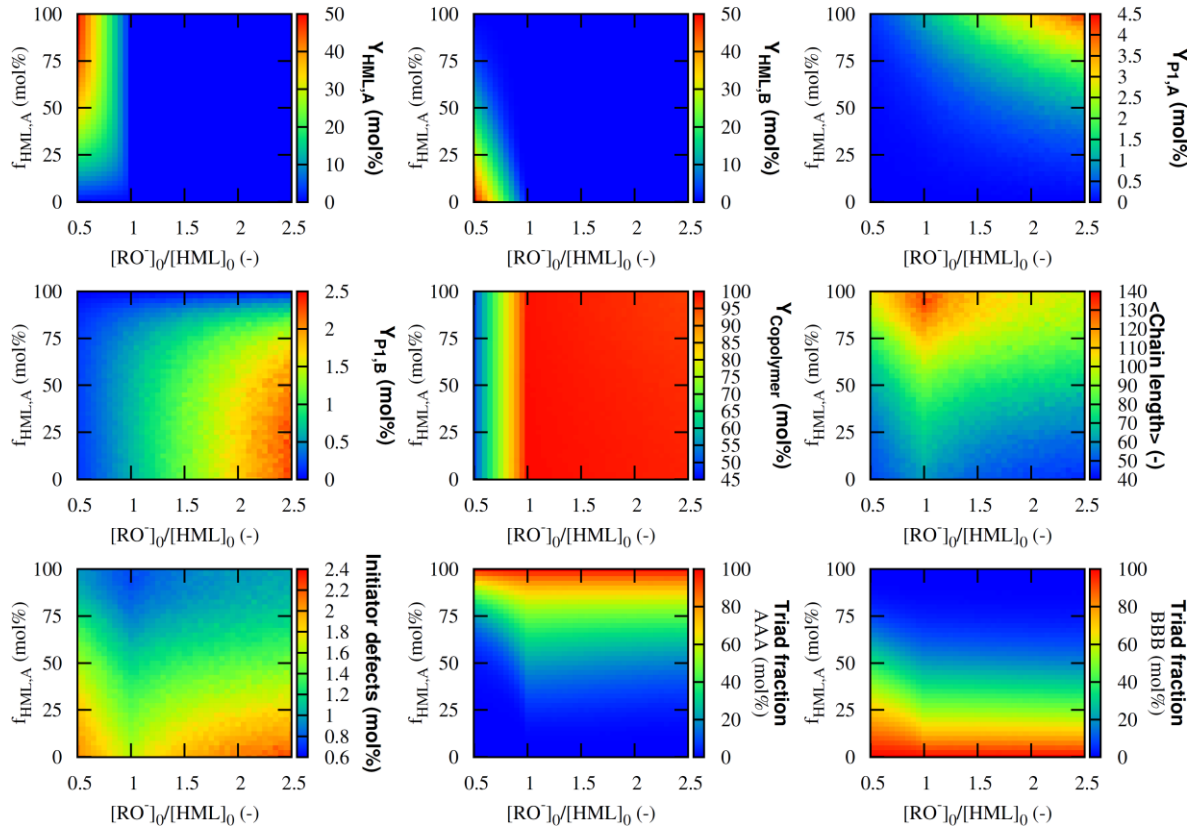

Figure 24: Effect of the base and the initial premonomer composition on the yields and properties for the copolymerizations of 8 with 9 (see Figures 3, 4 and 5); Reaction conditions: 308 K; $f_{HML,A}$ is defined as $[HML,A]_0/([HML,A]_0+[HML,B]_0)$

The effect of the base on the remaining copolymerizations is given in Appendix J and is in line with the above discussion.

3.3.6. Effect of the Hammett substituent constant σ on the copolymerization.

So far, the copolymerization is shown for specified premonomers, such as **1**-**9**. Each of these premonomers is characterized by the Hammett substituent constants σ of their substituents. Hence, instead of showing plots for each premonomer A and B, similar plots can be made for continuous variations of σ_A and σ_B, as was done for homopolyerizations before. In the following figures, the description is generalized by considering σ_B as a continuous variable. This representation implies by necessity that k_{E2} and k_{NA} of premonomer B are calculated via

Hammett's relation, which may yield slightly different rate coefficients than the rate coefficients used to construct the Hammett relations. To clarify: In the simulations before this point, the rate coefficients k_{E2} and k_{NA} as determined from the UV-vis experiments are used for premonomer B. In the simulations after this point, premonomer B is not specified but only characterized by a Hammett substituent constant σ_B. This implies that the rate coefficients $k_{E2,B}$ and $k_{NA,B}$ must be used to construct a Hammett relation for the kinetics of premonomer B. In order to judge the inaccuracies introduced, the real rate coefficients must be compared with their Hammett-regressed values. These are given in Appendix H, Figures H2 and H3. It can be seen that the differences are negligible except for the k_{E2} value of **4** and the k_{NA} value of **2**. Other than these two minor differences, the actual rate coefficients are in good agreement with their Hammett determined values. In this way, the ideas outlined in the previous section may be applied for premonomers B different from the ones in this work.

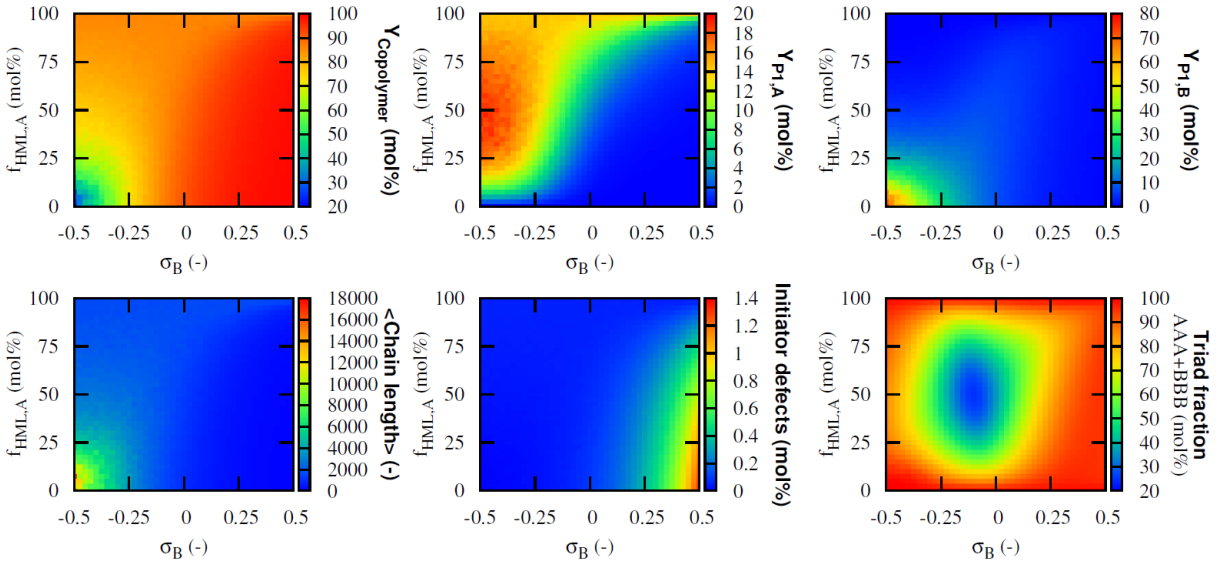

Figure 25: Effect of the Hammett substituent constant σ_B and the initial premonomer composition on the yields and properties for the copolymerization of 3 (see Figures 3, 4 and 5); Reaction conditions: $[RO^-]_0/[HML]_0$=1, 308 K; $f_{HML,A}$ is defined as $[HML,A]_0/([HML,A]_0+[HML,B]_0)$

Figure 25 shows the copolymerization of **3** (which possesses EDGs) with premonomer B, described by σ_B ranging from -0.5 to 0.5. As can be expected, the value of σ_B does not matter when the initial premonomer composition consists of purely premonomer A. As the initial fraction of premonomer B increases, the copolymer yield either increases when σ_B is positive

(EWG) or decreases when σ_B is negative (EDG). For the chain length, the reverse trend is seen (in agreement with earlier discussion). In the region of very low copolymer yield, the initial composition is pure premonomer B possessing a highly electron donating group. In this same region, the byproduct yield originating from premonomer B is highest because the polymerization is proceeding slowly. In contrast, the byproduct yield originating from premonomer A is high over a larger range of initial premonomer compositions and σ_B. Initiator defects in the copolymerization of **3** are generally low, unless **3** is copolymerized with a high amount of premonomer B possessing strongly electron withdrawing groups. The conjugated triad fraction of the AAA and BBB types shows that, as before, homopolymers are formed for pure premonomer A or pure premonomer B initial compositions. For initial premonomer compositions A:B of 50:50, it can be seen that a block-like copolymer is formed when premomer B possesses more electron donating groups than premonomer A. As the electron donating character of B decreases to resemble the electron donating character of the OC_{10} and OC_1 groups of **3**, a random copolymer is formed. For even higher values of σ_B, the kinetics of premonomer B correspond to the presence of electron withdrawing groups, resulting in a 100% conjugated triad fraction of the AAA and BBB type, i.e. a block copolymer results.

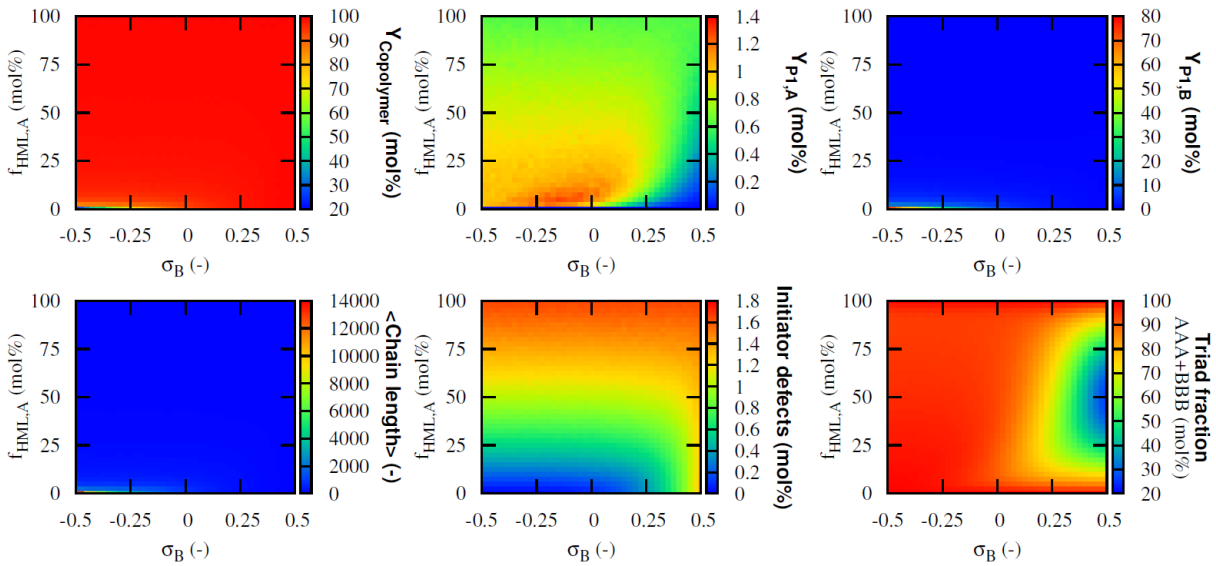

Figure 26: Effect of the Hammett substituent constant σ_B and the initial premonomer composition on the yields and properties for the copolymerization of 9 (see Figures 3, 4 and 5); Reaction conditions: $[RO^-]_0/[HML]_0$=1, 308 K; $f_{HML,A}$ is defined as $[HML,A]_0/([HML,A]_0+[HML,B]_0)$

Figure 26 shows the copolymerization of **9** (which possesses EWGs) with premonomer B, described by σ_B ranging from -0.5 to 0.5. As in Figure 25, the value of σ_B does not matter when the initial premonomer composition consists of purely premonomer A. In contrast to Figure 25, the copolymer yield is always high, except when a pure premonomer B mixture is used and premonomer B possesses EDGs. As before, the chain length plot shows the inverse behavior of the copolymer yield. The byproduct yield originating from premonomer A is low irrespective of the initial composition or B's substituents on the aromatic moiety, while the byproduct yield originating from premonomer B is only high when pure B with EDGs is started from. Hence, the sum of the byproduct yield of B and the copolymer yield is approximately 100%. As before, the initiator defects do not heavily depend on the electronic character of the substituents on the aromatic moiety of premonomer B, when premonomer A already possesses EWGs. Hence, the initiator defect content depends mostly on the initial premonomer composition (unless the initial content of A is very low). The conjugated triad fraction of the AAA and BBB type may be interpreted similarly to Figure 25: For similar electronic effects of the substituents on the aromatic moieties of A and B, a random copolymer results and for strongly different electronic effects, block copolymers are achieved. Intermediate differences of σ_B lead to microstructures with both random and block-like character.

The remaining copolymerizations of **1**, **2** and **4**-**8** are given in Appendix K.

3.4. Conclusions

The synthesis of PPV can be kinetically decoupled by modeling both diluted and concentrated conditions. In diluted conditions, it is found that large differences in monomer concentration occur. In more concentrated (i.e. polymerization) conditions, propagation reactivity can be simulated with Hammett's structure-reactivity relation in agreement with the findings of Cho et al. for the Wessling route.[68,69] The structure effect on the initiation reaction is assumed to be similar but more pronounced than on the propagation. Previous work on structure-reactivity of *p*-quinodimethane chemistry is thus unified in a kinetic model which correctly predicts that electron-poor PPVs inherently possess low chain lengths and that electron-rich PPVs, such as MDMO-PPV, are characterized by high chain lengths. The structure-reactivity relations outlined are considered essential toward understanding of the kinetics of precursor routes and ultimately optimization of conjugated materials. The modeled interplay between premonomer structure, yield, chain length and initiator defects during the synthesis of PPV

based homopolymers allows to model copolymerizations in a next step. The properties of PPVs with electron withdrawing substituents are only weakly affected by the addition of premonomers with electron donating groups, whereas the properties of PPVs with electron donating substituents, such as MDMO-PPV, can be affected significantly by such addition. The observed effect on the polymer properties is much greater than when varying the reaction conditions. The base concentration can only mildly affect the properties in case premonomers with EDG and premonomers with EWG are copolymerized. However, when two premonomers with EDGs are copolymerized, the base has a larger effect on the properties, comparable to the effect of the initial premonomer composition.

References

1. Spanggaard, H.; Sariciftci, F. C. *Sol. Energy Mater. Sol. Cells* **2004**, 83, 125-146.
2. Thompson, B. C.; Frechet, J. M. J. *Angew. Chem., Int. Ed.* **2008**, 47, 58-77.
3. Gunes, S.; Neugebauer, H.; Sariciftci, N. S. *Chem. Rev.* **2007**, 107, 1324-1338.
4. Gevorgyan, S. A.; Krebs, F. C. *Mol. Org. Electron. Devices* **2010**, 291-309.
5. Kietzke, T. *Mol. Org. Electron. Devices* **2010**, 253-289.
6. Cheng, Y.-J.; Yang, S.-H.; Hsu, C.-S. *Chem. Rev.* **2009**, 109, 5868-5923.
7. Cimrova, V.; Schmidt, W.; Rulkens, R.; Schulze, M.; Meyer, W.; Neher, D. *Adv. Mater.* **1996**, 8, 585-588.
8. Edman, L.; Pauchard, M.; Liu, B.; Bazan, G.; Moses, D.; Heeger, A. J. *Appl. Phys. Lett.* **2003**, 82, 3961-3963.
9. Cheng, C. H. W.; Boettcher, S. W.; Johnston, D. H.; Lonergan, M. C. *J. Am. Chem. Soc.* **2004**, 126, 8666-8667.
10. Kawai, T.; Yamaue, T.; Onoda, M.; Yoshino, K. *Synth. Met.* **1999**, *102*, 971-972.
11. Gomez, E. D.; Lee, S. S.; Kim, C. S.; Loo, Y.-L. *Mol. Org. Electron. Devices* **2010**, 109-152.
12. Grimsdale, A. C.; Chan, K. L.; Martin, R. E.; Jokisz, P. G.; Holmes, A. B. *Chem. Rev.* **2009**, 109, 897-1091.
13. Yang, J.H.; Garcia, A.; Nguyen, T.Q. *Appl. Phys. Lett.* **2007**, 90, 103514-103517.
14. Lee, W.; Mane, R.S.; Min, S.K.; Yoon, T.H.; Han, S.H.; Lee, S.H. *Appl. Phys. Lett.* **2007**, *90*, 263503/1-263503/3.
15. Holder, E.; Tessler, N.; Rogach, A. *J. Mater. Chem.* **2008**, 18, 1064-1078.
16. Peng, Z.; Xu, B. ; Zhang, J. ; Pan, Y. *Chem. Commun.* **1999**, 1855-1856.
17. Balanda, P. B.; Ramey, M. B.; Reynolds, J. R. *Macromolecules* **1999**, 32, 3970-3978.

18. Levitsky, I. A.; Kim, J.; Swager, T. M. *J. Am. Chem. Soc.* **1999**, 121, 1466-1472.
19. Horowitz, G. *Adv. Mater.* **1998**, 10, 365-377.
20. Kano, M.; Minari, T.; Tsukagoshi, K. *Appl. Phys. Express* **2010**, 3, 051601/1-051601/3.
21. Liu, B.; Yu, W. L.; Lai, Y. H.; Huang, W. *Chem. Commun.* **2000**, 551-552.
22. Patil, A. O.; Ikenoue, Y.; Wudl, F.; Heeger, A. J. *J. Am. Chem. Soc.* **1987**, 109, 1858-1859.
23. Tan, C. Y.; Pinto, M. R.; Kose, M. E.; Ghiviriga, I.; Schanze, K.S. *Adv. Mater.* **2004**, 16, 1208-1212.
24. Shi, S.; Wudl, F. *Macromolecules* **1990**, 23, 2119-2124.
25. Fujii, A.; Sonoda, T.; Fujisawa, T.; Ootake, R.; Yoshino, K. *Synth. Met.* **2001**, 119, 189-190.
26. Cheng, F.; Zhang, G. W.; Lu, X. M.; Huang, Y. Q.; Chen, Y.; Zhou, Y.; Fan, Q. L.; Huang, W. *Macromol. Rapid. Comm.* **2006**, 27, 799-803.
27. Gerard, M.; Chaubey, A.; Malhotra, B. D. *Biosens. Bioelectron.* **2002**, 17, 345-359.
28. Zhang, B.; Lin, H.; Tang, J.; Liu, J. S. *Chinese Sci. Bull.* **2009**, 54, 3515-3520.
29. Khan, A.; Müller, S.; Hecht, S. *Chem. Commun.* **2005**, 584-586.
30. Kim, K. N.; Kwon, Y. W.; Choi, D. H.; Jin, J. I. *Macromol. Chem. Physic.* **2009**, 210, 1372-1378.
31. Anslyn, E. V.; Dougherty, D. A., editors. *Modern Physical Organic Chemistry*. Sausalito: University Science Books; 2006.
32. Henckens, A.; Lutsen, L.; Vanderzande, D.; Knipper, M.; Manca, J.; Aernouts, T.; Poortmans, J. *SPIE Proc.* **2004**, 52-59.
33. Meier, H. *Angew. Chem.* **1992**, 104, 1425-1426.
34. Hide, F.; Diaz-Garcia, M. A.; Schwartz, B. J.; Heeger, A. J. *Acc. Chem. Res.* **1997**, 30, 430-436.
35. McGehee, M. D.; Heeger, A. J. *Adv. Mater.* **2000**, 12, 1655-1668.
36. Petty, M. C., Bryce, M. R., Bloor, D., editors. *Introduction to molecular electronics*. London: Edward Arnold; 1995.
37. Loutfy, R. O.; Hor, A. M.; Hsiao, C. K.; Baranyi, G.; Kazmaier, P. *Pure Appl. Chem.* **1988**, 60, 1047-1054.
38. Nalwa, H. S., editor. *Nonlinear optics of organic molecules and polymers*; New York: CRC; 1997.
39. Feringa, L.; Jager, W. F.; de Lange, B. *Tetrahedron* **1993**, 49, 8267-8310.

40. Katz, H. E. *Chem. Mater.* **2004**, 23, 4748-4756.
41. Henckens, A.; Colladet, K.; Fourier, S.; Cleij, T. J.; Lutsen, L.; Gelan, J. *Macromolecules* **2005**, 38, 19-26.
42. Henckens, A.; Duyssens, I.; Lutsen, L.; Vanderzande, D.; Cleij, T. J. *Polymer* **2006**, 47, 123-131.
43. Vandenbergh, J.; Wouters, J.; Adriaensens, P. J.; Mens, R.; Cleij, T. J.; Lutsen, L.; Vanderzande, D. J. M. *Macromolecules* **2009**, 42, 3661-3668.
44. Breselge, M.; Van Severen, I.; Lutsen, L.; Adriaensens, P.; Manca, J.; Vanderzande, D.; Cleij, T. *Thin Solid Films* **2006**, 511-512, 328-332.
45. Blom, P. W. M.; Tanase, C.; de Leeuw, D. M.; Coehoorn, R. *Appl. Phys. Lett.* **2005**, 86, 092105/1-092105/3.
46. Issaris, A.; Vanderzande, D.; Gelan, J. *Polymer* **1997**, 38, 2571-2574.
47. Hontis, L.; Vrindts, V.; Lutsen, L.; Vanderzande, D.; Gelan, J. *Polymer* **2001**, 42, 5793-5796.
48. Hontis, L.; Vrindts, V.; Vanderzande, D.; Lutsen, L. *Macromolecules* **2003**, 36, 3035-3044.
49. Wiesecke, J.; Rehahn, M. *Angew. Chem., Int. Ed.* **2003**, 42, 567-570.
50. Schwalm, T.; Wiesecke, J.; Immel, S.; Rehahn, M. *Macromolecules* **2007**, 40, 8842-8854.
51. Reichardt, C, editor. *Solvents and Solvent Effects in Organic Chemistry*. Weinheim: VCH; 1990.
52. Munters, T.; Martens, T.; Goris, L.; Vrindts, V.; Manca, J.; Lutsen, L.; De Ceuninck, W.; Vanderzande, D.; De Schepper, L.; Gelan, J.; Sariciftci, N.S.; Brabec, C. J. *Thin Solid Films* **2002**, 403-404, 247-251.
53. Pan, M.; Bao, Z. N.; Yu, L. P. *Macromolecules* **1995**, 28 (14), 5151-5153.
54. Liu, Y. B.; Lahti, P. M.; La, F. *Polymer* **1998**, 39, 5241-5244.
55. Lutsen, L. J.; Van Breemen, A. J.; Kreuder, W.; Vanderzande, D. J. M.; Gelan, J. M. J. V. *Helv. Chem. Acta.* **2000**, 83, 3113-3121.
56. Lutsen, L.; Adriaensens, P.; Becker, H.; Van Breemen, A. J.;Vanderzande, D.; Gelan, J. *Macromolecules* **1999**, 32, 6517-6525
57. Mozer, A. J.; Denk, P.; Scharber, M. C.; Neugebauer, H.; Sariciftci, N. S.; Wagner, P.; Lutsen, L.; Vanderzande D.; Kadashchuk, A.; Staneva, R.; Resel, R. *Synthetic Metals* **2005**, 153, 81-84.

58. Mozer, A. J.; Denk, P.; Scharber, M. C.; Neugebauer, H.; Sariciftci, N. S.; Wagner, P.; Lutsen, L.; Vanderzande, D. *J. Phys. Chem. B* **2004**, 108, 5235-5242.
59. Wu, P.-T.; Ren, G.; Jenekhe, S. A. *Macromolecules* **2010**, 43, 3306-3313.
60. Zhang, C.; Sun, J.; Li, R.; Sun S.-S.; Lafalce, E.; Jiang, X. *Macromolecules* **2011**, 44, 6389-6396.
61. Koetse, M. M.; Sweelssen, J.; Franse, T.; Veenstra, S. C.; Kroon, J. M.; Yang, X.; Alexeev, A.; Loos, J.; Schubert, U. S.; Schoo, H. F. M. *SPIE USE* **2003**, 6, 5215-5222.
62. Spanggaard, H.; Krebs, F. C. *Solar Energy Materials & Solar Cells* **2004**, 83, 125-146.
63. Becker, H.; Gelsen, O.; Kluge, E.; Kreuder, W.; Schenk, H.; Spreitzer, H. *Synth. Met.* **2000**, 111-112, 145-149.
64. Van Severen, I.; Breselge, M.; Fourier, S.; Adriaensens, P.; Manca, J.; Lutsen, L.; Cleij, T. J.; Vanderzande, D. *Macromol. Chem. Phys.* **2007**, 208, 196-206.
65. Junkers, T.; Vandenbergh, J.; Adriaensens, P.J.; Lutsen, L.; Vanderzande, D. *Polym. Chem.* **2012**, 3, 275-285.
66. Adriaensens, P.; Van der Borght, M.; Hontis, L.; Issaris, A.; van Breemen, A.; de Kok, M.; Vanderzande, D.; Gelan, J. *Polymer* **2000**, 41, 19, 7003-7009.
67. Hermosilla, L.; Catak, S.; Van Speybroeck, V.; Waroquier, M.; Vandenbergh, J.; Motmans, F.; Adriaensens, P.; Lutsen, L.; Cleij, T.; Vanderzande, D. *Macromolecules* **2010**, 43, 18, 7424-7433.
68. Cho, B.R. *Prog. Pol. Sci.* **2002**, 27, 2, 307-355.
69. Cho, B.R.; Kim, T. H.; Son, K. H.; Kim, Y. K.; Lee, Y. K.; Jeon, S. J. *Macromolecules* **2000**, 33, 22, 8167-8172.
70. Schwalm, T.; Wiesecke, J.; Immel, S.; Rehahn, M. *Macromolecules* **2007**, 40, 8842-8854.
71. Trahanovsky, W. S.; Lorimor, S. P. *J. Org. Chem.* **2006**, 71, 1784-1794.
72. Boudart, M., editor. *Kinetics of Chemical Processes*. Englewood Cliffs, NJ: Prentice Hall; 1968.
73. Van Steenberge, P.; Vandenbergh, J.; D'hooge, D. R.; Reyniers, M.-F.; Adriaensens, P. J.; Lutsen, L.; Vanderzande, D. J. M.; Marin, G. B. *Macromolecules* **2011**, 44, 8716-8726.
74. Pyun, S. Y.; Kim, W. G.; Jeong, J.-H.; Cho, B. R. *Bull. Korean Chem. Soc.* **2008**, 29, 2453-2458.
75. Alexandrova, L.; Salcedo, R. *Polymer* **1994**, 35, 21, 4656-4658.

76. Gillissen, S.; Jonforsen, M.; Kesters, E.; Johansson, T.; Theander, M.; Andersson, M. R.; Inganas, O.; Lutsen, L.; Vanderzande, D. *Macromolecules* **2001**, 34, 7294-7299.

77. Burn, P. L.; Holmes, A. B.; Kraft, A.; Bradley, D. D. C.; Brown, A. R.; Friend, R. H. *J. Chem. Soc., Chem. Commun.* **1992**, 32-34.

78. Brown, A. R.; Burn, P. L.; Bradley, D. D. C.; Friend, R. H.; Kraft, A.; Holmes, A. B. *Mol. Cryst. Liq. Cryst.* **1992**, 216, 111-116.

79. Vanderzande, D. J.; Issaris, A. C.; van der Borght, M. J.; van Breemen, A. J.; de Kok, M. M.; Gelan, J. M. *Macromol. Symp.* **1997**, 125, 189-203.

80. de Kok, M. M.; van Breemen, A. J. J. M.; Adriaensens, P. J.; van Dixhoorn, A.; Gelan, J. M.; Vanderzande, D. J. *Acta Polym.* **1998**, 49, 510-513.

81. de Kok, M.M.; Dissertation, 1999, Limburgs Universitair Centrum Diepenbeek, p. 81 of 152.

82. de Kok, M.M.; Dissertation, 1999, Limburgs Universitair Centrum Diepenbeek, p. 70 of 152.

83. de Kok, M.M.; Dissertation, 1999, Limburgs Universitair Centrum Diepenbeek, p. 33 of 152.

Chapter 4: Model based design of poly(2,5-dialkoxy-1,4-phenylene vinylene)s via the dithiocarbamate route

Summary

A kinetic Monte Carlo modeling study is presented for the synthesis of the dithiocarbamate precursor polymer toward poly(2,5-dialkoxy-1,4-phenylene vinylene)s. Based on UV-vis spectroscopy, Hammett's structure-reactivity relation, reported Gel Permeation Chromatography and ^{1}H NMR data, approximate values of rate coefficients for monomer formation, chain initiation and propagation are determined and used for computer simulations. Simulation data agree with reported experimental data and confirm that the regioregularity in poly[(2-methoxy-5-(3′,7′,-dimethyloctyloxy))-1,4-phenylene vinylene] (MDMO-PPV) stems from steric hindrance during the monomer formation when lithium bis(trimethylsilyl) amide (LHMDS) is the base. It is demonstrated that copolymers having a triad distribution similar to MDMO-PPV can be synthesized through LHMDS induced copolymerization of 2,5-Bis(N,N-diethyldithiocarbamate-methyl)-1,4-dimethoxybenzene and 2,5-Bis(N,N-diethyldithiocarbamate-methyl)-1,4-Bis(3′,7′-dimethyl octyloxy)-benzene by varying the initial premonomer composition. The resulting copolymers are characterized by the same yield, average chain length and structural defect content as MDMO-PPV, but possess the advantage that their triad distribution can be varied over a broad range. Reaction conditions are provided to synthesize poly(2,5-dialkoxy-1,4-phenylene vinylene)s with a targeted microstructure, which is important to design PPV materials with optimal properties for photovoltaic devices.

4.1. Introduction

The luminescence properties of poly(*p*-phenylene vinylene) (PPV) in solution were discovered by Burroughes and coworkers in 1990.[1] Shortly afterwards, the first Organic Light Emitting Diode (OLED), using PPV as active material, was reported by Friend and coworkers.[2] Since then, PPVs are used in various organic opto-electronic devices[3-9], which are preferred to their inorganic counterparts because they can be coated onto large, flexible surface areas and their molecular structure can be tuned to design novel active materials. Well-defined ordered morphologies of the active PPV material lead to better device performance.[10-12] PPVs with linear side chains[11,13], chiral substituents[14,15] or regioregular

polymers[10,16] achieving these well-defined ordered morphologies, have been reported. In particular, regioregular polymers are important for the design of stable morphologies in material blends for bulk heterojunction solar cells.[17]

Not many reports exist on regioregularity control.[18,19] The group of Vanderzande prepared[20] two isomers of asymmetric monosulfinyl chloromethylbenzenes in 50:50 ratio and demonstrated their polymerization toward regiorandom high chain length MDMO-PPV.[21] Using only one of the two isomers, they synthesize fully regioregular MDMO-PPV, albeit with poor solubility in common solvents, inhibiting further characterization. Joint work of the Vanderzande group and Mozer et al.[22,23] resulted in soluble MDMO-PPV with a 30:70 composition of isomeric comonomers, displaying a 3.5-fold higher hole mobility than its regiorandom (50:50) counterpart. The latter result is of particular importance toward device optimization because the hole mobility in MDMO-PPV films is currently the bottleneck of the performance of photovoltaic devices (the electron mobility in PCBM films is an order of 2 to 4 times larger). The 30:70 MDMO-PPV was used to fabricate a bulk hetero-junction solar cell with a very high fill factor.

For certain classes of conjugated polymers, the regioregularity does not strongly affect the opto-electronic properties and thus variable regioregularity can improve solubility. For example, the statistical copolymers of 3-butylthiophene and 3-octyltiophene of several compositions turn out[24] to be crystalline despite statistical arrangement of the side chains with different size. Power conversion efficiencies up to 3.0% are obtained in photovoltaic devices, which is significantly higher than for the respective homopolymers and their blends. A similar idea is reported[25] for the synthesis of poly(3-dodecylthienylenevinylene)s, in which also isomeric comonomers are used to introduce regiorandomness to improve solubility, while not affecting the crystallinity and photovoltaic performance strongly. The result is attributed to the long separation between the side chains, allowing all side chains to be stacked in the polymer backbone plane irrespective of the degree of regioregularity. The best solar cell device efficiencies were obtained for the poly(3-dodecylthienylenevinylene) with a 30:70 initial monomer ratio, coincidentally the same initial (pre)monomer composition as demonstrated[22,23] best for MDMO-PPV via the sulfinyl route.

From the above, it is clear that the regioregularity approach offers opportunity toward tuning of photovoltaic device properties. However, to relate the regioregularity to device

performance, a quantitative method to measure regioregularity is necessary. ^{1}H NMR readily offers information on the triad distribution of a copolymer, as recently demonstrated by Vandenbergh et al.[26] for the dithiocarbamate (DTC) precursor route using lithium-bistrimethylsilylamide (LHMDS) and K*t*BuO as base. Straightforward synthesis of poly(2-methoxy-5-(3',7'-dimethyloctyloxy)-1,4-phenylene vinylene) (MDMO-PPV) was demonstrated and, in contrast to the regiorandom polymers obtained via the Gilch route[27,28], the DTC-polymers displayed a partially regioregular character[26] when LHMDS was used as the base. Using ^{1}H NMR spectroscopy[26], four different environments for the methoxy groups in the copolymer side chain can be distinguished, corresponding to four triad types in MDMO-PPV (see Figure 1).

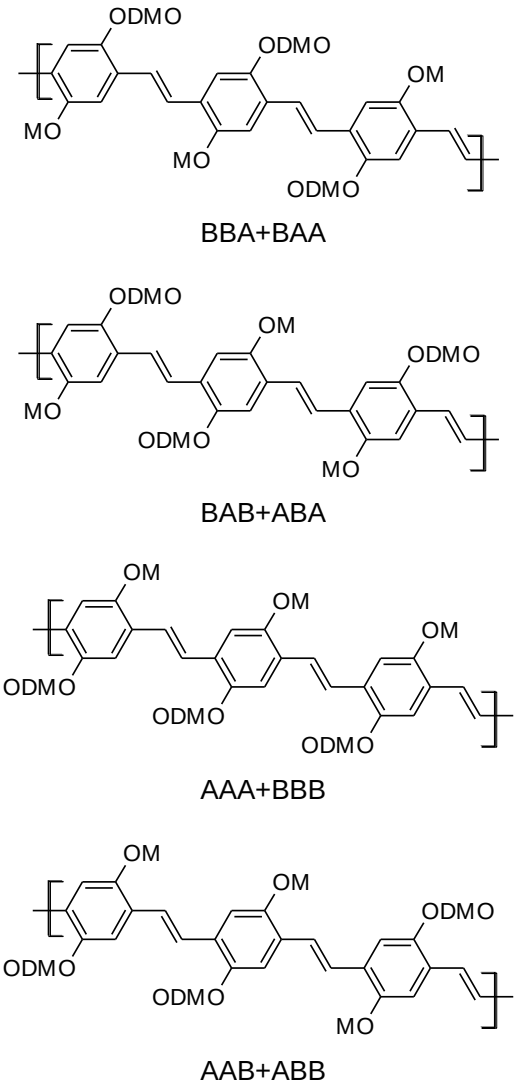

Figure 1: Triads in MDMO-PPV

MDMO-PPV synthesized with LHMDS shows a 47% fraction of regioregular triads (AAA+BBB, see Figure 1) whereas the K*t*BuO induced polymerization yields a fraction of about 25% for each triad type, i.e. a regiorandom polymer is obtained. An additional NMR study[26] on ^{13}C-labeled MDMO-PPV revealed the presence of only a minimal amount of structural defects in the microstructure of the copolymer indicating that recombinations are of minor importance and that propagation occurs almost exclusively by head-to-tail additions (Figure 2).[26] The latter has led to the proposition[26] that, in contrast to the K*t*BuO induced 1,6-elimination, the LHMDS induced 1,6-elimination exhibits regioselectivity leading to the preferential formation of monomer A (Figure 2) in the DTC route. This would affect the triad microstructure of the DTC-polymers and explain the partially regioregular character[26] of MDMO-PPV when synthesized using LHMDS as the base.

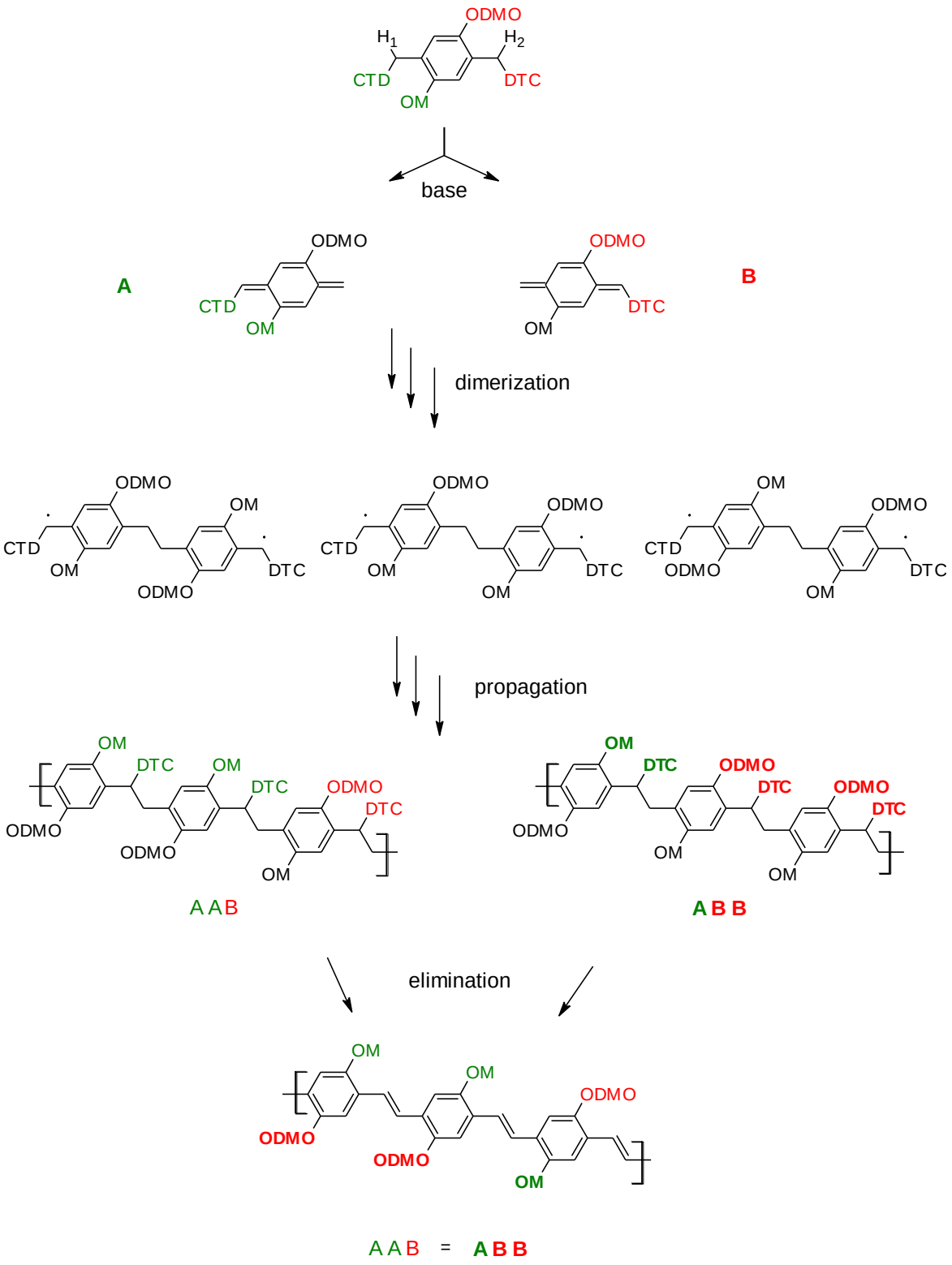

Figure 2: The dithiocarbamate route toward MDMO-PPV. Only 2 of the 8 triads in the precursor polymer and 1 of the 4 triads in the conjugated polymer are shown. All possible triads are shown in Figure 1 and 3. ODMO = 3,7-dimethyloctyloxy, OM = methoxy, DTC = Et_2N-C(S)-S

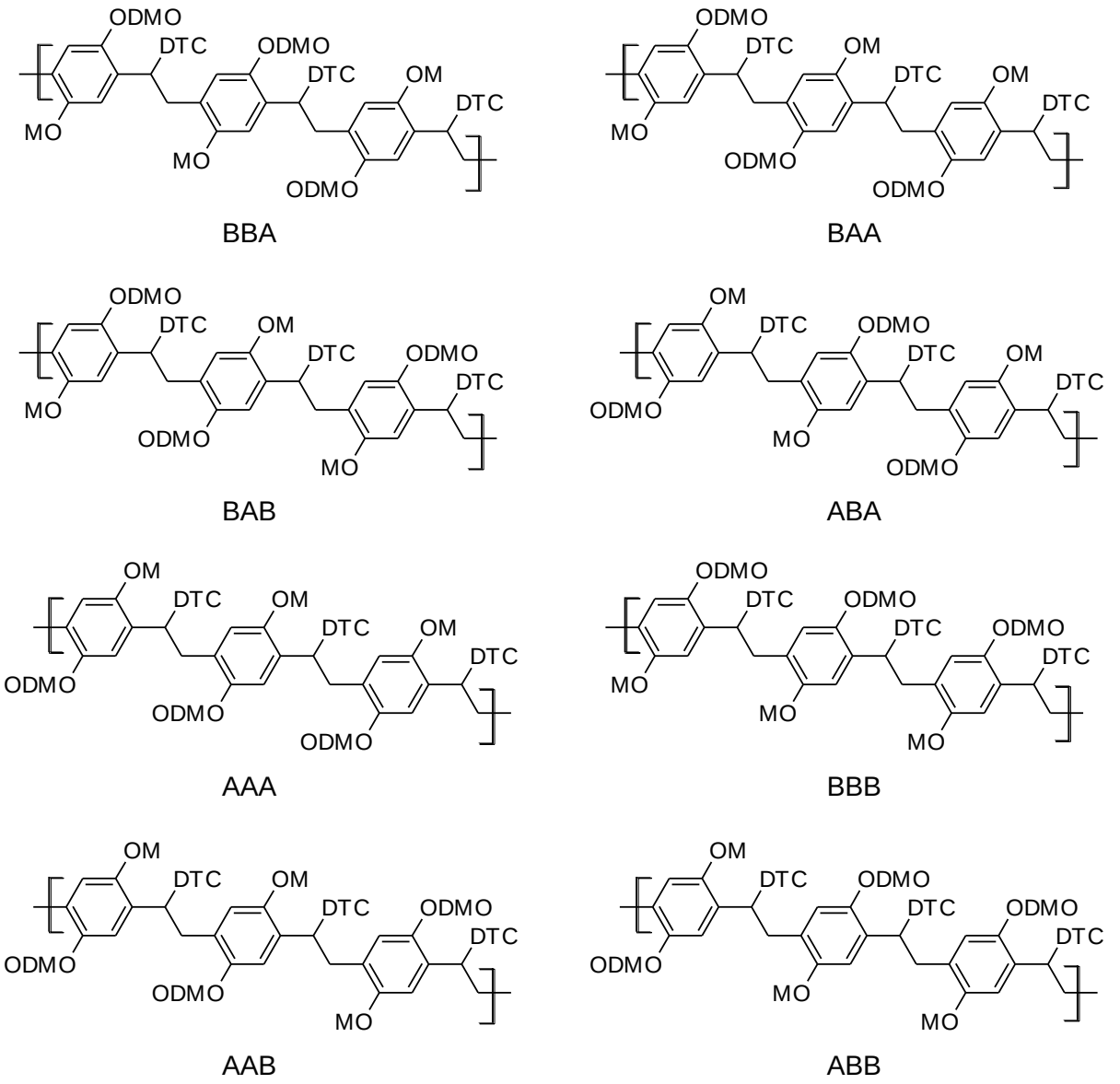

Figure 3: Triads in precursor MDMO-PPV via the DTC route

To obtain more insight into the origin of the regioselectivity during MDMO-PPV synthesis via the DTC route, a kinetic Monte Carlo (kMC) modeling study is performed for the synthesis of various poly(2,5-dialkoxy-1,4-phenylene vinylene)s as shown in Figure 2. The MDMO-premonomer is subjected to a base induced 1,6-elimination yielding two isomeric p-quinodimethane monomers which polymerize via a radical mechanism leading to the precursor polymer, of which all triads are shown in Figure 3. After thermal treatment and concomitant intramolecular eliminations, the final conjugated MDMO-PPV is obtained. The kinetic model considers four premonomers, shown in Figure 4. The first premonomer considered (DTC) has no substituents on the aromatic moiety, while DTC-MO and DTC-

ODMO are symmetrically substituted with OC_1 and OC_{10} groups respectively. In contrast, DTC-MO-MDMO is asymmetrically substituted with OC_1 and OC_{10} groups leading to precursor MDMO-PPV upon polymerization. The choice of these premonomers allows to investigate the electronic and steric effects of the OC_1 and OC_{10} groups on the yields and the precursor polymer microstructural properties of poly(2,5-dialkoxy-1,4-phenylene vinylene)s.

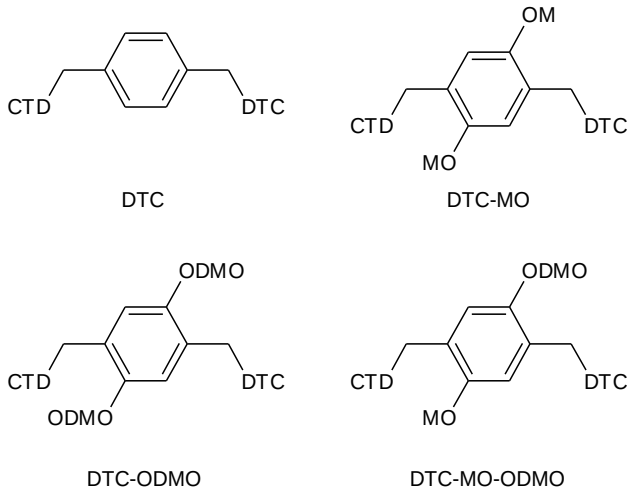

Figure 4: Considered premonomers: DTC is unsubstituted, DTC-MO and DTC-ODMO are symmetrically substituted, DTC-MO-ODMO is asymmetrically substituted, leading to MDMO-PPV

The kinetic modeling study increases complexity one step at a time. In a first step, the monomer formation of DTC (see Figure 2) is studied using UV-Vis spectroscopy and kinetic Monte Carlo simulations are used to illustrate the steric and electronic effects on the monomer formation of DTC-MO and DTC-ODMO and the comonomer formation of DTC-MO-ODMO (see Figure 4) for the bases KtBuO and LHMDS. Next, homopolymerization of the symmetrically substituted premonomers DTC, DTC-MO and DTC-MO-ODMO (see Figure 4) is simulated. In a third step, KtBuO and LHMDS induced polymerization of the asymmetric premonomer DTC-MO-ODMO (see Figure 4) is considered. Since 1,6-elimination of DTC-MO-ODMO leads to the in situ formation of two isomeric monomers A and B (see Figure 2), this case actually constitutes a copolymerization with in situ formation of the two comonomers. Kinetic Monte Carlo modeling is now used to illustrate the effect of the base on the regioregularity of the formed MDMO-PPV. Finally, the LHMDS induced copolymerizations of the symmetrically substituted premonomers are modeled (DTC, DTC-MO and DTC-ODMO in Figure 4). This final step of the study broadens the scope of the DTC

route to mixtures of premonomers. Simulations are used to explore the influence of the initial ratio of comonomers on the polymer microstructure and to formulate recommendations as to which reaction conditions lead to targeted triad distributions in poly(2,5-dialkoxy-1,4-phenylene vinylene)s. Terpolymerizations, which arise when an asymmetric premonomer is mixed with a symmetric premonomer, i.e. mixtures of DTC-MO-ODMO with either DTC, DTC-MO or DTC-ODMO, are not considered in the present study.

4.2. Experimental procedure

Unless otherwise stated, all reagents and chemicals were obtained from commercial sources (Acros and Aldrich) and used without further purification. Tetrahydrofuran (THF) was dried by distillation from sodium/benzophenone. The synthesis procedure of 1,4-Bis(N,N-diethyldithiocarbamate-methyl)-benzene has been reported elsewhere.[29] In situ UV-vis experiments were performed using a Cary 500 UV-Vis-NIR spectrophotometer equipped with a stop-flow module (Hi-Tech Limited)[30]. The optic path length of the sample cell was 10 mm. All spectroscopic and kinetic data were obtained using the ”Scanning kinetics” and ”Kinetics” software module supplied by Varian. For the K*t*BuO experiments, 10^{-4} mol L^{-1} solutions of 1,4-Bis(N,N-diethyldithiocarbamate-methyl)-benzene in THF are prepared. A 10^{-2} mol L^{-1} stock solution of K*t*BuO in THF was prepared. For the LHMDS experiments, 10^{-2} mol L^{-1} solutions of 1,4-Bis(N,N-diethyldithiocarbamate-methyl)-benzene in THF were prepared. The base solutions were prepared by dilution of a 1 mol L^{-1} LHMDS stock solution in THF to a 5 10^{-2} or a 10^{-1} mol L^{-1} solution. Upon mixing of the reacting solutions by the stop-flow accessory, all concentration values are halved. All solutions were degassed with nitrogen prior to the kinetic UV-vis experiment. The temperature of the reacting solutions was maintained at 298 K.

To determine the rate coefficients for the 1,6-elimination, the base (either K*t*BuO or LHMDS) was added in excess, creating pseudo-first order conditions. No indication for polymerization was found during the kinetic runs and the only products absorbing in the UV-vis spectrum are the premonomer (HML) and the *p*-quinodimethane monomer (M). The maximum wavelength of the UV-vis absorbance of the *p*-quinodimethane is approx. 318 nm[30,31], which is also the wavelength used in the UV-vis experiments in this study to monitor the *p*-quinodimethane. The contributions to the absorbance at 318 nm of the premonomer can be neglected. The *p*-quinodimethane concentration is thus directly proportional to the total absorbance at 318 nm.

4.3. Kinetic model

Recently, Van Steenberge et al. developed[31] a kinetic Monte Carlo (kMC) model to define optimal reactions conditions for PPV synthesis via the sulfinyl route using 1-(chloromethyl)-4-[(n-octylsulfinyl)methyl]-benzene as the premonomer. In this work, the modeling approach is extended to alkoxy substituted PPV synthesis via the DTC route by including the additional reaction steps due to the in situ formation of the two comonomers and the ensuing copolymerization. Also, the (pen)ultimate monomer units are tracked to allow a direct comparison with the reported[26] triad distribution of MDMO-PPV. Details of the kinetic Monte Carlo model can be found in Appendix A. All yields are normalized with the initial premonomer concentration.

The calculation of the reaction rates is based on the reaction scheme presented in Figure 2. The polymerization starts by contacting a premonomer solution with a solution of KtBuO or LHMDS in THF, leading to the actual monomer para-quinodimethane A or B via a base induced 1,6-elimination. The para-quinodimethane then dimerizes and may form 3 different diradical initiatiors. As in vinyl polymerizations, the para-quinodimethane monomer adds to the initiator radical and forms macrodiradicals. In order to track the formation of regioregular triads, macrodiradical types are distinguished based on their ultimate and penultimate monomer units, leading to $2^4 = 16$ possible types of macrodiradicals. Some of these 16 types are symmetric so that the actual number of distinct types is only 10. Each macroradical can react with both radical centers, with both monomers (as shown in Figure 2), leading to $10 \times 2 \times 2 = 40$ distinguished propagation types tracked by the model, each defining a sequence of three monomer units (a triad).

Approximate values for the rate coefficients are derived based on UV-vis data for the 1,6-elimination of DTC and data reported in literature[26] for GPC and ^{1}H NMR analysis of MDMO-PPV, originating from DTC-MO-ODMO, prepared via the DTC route. The electronic effects of the OC_1 and OC_{10} groups on the kinetics are modeled using Hammett free energy relations based on the findings of Cho et al.[32,33] for the Wessling route. The rate coefficients used in the simulations are presented in the next section together with a detailed description of how these rate coefficients are obtained.

4.4. Determination of rate coefficients

4.4.1. 1,6-Elimination

Figure 4 shows that the premonomers DTC, DTC-MO, DTC-ODMO each possess 4 structurally equivalent protons. Hence, their 1,6-elimination rate coefficients k_{E_2} can be written as $k_{E_2} = n_H \tilde{k}_{E_2}$ with $n_H = 4$ and $\tilde{k}_{E_2}$ the single event rate coefficient. For the asymmetric premonomer DTC-MO-ODMO, two different types of benzylic protons can be abstracted in an 1,6-elimination. The rate coefficients corresponding to these 2 distinct reactions are denoted $k_{E_{2,1}}$ and $k_{E_{2,2}}$. For each reaction site, 2 equivalent protons can be abstracted and, hence, $k_{E_{2,i}}$ can be written as: $k_{E_{2,i}} = n_{H,i} \tilde{k}_{E_{2,i}}$ with $n_{H,i} = 2$ and $\tilde{k}_{E_{2,i}}$ the single event rate coefficient of site i. Single-event rate coefficients are used to limit the number of Hammett relations.

The single event rate coefficient for DTC is further denoted as $\tilde{k}_{E_2}(H,H)$ and is found, after division by 4, by UV-vis monitoring of the para-quinodimethane from DTC and applying the Guggenheim method (see Appendix B for the method and the next section for the application). This is done for the bases LHMDS and K*t*BuO, the single event rate coefficients are given in Table 1.

Table 1: Values of single event rate coefficients (L mol^{-1} s^{-1}) for 1,6-elimination

	$\tilde{k}_{E_2}$			$\tilde{k}_{E_{2,1}}$	$\tilde{k}_{E_{2,2}}$
	DTC	DTC-MO	DTC-ODMO	DTC-MO-ODMO	DTC-MO-ODMO
K*t*BuO	2.43	-	-	0.75	0.75
LHMDS	4.55	1.40	0.47	1.40	0.47

To account for the electronic effect of the two OC_1 groups of DTC-MO and the single OC_1 group of DTC-MO-ODMO, the single event rate coefficient $\tilde{k}_{E_2}(H,H)$ for DTC is

extrapolated using Hammett's relation (see Appendix G) to obtain the single event rate coefficient $\tilde{k}_{E_2}(OR,OR)_u$ for DTC-MO (Table 1).

The validity of the Hammett free energy relation for the 1,6-elimination (and the other PPV reactions) of doubly substituted aromatics has been reported before[34,35]:

$$\log\left(\frac{k_{X,Y}}{k_{H,H}}\right) = \rho(\sigma_X + \sigma_Y) = \rho\sigma_t$$

The substituent constant σ_t expresses the effect of the substituents X and Y (on the aromatic moiety) on the reaction rate, independent of ρ. Similarly, ρ expresses the effect of the reaction type on the reaction rate, independent of σ_t. The substituent constants[36] used are $\sigma_t(H,H) = 0$ and $\sigma_t(OC_1,OC_{10}) = \sigma_t(OC_1,OC_1) = \sigma_t(OC_{10},OC_{10}) = -0.1$. In addition to the σ_t values, also the Hammett reaction constant ρ needs to be known. For the 1,6-elimination, an upper limit[37] for anionic reactions is used: $\rho_{E2} = 5$, see Table 2. These ρ and σ values allow to calculate the single event rate coefficent for DTC-MO, see Table 1. The single event rate coefficients for DTC and DTC-MO allow to perform simulations illustrating the electronic effect of the OC_1 groups on the 1,6-elimination.

Table 2: Values for the Hammett reaction constants ρ

	1,6-elimination	initiation	propagation
Reaction constant ρ	5[37]	5.14	0.6[37]

Likewise, to illustrate the steric effect of OC_{10} groups on the 1,6-elimination, single event rate coefficients for DTC-ODMO and DTC-MO-ODMO are necessary. The single event rate coefficient $\tilde{k}_{E_2}(OR,OR)_u$ for DTC-MO is assumed to be equal to the single event rate coefficient $\tilde{k}_{E_{2,1}}(OR,OR)_u$ for the unhindered protons of DTC-MO-ODMO. For the hindered protons, it is assumed that the electronic effect of the OC_1 and OC_{10} group is equal, so that $\tilde{k}_{E_{2,2}}(OR,OR)_h$ can be written as

$$\tilde{k}_{E_{2,2}}(OR,OR)_h = \frac{\tilde{k}_{E_{2,1}}(OR,OR)_u}{f_s}$$

with f_s a steric factor. The steric factor is determined from reported triad fractions of the LHMDS-based MDMO-PPV; a steric factor f_s of ≈ 3 is found. For the single event rate coefficient $\tilde{k}_{E_2}(OR,OR)_h$ of DTC-ODMO, the value of the single event rate coefficient $\tilde{k}_{E_{2,2}}(OR,OR)_h$ of DTC-MO-ODMO is used (Table 1).

4.4.2. Chain propagation

The determination of the propagation rate coefficients is illustrated for DTC-MO-ODMO, as an example. Denote $k_p(OR,OR)_{u,u}$ as a propagation step which is unhindered at the radical center (e.g. A° in Figure 5 for DTC-MO-ODMO) and unhindered at the double bond of the monomer (e.g. B in Figure 5 for DTC-MO-ODMO).

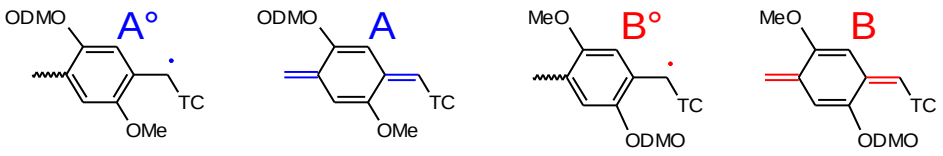

Figure 5: Propagating macroradical chain ends and monomer isomers in the dithiocarbamate route toward precursor MDMO-PPV formation

Hence, for DTC-MO-ODMO, $k_p(OR,OR)_{u,u} = k_{p,AB}$. Denote $k_p(OR,OR)_{u,h}$ as a rate coefficient for a propagation step in which the radical center is unhindered (e.g. A° in Figure 5 for DTC-MO-ODMO) and the double bond is hindered (e.g. A in Figure 5 for DTC-MO-ODMO). Hence, for DTC-MO-ODMO, $k_p(OR,OR)_{u,h} = k_{p,AA}$. Denote $k_p(OR,OR)_{h,u}$ as a rate coefficient for a propagation step in which the radical center is hindered (e.g. B° in Figure 5 for DTC-MO-ODMO) and the double bond is unhindered (e.g. B in Figure 5 for DTC-MO-ODMO). Hence, for DTC-MO-ODMO, $k_p(OR,OR)_{h,u} = k_{p,BB}$. Denote $k_p(OR,OR)_{h,h}$ as a rate coefficient for a propagation step which is hindered both at the radical center (e.g. B° in Figure 5 for DTC-MO-ODMO) and the double bond (e.g. A in Figure 5 for DTC-MO-ODMO). Hence, for DTC-MO-ODMO, $k_p(OR,OR)_{h,h} = k_{p,BA}$. To account for steric hindrance on the propagation, it is assumed that $0.9\ k_p(OR,OR)_{u,u} = k_p(OR,OR)_{u,h} = k_p(OR,OR)_{h,u}$ and $0.8\ k_p(OR,OR)_{u,u} = k_p(OR,OR)_{h,h}$. The factors 0.9 and 0.8 are deemed appropriate to describe the experimental data on KtBuO-induced MDMO-PPV reported in (26), taking into account experimental error (1%) on the reported triad fractions. $k_p(OR,OR)_{u,u}$ is then adjusted to fit the experimental data on MDMO-PPV reported in (26).

For the homopolymerization of DTC, $k_p(H,H)$ is determined via a Hammett relation from $k_p(OR,OR)_{u,u}$. A Hammett reaction constant of $\rho_p = 0.6$ is assumed for the propagation reaction[5], the value is in agreement with Cho's[34,35] ρ_p value of 0.7 for the Wessling route. For DTC-MO, the propagation rate coefficient for the homopolymerization is $k_p(OR,OR)_{u,u}$. For DTC-ODMO, the propagation rate coefficient for the homopolymerization is $k_p(OR,OR)_{h,h}$.

Table 3: Values of rate coefficients (L mol^{-1} s^{-1}) for homopolymerization reactions[a]

	K*t*BuO	LHMDS		
	DTC	DTC	DTC-MO	DTC-ODMO
k_{ini}	$1.2\ 10^{-5}$	$1.2\ 10^{-5}$	$3.6\ 10^{-6}$	$2.9\ 10^{-6}$
k_p	1.13	1.13	0.98	0.78

[a] *This table complements Table 1.*

Table 4: Values of rate coefficients (L mol^{-1} s^{-1}) for copolymerization reactions[a]

	K*t*BuO	LHMDS			
	DTC-MO-ODMO	DTC-MO-ODMO	DTC and DTC-MO	DTC and DTC-ODMO	DTC-MO and DTC-ODMO
$k_{ini,AA}$	$2.9\ 10^{-6}$	$2.9\ 10^{-6}$	$1.2\ 10^{-5}$	$1.2\ 10^{-5}$	$3.6\ 10^{-6}$
$k_{ini,AB}$	$3.2\ 10^{-6}$	$3.2\ 10^{-6}$	$6.6\ 10^{-6}$	$5.9\ 10^{-6}$	$3.2\ 10^{-6}$
$k_{ini,BB}$	$3.6\ 10^{-6}$	$3.6\ 10^{-6}$	$3.6\ 10^{-6}$	$2.9\ 10^{-6}$	$2.9\ 10^{-6}$
$k_{p,AA}$	0.88	0.88	1.13	1.13	0.98
$k_{p,AB}$	0.98	0.98	1.05	0.94	0.87
$k_{p,BA}$	0.78	0.78	1.05	0.94	0.87
$k_{p,BB}$	0.88	0.88	0.98	0.78	0.78

[a] *This table complements Table 1.*

The crosspropagation rate coefficients for the copolymerizations of DTC-MO with DTC-ODMO can be approximated by either $k_p(OR,OR)_{u,h}$ or $k_p(OR,OR)_{h,u}$ (same numerical value). The crosspropagation rate coefficients for the copolymerizations of DTC with DTC-MO and

DTC-ODMO are determined by the geometric means of already known propagation rate coefficients (Table 3 and 4). All propagation rate coefficients are then determined.

4.4.3. Chain initiation

The determination of the initiation rate coefficients is illustrated with the dimerization of the two monomers A and B shown in Figure 5. Denote $k_{ini}(OR,OR)_{h,h}$ as a rate coefficient for an initiation step which is hindered at both bond forming carbons of the monomers (e.g. A+A dimerization in Figure 5 for DTC-MO-ODMO). Hence, for DTC-MO-ODMO, $k_{ini}(OR,OR)_{h,h} = k_{ini,AA}$. Denote $k_{ini}(OR,OR)_{u,h}$ as a rate coefficient for an initiation step which is hindered at one of the bond forming carbons of the monomers (e.g. A+B dimerization in Figure 5 for DTC-MO-ODMO). Hence, for DTC-MO-ODMO, $k_{ini}(OR,OR)_{u,h} = k_{ini,AB}$. Contrary to the propagation reaction, there is no need to define $k_{ini,BA}$. Denote $k_{ini}(OR,OR)_{u,u}$ as a rate coefficient for an initiation step which is unhindered at both bond forming carbons of the monomers (e.g. B+B dimerization in Figure 5 for DTC-MO-ODMO). Hence, for DTC-MO-ODMO, $k_{ini}(OR,OR)_{u,u} = k_{ini,BB}$. To account for steric hindrance, it is assumed that $0.8\ k_{ini}(OR,OR)_{u,u} = k_{ini}(OR,OR)_{h,h}$ and $0.9\ k_{ini}(OR,OR)_{u,u} = k_{ini}(OR,OR)_{u,h}$. $k_{ini}(OR,OR)_{u,u}$ is then fitted from experimental data[26] on MDMO-PPV.

For the homoinitiation of DTC, $k_{ini}(H,H)$ is determined via a Hammett correlation from $k_{ini}(OR,OR)_{u,u}$. The necessary Hammet reaction constant ρ_{ini} is determined from experiment as follows. Henckens et al. report[38] M_m values of DTC-polymers originating from both unsubstituted and OC_8-premonomers. Dividing Henckens' M_m values with the molar masses of the repeating units, mass averaged polymerization degrees (x_m) are obtained. Solely for determining the ρ_{ini} value, it is assumed that x_m scaled with k_p/k_{ini}:

$$\frac{x_m(H,H)}{x_m(OC_8,OC_8)} = \frac{\left(\frac{k_p(H,H)}{k_{ini}(H,H)}\right)}{\left(\frac{k_p(OC_8,OC_8)}{k_{ini}(OC_8,OC_8)}\right)} = \frac{10^{\rho_{ini}\cdot\sigma_t}}{10^{\rho_p\cdot\sigma_t}} = 10^{(\rho_{ini}-\rho_p)\sigma_t}$$

leading to

$$\rho_{ini} = \frac{1}{\sigma_t}\log\left(\frac{x_m(H,H)}{x_m(OC_8,OC_8)}\right) + \rho_p$$

The ρ_{ini} value found is 5.14 (Table 2). For DTC-MO, the initiation rate coefficient for the homopolymerization is $k_{ini}(OR,OR)_{u,u}$. For DTC-ODMO, the initiation rate coefficient for the homopolymerization is $k_{ini}(OR,OR)_{h,h}$.

The crossinitiation rate coefficients for the copolymerizations of DTC-MO with DTC-ODMO can be approximated by $k_{ini}(OR,OR)_{h,u}$. The crossinitiation rate coefficients for the copolymerizations of DTC with DTC-MO and DTC-ODMO are determined as the geometric means of already known initiation rate coefficients (Table 3 and 4). All initiation rate coefficients are then determined.

4.5. Results and discussion

First, we discuss the monomer formation via 1,6-elimination of DTC, DTC-MO, DTC-ODMO and DTC-MO-ODMO in pseudo-first order conditions allowing kinetic decoupling of the monomer and the (co)polymer formation. Next, kMC simulation results for the homopolymerization of the symmetric premonomers DTC, DTC-MO and DTC-ODMO are presented, followed by a discussion of the polymerization of the asymmetric premonomer DTC-MO-ODMO yielding MDMO-PPV. Good agreement with reported experimental yield, chain length and triad distribution of MDMO-PPV is demonstrated. Finally, copolymerizations starting from symmetric premonomers DTC, DTC-MO and DTC-ODMO are presented to illustrate the use of kinetic modeling to tune the copolymer triad distribution. It is demonstrated that copolymers starting from DTC-MO and DTC-ODMO can be designed with the same yield, initiator defect content and average chain length as MDMO-PPV, but characterized by a different triad distribution.

4.5.1. Monomer formation

The kinetics of the 1,6-elimination of DTC with K*t*BuO and LHMDS in THF is studied using UV-vis spectroscopy. Interference of polymerization reactions is avoided by using pseudo-first order conditions, i.e. low initial premonomer concentrations combined with excess amounts of base. Under these reaction conditions, the in situ formed *p*-quinodimethane monomer can be monitored. The Guggenheim[39,40] method is applied to extract the pseudo-first order 1,6-elimination rate coefficients $k_{E2,KtBuO}$(DTC) and $k_{E2,LHMDS}$(DTC) as explained in the next section.

The K*t*BuO induced 1,6-eliminaton of DTC in THF is followed with UV-vis spectroscopy and the Guggenheim method is applied at low reaction times to extract the pseudo-first order

rate coefficient from the log(A_t-$A_{t+\Delta t}$) plot (Figure 6). The reaction condition was $[HML]_0$ = 5 10^{-5} mol L^{-1} and $[KtBuO]_0$ = 5 10^{-3} mol L^{-1}, yielding $k_{E2,KtBuO}$ as (0.0485 s^{-1})/(0.005 mol L^{-1}) = 9.7 L mol^{-1} s^{-1}. Similar values for the 1,6-elimination in the sulfinyl[7,8] route are found to be 1.2 L mol^{-1} s^{-1} and 14 L mol^{-1} s^{-1}.[30,41]

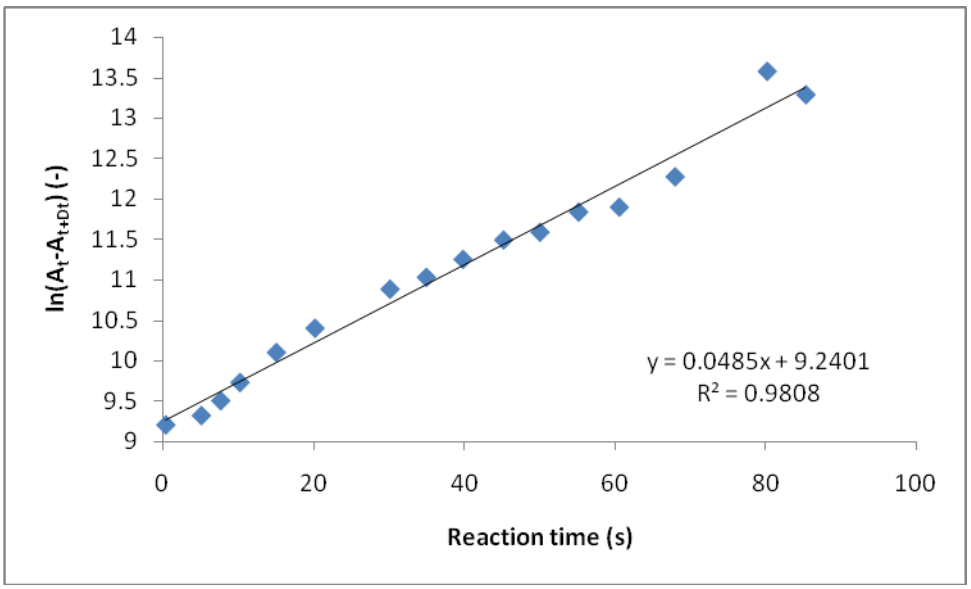

Figure 6: Guggenheim plot of absorbance A as a function of reaction time; The slope is the pseudo first order rate coefficient of the 1,6-elimination of DTC; Reaction condition: $[Premonomer]_0$ = 5 10^{-5} mol L^{-1} and $[KtBuO]_0$ = 5 10^{-3} mol L^{-1}, 308 K, solvent THF

A similar approach is followed to determine the 1,6-elimination kinetics of the LHMDS induced 1,6-elimination of DTC in THF, for two base concentrations, $[LHMDS]_0$ = 0.025 and 0.05 mol L^{-1} (Figure 7). The pseudo first order rate coefficient is found to be linearly depend on the base concentration, attesting to the first order dependency of the 1,6-elimination to the base. Constrained linear regression yields $k_{E2,LHMDS}$ as 18.2 L mol^{-1} s^{-1}, which is in line with the pKa,H_2O difference between KtBuO and LHMDS (resp. 19 and 36).

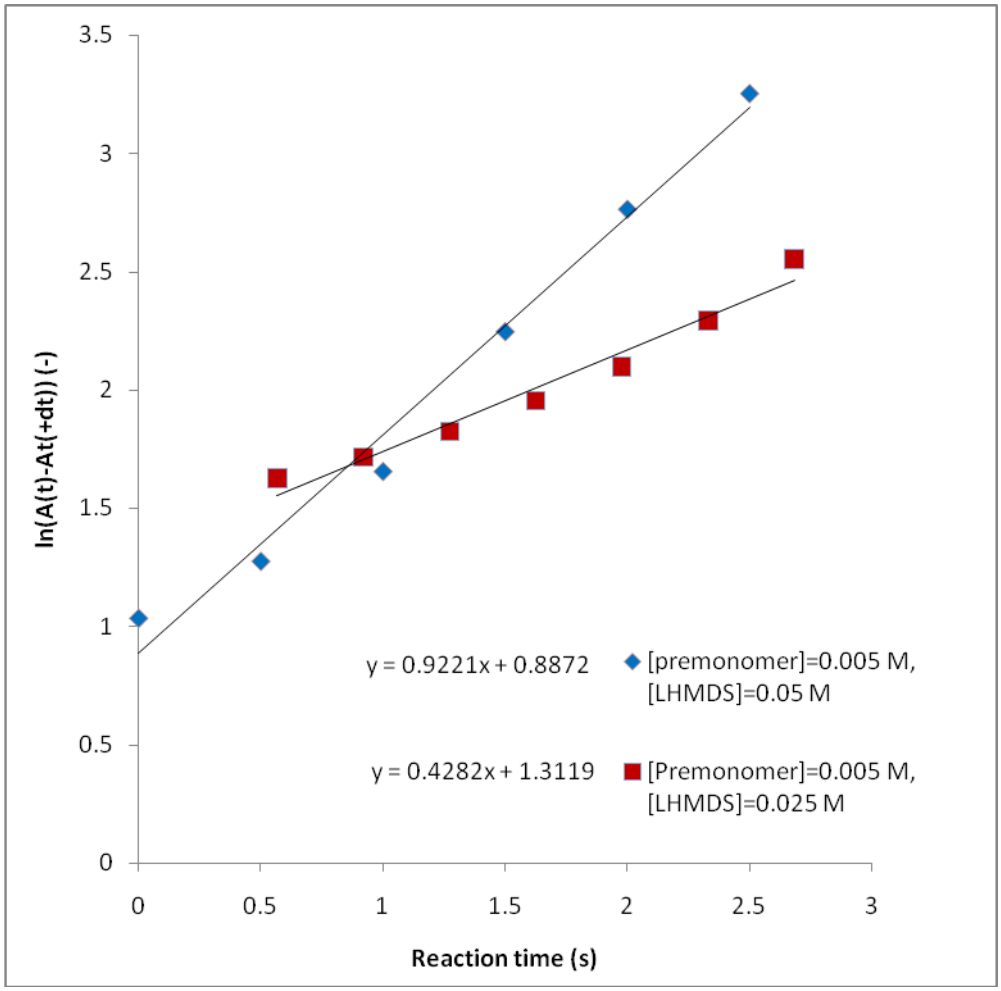

Figure 7: Guggenheim plot of absorbance A as a function of reaction time. The slopes are the pseudo first order rate coefficients of the 1,6-elimination of DTC; Reaction condition: $[Premonomer]_0$ = 0.005 mol L^{-1}, 308 K, solvent THF

Figure 8 shows the corresponding (pre)monomer yield under typical pseudo-first order conditions with the rate coefficients for initiation and propagation as discussed in the section about the determination of rate coefficients. It can be seen that the monomer is not consumed at such reaction conditions, implying a very low dimerization rate, which is in agreement with the UV-vis data. Clearly, LHMDS induces a faster elimination of DTC than K*t*BuO.

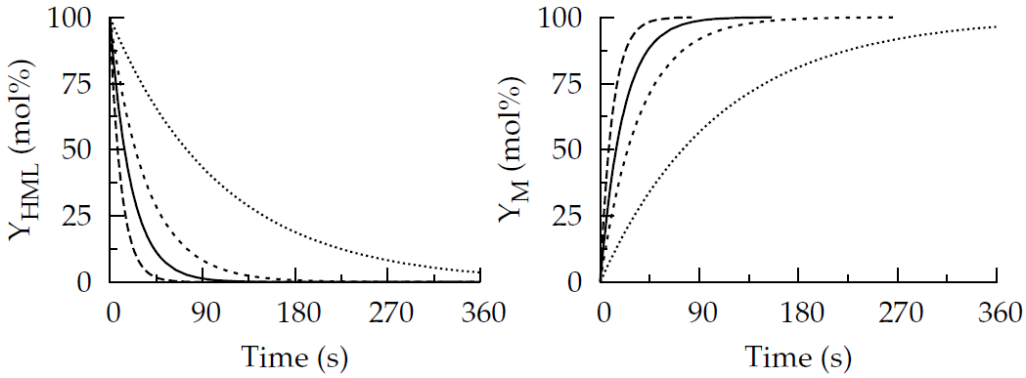

Figure 8: Simulated premonomer and monomer yield for DTC, DTC-MO and DTC-ODMO (see Figure 4) under pseudo-first order conditions: $[Base]_0 = 5\ 10^{-3}$ mol L^{-1} and $[Premonomer]_0 = 5\ 10^{-5}$ mol L^{-1}, 308 K, solvent THF; These initial concentrations are half of the values reported in the Experimental procedures, because a two-fold dilution occurs upon mixing the prepared base and premonomer solutions; ——— : KtBuO with DTC; - - - - - - : LHMDS with DTC; . . . . . : LHMDS with DTC-MO; ····· : LHMDS with DTC-ODMO

Figure 8 also shows the (pre)monomer yield for the LHDMS induced 1,6-elimination of DTC-MO and DTC-ODMO. For the determination of $k_{E2,LHMDS}$(DTC-MO) and $k_{E2,LHMDS}$(DTC-ODMO), UV-vis spectroscopy could unfortunately not be used, since the maximum of the absorption band of the alkoxy groups is too close to the maximum of the absorption band of the *p*-quinodimethane system. Therefore, approximate values as derived in the section about the Guggenheim method are used. Clearly, the presence of the electron donating OC_1 groups in DTC-MO decreases the 1,6-elimination rate as compared to DTC for the same LHMDS base. For the OC_{10} groups in DTC-ODMO, the same electronic effect is present but steric hindrance is now also operative and further decreases the LHMDS 1,6-elimination rate by approx. a factor 3.

Analogously, Figure 9 shows the simulation results for the monomer formation from DTC-MO-ODMO using approximate values for the rate coefficients as explained in the section about the determination of the rate coefficients. In this case, the asymmetric aromatic substitution leads to the formation of 2 isomeric *p*-quinodimethane monomers (**A**, **B**; see Figure 2). For K*t*BuO, these are formed in a 1:1 ratio due to low steric requirements. In contrast, for LHMDS the isomers are formed in a 3:1 ratio, due to a threefold reactivity

difference of the benzylic protons H_1 and H_2 (see Figure 2) for the regioselective abstraction by LHMDS, as explained in the section about the determination of the rate coefficients.

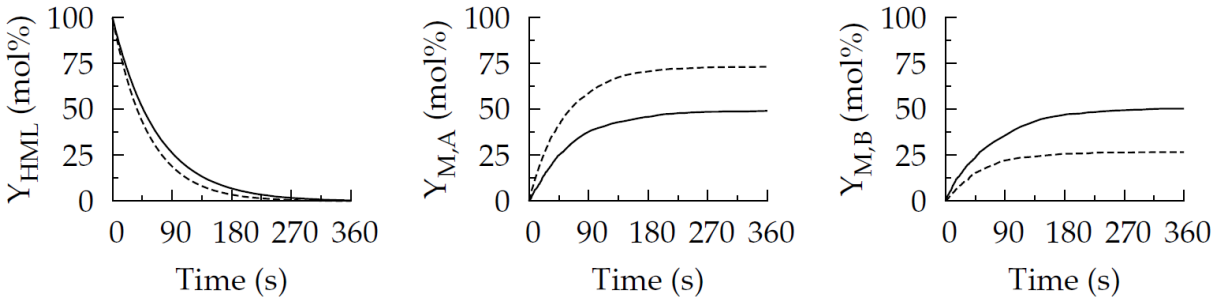

Figure 9: Simulated premonomer and monomer A and B yield of DTC-MO-ODMO (see Figure 4 and 5) under pseudo-first order conditions: $[Premonomer]_0 = 5\ 10^{-5}$ mol L^{-1} and $[Base]_0 = 5\ 10^{-3}$ mol L^{-1}, 308 K, solvent THF; ——— : KtBuO; - - - - - - : LHMDS

4.5.2. Homopolymerization

Figure 10 shows the simulated (pre)monomer yields and precursor polymer properties for the homopolymerizations of DTC, DTC-MO and DTC-ODMO for an initial base to premonomer ratio of 1.4. Although the fully conjugated homopolymer of DTC, which is obtained after the intramolecular elimination (see Figure 2), does not dissolve in THF, the synthesis of the precursor polymer from DTC is simulated to evaluate the influence of the presence of the OC_1 and OC_{10} substituents.

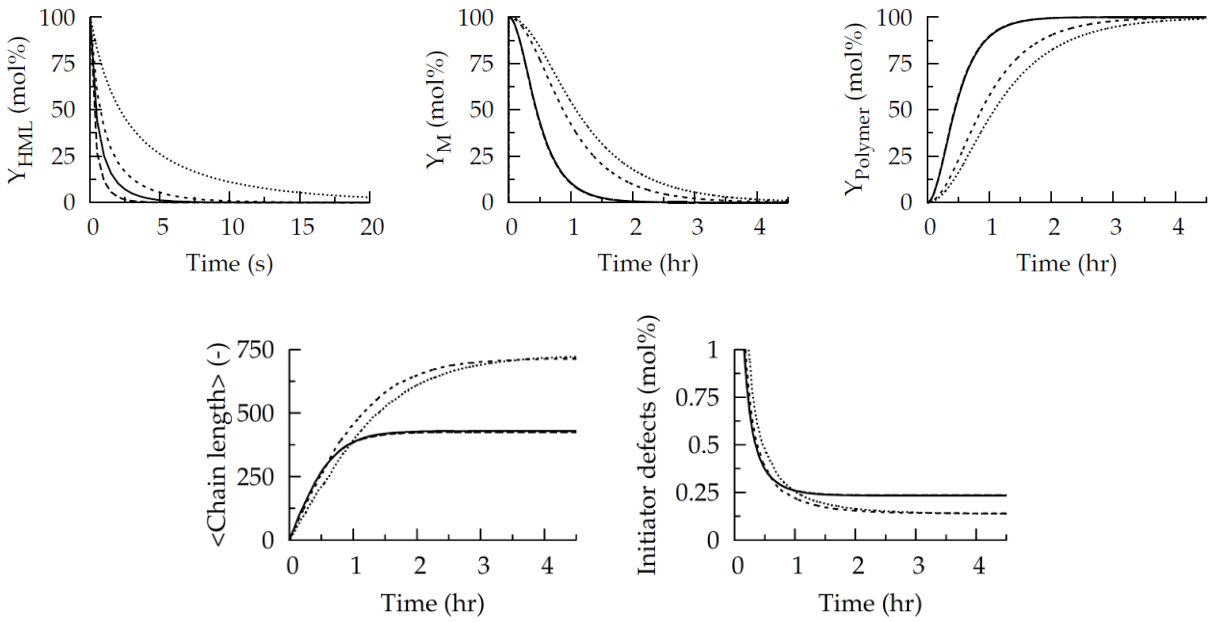

Figure 10: Simulated homopolymer yield and properties for homopolymerization of 1, 2 and 3 (see Figure 4) as a function of time; Reaction conditions[26]: $[Premonomer]_0$ = 0.154 mol L^{-1} and $[Base]_0$ = 0.22 mol L^{-1}, 308 K, solvent THF; The two simulations for 1 coincide in all plots except in the top left hand plot due to the different scaling of the x-axis; Molar mass of repeating units: 251, 311, 563 (resp. 1, 2, 3) g mol^{-1}; Initiator defect content is expressed per monomer unit; ——— : KtBuO with DTC; - - - - - - : LHMDS with DTC; . . . . . : LHMDS with DTC-MO; ····· : LHMDS with DTC-ODMO

For all four cases in Figure 10, the premonomer is consumed much faster than under pseudo-first order conditions, due to the higher initial concentrations used in polymer synthesis conditions. It takes approx. 5 seconds to reduce the premonomer yield of DTC-ODMO to 25% while in pseudo-first order conditions this requires some 135 seconds (Figure 8). Despite that the monomer is formed roughly two times faster when LHMDS instead of K*t*BuO is used, the polymer yield (top right hand plot in Figure 10) does not depend strongly on the base: almost identical polymerization rates are observed for DTC when using LHMDS and KtBuO. The limited influence of the base can be explained by the time scale of the 1,6-elimination being approx. 1800 times shorter than the time scale for polymerization: the premonomer half-life is approx. 1 s, while it takes about 0.5 hr for the monomer yield to decrease to 50%. The presence of the OC_1 groups in DTC-MO causes a large decrease of the polymerization rate. Steric hindrance exerted by the OC_{10} groups in DTC-ODMO decreases the polymerization rate even further.

The evolution of the average chain length with time shows an important influence of the electronic effect while the steric effect remains limited. After one hour, for the unsubstituted PPV an average chain length of approx. 375 is obtained while for the OC_1 and OC_{10} substituted PPVs an average chain length around 500 has already been reached. The final average chain length for DTC-MO and DTC-ODMO is approximately equal (750), which is markedly higher than the final average chain length for DTC (375). The steric effect of the length of the alkyl chain has however no significant influence on the final average chain length and only affects the time needed to reach it.

Figure 10 also shows that the initiator defect content decreases throughout the polymerization because the initiator defect content is highest when the average chain length is lowest. The initiator defect content is defined as the ratio of the number of initiation events to the sum of the number of initiation and propagation events.[31] The initiator defect content for DTC-MO and DTC-ODMO is approximately equal. A value of approx. 0.125 mol% is obtained, which is two times lower than the initiator defect content when using DTC.

4.5.3. MDMO-PPV synthesis

1,6-Elimination of the asymmetric premonomer DTC-MO-ODMO leads to the in situ formation of two isomeric *p*-quinodimethane monomers **A** and **B** (see Figure 2, the preferentially formed isomer is designated as "**A**"). MDMO-PPV synthesis from DTC-MO-ODMO thus constitutes a copolymerization. In general, head-to-tail coupling of the monomer units A and B can occur in 2 ways, creating four different types of environments for the methoxygroups in the conjugated MDMO-PPV, i.e. four types of conjugated triads can be distinguished (see Figure 1) To characterize the copolymer structure, the triad distribution of MDMO-PPV is simulated in addition to yield, chain length and initiator defect content.

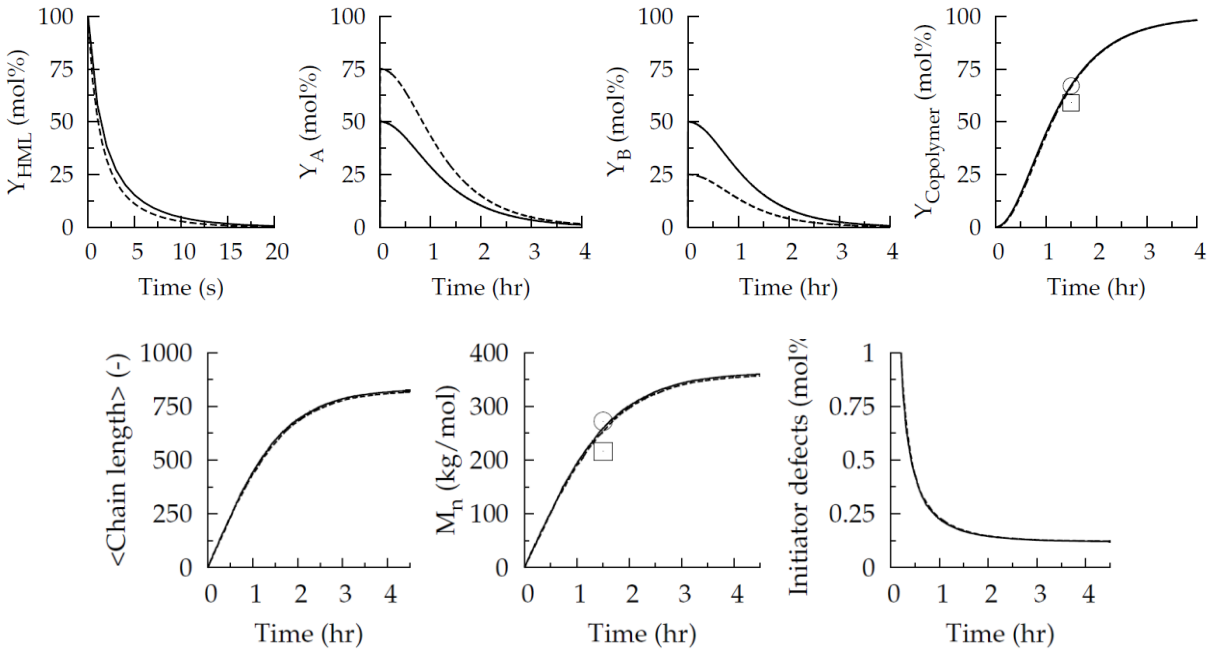

Figure 11: Simulated MDMO-PPV yield and properties as a function of time. Reaction conditions[26]: $[DTC\text{-}MO\text{-}ODMO]_0$ = 0.154 mol L^{-1} and $[Base]_0$ = 0.22 mol L^{-1}, 308 K, solvent THF; Experimental data are taken from (26); Molar mass of repeating unit: 437 g mol^{-1}; Initiator defect content is expressed per monomer unit; ——— : KtBuO; - - - - - - : LHMDS; □: KtBuO; ○: LHMDS

Figure 11 compares the K*t*BuO and LHMDS induced polymerization of DTC-MO-ODMO. Only a small effect of the base on the 1,6-elimination is observed. The monomer yield profiles show, that isomers **A** and **B** are formed and consumed in a 1:1 ratio when K*t*BuO is used, while they are formed and consumed in 3:1 ratio when LHMDS is the base. Despite the large difference in isomer concentrations due to the regioselectivity of the LHMDS induced 1,6 elimination, the copolymer yields do not strongly depend on the base, in agreement with experimental data.[26] A similar insensitivity to the base is seen for the average chain length and the initiator defect content, which is related to the approx. 1200 times shorter time scale for 1,6-elimination than for polymerization: the half-life of the premonomer is approx. 3 seconds, while it takes about 1 hr for the total monomer yield to decrease by 50% after premonomer consumption. The final average chain length is about 800 and the final initiator defect content 0.12 mol%, which are very similar values compared to those for the structurally related homopolymerizations of DTC-MO and DTC-ODMO under the same reaction conditions; a final average chain length of 750 and a final initiator defect content of 0.13 mol% are again obtained (Figure 11).

The effect of the regioselectivity of LHMDS induced 1,6-elimination on the monomer yield profiles is reflected in the triad distribution of MDMO-PPV as shown in Table 5.

Table 5: Simulated and experimental conjugated triad distribution in MDMO-PPV[a]

	K*t*BuO		LHMDS	
	Experiment	simulated	Experiment	simulated
BBA+BAA	22	25.0	20	18.7
BAB+ABA	25	24.7	17	18.6
AAA+BBB	27	25.3	47	44.1
AAB+ABB	26	24.9	16	18.7

[a]Experimental data taken from [26]. Reaction condition[26]: $[Premonomer]_0$ = 0.154 mol L^{-1} and $[Base]_0$=0.22 mol L^{-1}, 308 K. THF as solvent.

In agreement with the experimental observations, when K*t*BuO is used as the base, values for all 4 triad fractions close to 25% are obtained. Clearly, with K*t*BuO both isomeric p-quinodimethane monomers A and B are randomly incorporated and, hence, it can be concluded that K*t*BuO does not show a preference for abstraction of one of the benzylic protons in DTC-MO-ODMO. In contrast, with the more voluminous LHMDS, there is a significant preference for incorporation of monomer **A** as evidenced by the steep decline of monomer **A** and this is reflected in the high regioregular triad fraction (45% with the AAA fraction being 43% and the BBB fraction 2%, see Table 6).

Table 6: Simulated precursor triad distribution in MDMO-PPV[a]

	K*t*BuO	LHMDS
BAA	12.5	14.0
BBA	12.5	4.7
ABA	12.4	13.9
BAB	12.4	4.6
AAA	12.7	42.5
BBB	12.6	1.6
ABB	12.4	4.7
AAB	12.5	14.0

[a]Reaction condition[26]: $[Premonomer]_0$ = 0.154 mol L^{-1} and $[Base]_0$=0.22 mol L^{-1}, 308 K, solvent THF. This table reduces to Table 1 when grouping the triads as indicated in Figure 1.

The steric hindrance between LHMDS and the large OC_{10} substituent results in the preferred abstraction of a proton in the least sterically hindered position in DTC-MO-ODMO leading to the preferred formation of monomer A (Figure 2). Hence, the simulation data in Table 5 strongly support the suggestion of Vandenbergh et al.[26] that the LHMDS induced regioregularity in MDMO-PPV mainly originates from a difference in the 1,6-elimination reactivity of the H_1 and H_2 protons in DTC-MO-ODMO (see Figure 2). As mentioned in the section on the monomer formation, the sterically unhindered H_1 protons are approx. 3 times more reactive for 1,6-elimination than the sterically hindered H_2 protons.

The findings for the two bases K*t*BuO and LHMDS can be generalized to a variable 1,6-elimination relative reactivity of the hindered and unhindered benzylic protons in DTC-MO-ODMO by performing simulations for different values of f_s, which is defined as the ratio of the rate coefficient for abstraction of the sterically unhindered proton H_1 to the rate coefficient for abstraction of the sterically hindered proton H_2. When the time scale of 1,6-elimination is much shorter than the time scale for polymerization, the premonomer is consumed completely before any polymerization occurs and the triad distribution only depends on the value of f_s. The remaining rate coefficients used for these simulations retain their original values given in the section about determination of rate coefficients (Tables 1, 3 and 4).

The results of such simulations are presented in Figure 11 at complete conversion. For f_s = 1 (no regioselectivity) and f_s = 3 (strong hindrance), the triad distributions corresponding to the K*t*BuO and, respectively, LHMDS induced polymerization are obtained. In the limiting case of highly sterically hindered bases and/or even more bulky substituents, a homopolymer results, i.e. the unhindered protons H_1 (Figure 2) are selectively abstracted, forming monomer **A** only leading to a triad fraction AAA of 100%. A broad range of degrees of regioregularity can be obtained for intermediate f_s values. However, in practice it is difficult to have such a range of bases readily available.

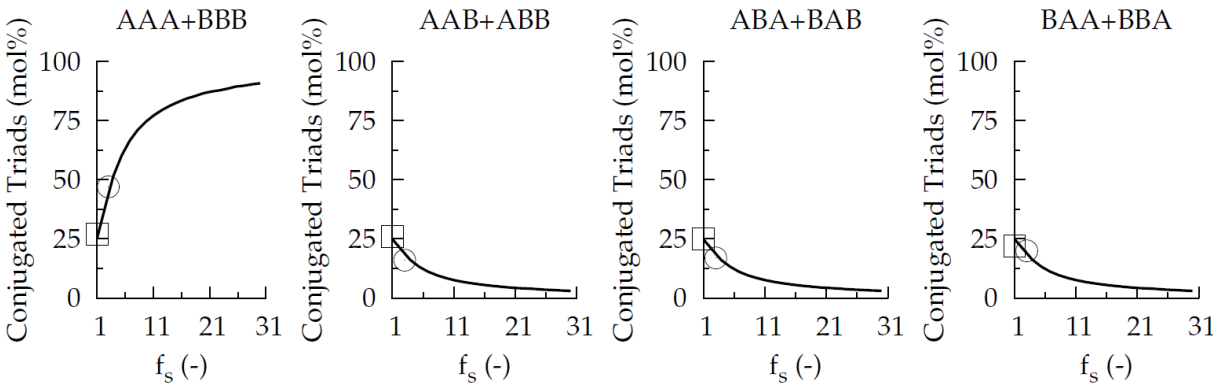

Figure 12: Conjugated triad distribution in MDMO-PPV as a function of the ratio f_s. f_s is a regioselectivity factor defined as the ratio of the rate coefficient for abstraction of the sterically unhindered proton H_1 to the rate coefficient for abstraction of the sterically hindered proton H_2. The rate coefficient for abstraction of the sterically unhindered proton H_1 is taken from paragraph 4.4.1 (Table 1, 1.40 L mol^{-1} s^{-1}) while the rate coefficient for abstraction of the sterically hindered proton H_2 is varied from 0.047 to 1.40 L mol^{-1} s^{-1} (corresponding to a 31:1 f_s ratio). Reaction condition[26]: [DTC-MO-ODMO]$_0$ = 0.154 mol L^{-1} and [Base]$_0$=0.22 mol L^{-1}, 308 K, solvent THF. Markers indicate experimental data reported in (26); □: KtBuO; ○: LHMDS

A more convenient method to control the triad distribution of poly(2,5-dialkoxy-1,4-phenylene vinylene)s consists of the polymerization of mixtures of symmetric premonomers. This approach allows to perform copolymerizations starting with variable initial ratios of the two premonomers instead of starting from a single asymmetric premonomer and varying the base to achieve the required ratio of the two comonomers by in situ 1,6-elimination. Therefore, the formation of poly(2,5-dialkoxy-1,4-phenylene vinylene)s via

copolymerizations of the symmetrical premonomers DTC, DTC-MO and DTC-ODMO is studied.

4.5.4. Copolymerization of symmetric premonomers

As outlined in the introduction, the copolymerization of isomeric premonomers is of particular relevance to obtain variable regioregularity.[22,23] MDMO-PPV with a composition of **A**:**B** = 30:70 (A; B see Figure 5) showed a hole mobility approximately 3.5 times larger than the regiorandom MDMO-PPV, at all measured electric fields. However, polymer yields and chain length as a function of the initial premonomer composition do not show a clear trend[23] and hence the effect of the initial premonomer composition is unknown. Kinetic modeling shows a clear trend in yield, chain length and triad distribution.

Figure 13 shows the simulation results for the copolymerizations of DTC with DTC-MO (left), DTC with DTC-ODMO (middle) and DTC-MO with DTC-ODMO (right) as a function of time and the initial premonomer composition $f_{HML,A} = [HML,A]_0/([HML,A]_0+[HML,B]_0)$, with **A** the first mentioned premonomer in the above series. Note that for these copolymers, the triads in the copolymers are defined based on the side chain of the monomer unit (see Appendix L). E.g. in copoly(DTC-MO)-(DTC-ODMO), each monomer A in a triad contains 2 OC_1 groups while each monomer B in a triad contains 2 OC_{10} groups. In contrast, for the earlier MDMO-PPV, Vandenbergh et al.[26] defined the triads based on the orientation of a side chain with respect to the previous monomer unit while each monomer unit in the triad has one OC_1 and one OC_{10} group, although with a possibly different orientation. From top to bottom in Figure 13, the yields of both premonomers, comonomers and the copolymer are presented.

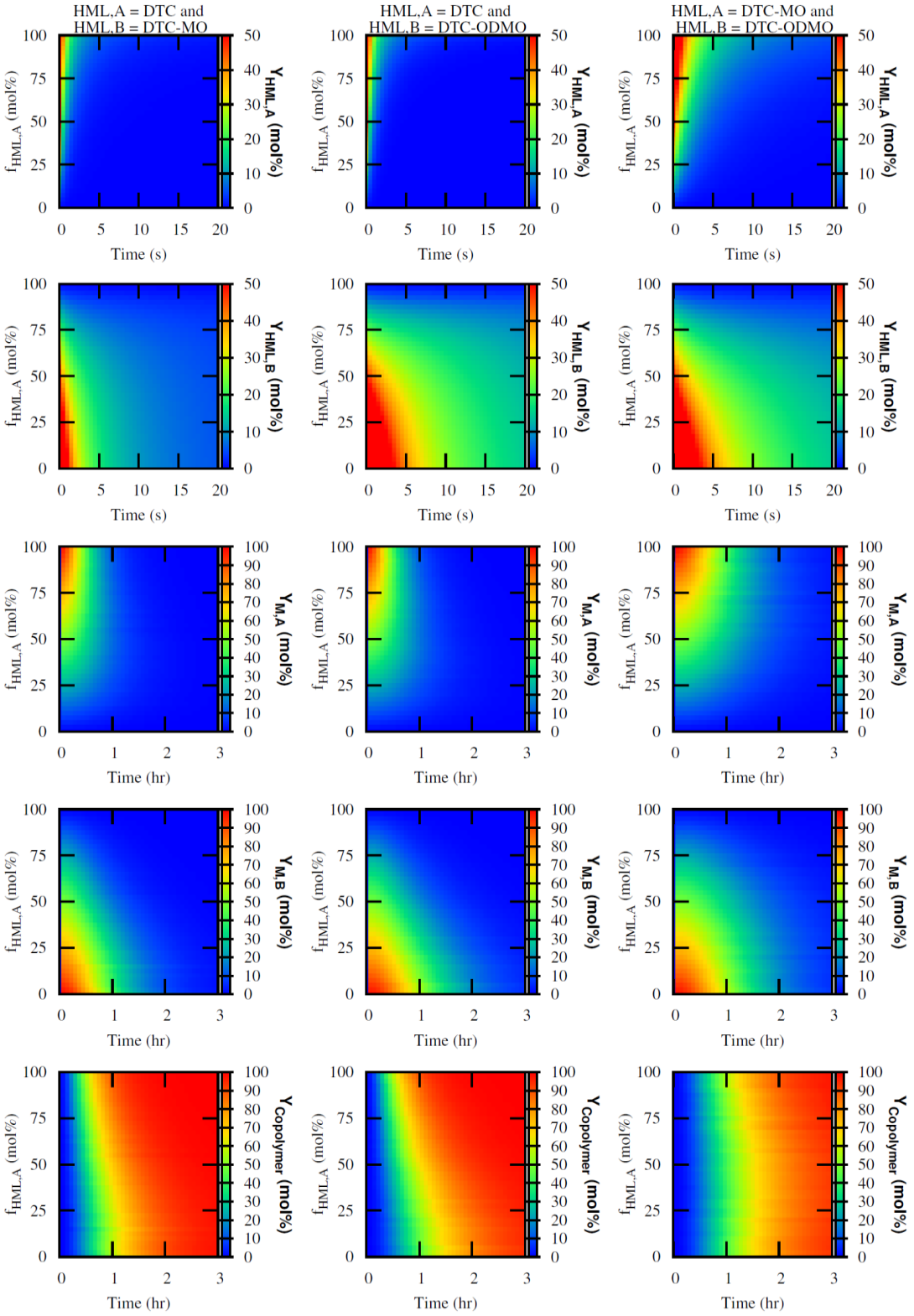

Figure 13: Yields as a function of time and initial premonomer composition of the copolymerizations of: left: DTC with DTC-MO, center: DTC with DTC-ODMO, right: DTC-MO with DTC-ODMO (see Figure 4); Reaction condition: $[HML,A]_0+[HML,B]_0 = [LHMDS] = 0.154$ mol L^{-1}, 308 K, solvent THF; $f_{HML,A}$ is defined as $[HML,A]_0/([HML,A]_0+[HML,B]_0)$

It can be seen that, as before, all premonomers are consumed completely and monomer yields of 100% are obtained before any polymerization occurs. For all three copolymerizations, the comonomer that is formed mostly is the one that is derived from the premonomer that is predominantly present in the initial premonomer mixture. For the two copolymerizations involving DTC, the copolymerization proceeds faster with increasing initial content of DTC. If DTC-MO is copolymerizing with DTC-ODMO, the polymer yield does not depend much on the initial premonomer composition as both premonomers possess alkoxy groups. In this case, it takes about 1 hr for the total monomer yield to decrease to 50% after premonomer consumption, as evidenced by the green region in the copolymer yield at that time. Note that this time is almost identical to the time needed for the MDMO-monomer yield to decrease to 50% in the earlier discussed MDMO-PPV formation from DTC-MO-ODMO (Figure 11). Moreover, the copolymer yield versus time profiles over the entire range of initial premonomer compositions are very similar to the one observed for MDMO-PPV. It will be shown in the next paragraph that also the properties of copoly(DTC-MO)-(DTC-ODMO) and MDMO-PPV are very similar.

Figure 14 shows, for the same 3 copolymerizations, from top to bottom, the average chain length, the initiator defect content and the conjugated triad fraction of the AAA + BBB type as a function of time and the initial premonomer composition.

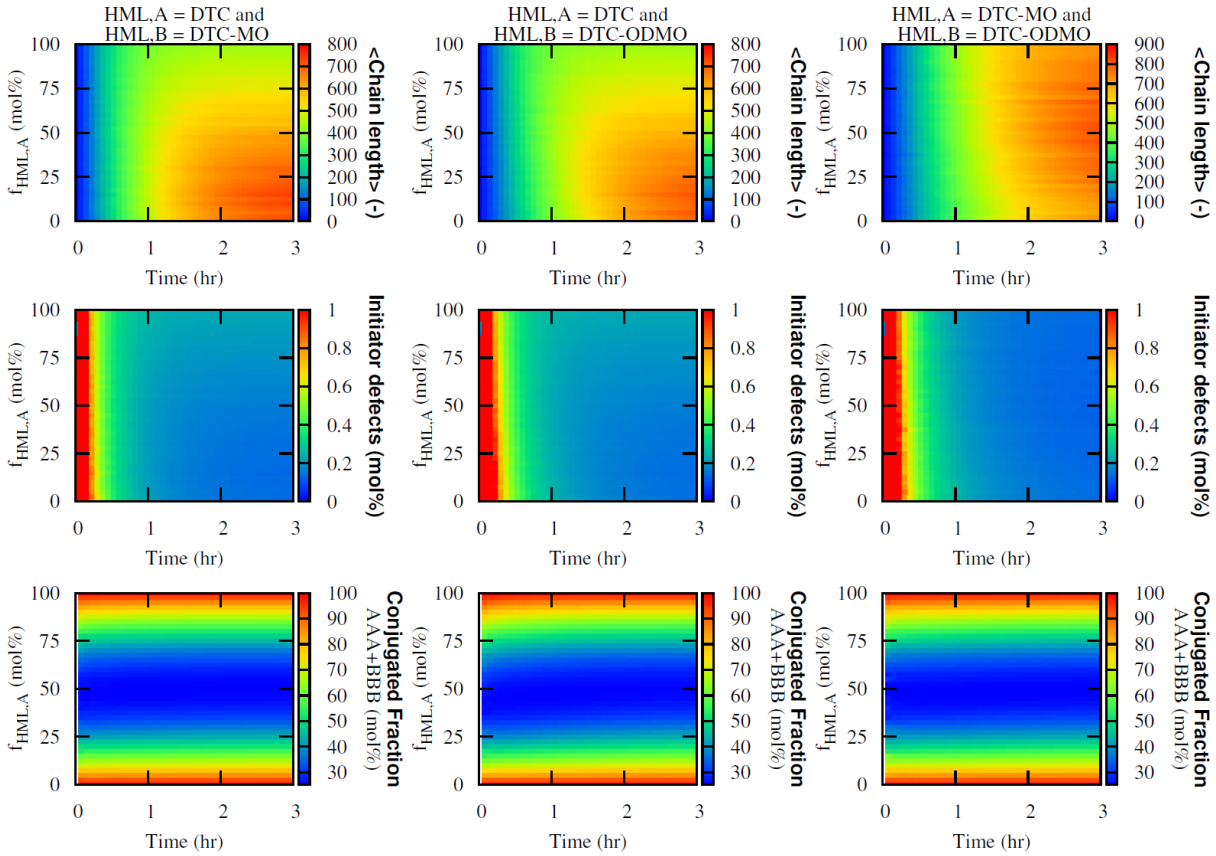

Figure 14: Properties as a function of time and initial premonomer composition of the copolymerizations of: left: DTC with DTC-MO, center: DTC with DTC-ODMO, right: DTC-MO with DTC-ODMO (see Figure 4); Reaction condition: $[HML,A]_0+[HML,B]_0 = [LHMDS]_0 = 0.154$ mol L^{-1}, 308 K, solvent THF; $f_{HML,A}$ is defined as $[HML,A]_0/([HML,A]_0+[HML,B]_0)$; Initiator defect content is expressed per monomer unit

For the two copolymerizations involving DTC, significantly lower average chain lengths are obtained when a higher initial content of the unsubstituted premonomer DTC is used. For instance, the average chain length at complete conversion (i.e. after 3 hrs.) of copoly(DTC)-(DTC-MO) decreases from 700 for an initial content of 25% of DTC to 500 for an initial content of 75% of DTC while for the homopolymerization of DTC-MO the final average chain length amounts to 750. If DTC-MO is copolymerized with DTC-ODMO, the profile of the average chain length versus time is rather insensitive to the initial premonomer ratio. Moreover, for the entire range of initial premonomer compositions, the evolution of the average chain lengths with time is very similar to that observed for MDMO-PPV (Figure 11). At complete conversion, the observed average chain lengths amount to about 800. A similar value was observed previously for MDMO-PPV (Figure 11).

In all three copolymerizations, the initiator defect content is higher than 1 mol% in the early stages of the polymerization and decreases as the polymerization proceeds. At the start of the polymerization, the chains are very short and each chain contains an initiation defect, as explained before. Note that the final initiator defect contents are comparable with the initiator defect content of MDMO-PPV since values between 0.13 and 0.25 mol% are obtained.

Figure 14 further illustrates that block-like copolymers are obtained when one of the premonomers is abundantly present in the initial premonomer mixture, as evidenced by the high AAA+BBB triad fractions in this region. In contrast, random copolymers (and corresponding triad fractions of the AAA+BBB types around 25%) are found when the initial premonomer mixture contains a substantial fraction of both premonomers.

In particular, it can be seen that when the initial premonomer mixture consists of 75% premonomer A, the AAA+BBB triad fraction is about 44% with the AAA fraction being 42.5% and the BBB fraction equal to 1.5%, which is almost identical to the regioregular triad fraction as obtained when reacting LHMDS with DTC-MO-ODMO (Table 1). The converse initial premonomer composition also yields a 44% triad fraction of the AAA+BBB type, but with the AAA fraction being 1.5% and the BBB fraction 42.5%. These two triad distributions indicate degrees of randomness/blockyness of copoly(DTC-MO)-(DTC-ODMO) similar to LHMDS synthesized MDMO-PPV. However, as noted previously, the AAA and BBB triads in copoly(DTC-MO)-(DTC-ODMO) are not structurally identical to the regioregular triads in MDMO-PPV, due to the different molecular structures of the corresponding monomers **A** and **B**. The similarities between copoly(DTC-MO)-(DTC-ODMO) and MDMO-PPV in average chain length, yield, defects and triad microstructure are related to the fact that the initial premonomer mixture of [DTC-MO]:[DTC-ODMO] = 75:25 mimicks the difference in reactivity of the benzylic protons H_1 and H_2 in DTC-MO-ODMO for LHMDS induced in situ 1,6-elimination. However, a difference in aggregation behavior can be expected between MDMO-PPV and copoly(DTC-MO)-(DTC-ODMO) due to the difference in molecular structure: with increasing amount of OC_{10} groups, Van der Waals forces increase and chain stacking behavior is expected to improve.

Concluding, these findings imply that copolymerization of DTC-MO and DTC-ODMO (with [DTC-MO]:[DTC-ODMO] = 75:25 or 25:75) can be used to synthesize copoly(DTC-MO)-

(DTC-ODMO) with similar yield, average chain length, defects and triad microstructure as MDMO-PPV. In addition, by varying the initial premonomer ratio [DTC-MO]:[DTC-ODMO], the triad distribution of the resulting copolymers can be varied in a broad range from random to blocky, with the yield, average chain length and initiator defect content remaining similar to those of MDMO-PPV.

4.6. Conclusions

To understand LHMDS-induced regioregularity in MDMO-PPV via the DTC route, monomer formation kinetics are decoupled from polymerization allowing to study the influence of the the electronic and steric effects of the methoxy and the bulky 3,7-dimethyloctyloxy group on both the monomer formation and the polymerization. The presented kMC model allows to simulate the reported effect of the LHMDS induced regioselectivity in the 1,6-elimination on the yield, average chain length and the resulting triad distribution in MDMO-PPV synthesis via the DTC route. Based on the understanding of how the base and the electronic and steric effects influence the MDMO-PPV reaction sequence, a convenient method is proposed to achieve a broad range of triad distributions for PPVs. Copolymerization of mixtures of the symmetric premonomers DTC-MO and DTC-ODMO allow mimicking the yield, average chain length and initiator defect content of MDMO-PPV whilst varying the triad distribution and influencing the chain stacking behavior of the PPV.

References

1. Burroughes, J.; Bradley, D.; Brown, A.; Marks, R.; Friend, R.; Holmes A. *Nature* **1990**, 347, 539-541.
2. Friend, R.; Gymer, R.; Holmes, A.; Burroughes, J.; Marks, R.; Taliani, C.; Bradley, D.; Dos Santos, D.; Bredas, J.; Logdlund, M.; Salaneck W. *Nature* **1999**, 397, 121-128.
3. Meier, H. *Angew. Chem.* **1992**, 104, 1425-1426.
4. Hide, F.; Diaz-Garcia, M. A.; Schwartz, B. J.; Heeger, A. J. *Acc. Chem. Res.* **1997**, 30, 430-436.
5. McGehee, M. D.; Heeger, A. J. *Adv. Mater.* **2000**, 12, 1655-1668.
6. Petty, M. C.; Bryce, M. R.; Bloor, D., editors. *Introduction to molecular electronics.* London: Edward Arnold; 1995.
7. Loutfy, R. O.; Hor, A. M.; Hsiao C. K.; Baranyi, G.; Kazmaier, P. *Pure Appl. Chem.* **1988**, 60, 1047-1054.

8. Nalwa, H.S., editor. *Nonlinear optics of organic molecules and polymers*. New York: CRC; 1997.
9. Feringa, L.; Jager, W. F.; de Lange, B. *Tetrahedron* **1993**, 49, 8267-8310.
10. Mozer, A. J.; Denk, P.; Scharber, M. C.; Neugebauer, H.; Sariciftci, N. S.; Wagner, P.; Lutsen, L.; Vanderzande, D. *J. Phys. Chem. B* **2004**, 108, 5235-5242.
11. van Breemen, A. J. J. M.; Herwig, P. T.; Chlon, C. H. T.; Sweelsen, J.; Schoo, H. F. M.; Benito, E. M.; de Leeuw, D. M.; Tanase, C.; Wildeman, J.; Blom, P. W. M. *Adv. Funct. Mater*. **2005**, 15, 872-876.
12. Breban, L.; Lutsen, L.; Vanhoyland, G.; D'Haen, J.; Manca, J.; Vanderzande, D. *Thin Solid Films* **2006**, 511-512, 695.
13. Chen, S. H.; Su, A. C.; Han, S. R.; Chen, S. A.; Lee, Y. Z.; *Macromolecules* **2004**, 37, 181-186.
14. Peeters, E.; Delmotte, A.; Janssen, R. A. J.; Meijer, E. W. *Adv. Mater.* **1997**, 9, 493-496.
15. Kemerink, M.; van Duren, J. K. J.; Jonkheijm, P.; Pasveer, W. F.; Koenraad, P. M.; Janssen, R. A. J.; Salemink, H. W. M.; Wolters, J. H. *Nano Lett.* **2003**, 3, 1191-1196.
16. Tajima, K. Tajima; Suzuki, Y.; Hashimoto, K. *J. Phys. Chem. C* **2008**, 112, 8507-8510.
17. Mozer, A. J.; Denk, P.; Scharber, M. C.; Neugebauer, H.; Sariciftci, N. S.; Wagner, P.; Lutsen, L.; Vanderzande, D.; Kadashchuk, A.; Staneva, R.; Resel, R. *Synth. Met.* **2005**, 153, 81-84.
18. Pan, M.; Bao, Z. N.; Yu, L. P. *Macromolecules* **1995**, 28, 14, 5151-5153.
19. Liu, Y. B.; Lahti, P. M.; La, F. *Polymer* **1998**, 39, 5241-5244.
20. Lutsen, L. J.; Van Breemen, A. J.; Kreuder, W.; Vanderzande, D. J. M.; Gelan, J. M. J. V. *Helv. Chem. Acta.* **2000**, 83, 3113-3121.
21. Lutsen, L.; Adriaensens, P.; Becker, H.; Van Breemen, A. J.; Vanderzande, D.; Gelan, J. *Macromolecules* **1999**, 32, 6517-6525.
22. Mozer, A. J.; Denk, P.; Scharber, M. C.; Neugebauer, H.; Sariciftci, N. S.; Wagner, P.; Lutsen, L.; Vanderzande D.; Kadashchuk, A.; Staneva, R.; Resel, R. *Synth. Met.* **2005**, 153, 81-84.
23. Mozer, A. J.; Denk, P.; Scharber, M. C.; Neugebauer, H.; Sariciftci, N. S.; Wagner, P.; Lutsen, L.; Vanderzande, D. *J. Phys. Chem. B* **2004**, 108, 5235-5242.
24. Wu, P.-T.; Ren, G.; Jenekhe, S. A. *Macromolecules* **2010**, 43, 3306-3313.

25. Zhang, C.; Sun, J.; Li, R.; Sun S.-S.; Lafalce, E.; Jiang, X. *Macromolecules* **2011**, 44, 6389-6396.
26. Vandenbergh, J.; Wouters, J.; Adriaensens, P. J.; Mens, R.; Cleij, T. J.; Lutsen, L.; Vanderzande, D. J. M. *Macromolecules* **2009**, 42, 11, 3661-3668.
27. Schwalm, T.; Wiesecke, J.; Immel, S.; Rehahn, M. *Macromol. Rapid Commun.* **2009**, 30, 1295-1322.
28. Junkers, T.; Vandenbergh, J.; Adriaensens, P.J.; Lutsen, L.; Vanderzande, D. *Polym. Chem.* **2012**, 3, 275-285.
29. Henckens, A.; Duyssens, I.; Lutsen, L.; Vanderzande, D.; Cleij T.J. *Polymer* **2006**, 47, 123-131.
30. Hermosilla, L.; Catak, S.; Van Speybroeck, V.; Waroquier, M.; Vandenbergh, J.; Motmans, F.; Adriaensens, P.; Lutsen, L.; Cleij, T.; Vanderzande, D. *Macromolecules* **2010**, 43, 18, 7424-7433.
31. Van Steenberge, P.; Vandenbergh, J.; D'hooge, D. R.; Reyniers, M.-F.; Adriaensens, P. J.; Lutsen, L.; Vanderzande, D. J. M.; Marin, G. B. *Macromolecules* **2011**, 44, 8716-8726.
32. Cho, B. R. *Prog. Polym. Sci.* **2002**, 27 (2), 307-355.
33. Cho, B. R.; Kim, T. H.; Son, K. H.; Kim, Y. K.; Lee, Y. K.; Jeon, S. J. *Macromolecules* **2000**, 33 (22), 8167-8172.
34. Cho, B. R. *Prog. Polym. Sci.* **2002**, 27 (2), 307-355.
35. Cho, B. R.; Kim, T. H.; Son, K. H.; Kim, Y. K.; Lee, Y. K.; Jeon, S. J. *Macromolecules* **2000**, 33 (22), 8167-8172.
36. Hansch, C.; Leo, A.; Taft, R. W. *Chem. Rev.* **1991**, 91, 2, 165-195.
37. Qiu, J.; Matyjaszewski, K. *Macromolecules* **1997**, 30, 5643-5648.
38. Henckens, A.; Duyssens, I.; Lutsen, L.; Vanderzande, D.; Cleij T. J. *Polymer* **2006**, 47, 123-131.
39. Frost, A. A.; Pearson, R. G., editors. *Kinetics and Mechanism*. Tokyo: Wiley; 1961.
40. Fleck, G., editor. *Chemical Reactions and Mechanisms*. New York: Holt, Rinehart and Winston, Inc.; 1971.
41. Pyun, S. Y.; Kim, W. G.; Jeong, J.-H.; Cho, B. R. *Bull. Korean Chem. Soc.* **2008**, 29, 2453-2458.

Chapter 5: Linear gradient quality of ATRP copolymers

Summary

The linear gradient quality and the control over chain length and end-group functionality in the copolymerization of acrylates and methacrylates via atom transfer radical polymerization (ATRP) were evaluated by detailed kinetic Monte Carlo simulations with individual tracking of macromolecules. In all simulations, diffusional limitations on termination were taken into account. The linear gradient quality is characterized by a linear gradient deviation <GD>. For a <GD> value of 0.06 or lower, the linear gradient quality is defined as excellent, whereas for <GD> values higher than 0.25 gradient copolymers of poor quality are formed (targeted chain length (TCL) = 100). Under batch ATRP conditions, using a catalytic system consistent with Cu(I)Br/PMDETA (PMDETA = N,N,N',N'',N''-pentamethyldiethylenetriamine (PMDETA) an excellent control over chain length and end-group functionality is possible and copolymers with a good linear gradient quality at final conversion can be prepared with an appropriate ATRP catalytic system. Moreover for sufficiently high conversions, a linear correlation exists between <GD> and the polydispersity index (PDI), allowing an approximate assessment of the linear gradient quality based on PDI. This linear correlation depends on the TCL. For higher TCL lower <GD> values are obtained for a given PDI. This work has been published in *Macromolecules* **2012**, 45, 8519-8531.

5.1. Introduction

Controlled radical polymerization (CRP) techniques allow the synthesis of well-defined macromolecules with predetermined chain length, low polydispersity index (PDI), high end-group functionality and controlled topology.[1, 2] In contrast to conventional free radical polymerization (FRP), in CRP, radicals are temporarily deactivated to a dormant form by a mediating agent. As illustrated in Scheme 1, in atom transfer radical polymerization (ATRP),[3-9] one of the most often used CRP techniques, this activation/deactivation process is catalyzed by a transition metal complex. For appropriately chosen transition metal complexes and polymerization conditions, all dormant polymer chains can grow concurrently and the impact of termination reactions is minimal, allowing the facile incorporation of end-group functionality X, i.e. most of the macromolecules are dormant instead of dead. If initiation and exchange reactions between the dormant and active form are fast, the polymers are characterized by a low PDI.

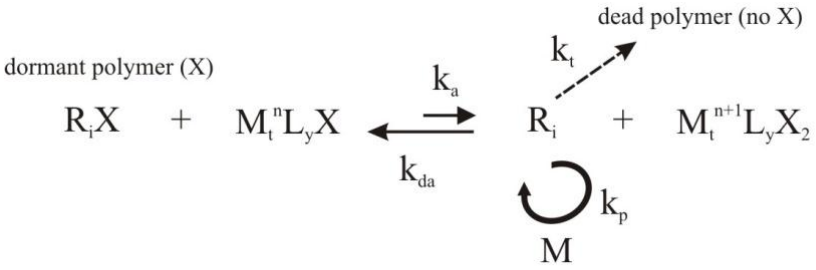

Scheme 1: Principle of ATRP; M_t: transition metal; L: ligand; X: halogen atom; n: oxidation state; M: monomer; $k_{a,da,p,t}$: rate coefficient for activation, deactivation, propagation, termination; ATRP initiator R_0X; i: chain length; $K_{eq} = k_a/k_{da}$

ATRP is a powerful polymerization technique for the synthesis of block and gradient copolymers.[2, 10-12] Block copolymers ($M_1 \ldots M_1M_2 \ldots M_2$) can be efficiently prepared if the first block is synthesized with high end-group functionality, followed by efficient cross-propagation after addition of the second monomer. The latter requires appropriate selection of the comonomers and can be enhanced by halogen exchange processes.[13, 14] In contrast to the sharp transition of composition observed in block copolymers, gradient copolymers exhibit a gradual shift in the copolymer composition from one chain end to the other. They can be obtained if activation-growth-deactivation cycles are efficient and if the rate of incorporation of one comonomer progressively increases, as dictated by either reactivity ratios or monomer feed.[11] In a controlled ATRP, a concurrent growth of essentially all macromolecules takes place during the entire reaction time, implying the flexibility to obtain intramolecular

heterogeneity of the copolymer composition.[15] In contrast, in FRP, intermolecular heterogeneity results because of the slow initiation and absence of intermittent activation-growth-deactivation cycles. In the absence of a mediating agent, an entire (dead) polymer chain is formed in a short time, ca. 1 s, compared to the total reaction time (> 1 h). Hence, the final reaction mixture contains polymer molecules obtained at different reaction times, which explains why FRP cannot be used to create gradient copolymers.

Several experimental[11, 16-19] and kinetic modeling studies[15, 20-26] were reported in which the influence of copolymerization conditions on the monomer sequence and, hence, the copolymer properties was investigated in CRP processes. It was shown that copolymer composition drift can exist under both homogeneous and heterogeneous ATRP batch conditions[11, 19, 27] and a semi-batch approach can be beneficial.[15, 21, 28, 29] For example, simulations based on the method of moments and the kinetic Monte Carlo (kMC) technique showed that semi-batch ATRP allows to optimize the comonomer feed rates to achieve a desired overall copolymer composition.[15, 21] However, in these modeling studies the copolymer composition was not explicitly tracked.

Recently, using more advanced kMC simulations, the kinetics of segment formation in nitroxide mediated polymerization (NMP) were studied.[22-24] In those studies, every polymer chain was represented by a sequence of segment lengths, e.g. the 'polymer' chain 'ABBAAAB' was recorded as '1231'. It was proposed that if the transient radical life time is too short, segment formation can be controlled by deactivation, instead of selective preference during propagation. However, an explicit evaluation of the linear gradient quality still remains elusive, since it requires tracking the monomer incorporation in each growing chain during the entire reaction time, as opposed to the overall instantaneous monomer incorporation as is done in most modeling studies.[15, 20, 21, 26]

It should be emphasized that the development of gradient copolymers is inhibited by the absence of a proper experimental technique to quantify the gradient quality. A better understanding of the relationship between the polymer microstructure and the polymer properties will be possible in case such analysis method is available.[7a] Recently, some attempts to visualize gradients in copolymers have been reported for brushes using atomic force microscopy (AFM).[30-34]

The control over chain length and end-group functionality should be related to the control over gradient quality, since an ideal gradient implies a uniform distribution of the

comonomers. In other words, the gradient quality could be measured indirectly or at least qualitatively assessed by a measurement of the PDI and/or end-group functionality. To verify this hypothesis, evaluation of the gradient quality by simulation is necessary.

In this work, for the first time, the linear gradient quality of ATRP copolymers is evaluated by kMC simulations which explicitly track the monomer sequence of each polymer chain. To quantify the linear gradient quality, a parameter to characterize the linear gradient deviation <GD> is introduced. The <GD> is a well-defined parameter that reflects the average deviation for each polymer chain from the theoretically ideal linear gradient profile of the same chain length and hence is a new copolymer property in addition to the average chain length (x_n) and PDI. The kMC simulations show that batch ATRP conditions allow to synthesize copolymers with a good linear gradient quality. Moreover, for sufficiently high conversions it is demonstrated that a correlation exists between <GD> and PDI. Thus, the measured PDI can be used as a first assessment of the linear gradient quality.

5.2. Kinetic model

The kinetic Monte Carlo (kMC) technique was used to model ATRP copolymerizations of acrylates (monomer A) and methacrylates (monomer B). Using the same kMC algorithm as previously applied for the optimization of the synthesis of poly(p-phenylenevinylene)s,[35] the CLD and its average properties, such as the average chain length (x_n) and the polydispersity index (PDI), are calculated as a function of conversion. In this work, the algorithm is extended to allow (i) a bivariate description of the copolymerization, i.e. the calculation of the distribution of the fraction of monomers A/B per chain length, and (ii) the explicit representation of all reaction events. In particular, the explicit representation of A and B propagation events allows to determine the (linear) gradient quality of the copolymer obtained. For the bivariate description, the reader is referred to Appendix M.[36-38]

5.2.1. Reactions

Table 1 gives an overview of the reactions considered in the copolymerization of acrylates (A) and methacrylates (B) starting from an ATRP initiator (R_0X). To describe the reactivity of the different macromolecular species, a terminal kinetic model is used, i.e. only the last incorporated monomer unit is taken into account. The model considers activation, deactivation, propagation and termination reactions. Based on recent literature reports on CRP (co)polymerization,[39-43] backbiting reactions of secondary acrylic species (R_A) are neglected in a first approximation. It was demonstrated that under controlled ATRP homopolymerization conditions the amount of short chain branching is lower than under FRP

conditions,[39-43] and that the presence of tertiary B monomer units lowers the probability for backbiting even further,[43] justifying this assumption. Based on literature data[44, 45] chain transfer to monomer is also neglected.

The simulations are performed at a polymerization temperature of 353 K and a reference catalytic system is selected. For this reference catalytic systemit is assumed that, based on the work of Seeliger et al.[46], activation of tertiary methacrylate dormant species (R_BX to R_B) is ten times faster than activation of secondary acrylate species (R_AX to R_A). The absolute activity of the reference catalytic system is similar to that of Cu(I)Br/PMDETA (PMDETA = N,N,N',N'',N''-pentamethyldiethylenetriamine) extrapolated to 353 K.[46-48] All deactivation rate coefficients are given a typical value of 10^7 L mol^{-1} s^{-1}. For the activation/deactivation of R_0X/R_0, the same rate coefficient is used as for R_AX/R_A. For propagation, rate coefficients reported in literature are used. Secondary acrylate radicals are assumed to terminate exclusively by recombination and tertiary methacrylate radicals solely by disproportionation.[44] Rate coefficients for both termination processes are chain length dependent, i.e. diffusional limitation are accounted for.

Table 1: Reactions and intrinsic chemical rate coefficients for ATRP of acrylates (A) and methacrylates (B) using a reference ATRP catalytic system; 353 K; R_0: ATRP initiator related; i: chain length; for termination: apparent rate coefficients via RAFT-CLD-T method[49, 50]

Reaction	k_{chem} (L mol^{-1} s^{-1})[a]	Reference
Activation of R_0X	1	this work
Activation of $R_{A,i}X$	1	this work
Activation of $R_{B,i}X$	10	this work
Deactivation of R_0	10^7	this work
Deactivation of $R_{A,i}$	10^7	this work
Deactivation of $R_{B,i}$	10^7	this work
Propagation of R_0 with A	$5.0\ 10^4$	this work
Propagation of R_0 with B	$1.5\ 10^5$	this work
Propagation of $R_{A,i}$ with A	$5.0\ 10^4$	[51]
Propagation of $R_{A,i}$ with B[b]	$1.5\ 10^5$	[11]
Propagation of $R_{B,i}$ with A[b]	$4.3\ 10^2$	[11]
Propagation of $R_{B,i}$ with B	$1.3\ 10^3$	[52]
Termination by recombination of R_0 with R_0	RAFT-CLD-T[c]	[50]
Termination by recombination of R_0 with $R_{A,i}$	RAFT-CLD-T	[50]
Termination by recombination of R_0 with $R_{B,i}$	RAFT-CLD-T	[50]
Termination by recombination of $R_{A,i}$ with $R_{A,j}$	RAFT-CLD-T	[50]
Termination by recombination of $R_{A,i}$ with $R_{B,j}$	RAFT-CLD-T	[50]
Termination by disproportionation of R_0 with $R_{B,j}$	RAFT-CLD-T	[50]
Termination by disproportionation of $R_{A,i}$ with $R_{B,j}$	RAFT-CLD-T	[50]
Termination by disproportionation of $R_{B,i}$ with $R_{B,j}$	RAFT-CLD-T	[50]

[a]for termination reaction chain length dependent k_{app} values are used to account for diffusional limitations

[b]calculation based on reactivity ratios

[c]R_0 treated as $R_{A,1}$; correlation for methyl acrylate is used for *n*-butyl acrylate in first approximation; AB cross-termination based on geometric mean of the corresponding homoterminations; evaluated at average chain length

For homo-termination, diffusional limitations are accounted for via apparent rate coefficients based on the 'reversible addition fragmentation chain transfer-chain length dependent-termination (RAFT-CLD-T)'- technique.[49, 50] For the RAFT-CLD-T parameters of nBuA, those for methyl acrylate are taken in first approximation at the considered polymerization temperature of 353 K. For cross-termination, the apparent rate coefficients are calculated as the square root of the product of the corresponding apparent homo-termination rate coefficients, i.e. the geometric mean is used. In a first approximation, the apparent termination rate coefficients are evaluated at the average chain length. For simplicity, diffusional limitations on deactivation are neglected since they can become only important at high conversion depending on the deactivator mobility[53-55]. For the remaining reaction steps, diffusional limitations are neglected based on literature data.[35]

5.2.2. Evaluation of linear gradient quality

Figure 2 shows the general kMC flow sheet followed in this work to evaluate the linear gradient quality of a copolymer. Only unidirectional linear gradients are considered. The reaction event history of the copolymer is tracked using a matrix 'ReactionEventHistory' starting from a representative number of ATRP initiator molecules, similar to the kMC model of Szymanski[25] for a living polymerization and Wang and Broadbelt on NMP.[22-24] In the matrix, every macrospecies is represented by one row. In contrast to Wang and Broadbelt[22-24], the reaction event history of all macromolecular species is recorded in a single matrix avoiding the time consuming switching of macromolecules from the 'active' to the 'dormant' matrix, corresponding to the population of macroradicals and dormant polymer molecules, respectively. Each reaction event is represented by a label (e.g. propagation with A corresponds with the label '1': green unit in Figure 2).

Next, the copolymer composition is derived from the 'ReactionEventHistory' matrix. As explained in Appendix N, this involves removing the excessive labels and sorting dead and dormant polymer molecules, i.e. only the propagation events are withheld for the construction of a second matrix named 'CopolymerComposition'. For each polymer chain k in the matrix 'CopolymerComposition', the quality of the linear gradient is characterized by a linear gradient deviation parameter GD(k). For values close to zero, as explained below, the considered polymer chain resembles a perfect linear gradient.

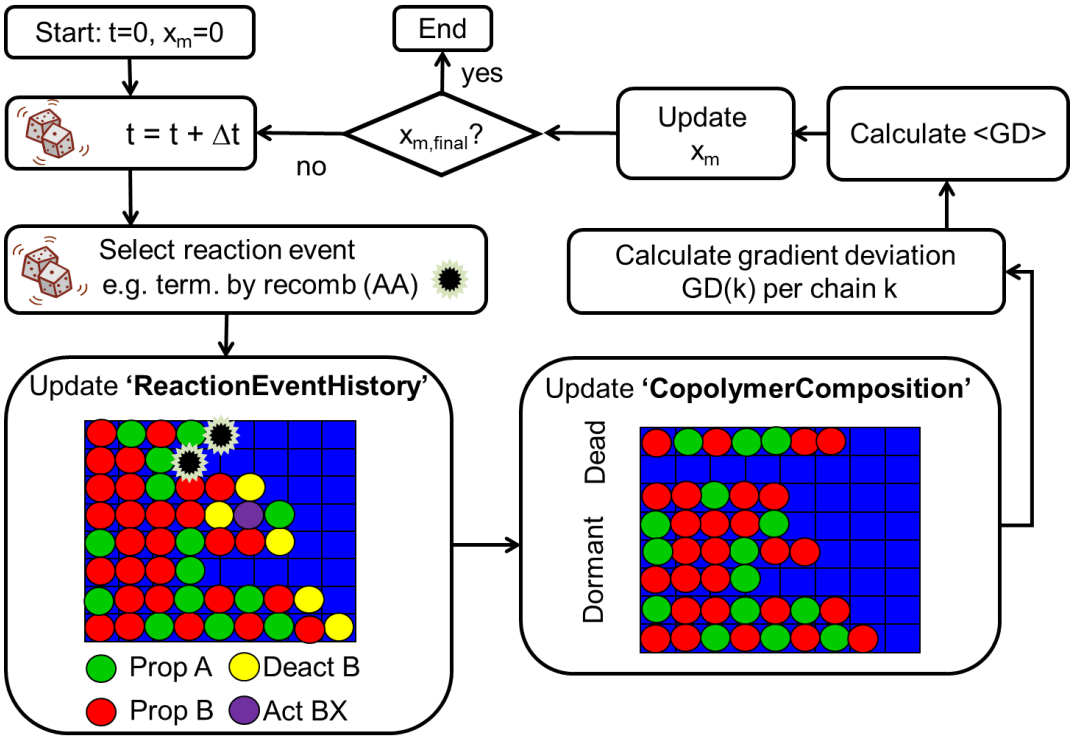

Figure 2: General kMC flow sheet for linear gradient quality evaluation; x_m = conversion; not all reaction events shown (see Appendix N); GD: gradient deviation

As illustrated in Figure 3, two considerations should be made for a unique linear gradient evaluation (Appendix O). First, for each polymer chain in the matrix 'CopolymerComposition' the same linear gradient quality should be obtained whether it is stored from 'left to right' or 'right to left' (e.g. Figure 3 top left and right). Second, the same linear gradient quality must be obtained if the comonomers A and B are interchanged, since the linear gradient quality should be independent of the monomer type (e.g. Figure 3 top vs. bottom).

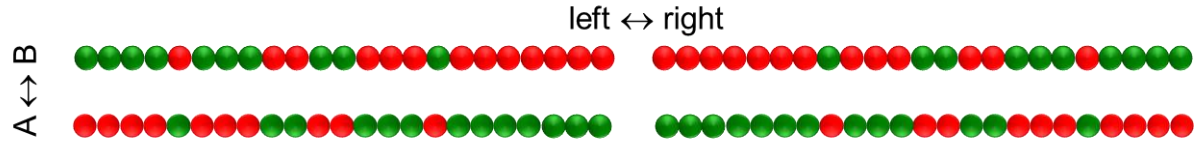

Figure 3: Four polymer chains with the same gradient quality; top two: stored from 'left to right' and from 'right to left'; bottom two: A and B switched; A = green; B = red

In general, as explained in Appendix O, these considerations require the calculation of four linear gradient deviation values per polymer chain k. These evaluations differ in the direction the polymer chain k is followed (from 'left to right' or reverse) and the selected theoretical ideal reference linear gradient polymer chain ('A to B' or 'B to A', both defined from 'left to right'). The linear gradient quality is subsequently obtained by selecting the minimum of these four values.

For the particular batch ATRP studied in this work, only one linear gradient deviation has to be calculated for sufficiently high conversions. As explained in Appendix O, only a comparison with a 'B to A' ideal linear gradient from 'left to right' is required, since formation of tertiary B macroradicals is favored[19] (A: acrylate; B: methacrylate). In the following paragraph the latter evaluation is therefore discussed in detail and referred to as the first evaluation. The other three evaluations, which are very similar, are discussed in Appendix O.

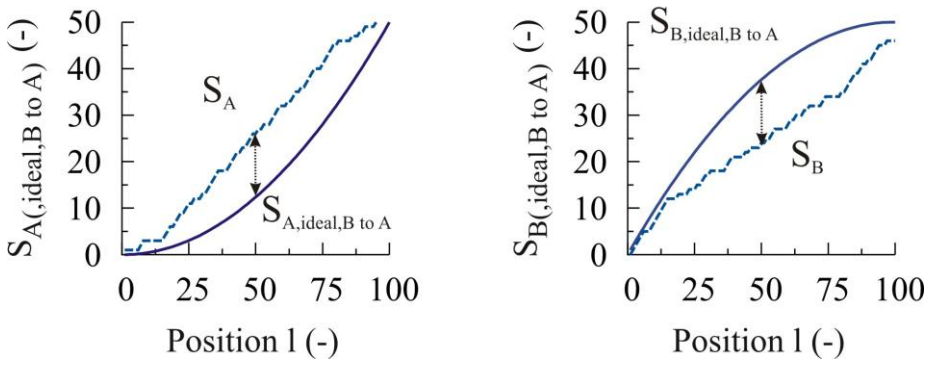

Figure 4: 'B to A' linear gradient evaluation ('left to right') for a single polymer chain

For a 'B to A' evaluation from 'left to right' (first evaluation), as illustrated in Figure 4, the simulated cumulative amount of monomer A (S_A) and B (S_B) (counted from 'left to right') is compared to the theoretical cumulative amount of monomer A ($S_{A,ideal,B\ to\ A}$) and B ($S_{B,ideal,B\ to\ A}$) in the corresponding 'B to A' theoretical ideal linear gradient profile. As explained in Appendix P, ideal profiles are parabolic as function of (chain) position l in agreement with the linear evolution of the corresponding probabilities. Clearly, only if the surface between the simulated and ideal profiles is small, the considered polymer chain k can be regarded as a good gradient. Therefore, as explained in Appendix Q taking into account averaging and normalization, Equation (1) can be used to quantify the linear gradient quality for the first evaluation:

$$GD_{BtoA}\ (k) = \sum_{l=1}^{i} \frac{1}{2} \frac{\left|S_A(k,l) - S_{A,ideal,BtoA}(k,l)\right| + \left|S_B(k,l) - S_{B,ideal,BtoA}(k,l)\right|}{i^2} \quad (1)$$

Three similar equations result for the other three evaluations (see Appendix O) allowing the calculation of the minimal GD(k) value for a single chain k and hence the calculation of an average GD value (<GD*>) for all polymer chains:

$$< GD^* >= \sum_{k=1}^{k_{max}} \frac{GD(k)}{k_{max}} \quad (2)$$

For ideal linear gradient copolymers (Appendix P) <GD*> values close to 0 are obtained. For example for an ideal linear gradient copolymer with a TCL of 100 (Figure P1 (left)) and 500 (Figure P1 (right)) a <GD*> of 0.02 and 0.01 is respectively obtained. Higher chain lengths inherently allow a better representation of the required continuous change of the incorporation of monomer B to A explaining the effect of TCL on <GD*> in case ideal linear gradients are considered. As illustrated in Appendix R, from TCLs higher than 500 onward the effect of TCL on <GD*> is less significant and polymers with a <GD*> of 0.01 can thus be considered as 'excellent' gradient polymers. On the other hand, for a pure homopolymer, which mathematically can be considered as the worst case, a value of 0.175 is obtained. This indicates that, in principle, <GD*> values range between 0 and 0.175. These values were thus rescaled linearly to be ranged between 0 and 1:

$$< GD >= \frac{< GD^* >}{0.175} \quad (3)$$

For an ideal linear gradient copolymer with TCL = 500 a <GD> of ca. 0.06 is obtained. Hence, ideal linear gradient copolymers result in case <GD> values close to 0.06 are obtained. In particular, simulations (see further) revealed that a rescaled value of 0.25 can be used to distinguish good from bad linear gradient copolymers for a TCL of 100. In a first approximation this limiting value can also be used for higher TCLs.

Finally, for a polymer consisting of polymer chains similar to the one in Figure 4 a <GD> of 0.4 is obtained, which corresponds to <GD*> = 0.07. Here, a bad gradient polymer chain is depicted since on a cumulative basis a deviation of 700 monomer units is obtained.

5.3. Results and discussion

In this section, first the copolymer properties are discussed for the reference ATRP catalytic system under the following batch conditions: $[A+B]_0/[R_0X]_0/[Cu(I)XL]_0/[Cu(II)X_2L]_0$ = 100/1/1/1 with $[A]_0 = [B]_0$. Note that a targeted chain length (TCL) of 100 is considered. From intermediate conversions onward the control over chain length distribution and livingness is excellent, whereas a good linear gradient quality, i.e. a <GD> lower than 0.25, is obtained at high conversion. Next it will be demonstrated that for the considered TCL a correlation exists between <GD> and PDI at sufficiently high conversion (> 0.25) while varying the ATRP catalytic system and its initial concentration. Only if a low PDI can be obtained, good linear gradient polymers can be prepared. For higher TCLs, it is shown that a slightly different correlation is obtained, leading to a higher gradient quality under controlled ATRP conditions. This work exclusively considers unidirectional linear gradient polymers, i.e. those formed from typical monofunctional ATRP initiators such as ethyl α-bromoisobutyrate (EBiB) or methyl 2-bromopropionate (MBP). However, the methods developed here could be extended in the future to characterize more complex gradient polymers such as ABA linear gradient polymers or gradient star polymers.

5.3.3. Linear gradient quality in ATRP

Figure 5 shows the evolution of the average chain length x_n, PDI and end-group functionality with conversion for the reference ATRP catalytic system (Table 1) and a TCL of 100, without Cu(II) species initially added and with Cu(I) equimolar to the ATRP initiator. This reference catalytic system, as mentioned earlier has similar activation rate coefficients to those of Cu(I)Br/PMDETA.[46] Note that the PDI is calculated from the simulated chain length distribution, whereas experimentally the PDI is determined from the molecular weight distribution. Both an excellent control over chain length and livingness is obtained. From relatively low conversion onwards, a linear increase of x_n with conversion is observed ($x_{n,ideal} = x_m [A+B]_0/[R_{ini}X]_0$). At high conversion, PDI values close to 1 are obtained and only a small loss of end-group functionality takes place during the polymerization (ca. 10 %).

The excellent control over chain length and livingness is confirmed by the simulation results shown in Figure 6, in which the matrix CopolymerComposition is illustrated for a representative number of polymer chains at a conversion of 0.25, 0.5, 0.75 and 1. For each conversion, the average chain length is shown as the mid-value of the abscissa and the dead polymer molecules are visualized above the full blue horizontal line. For an ideal ATRP, i.e. with instantaneous initiation and absence of termination, the sample would consist of 1000

dormant polymer chains with uniform chain length. It can be concluded from Figure 6 that most of the polymer chains are indeed dormant and consume an approximate equal amount of monomer as the ATRP proceeds, i.e. their chain length increases linearly with conversion. On the other hand, the dead polymer molecules have a relatively low chain length and are mainly formed at low conversion.

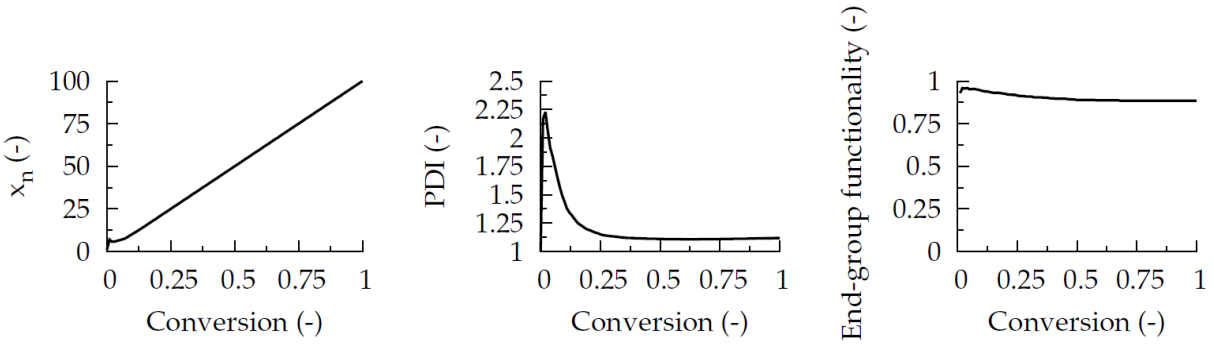

Figure 5: Left: average chain length x_n; middle: polydispersity index (PDI); right: end-group functionality as a function of conversion; $[A+B]_0/[R_0X]_0/[Cu(I)L_yX]_0$ = 100/1/1 with $[A]_0 = [B]_0$ and $[Cu(II)L_yX_2]_0$ = 0; ATRP reference catalytic system (Table 1)

During the ATRP, both monomer A (green) and B (red) are incorporated into the dormant polymer molecules. Initially, propagation with B (mostly red units; top left) is preferred and A is incorporated at higher conversion (mostly green units at high positions; bottom right). The dead polymer molecules consist mostly of monomer B (red), since they are mainly formed at low conversion. Overall, a gradient-like copolymer is obtained since the livingness of the ATRP is relatively high (Figure 5 right).

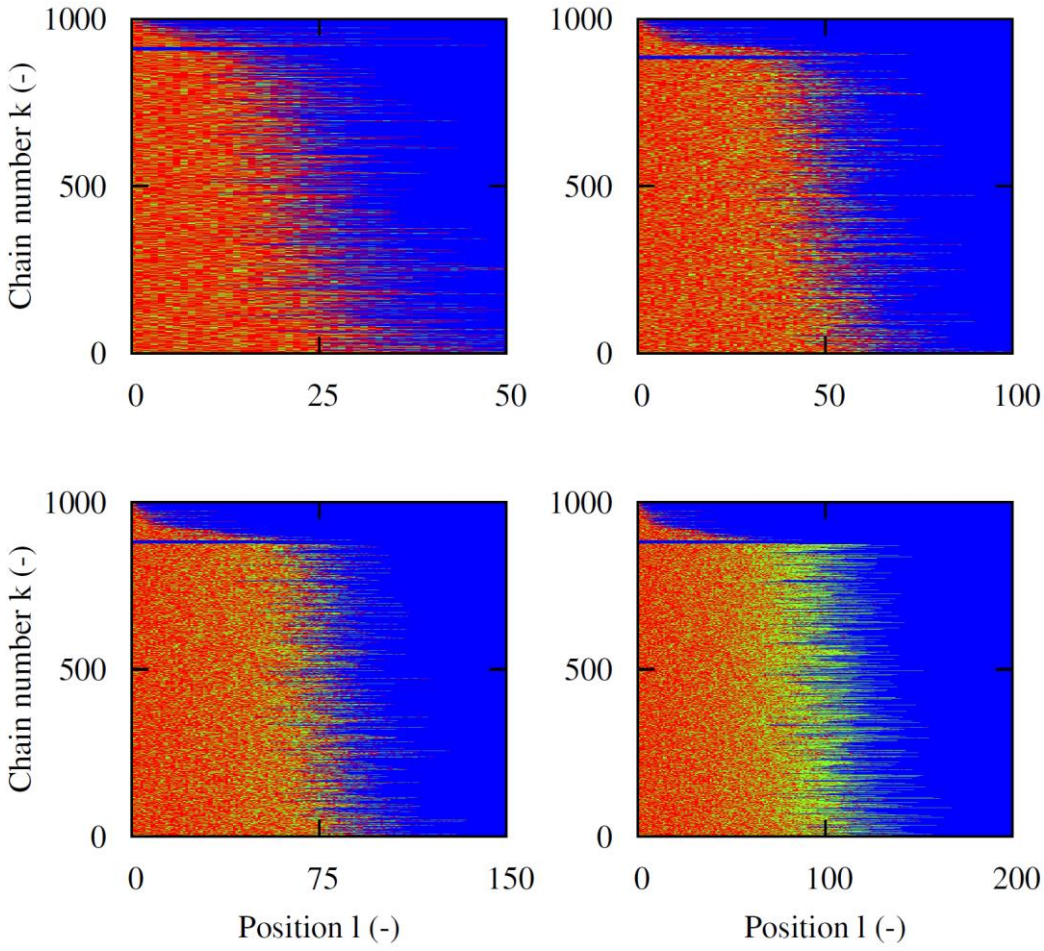

Figure 6: Copolymer composition at a conversion of 0.25, 0.5, 0.75 and 1 (left to right and top to bottom); $[A+B]_0/[R_0X]_0/[Cu(I)L_yX]_0$ = 100/1/1 with $[A]_0 = [B]_0$ and $[Cu(II)L_yX_2]_0 = 0$; ATRP reference catalytic system (Table 1); green: A; red: B; blue: absence of monomer

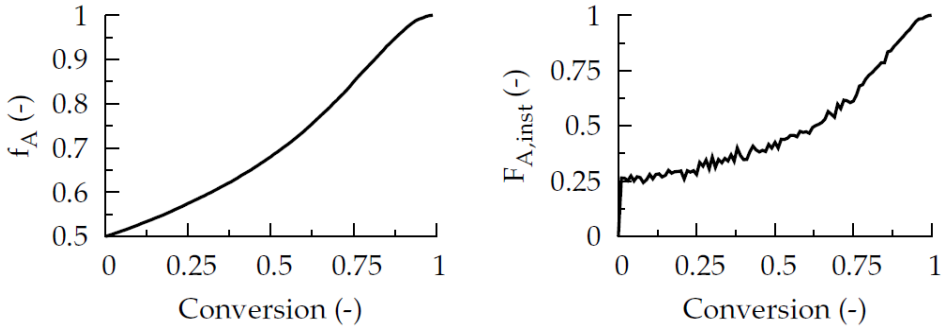

Figure 7: Left: monomer composition f_A; right: overall instantaneous copolymer composition $F_{A,inst}$ as a function of conversion for monomer A; $[A+B]_0/[R_0X]_0/[Cu(I)L_yX]_0$ = 100/1/1 with $[A]_0 = [B]_0$ and $[Cu(II)L_yX_2]_0 = 0$; ATRP reference catalytic system (Table 1)

This gradient-like behavior is also reflected in Figure 7 in which the monomer composition and the overall instantaneous copolymer composition are given for monomer A as a function of conversion. As polymerization proceeds, the monomer feed becomes enriched in A (Figure 7(a)) and more of A is incorporated into the copolymer chains (Figure 7(b)). Similarly, the chemical composition-chain length distribution (CC-CLD) (Figure 8) shows a gradual shift to higher amounts of monomer A at higher conversion. For example, at a conversion of 0.25 (top left) only 5 monomer A units are incorporated into polymer chains which possess an average chain length of 25. However, at a conversion of 0.50 (top right), at which the average chain length is 50, the number of monomer A units gradually increases to ca. 15. At final conversion (bottom right), the contribution of monomer A units in most polymer chains is ca. 50%, as required for a linear gradient copolymer. Note that in agreement with Figure 6, dead polymer molecules are mainly formed at low conversion and their chain length is relatively low, i.e. they are mainly situated in the left bottom corner of the CC-CLD.

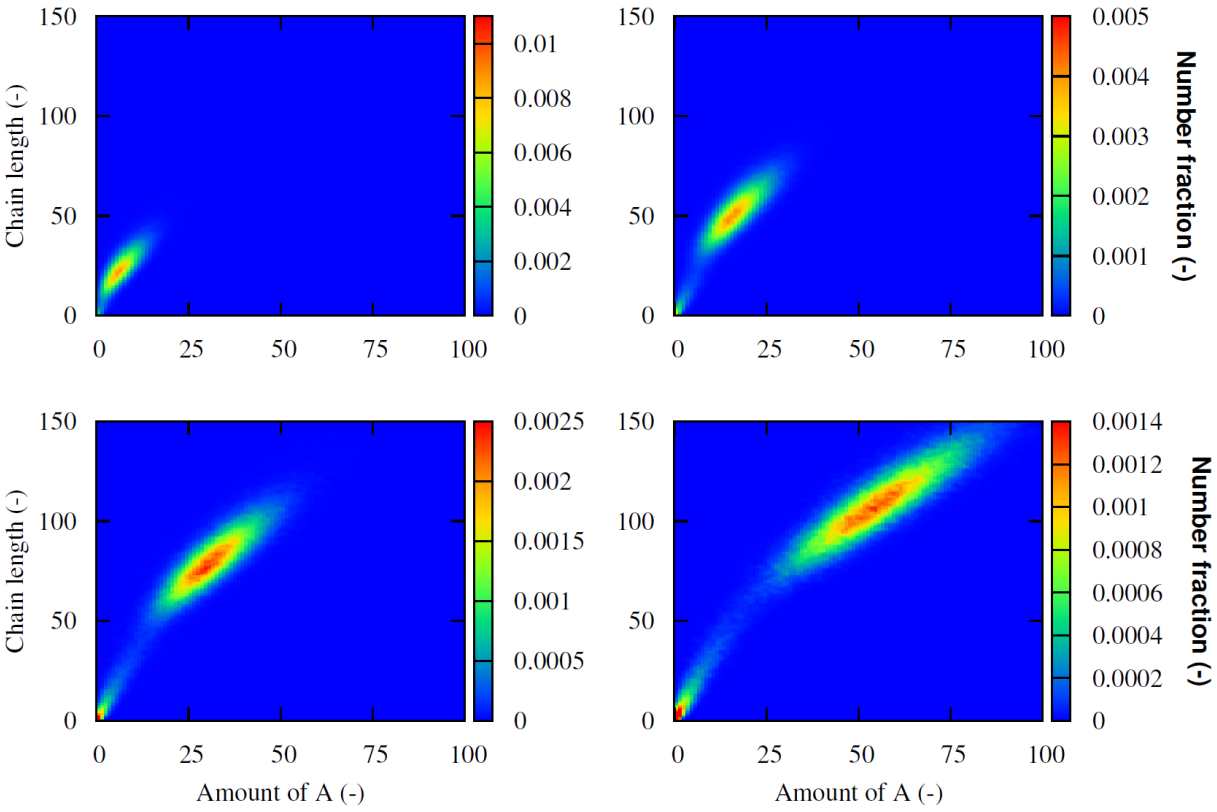

Figure 8: CC-CLD at a conversion of 0.25,0.5, 0.75 and 1 (left to right and top to bottom); $[A+B]_0/[R_0X]_0/[Cu(I)L_yX]_0$ = 100/1/1 with $[A]_0 = [B]_0$ and $[Cu(II)L_yX_2]_0 = 0$; ATRP reference catalytic system (Table 1); simulation for 10^5 ATRP initiator molecules

Figure 9 shows that the copolymer at final conversion (Figure 6; bottom right; x_n = 100; conversion = 1) is a gradient copolymer of mediocre linear gradient quality. A <GD> of 0.20 is obtained which is ca. two times higher than the value for the sample of ideal gradient copolymer chains with the same TCL of 100 (Figure P.1(left)) and even three times higher than for the sample of ideal gradient copolymer chains (Figure P.1(right)) for a TCL of 500. As explained above, the latter polymer is characterized by a <GD> of 0.06, which is the upper limit for excellent gradients.

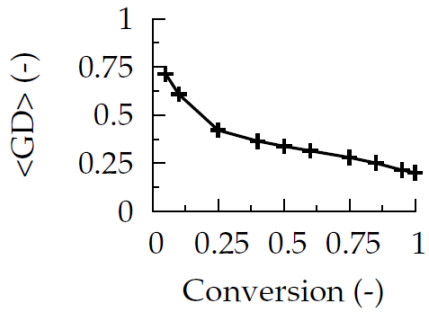

Figure 9: Average gradient deviation (<GD>) as a function of conversion; $[A+B]_0/[R_0X]_0/[Cu(I)L_yX]_0$ = 100/1/1 with $[A]_0 = [B]_0$ and $[Cu(II)L_yX_2]_0 = 0$; ATRP reference catalytic system (Table 1); the lowest <GD> value is obtained for the polymer obtained at final conversion (Figure 6 (bottom right))

Note that if the ATRP would be stopped earlier, higher <GD> values are obtained. For example, the polymer represented by Figure 6 (top left; conversion = 0.25) is a poor gradient copolymer since too much monomer B (red) is present, which is reflected by the <GD> of 0.45. Only at conversions higher than 0.75, <GD> becomes lower than 0.25 and the linear gradient quality is good, indicating that for a TCL of 100 this <GD> value can be used to distinguish good from bad gradients. For completeness, in Appendix S, the variance of the GD distribution is given as a function of conversion. It can be seen that from low conversion onward, this variance is low, indicating that <GD> is sufficient to characterize the GD distribution.

5.3.4. Effect of catalytic system reactivity on linear gradient quality

Figure 10 shows the effect of the deactivation rate coefficient $k_{da,chem}$ on the average chain length, PDI, end-group functionality and <GD> as a function of conversion under batch conditions for normal ATRP, without Cu(II) species initially added and with Cu(I) equimolar to the ATRP initiator (TCL = 100). For the reference catalytic system, a value of 10^7 L mol^{-1} s^{-1} was used (dashed line in Figure 10). The value of $k_{da,chem}$ is varied between 10^5 and 10^8 L

mol^{-1} s^{-1} with all other rate coefficients unchanged (Table 1). In ATRP, deactivation rate coefficients are typically in the order of 10^7 L mol^{-1} s^{-1}, although certain catalytic systems with a bridged-cyclam as a ligand, can display deactivation rate coefficients of 10^5 L mol^{-1} s^{-1}.[56] For catalytic systems characterized by lower $k_{da,chem}$, the control over chain length and livingness is worse and the linear gradient quality decreases. The lower PDI for higher $k_{da,chem}$ is due to the shorter transient radical lifetime, implying that fewer monomer units are added per activation-growth-deactivation cycle, and that all macrospecies can grow concurrently. Since all $k_{a,chem}$ values are fixed, lower ATRP equilibrium coefficients (K_{eq}'s; Scheme 1) are obtained, resulting in lower radical concentrations and fewer dead chains. This suggests that the linear gradient quality could be assessed by a measurement of the PDI and/or end-group functionality.

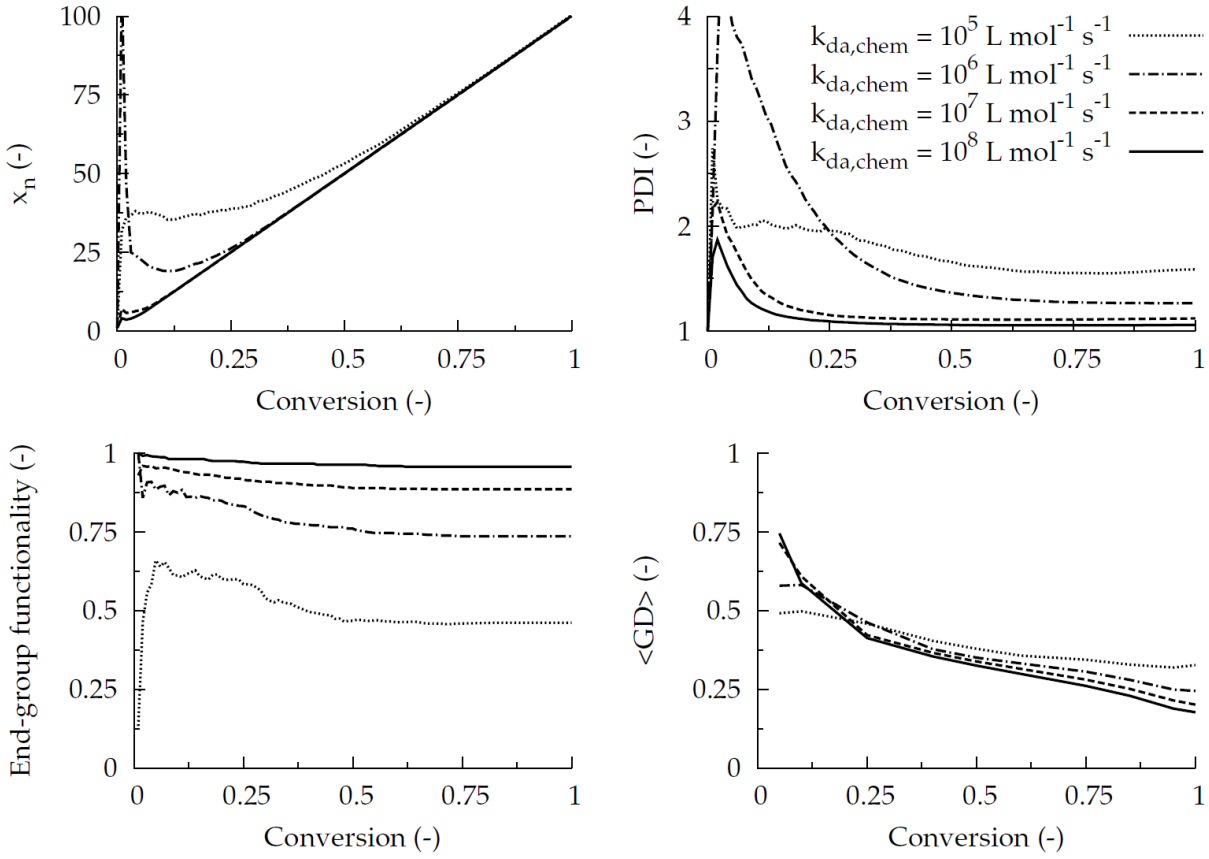

Figure 10: Top left: average chain length x_n; top right: polydispersity index (PDI); bottom left: end-group functionality and bottom right average gradient deviation (<GD>) as a function of conversion for $k_{da,chem}$ equal to 10^5 (dotted line), 10^6 (dashed dotted line), 10^7 (dashed line) and 10^8 (full line) L mol^{-1} s^{-1}; $[A+B]_0/[R_0X]_0/[Cu(I)L_yX]_0$ = 100/1/1 with $[A]_0 = [B]_0$ and $[Cu(II)L_yX_2]_0 = 0$

The implied correlation (Figure 10) may be more clearly visualized by directly plotting the PDI, end-group functionality and average gradient deviation <GD> as a function of $k_{da,chem}$ at a conversion of 1 (Figure 11).

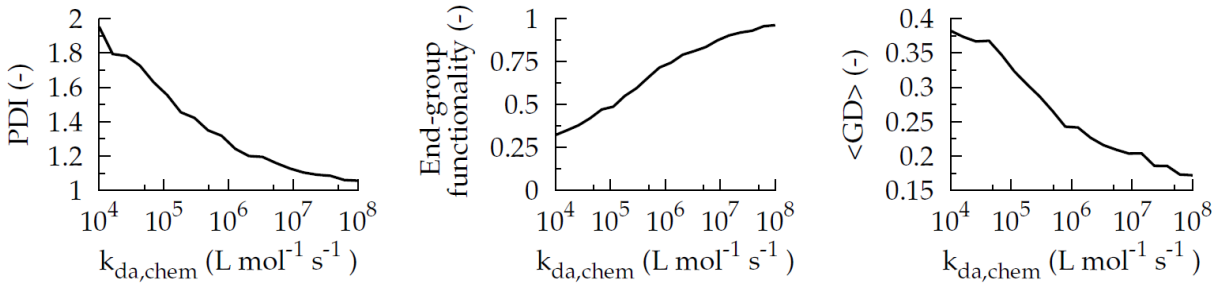

Figure 11: Left: PDI; middle: end-group functionality; right: <GD> as a function of $k_{da,chem}$ at a conversion of 1; $[A+B]_0/[R_0X]_0/[Cu(I)L_yX]_0$ = 100/1/1 with $[A]_0 = [B]_0$ and $[Cu(II)L_yX_2]_0 = 0$

This is further confirmed in Figure 12, in which the effect of $k_{da,chem}$ on the copolymer composition is shown at a conversion of 1. As before, the average chain length is shown as the mid-value of the abscissa and the dead polymer molecules are visualized above the full blue line. It can be deduced that for low $k_{da,chem}$ (Figure 12 top left; $k_{da,chem} = 10^5$ L mol^{-1} s^{-1}) the fraction of dead polymer molecules is very high and these polymer molecules possess no linear gradient character, since they mainly contain monomer B (red). A broad range of chain lengths is obtained in agreement with the high PDI value of 1.7 (Figure 10 top right; $k_{da,chem} = 10^5$ L mol^{-1} s^{-1}). On the other hand, if $k_{da,chem}$ is sufficiently high, a narrow CLD results, consisting mainly of dormant polymer chains and the linear gradient quality is good (e.g. Figure 12 bottom right; PDI = 1.05; $k_{da,chem} = 10^8$ L mol^{-1} s^{-1}).

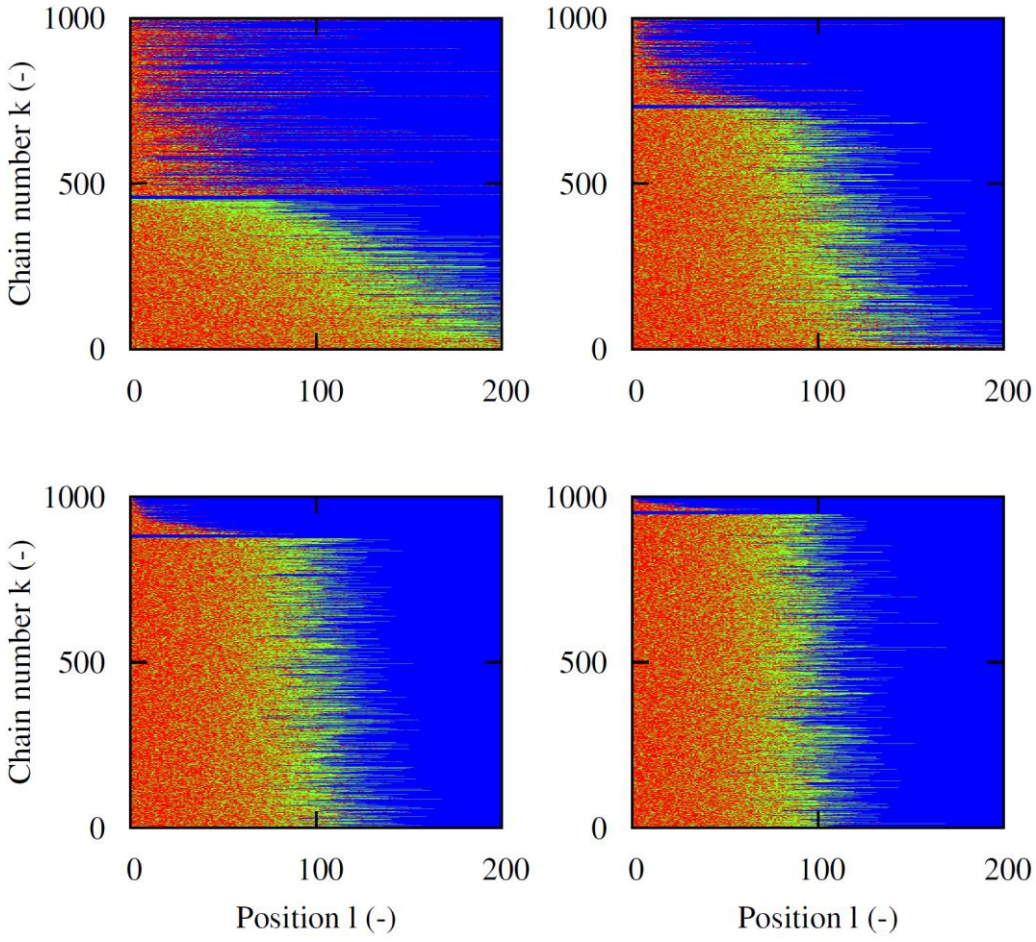

Figure 12: Copolymer composition at a conversion of 1 for $k_{da,chem}$ equal to (top left) 10^5, (top right) 10^6, (bottom left) 10^7 and (bottom right) 10^8 L mol^{-1} s^{-1}; $[A+B]_0/[R_0X]_0/[Cu(I)L_yX]_0$ = 100/1/1 with $[A]_0 = [B]_0$ and $[Cu(II)L_yX_2]_0 = 0$; green A; red B; blue: absence of monomer

Simulations over a broader range of catalyst reactivity revealed that for sufficiently high conversions (> 0.25) the gradient quality can be indirectly assessed by a measurement of the PDI, although not by the end-group functionality. Figure 13 shows the PDI, end-group functionality and <GD> profile for various activation rate coefficients $k_{a,chem}$ for a fixed $k_{da,chem}$ of 10^7 L mol^{-1} s^{-1}. An activation rate coefficient of 10^1 L mol^{-1} s^{-1} for the acrylate is consistent with the value expected in case tris(2-pyridylmethyl)amine (TPMA) is used as ligand,[56] while an activation rate coefficient in the order of 10^{-3} L mol^{-1} s^{-1} for the acrylate is expected in case bipyridine is used as ligand.[56] In each simulation, the activation of tertiary dormant species ($k_{a,chem,BX}$) is assumed ten times faster than for secondary species ($k_{a,chem,AX}$). The <GD> and PDI profile display a minimum situated at $k_{a,chem}$ equal to 10^1 L mol^{-1} s^{-1}. On

the other hand, the end-group functionality decreases as a function of $k_{a,chem}$ and therefore cannot be used to assess the linear gradient quality.

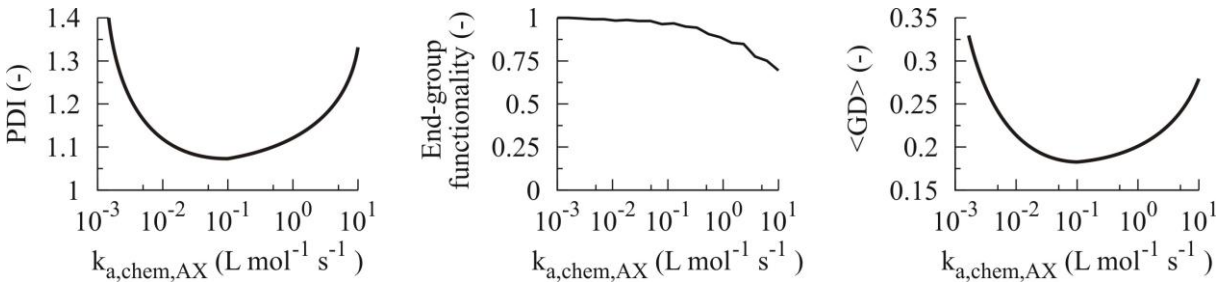

Figure 13: Left: PDI; middle: end-group functionality; right: <GD> as a function of $k_{a,chem,AX}$ at a conversion of 1; $[A+B]_0/[R_0X]_0/[Cu(I)L_yX]_0 = 100/1/1$ with $[A]_0 = [B]_0$ and $[Cu(II)L_yX_2]_0 = 0$; $k_{da,chem} = 10^7$ L mol^{-1} s^{-1} and $k_{a,chem,BX} = 10\ k_{a,chem,AX}$

For low $k_{a,chem}$ values, termination can be suppressed, although initiation is far from instantaneous. For extremely low $k_{a,chem}$ values (Figure 14, left), the livingness is almost perfect but the dormant polymer chains formed first (lowest chain numbers) consist mostly of monomer B (red) and possess a too high chain length. The reverse happens at high conversion explaining the low <GD> values for low $k_{a,chem}$ values. Note that in this case the ATRP initiator is not fully consumed even at final conversion as evidenced by the blue zone at the top of the figure, i.e. a very slow ATRP initiation occurs. On the other hand, for high $k_{a,chem}$ values, initiation is fast but termination cannot be sufficiently suppressed. In Figure 14 (right), a very high number of dead polymer chains result consisting mainly of monomer B (red), which results in high <GD> values, despite a relatively good gradient composition for the dormant polymer molecules.

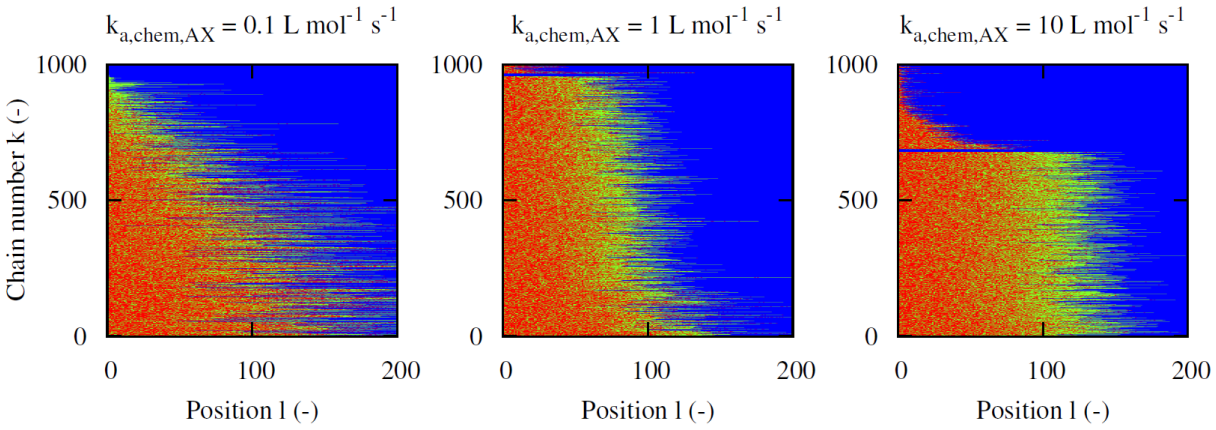

Figure 14: Copolymer composition at a conversion of 1 for $k_{a,chem,AX}$ equal to (left) 10^{-3}, (middle) 10^{-1}, (right) 10^{1} L mol^{-1} s^{-1}; $[A+B]_0/[R_0X]_0/[Cu(I)L_yX]_0$ = 100/1/1 with $[A]_0 = [B]_0$ and $[Cu(II)L_yX_2]_0 = 0$; green: A; red: B; blue: absence of monomer; full blue line: separation of dead (top) and dormant (bottom) polymer chains; $k_{da,chem} = 10^7$ L mol^{-1} s^{-1} and $k_{a,chem,BX} = 10\ k_{a,chem,AX}$

Hence, the best control over gradient quality is obtained at intermediate $k_{a,chem}$ values, since then ATRP initiation is sufficiently fast and termination is adequately suppressed. Figure 14 (middle) shows that for a $k_{a,chem,AX} = 10^{-1}$ L mol^{-1} s^{-1} both a good control over chain length and gradient quality is obtained, which is also reflected in the low values for PDI and <GD> from Figure 13, respectively 1.1 and 0.18. In Appendix T it is illustrated that similar results are obtained for $k_{da,chem}$ equal to 10^6 L mol^{-1} s^{-1}, further confirming the proposed correlation between PDI and <GD> at sufficiently high conversion.

5.3.5. Effect of initial activator concentration on linear gradient quality

Figure 15 shows the effect of the initial activator concentration on the evolution of the average chain length x_n, PDI, end-group functionality and <GD> with conversion for the reference ATRP catalytic system (Table 1) and a TCL of 100. In all simulations, no deactivator is present at the start of the ATRP. For lower initial activator concentrations, the livingness is higher and the control over chain length is less. However, at high conversions only for an initial molar ratio of ATRP initiator to activator of 0.01 a slightly higher PDI is obtained, which is reflected in the slightly higher <GD> value at high conversion. Note that the end-group fidelity can again not be used to assess the linear gradient quality, since this property changes oppositely with respect to the initial amount of activator.

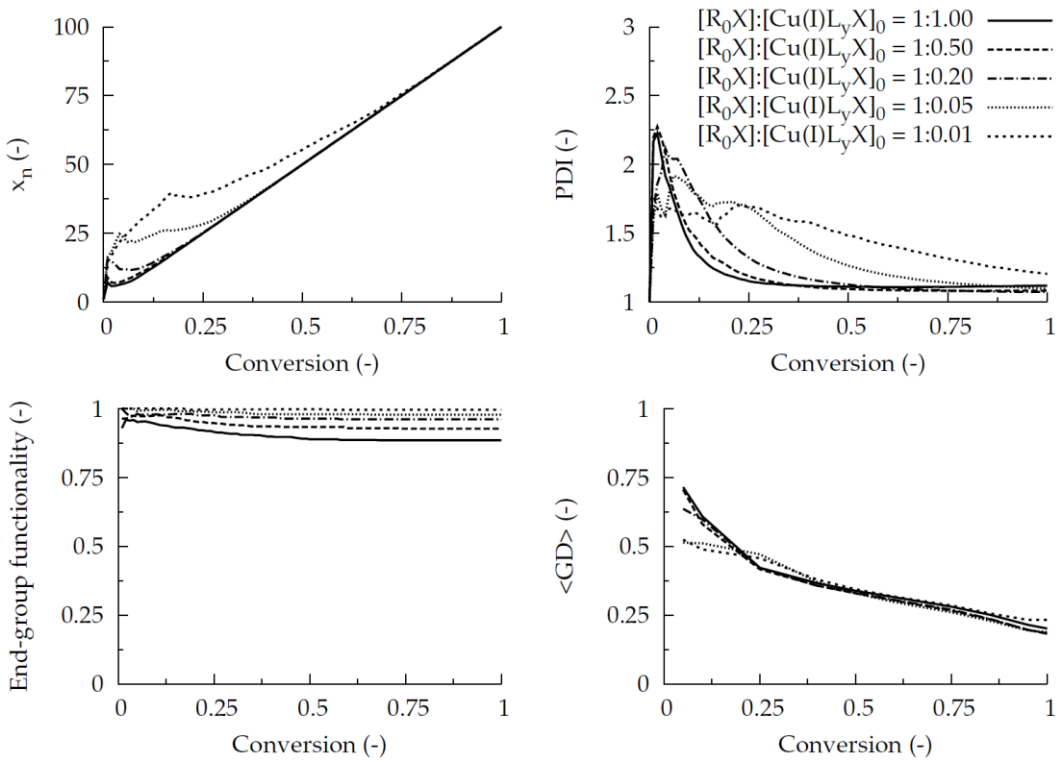

Figure 15: Top left: average chain length x_n; top right: polydispersity index (PDI); bottom left: end-group functionality and bottom right average gradient deviation (<GD>) as a function of conversion for $[R_0X]_0$:$[Cu(I)L_yX]_0$ equal to 1:0.01, 1:0.05, 1:0.20, 1:0.50, 1 and the reference catalytic system (Table 1); $[A+B]_0/[R_0X]_0$ = 100/1 with $[A]_0 = [B]_0$ and $[Cu(II)L_yX_2]_0 = 0$

5.3.6. Effect of initial deactivator concentration on linear gradient quality

In addition to the effect of the initial activator concentration, it is also important to determine the effect of adding deactivator at the start of the polymerization, since this could provide a simple tool for tuning polymer properties. Figure 16 shows the effect of the initial deactivator concentration on the average chain length, PDI, end-group functionality and <GD> profile for a fixed $k_{da,chem}$ of 10^7 L mol^{-1} s^{-1}. It can be seen that at high conversion the effect is limited. A slightly lower PDI and thus <GD> is obtained in case a non-zero initial deactivator concentration is applied.

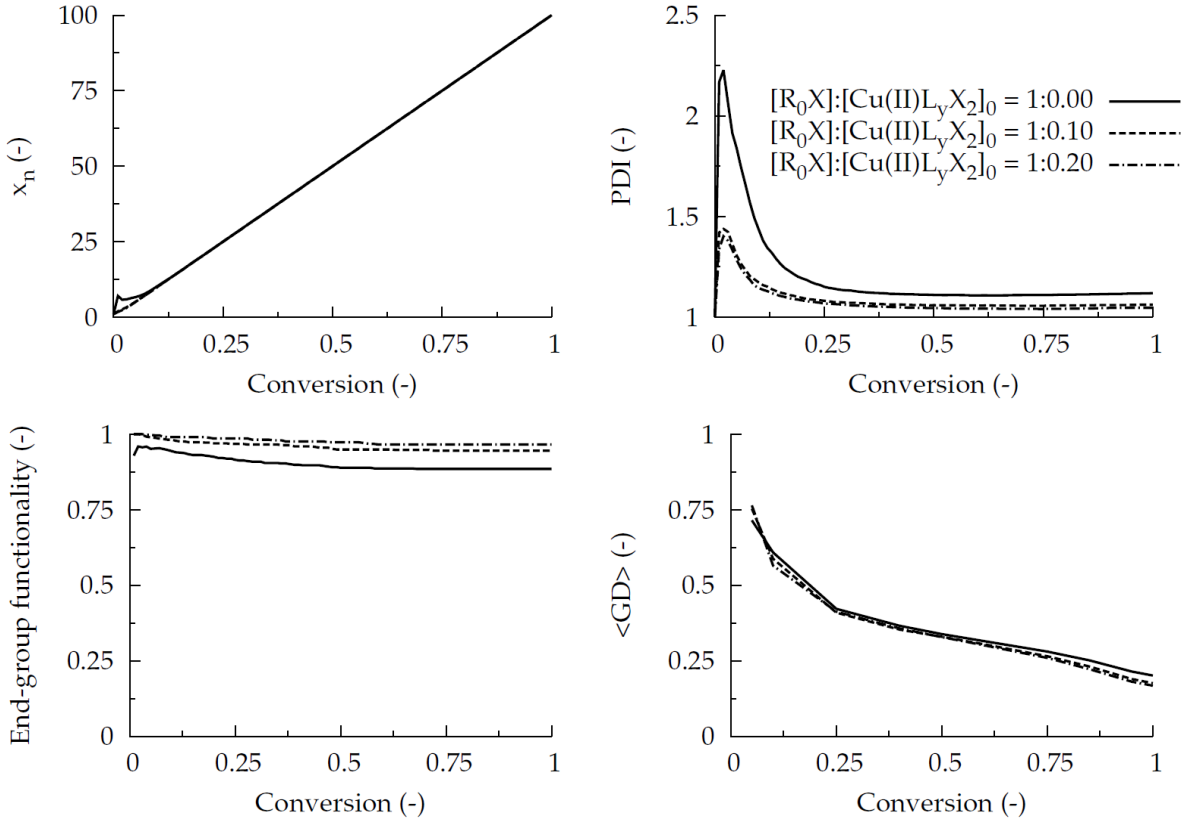

Figure 16: Top left: average chain length x_n; top right: polydispersity index (PDI); bottom left: end-group functionality and bottom right average gradient deviation (<GD>) as a function of conversion for $[R_0X]_0$:$[Cu(II)L_yX_2]_0$ equal to 1:0, 1:0.10, 1:0.20 and the reference catalytic system (Table 1); $[A+B]_0/[R_0X]_0/([Cu(I)L_yX]_0+[Cu(II)L_yX_2]_0)$ = 100/1/1 with $[A]_0 = [B]_0$

5.3.7. Correlation between linear gradient quality and PDI

As discussed above, the PDI can be potentially used to assess the linear gradient quality in batch ATRP, using copolymerization of acrylates and methacrylates, as an example. Figure 17 (bottom) shows a quasi-linear correlation between PDI and <GD> at final conversion for the simulations discussed above, i.e. a variation of (i) $k_{da,chem}$, (ii) $k_{a,chem}$, (iii) initial activator concentration and (iv) initial deactivator concentration. In all simulations, TCL is equal to 100. Clearly, low <GD> values and thus a good linear gradient quality can be obtained only when the control over chain length distribution is good, i.e. low PDI values result. This is again due to the efficient deactivation of macroradicals leading to a concurrent growth of all polymer chains.

Practically, ATRPs are seldom conducted until complete conversion and a conversion of e.g. 0.85 is reached. Figure 17 (top) shows that also at this conversion the correlation between PDI and <GD> holds although slightly higher GD values are obtained at lower PDIs. This slight increase at low PDIs can be attributed to the unequal presence of monomer A and B units in the polymer chains. E.g. Figure 7 shows that, at a conversion of 0.85, the monomer feed consist mostly of monomer A and hence only at final conversion both monomers are equally present in the polymer chains, which is a prerequisite for a linear gradient polymer. For higher PDIs, however, the beneficial effect of an equal presence of monomer A and B becomes less important, since the composition of the copolymer chains as such differs too much from the ideal one.

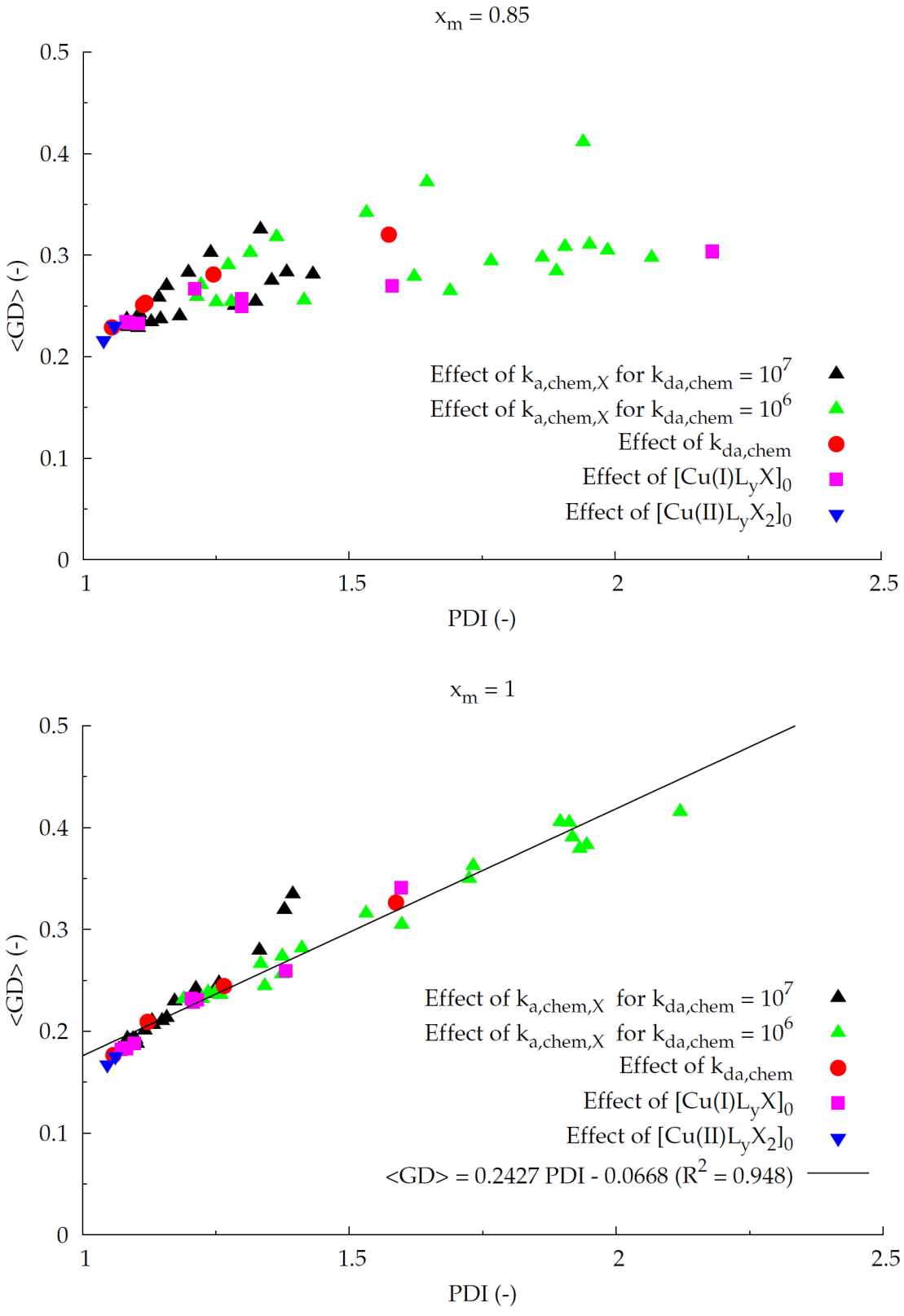

Figure 17: Correlation between PDI and <GD> at a conversion of 0.85 (top) and final conversion (bottom), in batch ATRP of acrylates and methacrylates (TCL = 100); red circles: Figure 10; green up-pointing triangles: Figure 13; magenta squares: Figure 15 and down-pointing triangles: Figure 16; $[A]_0 = [B]_0$

5.3.8. Effect of targeted chain length on linear gradient quality

The above simulation results were all limited to a TCL of 100. However, it can be expected that a better linear gradient quality can be obtained in case a higher TCL is selected. As explained in Appendix R, theoretically <GD> values very close to 0 can be obtained for TCLs of 500 and higher, since inherently higher chain lengths allow a more continuous transition from 'B to A'. Hence, it can be expected that a similar but different correlation is valid between PDI and <GD> for higher TCLs, at least under controlled ATRP conditions.

Figure 18 shows the effect of TCL on the correlation between the final PDI and <GD>. The correlations are visualized for a TCL of 100 and 500 in case $k_{a,chem}$ is varied while fixing $k_{da,chem}$ at 10^7 L mol^{-1} s^{-1}. In both cases a quasi-linear behavior is observed. However, only for sufficiently low PDIs the correlations are significantly different, i.e. lower <GD> values result for a higher TCL, in agreement with the decreasing <GD> values for 'perfect' ideal gradients as a function of TCL (see Appendix R). For higher PDIs, however, the beneficial effect of a higher TCL becomes less important, similar to the fading advantage of an equal presence of monomer A and B in the polymer chains, as explained above. Regression analysis and a statistical test for the significance of the difference between both correlations is provided in Appendix U.

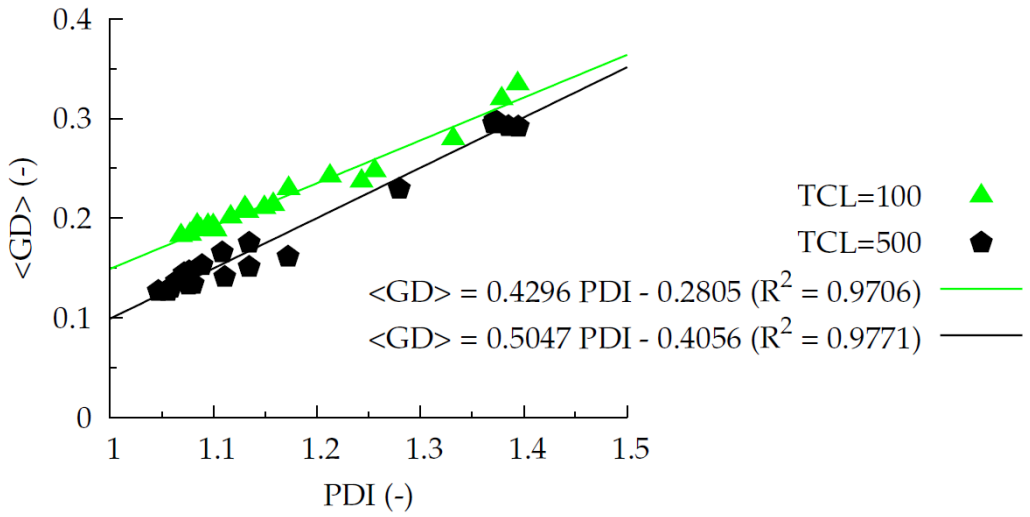

Figure 18: Correlation between final PDI and <GD>, i.e. at final conversion, in batch ATRP of acrylates and methacrylates for a TCL of 100 and 500; $[A]_0 = [B]_0$; variation of rate coefficients as for Figure 13

5.4. Conclusions

For the first time, the linear gradient quality of ATRP copolymers is evaluated based on the explicit tracking of the copolymer composition of each polymer chain. Per copolymer chain k, a linear gradient deviation GD(k) is calculated with respect to theoretical ideal linear gradient profile for the same chain length.

For a <GD> value of 0.06 or lower, the gradient quality of the copolymer is defined as excellent, whereas e.g. for a TCL of 100 the gradient quality is poor if <GD> becomes higher than 0.25. The applied strategy can be used for other CRP or living polymerization techniques in a straightforward manner and its evaluation criterion can be extended to copolymers of any gradient type, provided that a corresponding linear correlation is derived.

Under batch ATRP conditions, using a catalyst consistent with Cu(I)Br/PMDETA, a copolymer with good linear gradient quality can be obtained if a high conversion is reached and an appropriate catalytic system is selected, leading to a low PDI. For higher TCLs, this correlation between PDI and <GD> shifts to lower <GD> values in case a well-controlled ATRP results.

References

1. Braunecker, W. A.; Matyjaszewski, K. *Progress in Polymer Science* **2007,** 32, (1), 93-146.
2. Davis, K.; Matyjaszewski, K. *Adv. Polym. Sci.* **2002,** 159, 1-13.
3. Matyjaszewski, K.; Xia, J. *Chemical Reviews* **2001,** 101, (9), 2921-2990.
4. Kamigaito, M.; Ando, T.; Sawamoto, M. *Chemical Reviews* **2001,** 101, (12), 3689-3746.
5. Tsarevsky, N. V.; Matyjaszewski, K. *Chemical Reviews* **2007,** 107, (6), 2270-2299.
6. Matyjaszewski, K. *Macromolecules* **2012,** 45, (10), 4015-4039.
7. Patten, T. E.; Matyjaszewski, K. *Advanced Materials* **1998,** 10, (12), 901-915.
8. Matyjaszewski, K. *Israel Journal of Chemistry* **2012,** 52, (3-4), 206-220.
9. Matyjaszewski, K.; Spanswick, J. *In: Matyjaszewski K and Möller M (eds.) Polymer Science: A Comprehensive Reference* **2012,** Vol. 3, 377-428; Amsterdam: Elsevier BV.
10. Matyjaszewski, K.; Shipp, D. A.; McMurtry, G. P.; Gaynor, S. G.; Pakula, T. *Journal of Polymer Science Part A: Polymer Chemistry* **2000,** 38, (11), 2023-2031.
11. Matyjaszewski, K.; Ziegler, M. J.; Arehart, S. V.; Greszta, D.; Pakula, T. *Journal of Physical Organic Chemistry* **2000,** 13, (12), 775-786.
12. Klumperman, B., 6.12 - Controlled Composition: Statistical, Gradient, and Alternating Copolymers. In *Polymer Science: A Comprehensive Reference*, Editors-in-Chief: Matyjaszewski, K.; Möller, M., Eds. Elsevier: Amsterdam, 2012; pp 433-453.
13. Peng, C.-H.; Kong, J.; Seeliger, F.; Matyjaszewski, K. *Macromolecules* **2011,** 44, (19), 7546-7557.
14. Shipp, D. A.; Wang, J.-L.; Matyjaszewski, K. *Macromolecules* **1998,** 31, (23), 8005-8008.
15. Al-Harthi, M.; Khan, M. J.; Abbasi, S. H.; Soares, J. B. P. *Macromolecular Reaction Engineering* **2009,** 3, (4), 148-159.
16. Kim, J.; Mok, M. M.; Sandoval, R. W.; Woo, D. J.; Torkelson, J. M. *Macromolecules* **2006,** 39, (18), 6152-6160.
17. Park, J.-S.; Kataoka, K. *Macromolecules* **2006,** 39, (19), 6622-6630.
18. Beginn, U. *Colloid & Polymer Science* **2008,** 286, (13), 1465-1474.
19. Ziegler, M. J.; Matyjaszewski, K. *Macromolecules* **2001,** 34, (3), 415-424.
20. Wang, R.; Luo, Y.; Li, B.; Sun, X.; Zhu, S. *Macromolecular Theory and Simulations* **2006,** 15, (4), 356-368.

21. Wang, R.; Luo, U.; Li, B.-G. *AIChE* **2007,** 53, 174-186.
22. Wang, L.; Broadbelt, L. J. *Macromolecules* **2009,** 42, (20), 7961-7968.
23. Wang, L.; Broadbelt, L. J. *Macromolecules* **2009,** 42, (21), 8118-8128.
24. Wang, L.; Broadbelt, L. J. *Macromolecules* **2010,** 43, (5), 2228-2235.
25. Szymanski, R. *e-Polymers* **2009,** no. 44.
26. Ye, Y.; Schork, F. J. *Industrial & Engineering Chemistry Research* **2009,** 48, (24), 10827-10839.
27. Arehart, S. V.; Matyjaszewski, K. *Macromolecules* **1999,** 32, (7), 2221-2231.
28. Min, K.; Oh, J. K.; Matyjaszewski, K. *Journal of Polymer Science, Part A: Polymer Chemistry* **2007,** 45, (8), 1413-1423.
29. Min, K. E.; Li, M.; Matyjaszewski, K. *Journal of Polymer Science, Part A: Polymer Chemistry* **2005,** 43, (16), 3616-3622.
30. Sheiko, S. S.; Sumerlin, B. S.; Matyjaszewski, K. *Progress in Polymer Science* **2008,** 33, (7), 759-785.
31. Lee, H.-i.; Pietrasik, J.; Sheiko, S. S.; Matyjaszewski, K. *Progress in Polymer Science* **2010,** 35, (1-2), 24-44.
32. Boerner, H. G.; Duran, D.; Matyjaszewski, K.; da Silva, M.; Sheiko, S. S. *Macromolecules* **2002,** 35, (9), 3387-3394.
33. Lee, H.-I.; Matyjaszewski, K.; Yu, S.; Sheiko, S. S. *Macromolecules* **2005,** 38, (20), 8264-8271.
34. Lord, S. J.; Sheiko, S. S.; LaRue, I.; Lee, H.-I.; Matyjaszewski, K. *Macromolecules* **2004,** 37, (11), 4235-4240.
35. Van Steenberge, P. H. M.; Vandenbergh, J.; D,'hooge, D. R.; Reyniers, M.-F. o.; Adriaensens, P. J.; Lutsen, L.; Vanderzande, D. J. M.; Marin, G. B. *Macromolecules* **2011,** 44, (22), 8716-8726.
36. Krallis, A.; Meimaroglou, D.; Kiparissides, C. *Chemical Engineering Science* **2008,** 63, (17), 4342-4360.
37. Chaffey-Millar, H.; Stewart, D.; Chakravarty, M. M. T.; Keller, G.; Barner-Kowollik, C. *Macromolecular Theory and Simulations* **2007,** 16, (6), 575-592.
38. Gillespie, D. T. *J. Phys. Chem.* **1977,** 81, 2340-2261.
39. Ahmad, N. M.; Charleux, B.; Farcet, C.; Ferguson, C. J.; Gaynor, S. G.; Hawkett, B. S.; Heatley, F.; Klumperman, B.; Konkolewicz, D.; Lovell, P. A.; Matyjaszewski, K.; Venkatesh, R. *Macromolecular Rapid Communications* **2009,** 30, (23), 2002-2021.

40. Yu-Su, S. Y.; Sun, F. C.; Sheiko, S. S.; Konkolewicz, D.; Lee, H.-i.; Matyjaszewski, K. *Macromolecules* **2011,** 44, 5928–5936.
41. D'hooge, D. R.; Reyniers, M.-F.; Stadler, F. J.; Dervaux, B.; Bailly, C.; Du Prez, F. E.; Marin, G. B. *Macromolecules* **2010,** 43, (21), 8766-8781.
42. Konkolewicz, D.; Sosnowski, S.; D'hooge, D. R.; Szymanski, R.; Reyniers, M.-F.; Marin, G. B.; Matyjaszewski, K. *Macromolecules* **2011,** 44, (21), 8361-8373.
43. Hlalele, L.; Klumperman, B. *Macromolecules* **2011,** 44, (18), 7100-7108.
44. Li, D.; Grady, M. C.; Hutchinson, R. A. *Industrial & Engineering Chemistry Research* **2004,** 44, (8), 2506-2517.
45. D'hooge, D. R.; Konkolewicz, D.; Reyniers, M.-F.; Marin, G. B.; Matyjaszewski, K. *Macromolecular Theory and Simulations* **2012,** 21, (1), 52-69.
46. Seeliger, F.; Matyjaszewski, K. *Macromolecules* **2009,** 42, (16), 6050-6055.
47. Tang, W.; Matyjaszewski, K. *Macromolecules* **2006,** 39, (15), 4953-4959.
48. Tang, W.; Matyjaszewski, K. *Macromolecules (Washington, DC, United States)* **2007,** 40, (6), 1858-1863.
49. Johnston-Hall, G.; Stenzel, M. H.; Davis, T. P.; Barner-Kowollik, C.; Monteiro, M. J. *Macromolecules* **2007,** 40, (8), 2730-2736.
50. Johnston-Hall, G.; Monteiro, M. J. *Journal of Polymer Science Part A: Polymer Chemistry* **2008,** 46, (10), 3155-3173.
51. Asua, J. M.; Beuermann, S.; Buback, M.; Castignolles, P.; Charleux, B.; Gilbert, R. G.; Hutchinson, R. A.; Leiza, J. R.; Nikitin, A. N.; Vairon, J.-P.; van Herk, A. M. *Macromolecular Chemistry and Physics* **2004,** 205, (16), 2151-2160.
52. Beuermann, S.; Buback, M.; Davis, T. P.; Gilbert, R. G.; Hutchinson, R. A.; Olaj, O. F.; Russell, G. T.; Schweer, J.; van Herk, A. M. *Macromolecular Chemistry and Physics* **1997,** 198, (5), 1545-1560.
53. D'hooge, D. R.; Reyniers, M.-F.; Marin, G. B. *Macromolecular Reaction Engineering* **2009,** 3, (4), 185-209.
54. Zetterlund, P. B. *Macromolecules* **2010,** 43, (3), 1387-1395.
55. Wang, A. R.; Zhu, S. *Macromolecules* **2002,** 35, (27), 9926-9933.
56. Tang, W.; Kwak, Y.; Braunecker, W.; Tsarevsky, N. V.; Coote, M. L.; Matyjaszewski, K. *Journal of the American Chemical Society* **2008,** 130, (32), 10702-10713.

Chapter 6: General conclusions and future prospects

6.1. General conclusions

A kinetic Monte Carlo (kMC) methodology has been developed which allows to optimize radical polymerization processes. Depending on the desired level of detail, both multivariate and explicit descriptions can be selected. The methodology has been successfully applied to two radical processes: the radical polymerization of *p*-quinodimethane derivatives obtained from *p*-xylene premonomers toward poly(p-phenylene vinylene)s (PPVs) and atom transfer radical polymerization (ATRP). For the PPV process, the premonomers 1-(chloromethyl)-4-[(n-octylsulfinyl)methyl]benzene (and derivatives) and 2,5-bis(N,N-diethyldithiocarbamate-methyl)-1-(3,7-dimethyloctyloxy)-4-methoxybenzene are considered resp. via the sulfinyl and the dithiocarbamate (DTC) precursor route. For the ATRP process, acrylates and methacrylates are considered as comonomers.

For the premonomer 1-(chloromethyl)-4-[(n-octylsulfinyl)methyl]benzene in sBuOH, kMC simulations show that intramolecular and intermolecular recombination can be neglected and that the final polymer yield and average polymer properties are only determined by the ratio of the initial base to premonomer concentration, while the absolute initial concentrations determine in turn the rate at which the final yields and properties are reached. Rate coefficients are based on comparison with experimental data. The effect of the leaving group, polarizer, aromatic moiety and aromatic substituents on the monomer formation can be modeled based on reported ab initio data and kinetic UV-vis data. The effect of aromatic substituents on the (co)polymer yield and properties can be modeled using Hammett relations. In particular, it is shown that PPVs with electron donating substituents possess high chain lengths while PPVs with electron withdrawing substituents possess low chain lengths.

For the premonomer 2,5-bis(N,N-diethyldithiocarbamate-methyl)-1-(3,7-dimethyloctyloxy)-4-methoxybenzene, kMC simulations reveal that the regioregular character in the resulting poly(2-methoxy-5-(3',7'-dimethyloctyloxy)-1,4-phenylenevinylene) (MDMO-PPV) can be influenced by the base type. For bulky bases leading to a regioselective 1,6-elimination, the regioregular triad is formed more and, hence, such bases should be selected for improved photovoltaic performance. In particular, based on ^{1}H NMR data of the triad distribution the kMC model allowed to determine that for lithium bis(trimethylsilyl)amide (LHMDS) the

reactivity of 1,6-elimination of the premonomer via the unhindered protons is three times higher than via the hindered protons.

For the ATRP of acrylates and methacrylates, an explicit calculation of the copolymer composition is performed using the kMC technique allowing for the first time an evaluation of the linear gradient quality. Per copolymer chain k, a gradient deviation GD(k) is calculated with respect to perfect theoretical gradient copolymer chains of the same chain length. For a <GD> value of 0.25 or lower, the gradient quality of the copolymer is defined as good. The applied strategy can be applied to other controlled radical polymerization or living polymerization techniques in a straightforward manner and can be easily extended to copolymers of any gradient type. Under batch ATRP conditions, a copolymer characterized by a low PDI value and high end-group functionality can be obtained with good gradient quality. More important, the gradient quality can be assessed by a measurement of the PDI. Low PDI values lead to low <GD> values and thus a high gradient quality.

6.2. Future prospects

The potential of kMC techniques to develop univariate descriptions of the microstructure of linear polymers has been illustrated in Chapters 2, 3 and 4. There it is demonstrated that the chain length can be used as the only stochastic variable to optimize PPV properties at laboratory scale. Similar to the deterministic approach, diffusional limitations can be accounted for using apparent rate coefficients. However, as explained in Chapter 1, in case branching becomes very important and monomer sequences have to be tracked as well, methods using individual tracking of macromolecules are necessary.

A first step toward methods using individual tracking of macromolecules to describe the polymer microstructure at laboratory scale has been made in this work through the development of a kinetic model for ATRP copolymerization (Chapter 5). Not only the monomer content and chain length are described, but also the monomer connectivity in each polymer chain. Diffusion limitations of the termination kinetics have been considered based on the average chain length.

A logical next step is extending the models toward arbitrary topology, paving the way to describe apparent reactivity of the macromolecules not only depending on their chain length but also on their branching degree, their number of reactive centers, etc. In the long run, this allows to model the architecture of e.g. branched polymers, brushes, stars, networks, dendrites

and thus to optimize existing polymerization processes and to support the development of new functional polymers. For such simulations, sufficiently large samples of macromolecules must however be generated to obtain accurate results. Hence, partitioning of the reaction volume and subsequent parallelization may be necessary. Such parallelization has recently been performed for univariate descriptions of linear polymers, but only to decrease calculation time, not to track explicitly a large sample of polymer molecules.

In addition, it is desired to use models which individually track macromolecules when performing the polymerization at industrial reactor scale. In these cases, large reaction volumes are used and the polymerization is frequently performed in a dispersed medium, e.g. emulsion and suspension, to gain further control over the polymer properties and/or to allow an efficient scale-up e.g. to address heat transfer issues. Such processes may be considered to behave as a large number of droplets/particles interacting with each other via the continuous phase. The natural problem arising here is that in general each droplet/particle should be characterized by its own ‘concentrations’. Deterministic models have been found limiting to describe such processes, due to the large number of variables needed. The parallelizability of kMC methods may aid in describing these processes, for example by executing a number of independent simulations, each simulating a part of the total number of droplets. Coalescence, aggregation, nucleation or breakage phenomena involving all droplets may be treated by a master simulation, i.e., the particle size distribution (PSD) is calculated at a larger scale.

A final future prospect to be mentioned here is related to the influence of molecular diffusion and mixing effects at these larger scales. Due to the viscosity increase along the polymerization, apparent kinetics result mainly due to the reduced mobility of macrospecies with high chain length. Accurate apparent rate coefficients, based on the explicit representation of their microstructure, are necessary to optimize polymer properties. Furthermore, at industrial scales the bulk concentrations and/or the PSD can become dependent on the spatial coordinate necessitating the combination of the previous models with mixing models and eventually computational fluid dynamics calculations.

Appendices

Appendix A: Kinetic Monte Carlo model

The kinetic Monte Carlo method is used to calculate the entire molar mass distribution. This method is easy to implement and does not rely on assumptions such as the quasi steady state approximation for reactive species. Unlike other numerical methods, no manual fine-tuning of numerical integration parameters is necessary, due to the brute-force nature of the method.

A kinetic Monte Carlo (kMC) model was developed on the basis of the stochastic simulation algorithm developed by Gillespie.[1-2] Instead of species concentrations, these models track discrete particles in a microscopic-scale homogeneous reaction volume V representative of the complete system. Additionally, these models are based on a simple iterative procedure that does not involve the integration of coupled differential equations.

In the "stochastic simulation algorithm",[1] reactions are described using reaction events. Hence, all concentrations must be converted to numbers of molecules:

$$n_A = C_A \cdot V \cdot N_A \qquad \text{(A1)}$$

n_A is the number of molecules of molecule A, C_A is the concentration of molecule A, V is the simulated reaction volume (many orders of magnitude smaller than the real reaction volume) and N_A is the Avogadro number. In order to calculate rates (and probabilities), the macroscopic rate coefficients k_{mac} of the considered reactions are converted to microscopic rate coefficients k_{mic} as follows:

For unimolecular reactions: $k_{mic} = k_{mac}$

For bimolecular reactions between distinguishable species: $k_{mic} = \frac{k_{mac}}{V \cdot N_A}$

For bimolecular reactions between indistinguishable species: $k_{mic} = \frac{2 \cdot k_{mac}}{V \cdot N_A}$

In order to calculate a reaction rate (and probability) in a next step, the number of combinations of molecules h leading to that particular reaction is calculated as follows:

For unimolecular reactions: $h = n_A$

For bimolecular reactions between distinguishable species: $h = n_A n_B$

For bimolecular reactions between indistinguishable species: $h = \frac{n_A(n_A-1)}{2}$

The rate R (in s^{-1}) of a reaction is then calculated as:

$$R = h \cdot k_{mic} \qquad \text{(A2)}$$

and represents the number of reaction events occurring per second in the volume V. This is done for every reaction ν (1, ..., M):

$$R(\nu) = h(\nu) \cdot k_{mic}(\nu) \qquad \text{(A3)}$$

The calculation of the reaction rates is based on the reaction scheme presented in Figure 4 in Chapter 2. The actual monomer para-quinodimethane is formed via a base induced 1,6-elimination and can be consumed by the base via a nucleophilic addition, yielding an ether byproduct P_1. Next to these anionic reactions, the para-quinodimethane may also dimerize and form a diradical initiator. The para-quinodimethane monomer adds to the initiator radical and forms macrodiradicals, which may recombine (not shown in Figure 4 in Chapter 2). In particular for the polymerization of p-quinodimethanes, the following functions h(ν) and k_{mic}(ν) are obtained (Table A1):

Table A1: Definition of kinetic Monte Carlo rate expressions; n_i denotes the number of molecules of species i; RO^- is the base, HML the premonomer, M the monomer, R_{tot} the α,ω-macrobiradicals and R_2, R_3, R_4 oligomeric radicals with chain lengths 2,3,4 respectively; IUPAC convention is used for termination by recombination

reaction	ν	$k_{mic}(\nu)$	h(ν)
1,6-elimination	1	$k_{E2}\,(VN_A)^{-1}$	$n_{RO^-}\, n_{HML}$
nucleophilic addition	2	$k_{NA}\,(VN_A)^{-1}$	$n_{RO^-}\, n_M$
initiation	3	$2\,k_{ini}\,(VN_A)^{-1}$	$n_M\,(n_M - 1)/2$
propagation	4	$k_p\,(VN_A)^{-1}$	$n_M\, n_{Rtot}$
recombination	5	$2\,k_{rc}\,(VN_A)^{-1}$	$n_{Rtot}\,(n_{Rtot} - 1)/2$
cyclization	6	k_{cyc}	$n_{R2} + n_{R3} + n_{R4}$

For well-mixed reaction volumes, it can be proven[1,2] that the time τ between two reaction events (not necessarily of the same reaction) is exponentially distributed. A sample from this distribution can be calculated[1,2] as follows:

$$\tau = \frac{-\ln r_1}{\sum_{\nu=1}^{\nu=M} R(\nu)} \qquad \text{(A4)}$$

Where r_1 is a sample from a uniform distribution between 0 and 1. Hence, if the simulation is starts at t = 0, the time of the first event is given by τ. Note that the time between two reaction events decreases with R, the number of reaction events occurring per second in the reaction volume.

To determine which reaction is taking place at this time τ, the reaction rates are rescaled to obtain probabilities P(ν):

$$P(\nu) = \frac{R(\nu)}{\sum_{\nu=1}^{\nu=M} R(\nu)} \qquad \text{(A5)}$$

In case five reactions are considered, an example distribution of reaction probabilities with respect to ν (the number designating the reaction) is depicted in Figure A1 (left).

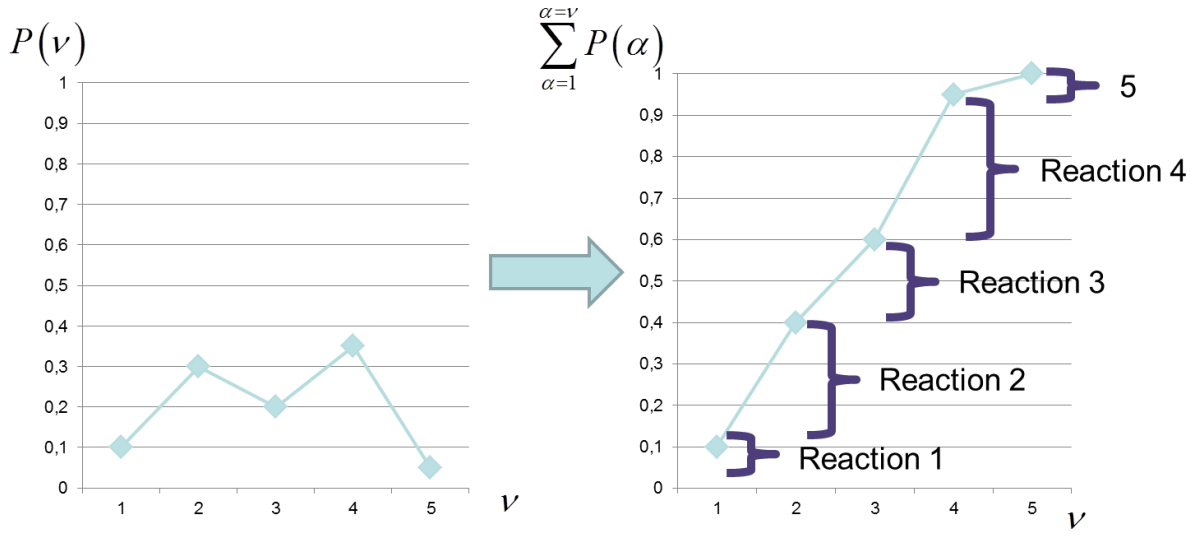

Figure A1: Sampling the reaction event from known reaction rates in the stochastic simulation algorithm; left: distribution of reaction probabilities; right: cumulative distribution of reaction probabilities

At this point, two methods can be distinguished, depending on how the reaction event is sampled from P(ν): the "direct method" and the "logarithmic direct" method.

A.1. Direct method

The direct method is suitable for reactions between species which are not distributed. To sample a reaction event from P(ν) (still at time τ) according to the direct method, one option is to calculate the cumulative probability function $\sum_{\alpha=1}^{\alpha=\nu} P(\alpha)$ (Figure A1 (right)). If a random value between 0 and 1 is chosen on the y-axis, the accolades indicate which reaction occurs. Thus, a value for ν obtained by such approach is a sample of a stochastic variable with distribution P(ν). Hence, Figure A1 illustrates the following criterion for the sampling of a reaction event:

$$\sum_{\nu=1}^{\nu=\mu-1} P(\nu) < r_2 < \sum_{\nu=1}^{\nu=\mu} P(\nu) \qquad \text{(A6)}$$

in which r_2 is a second sample of the uniform distribution between 0 and 1, μ is the number designating the reaction from which an event was sampled. Equations A4 and A6 have been rigorously proven.[1,2] Practically, μ is determined with a linear search on the cumulative reaction probability (Equation A6).

Once the sample of the reaction event at time τ is determined, the numbers of molecules related to that particular reaction are updated. E.g. for the generic reaction event A+B → C:

before the execution: $n_A = 10$ $n_B = 10$ $n_C = 0$

after the execution: $n_A = 9$ $n_B = 9$ $n_C = 1$

At this point, the first event has been finalized and the second event begins by updating the number of combinations of molecules h and recalculating the probabilities, the timestep τ, and so on. The stochastic simulation algorithm ends at predefined time or when all reaction rates are 0.

The only adjustable parameter in the kMC model is the size of the control volume V, which was increased until the stochastic noise in the simulated responses disappeared. A different approach to obtain noise-free results is to perform a large number of runs with small control volumes.[4]

As mentioned before, the direct method is suitable for species which are not distributed with respect to their chain length. For fast calculation of reactions between species which are distributed with respect to their chain length, the "logarithmic direct"[4,5] method is used.

A.2. Logarithmic direct method

If the reaction event to be sampled involves distributed species, such as polymers, binary searches using partial sums of probabilities (logarithmic method) are more suitable[4-5] (see Chapter 1) than linear searches on the cumulative probabilities (direct method).

A.2.1. Propagation reactions

For example, consider propagation reactions up to a chain length of 1024. In the direct method, R(ν) with ν = 1, ..., 1024 for the propagation reactions would be defined, using a time-consuming linear search over 1024 elements in an array to determine μ (the propagation radical). This would lead (on average) to 512 searches for symmetrical macroradical distributions. In contrast, the logarithmic method defines a single overall propagation reaction rate according to:

$$R(1) = k_{p,mic} \cdot n_{Rtot} \cdot n_M \qquad \text{(A7)}$$

Which is the total propagation rate of all the macroradicals. If this (pseudo) reaction channel is selected by the algorithm, then a macroradical with a specified chain length must be sampled in an additional step to calculate/update the CLD of the macroradicals. The sampling of the macroradical is performed using a binary tree in $\log_2(1024) = 10$ steps as explained in Chapter 1, as opposed to 512. Note that this additional step is not present in the direct method, because in the direct method both the propagation reaction and the chain length of the macroradical are sampled in one step.

The binary tree can be contained in an array by numbering the tree nodes from left to right and top to bottom (Figure A2; shown for a maximum chain length of 8), which is a natural numbering for the nodes of a binary tree to allows traversing up and down along the tree by simple instructions. E.g. traversing down the tree to the left corresponds to multiplying the node number by two, whereas a right turn corresponds to multiplying by two and adding one.

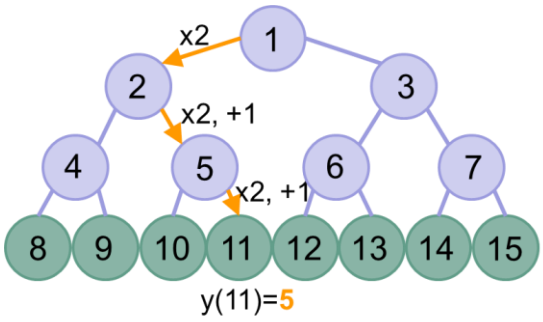

Figure A2: Arrangement of a binary tree in an array; the lower 8 nodes represents the chain lengths 1, …, 8

The numbers of radicals with a given chain length (1, …, 8) are stored in the second half of the tree (green; Figure A3). The first half (purple) of the tree is reserved for partial sums to optimize searching. Note that each leaf is the sum of the two underlying leafs, which differs markedly from the strategy utilizing the cumulative distribution to sample reactants/reactions (Figure A1). Figure A3 shows a total number of radicals of 39, of which 10 radicals have a chain length of 1, 9 radicals of chain length 2,… and 1 radical of chain length 8.

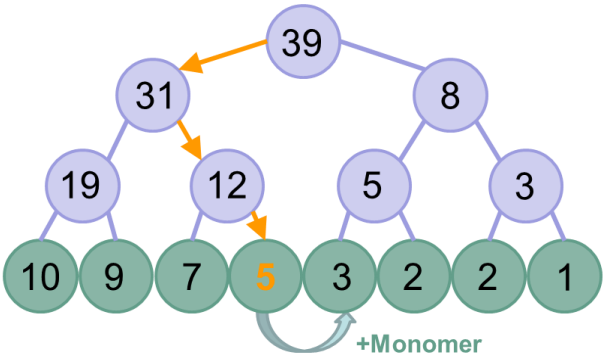

Figure A3: (Macro)radicals of chain lengths 1, …, 8 contained in a binary tree data structure; $\log_2(8) = 3$ choices determine the radical (orange arrows)

To sample a macroradical (with known chain length) after selecting a propagation event according to Equation (A7), a third sample of the uniform distribution between 0 and 1 is used and multiplied by the total number of radicals: e.g. 0.769 * 39 = 30. For simplicity and explaining the algorithm, it can be said that the 30th radical (of the 39 radicals present) is sought.

In the first step traversing down the three, the algorithm checks whether this number (30) is larger than or equal to the value in node 2 (containing the number 31; Figure A3). If this would be the

case, the algorithm continues the search in the right sub-tree of the first node, which contains the "last" 8 radicals of the 39 radicals in the mixture. However, since 30 < 31, the radical to be determined is contained in the left sub-tree of the second node in Figure A3, which contains the "first" 31 radicals of the 39 radicals in the mixture. For this reason, the algorithm chooses to traverse down to the left sub-tree of the first node. This step has reduced the size of the three. The next step is similar, but the tree is smaller.

In the second step, the algorithm compares 30 with 19, since 30 > 19 the radical must now be in the right sub-tree of the second node, discarding the 19 radicals in node 4. Hence, when a "right" choice is made, the number 30 is decreased by these 19 radicals: 30 – 19 = 11, indicating that the 11^{th} radical of the 12 radicals in node 5 is sought. The second step has further reduced the size of the tree.

In the third and final step, 11 is compared with 7 and the algorithm chooses "right" because the 11^{th} radical must be in the last 5 radicals contained in the sub-tree of node 11. At this point the end of the tree is reached.

Now, the chain length of the macroradical must be updated for the propagation event. Node 11 corresponds to a chain length of 4 by definition (Figure A2). To execute the propagation, the value of node 11 is decreased by a value of one and a radical of chain length 5 is added to node 12 by increasing its value by one. The propagation reaction is then finalized and a next reaction is started.

Note that the above illustration is for a a maximum chain length of 8 and a three height of 3 ($\log_2(8) = 3$) and can be extended easily to chain lengths of 1024 (height 10) and higher.

A.2.2. Recombination reactions

Similar to propagation reactions, recombination reactions are described using an overall recombination rate:

$$R(1) = k_{tc,mic} \cdot \frac{n_{Rtot} \cdot (n_{Rtot} - 1)}{2} \qquad \text{and}$$

$$k_{tc,mic} = \frac{2 \cdot k_{tc,mac}}{V \cdot N_A} \qquad \text{(A8)}$$

If a recombination reaction event is sampled, then in an additional step two macroradicals should be sampled from the binary tree. This is very similar to the binary search for locating a propagating radical, with the exception it has to be performed twice for two recombining radicals. If the chain lengths of the recombining radicals are i and j, then the numbers of macroradicals of chain length i and j in the binary tree are decreased by unity. From the found chain lengths of the two sampled (recombining) macroradicals, the number of dead polymers with a chain length i + j is increased in a *new* binary tree for the dead polymer molecules.

For disproportionation reactions, the chain lengths i and j of the two sampled macroradicals are used for the formation of two dead polymer molecules.

References

1. Gillespie, D. T. *J. Phys. Chem.* **1977**, 81, 25, 2340-2361.
2. Gillespie, D. T. *J. Comput. Phys.* **1976**, 22, 403-434
3. Szymanski, R. e-polymers **2009**, 044.
4. Chaffey-Millar, H.; Stewart D.; Chakravarty, M. M. T.; Keller, G.; Barner-Kowollik, C. *Macromol. Theor. Simul.* **2007**, 16, 6, 575-592.
5. Gibson, M. A.; Bruck, J. *J. Phys. Chem. A* **2000**, 104, 9, 1876-1889.

Appendix B: Mathematical details of the Guggenheim method

For the reaction scheme HML → M → P_1 , with rate coefficients $k_1 = k_{E2}\,[RO^-]_0$ and $k_2 = k_{NA}\,[RO^-]_0$, it can be proven that the concentration of the intermediate is given by ($k_1 \neq k_2$)

$$[M] = [HML]_0 \frac{k_1}{k_1 - k_2}\left(e^{-k_2 t} - e^{-k_1 t}\right) \qquad \text{(B1)}$$

The absorbance corresponding to this concentration can be expressed with the law of Bouguer-Lambert-Beer:

$$A_M(t) = l\varepsilon[M] = l\varepsilon[HML]_0 \frac{k_1}{k_1 - k_2}\left(e^{-k_2 t} - e^{-k_1 t}\right) \qquad \text{(B2)}$$

For high reaction times and $k_1 >> k_2$, the second term disappears and k_2 can easily be determined via linear regression from:

$$\ln\left(A_M(t)\right) = \ln\left(l\varepsilon[HML]_0 \frac{k_1}{k_1 - k_2}\right) - k_2 t \quad \text{for} \quad t \to \infty \qquad \text{(B3)}$$

To determine the k_1-value, low reaction times ($t \to 0$) are needed to ensure the second reaction (k_2) is not interfering:

$$A_M(t) = l\varepsilon[HML]_0 \frac{k_1}{k_1 - k_2}\left(1 - e^{-k_1 t}\right) \text{ for } \quad t \to 0 \qquad \text{(B4)}$$

It must be clear at this point that a logarithmic plot will not yield a straight line from which a rate coefficient can be regressed. Expressing the absorbance as a function of $t + \Delta t$:

$$A_M(t + \Delta t) = l\varepsilon[HML]_0 \frac{k_1}{k_1 - k_2}\left(1 - e^{-k_1 (t + \Delta t)}\right) \qquad \text{(B5)}$$

Subtracting both expressions cancels the constant term:

$$A_M(t + \Delta t) - A_M(t) = l\varepsilon[HML]_0 \frac{k_1}{k_1 - k_2}\left(1 - e^{-k_1 \Delta t}\right)e^{-k_1 t} \qquad \text{(B6)}$$

Which yields an

expression from which k_1 can be regressed:

$$\ln\left[A_M\left(t+\Delta t\right)-A_M\left(t\right)\right]=\ln\left[l\varepsilon\left[HML\right]_0\frac{k_1}{k_1-k_2}\left(1-e^{-k_1\Delta t}\right)\right]-k_1t \qquad \text{(B7)}$$

Note that Δt is a parameter in this method. In the application of the Guggenheim method, various values of Δt were used. However, none of them gave a meaningful difference as long as properly selected exponential regions of the absorbance $A_M(t)$ were used as input for the Guggenheim method.

Appendix C: Linear regression for determination of k_{E2} and k_{NA}

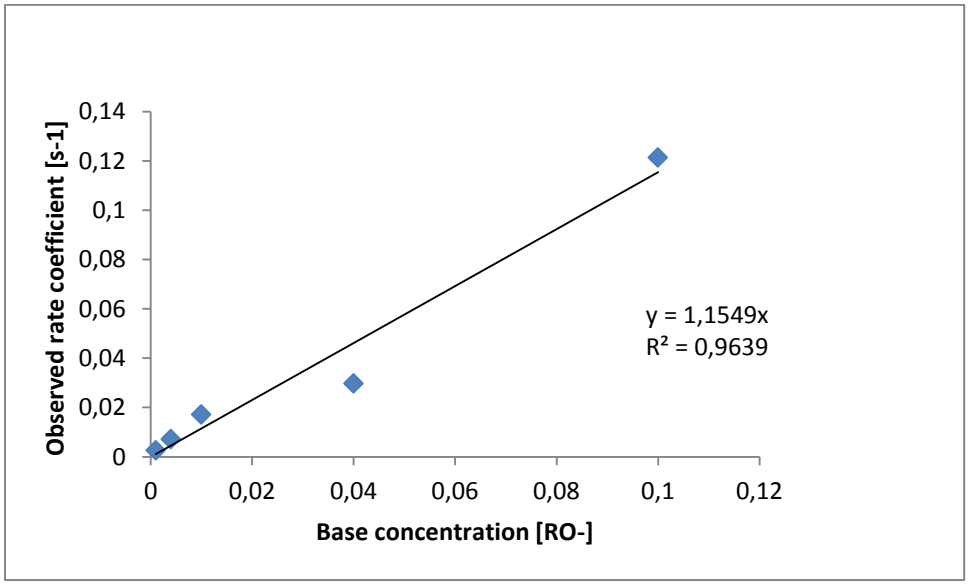

Figure C1: Observed rate coefficient for 1,6-elimination as a function of the base concentration. Reaction conditions: 298 K, $[HML]_0 = 10^{-4}$ mol L^{-1}, $[RO^-]_0 = 10^{-3}$ mol L^{-1} – 10^{-1} mol L^{-1}. Symbols: slopes from the straight lines determined from the Guggenheim method (Figure 6 in Chapter 2). Full line: linear regression. The slope of the straight line is the intrinsic rate coefficient for the 1,6-elimination

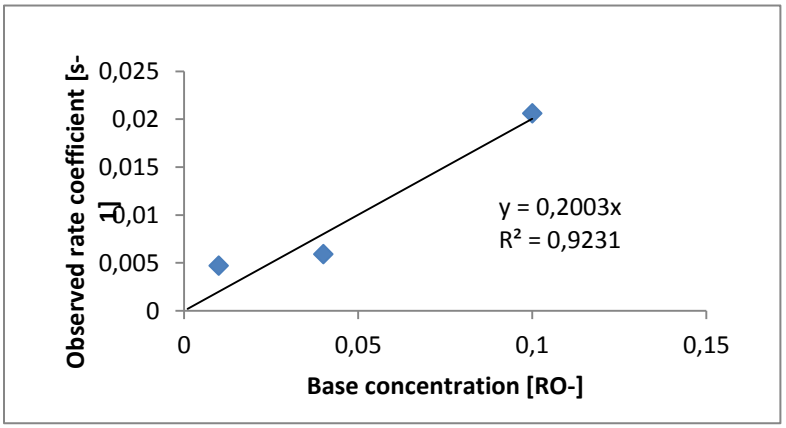

Figure C2: Observed rate coefficient for conjugate nucleophilic addition as a function of the base concentration. Reaction conditions: 298 K, $[HML]_0 = 10^{-4}$ mol L^{-1}, $[RO^-]_0 = 10^{-2}$ mol L^{-1} – 10^{-1} mol L^{-1}. Symbols: slopes from the straight lines determined from the Guggenheim method (Figure 7 in Chapter 2). Full line: linear regression. The slope of the straight line is the intrinsic rate coefficient for the conjugate nucleophilic addition

Appendix D: Mass chain length distributions for the sulfinyl route

The simulated chain length distributions corresponding to the experimental data of van Breemen et al.[55] (Table 2 in Chapter 2) are given for 3 different times throughout the polymerization process.

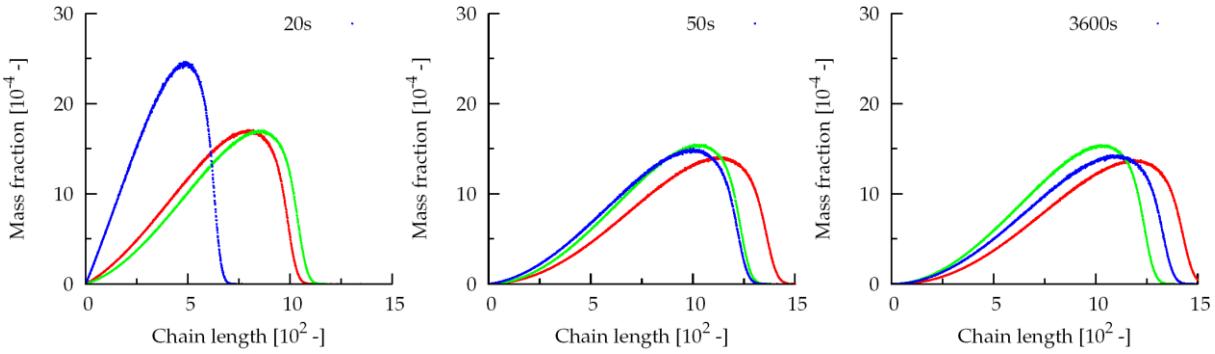

Figure D1: Simulated molar mass distributions as a function of base concentration and polymerization time (20, 50 and 3600s). Reaction conditions: 308 K, $[HML]_0$ = 0.1 mol L^{-1}, $[RO^-]_0$ = 0.05 mol L^{-1} (blue line), 0.13 mol L^{-1} (red line), 0.20 M (green line)

Appendix E: Procedures

All reported mass averaged molar mass and structural defects are calculated based on the α,ω-macrodiradical population. This makes sense when comparing simulations with experiments: in practice, ^{13}C NMR is performed on the high molar mass fraction only since the cyclic oligomers are not isolated with the polymer. A similar remark must be made for the mass averaged molar mass in this simulation: including the cyclic oligomer population in the calculation of the mass averaged molar mass is equivalent to including a sharp peak around chain lengths i = 2, 3 and 4 in the Size Exclusion Chromatogram (SEC) elugram integration to determine the average molar masses of the product. For the above reasons, only the α,ω-macrodiradical population is used to calculate the polymer characteristics.

Appendix F: Effect of reaction conditions on monomer and precursor PPV formation

After ensuring that termination reactions can be neglected, the effect of the reaction conditions on the PPV process can be investigated over a broad range of concentrations. Kinetic Monte Carlo simulations are used to illustrate the effect of the reaction conditions on the yields of the 3 main compounds (premonomer, byproduct and polymer). As illustrated in Figure F1, a gradual transition in the product yields, going from purely byproduct over almost exclusively radical polymer to only starting product (premonomer), is observed.

In Figure F1, the graphs are arranged as follows: from left to right the effect of increasing initial premonomer concentration can be seen while from top to bottom the effect of increasing initial base concentration can be observed. Qualitatively, 3 regimes exist depending on the ratio $[RO^-]_0/[HML]_0$. The 3 cases on the leading diagonal, for which $[RO^-]_0/[HML]_0 = 1$, show the highest polymer yield. The 3 cases in the upper right corner of Figure 10, for which $[RO^-]_0/[HML]_0 < 1$, show the highest premonomer yield. The 3 cases in the lower left hand corner of Figure 10, for which $[RO^-]_0/[HML]_0 > 1$, show the highest byproduct yield. Hence, a shift in product yield is possible when increasing or decreasing one of the reactant concentrations by an order of magnitude. On the other hand, when both reactant concentrations are increased or decreased by an order of magnitude (e.g. the 3 figures on the leading diagonal), no shift in product yields is observed. Instead, the reaction kinetics slow down or speed up by an order of magnitude (note the appropriate scaling of the x-axis), yielding identical final values of the properties and yields. In other words, the final polymer properties and yields are only influenced by the ratio $[RO^-]_0/[HML]_0$. This can be understood by the bimolecular nature of all involved reactions and, hence, the independence of the relative reaction rates on the absolute values of the concentrations. It must be stressed that there is no dilution effect on the final yields and properties because unimolecular reactions are absent in the model. The direct consequence of the above observation is that a single independent variable, i.e. $[RO^-]/[HML]_0$, can be used to visualize the results.

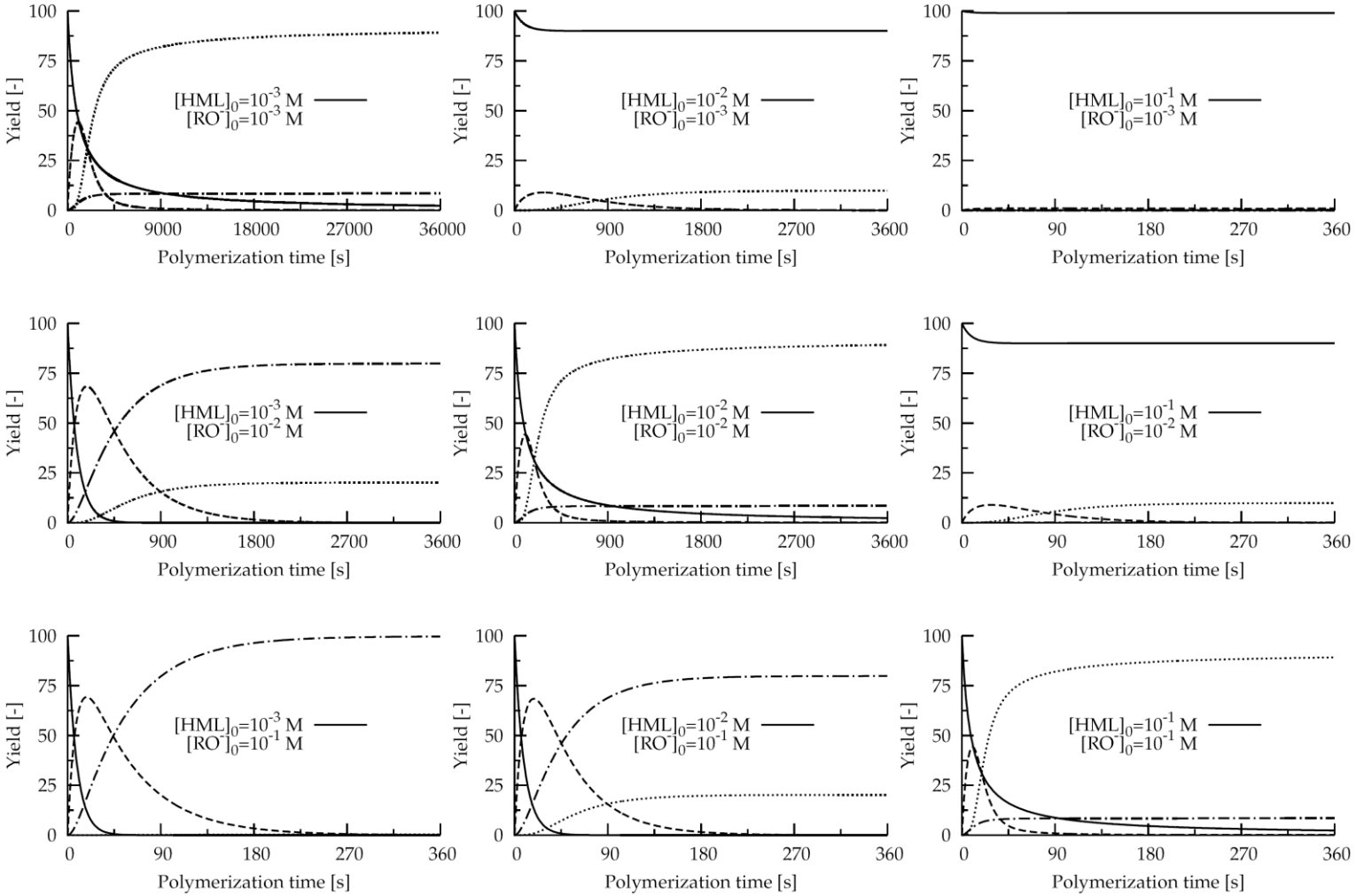

Figure F1: Influence of initial premonomer and base concentration on the simulated yields of premonomer HML, p-quinodimethane M, substitution product P_1 and polymer. Reaction conditions: 308 K, $[HML]_0 = 10^{-3}$ mol L^{-1}, 10^{-2} mol L^{-1}, 10^{-1} mol L^{-1}, $[RO^-]_0 = 10^{-3}$ mol L^{-1}, 10^{-2} mol L^{-1}, 10^{-1} mol L^{-1}. Full line: premonomer yield. Dashed line: monomer yield. Dashed-dotted line: substitution product yield. Dotted line: polymer yield

Appendix G: The Hammett relation

The Hammett relation for a reaction family, in which the members are distinguished by varying substituents, may be written as:

$$\log \frac{k}{k_0} = \rho\sigma \qquad \text{(G1)}$$

in which ρ depends, in principle, only on the type of the reaction family and the reaction conditions but not the substituent, whereas σ depends only on the substituent but not the nature of the reaction family or the reaction conditions. The reference substituent is always chosen to be the hydrogen atom, and σ is chosen to be 0 for the hydrogen atom. In this case, the rate coefficient of the reaction is k_0, the reference rate coefficient of the reaction.

If the substituent is more electronegative than the hydrogen atom, then σ is positive. If the substituent is less electronegative than the hydrogen atom, then σ is negative. Hence, for an increase of the rate coefficient k when the substituent becomes electronegative, ρ should be positive.

Appendix H: Determination of rate coefficients and Hammett relations for the sulfinyl route

Hermosilla et al. report[1] UV-vis data and calculated deprotonation energies in diluted conditions and high base excess. These data are suitable to determine rate coefficients for the 1,6-elimination and the nucleophilic addition, without interference of polymerization reactions. The 1,6-elimination rate coefficients are determined from reported deprotonation energies and the conjugate nucleophilic addition rate coefficients are determined from the times of maximum UV-vis absorbance. The resulting rate coefficients are given in Table H1. From these rate coefficients, Hammett reaction constants ρ_{E2} = 3.86 and ρ_{NA} = 1.56 result (Table H2), both indicating negatively charged transition states. In the following two sections, detailed explanations are given.

H.1. 1,6-elimination

To model the effect of the leaving group, the leaving group is changed from Cl (premonomer **1**) to Br (premonomer **10**). The k_{E2}(L=Br) value of **10** is determined by calculating a reactivity ratio k_{E2}(L=Br)/k_{E2}(L=Cl) based on the k_{E2} values reported by Hermosilla et al. and then multiplying this reactivity ratio with the k_{E2}(L=Cl) value reported in (2). Ratios determined by UV-vis are used because they are in good agreement with ratios from theoretical modeling.[1]

To model the effect of the polarizer, the polarizer is changed from P=SOC_8 (premonomer **1**) to P=SO_2C_8 (premonomer **13**). The k_{E2}(P=SO_2C8) value of **13** was determined by calculating a reactivity ratio k_{E2}(P=SO_2C_8)/k_{E2}(P=SOC_8) based on the k_{E2} values reported by Hermosilla et al. and then multiplying this reactivity ratio with the k_{E2}(P=SOC8) value reported in (2). Ratios determined by UV-vis are used because they are in good agreement with ratios from theoretical modeling.[1]

To model the effect of the substituents on the aromatic moiety, the logarithms of the known k_{E2} values of premonomers **1**, **10** and **13** are correlated with their known deprotonation energies (Figure H1).

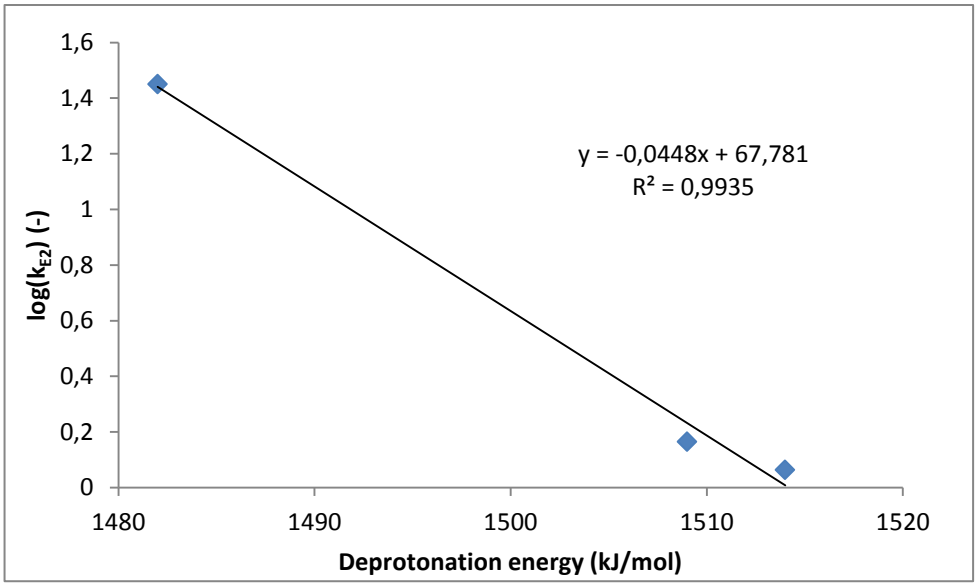

Figure H1: Correlation of deprotonation energies of premonomers 1, 10 and 13 with rate coefficients from UV-vis spectroscopy; Deprotonation energies taken from (1)

From the reported deprotonation energies of premonomers **2**, **4**, **9**, **11** and **12**, the correlation allows to calculate the corresponding k_{E2} values. No deprotonation energies for the remaining premonomers are available in literature, hence Hammett's relation is used: From the k_{E2} values of **1**, **2**, **4** and **9** Hammett's ρ_{E2} value is calculated to be 3.86 (Figure H2), allowing to calculate the remaining k_{E2} values. The used Hammett substituent constants σ are calculated as $\sigma_{meta} + \sigma_{ortho}$. σ_{ortho} is assumed[3] to be 75% of σ_{para}. σ_{meta} and σ_{para} are taken from (4).

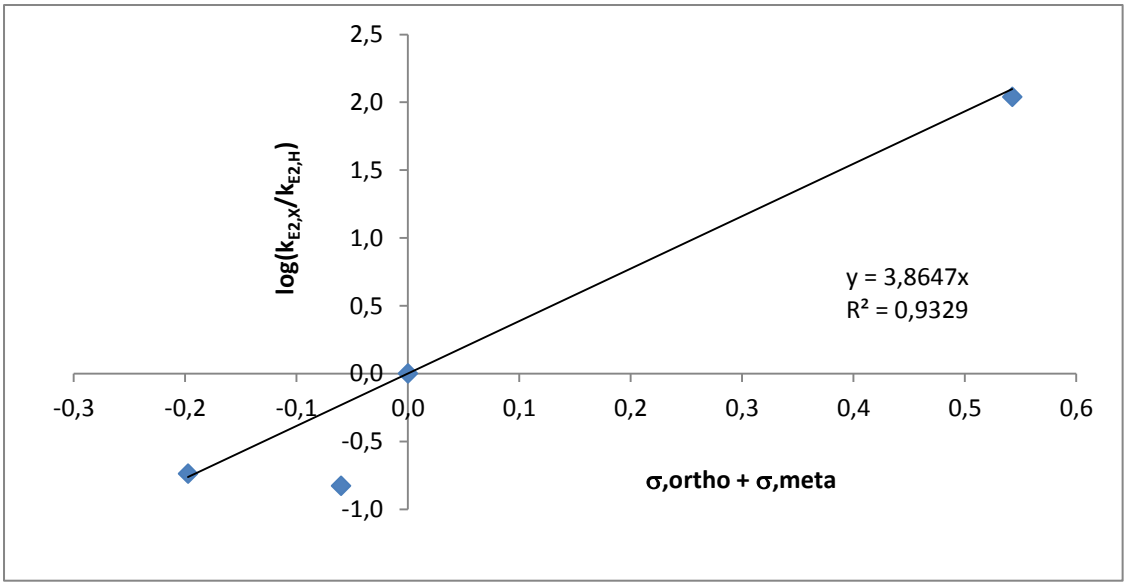

Figure H2: Hammett plot for the 1,6-elimination of premonomers 1, 2, 4 and 9; Reaction condition: 298 K

H.2. Conjugate nucleophilic addition

Because the leaving group has parted during the formation of the para-quinodimethane, there is no effect of leaving group on the k_{NA} for premonomer **10**, the value is taken equal to the k_{NA} for premonomer **1**.

To model the effect of the polarizer, the Guggenheim method is performed using Hermosilla's UV-vis spectra to obtain pseudo-first order rate coefficients. Again a reactivity ratio $k_{NA}(P=SO_2C_8)/k_{NA}(P=SOC_8)$ is determined. Multiplication with the k_{NA} value for premonomer **1** yields the k_{NA} value for premonomer **13**. Ratios determined by UV-vis are used because they are in good agreement with ratios from theoretical modeling.[1]

The reliability of the k_{NA} values for premonomers **1**, **10** and **13** can be verified as follows. It has been demonstrated[1] that, in diluted UV-vis conditions and the base in excess, the only reactions occurring are:

$$HML \rightarrow M \rightarrow P_1 \qquad \text{(H1)}$$

With pseudo first order rate coefficients $k_{E2}[RO^-]_0$ and $k_{NA}[RO^-]_0$ ($[RO^-]_0 = 25\ 10^{-2}$ M). For this two-step mechanism, it can be proven by mass conservation that the time of maximum concentration of the intermediate M is:

$$t_{max,analytic} = \frac{\ln\left(\frac{k_{E2}}{k_{NA}}\right)}{(k_{E2} - k_{NA})[RO^-]_0} \qquad \text{(H2)}$$

$t_{max,analytic}$ is thus calculated from the k_{E2} and k_{NA} values for **1**, **10** and **13** and compared to the reported[1] $t_{max,experimental}$ values in Figure 6 in Chapter 3, which shows a parity plot. It appears that the k_{NA} values for premonomers **1**, **10** and **13** determined via both independent methods are in excellent agreement. Hence, the use of Equation (H2) is deemed reliable and is also used for the k_{NA} values of **2**, **4**, **9**, **11** and **12**: t_{max} is reported[1] and k_{E2} is known from correlating deprotonation energies as demonstrated in the previous section, hence equation (H2) can be solved for k_{NA} values for **2**, **4**, **9**, **11** and **12**. Based on the found k_{NA} values for the premonomers with substituents on the aromatic moiety **1**, **2**, **4** and **9**, Hammett's reaction constant for the nucleophilic addition was determined as $\rho_{NA} = 1.56$ (Figure H3).

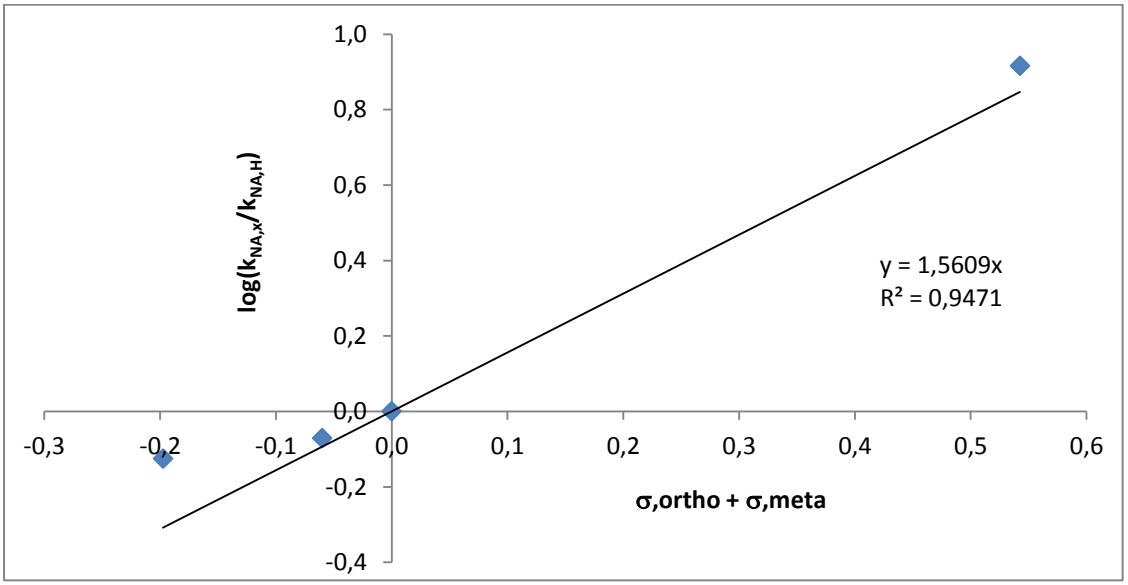

Figure H3: Hammett plot for the conjugate nucleophilic addition reaction of premonomers 1, 2, 4 and 9; Reaction condition: 298 K

The positive ρ_{NA} value is expected based on the negatively charged transition state. The rate coefficients for conjugate nucleophilic addition of the remaining premonomers can then be calculated using the found Hammett relation.

H.3. Propagation

If the premonomers differ in leaving group, polarizer or aromatic moiety, the reference k_p value[1] is assumed. If the premonomer possesses substituents on the aromatic moiety, the propagation reactivity is described by Hammett's linear free energy relation. The use of the Hammett equations has been demonstrated for the Wessling route by Cho et al.,[5,6] who observed that the Hammett reaction constant ρ_{NA} for the conjugate nucleophilic addition was approximately equal to the reaction constant ρ_p for the propagation reaction. In this work, it is assumed that the same is valid for the sulfinyl route (ρ_p = 1.56, Table H2), after which the rate coefficients for propagation can be determined from the reference[2] k_p and the Hammett reaction constant ρ_p. The resulting values are given in Table H1.

Table H1: Substituent σ constants and rate coefficients (M^{-1} s^{-1}) for premonomers 1-13 in solvent sBuOH

Premonomer	L	P	X	Y	σ	k_{E2}	k_{NA}	k_{ini}	k_p
1	Cl	SOR	H	H	0	1.16	0.20	$2.89\ 10^{-3}$	$6.71\ 10^{2}$
2	Cl	SOR	Me	Me	-0.20	0.21	0.15	$1.80\ 10^{-4}$	$3.30\ 10^{2}$
3	Cl	SOR	OC_{10}	OMe	-0.10	0.47	0.14	$6.85\ 10^{-4}$	$4.64\ 10^{2}$
4	Cl	SOR	OMe	OC_{10}	-0.06	0.17	0.17	$1.24\ 10^{-3}$	$5.40\ 10^{2}$
5	Cl	SOR	OMe	SMe	-0.05	0.73	0.17	$1.38\ 10^{-3}$	$5.55\ 10^{2}$
6	Cl	SOR	H	OMe	0.12	3.37	0.31	$1.56\ 10^{-2}$	$1.03\ 10^{3}$
7	Cl	SOR	OMe	Br	0.19	6.15	0.39	$4.02\ 10^{-2}$	$1.32\ 10^{3}$
8	Cl	SOR	H	Br	0.39	37.26	0.81	$6.90\ 10^{-1}$	$2.72\ 10^{3}$
9	Cl	SOR	Cl	Cl	0.54	127.12	1.65	5.87	$4.71\ 10^{3}$
10	Br	SOR	H	H	-	1.46	0.20	$2.89\ 10^{-3}$	$6.71\ 10^{2}$
11[a]	Cl	SOR	pyrH	pyrH	-	24.40	0.28	$2.89\ 10^{-3}$	$6.71\ 10^{2}$
12	Cl	SOR+Cl	H	H	-	22.01	42.0	$2.89\ 10^{-3}$	$6.71\ 10^{2}$
13	Cl	SO_2R	H	H	-	28.23	0.64	$2.89\ 10^{-3}$	$6.71\ 10^{2}$

[a] *Premonomer 11 contains a pyridine moiety. R = n-octyl. X = ortho substituent with respect to P. Y = meta substituent with respect to P.*

The rate coefficients for the reference polymerization of **1** have been reported.[2] Note that exactly half of the reported propagation value is given in Table H1. The factor 2 emerges because the two radical centers on the macromolecule are lumped[2] together in the propagation step. When delumping the two propagation reactions on each radical center of the chain ends, as is done in this work, both radical centers must be considered separately and each radical chain end is propagating with half of the "lumped" reactivity.

H.4. Radical initiation

As mentioned in Chapter 3, the uncertainty lies with the initiation reaction, for which no tangible data is reported. If the premonomers differ in leaving group, polarizer or aromatic moiety, the reference[2] k_{ini} value is assumed. If the premonomer possesses substituents on the aromatic moiety, the initiation reactivity is described by Hammett's linear free energy relation. Although Cho et al. report kinetic studies[5,6] using Hammett relations for the propagation, they do not use Hammett's relation for the initiation reaction. Cho et al. assume that the propagation radicals are in quasi-steady state, obviating the need for any initiation (and termination) reaction and corresponding Hammett description. However, there is no proof of termination reactions and hence the use of the quasi-steady state approximation is questionable. Short of better alternatives, the Hammett relation is assumed in this work for the initiation reaction. It is assumed that substitution with electron donating groups retards the dimerization, similar to the propagation reaction but more pronounced. In this work, ρ_{ini} was determined from the equation $\rho_{ini,sulfinyl} - \rho_{prop,sulfinyl} = \rho_{ini,dithiocarbamate} - \rho_{prop,dithiocarbamate}$. This means that the difference in sensitivity of the propagation and initiation reaction is assumed to be the same for both the sulfinyl and dithiocarbamate routes. The equation involving Hammett reaction constants can be re-written as a function of the rate coefficients as follows:

$$\rho_{ini,sulfinyl} - \rho_{prop,sulfinyl} = \rho_{ini,DTC} - \rho_{ini,DTC} \Leftrightarrow$$

$$\frac{10^{\sigma\rho_{prop,sulfinyl}}}{10^{\sigma\rho_{ini,sulfinyl}}} = \frac{10^{\sigma\rho_{prop,DTC}}}{10^{\sigma\rho_{ini,DTC}}} \Leftrightarrow$$

$$\frac{\left(\frac{k_{prop,sulfinyl,X}}{k_{prop,sulfinyl,H}}\right)}{\left(\frac{k_{ini,sulfinyl,X}}{k_{ini,sulfinyl,H}}\right)} = \frac{\left(\frac{k_{prop,DTC,X}}{k_{prop,DTC,H}}\right)}{\left(\frac{k_{ini,DTC,X}}{k_{ini,DTC,H}}\right)} \Leftrightarrow$$

$$\frac{k_{prop,sulfinyl,X}}{k_{ini,sulfinyl,X}} \propto \frac{k_{prop,DTC,X}}{k_{ini,DTC,X}} \qquad \text{(H3)}$$

Returning to the original equation and using the Hammett reaction constants for the DTC route given in Chapter 4:

$$\rho_{ini,sulfinyl} - \rho_{prop,sulfinyl} = \rho_{ini,DTC} - \rho_{prop,DTC} \Leftrightarrow$$

$$\rho_{ini,sulfinyl} = \rho_{ini,DTC} - \rho_{prop,DTC} + \rho_{prop,sulfinyl} \Leftrightarrow$$

$$\rho_{ini,sulfinyl} = 5.14 - 0.60 + 1.56 = 6.10 \qquad \text{(H4)}$$

The value found is ρ_{ini} = 6.1 and is given in Table H2 for comparison with other Hammett reaction constants.

Table H2: Values for the Hammett reaction constants ρ

	1,6-elimination	nucleophilic addition	initiation	propagation
sulfinyl route[a]	3.86	1.56	6.10	1.56
dithiocarbamate route[7]	5.00	-	5.14	0.60

[a] *this work.*

As mentioned in Chapter 3 in the section on the monomer formation, a slight overestimation of ρ_{ini} is possible. Perhaps $\rho_{ini,sulfinyl} = \rho_{ini,dithiocarbamate}$ should be preferred to describe the monomer formation, but this ignores the difference in polarizer altogether. Note that ρ^{ini} is larger than ρ_p, which is consistent with Chapter 4 on the dithiocarbamate route. As can be seen in Table H2, the initiation reactions of both routes are highly sensitive to structure effects, with Hammett reaction constants larger than 5. These high values are normally only observed[7] for ionic reactions, but for the dimerization of two *p*-quinodimethanes yielding a biradical, extreme ρ_{ini} values are not illogical. As outlined in the introduction and demonstrated in Chapter 3, the value leads to experimentally observed behavior.

References

1. Hermosilla, L.; Catak, S.; Van Speybroeck, V.; Waroquier, M.; Vandenbergh, J.; Motmans, F.; Adriaensens, P.; Lutsen, L.; Cleij, T.; Vanderzande, D. *Macromolecules* **2010**, 43, 18, 7424-7433.
2. Van Steenberge, P.; Vandenbergh, J.; D'hooge, D.R.; Reyniers, M.-F.; Adriaensens, P.J.; Lutsen, L.; Vanderzande, D.J.M.; Marin, G.B. *Macromolecules* **2011**, 44, 8716-8726.
3. Charton, M.; *Can. J. Chem.* **1960**, 38, 2493-2499.
4. Hansch, C.; Leo, A.; Taft, R.W. *Chem. Rev.* **1991**, 91, 165-195.
5. Cho, B. R. *Prog. Pol. Sci.* **2002**, 27, 2, 307-355.
6. Cho, B. R.; Kim, T. H.; Son, K. H.; Kim, Y. K.; Lee, Y. K.; Jeon, S. J. *Macromolecules* **2000**, 33, 22, 8167-8172.
7. Qiu, J.; Matyjaszewski, K, *Macromolecules* **1997**, 30, 5643-5648.

Appendix I: Effect of the initial premonomer composition on the copolymerizations via the sulfinyl route

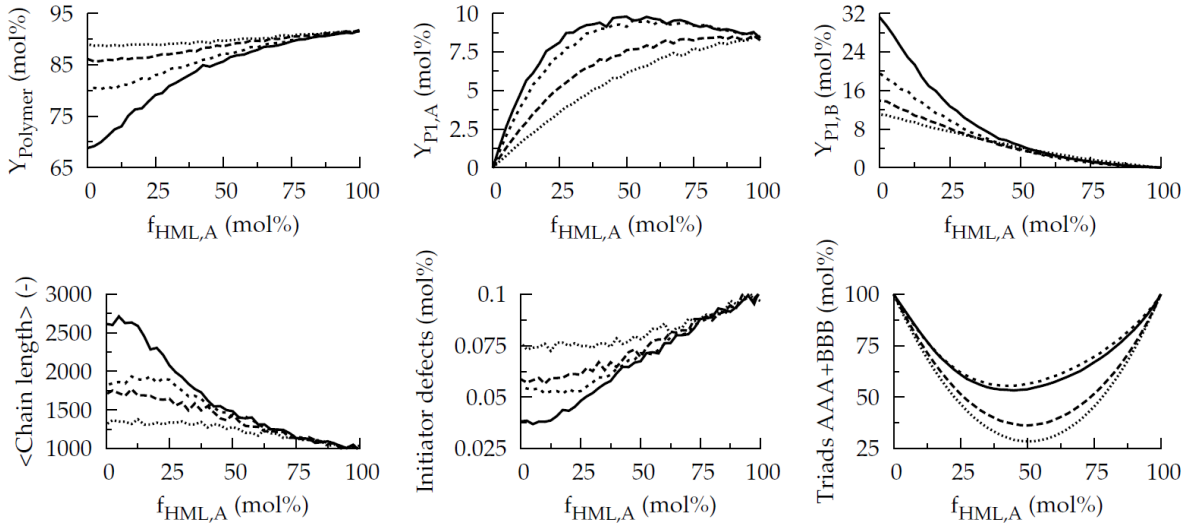

Figure I1: Effect of initial premonomer composition on the yields and properties for the copolymerizations of 1 (possessing no substituents) with 1-5 (possessing EDGs) (see Figures 3, 4 and 5 in Chapter 3); Reaction conditions: $[RO^-]_0/[HML]_0$ = 1, 308 K; $f_{HML,A}$ is defined as $[HML,A]_0/([HML,A]_0+[HML,B]_0)$; HML,A = 1 and HML,B: ——— : 1 with 2; - - - - - : 1 with 3; . . . . . : 1 with 4; ····· : 1 with 5

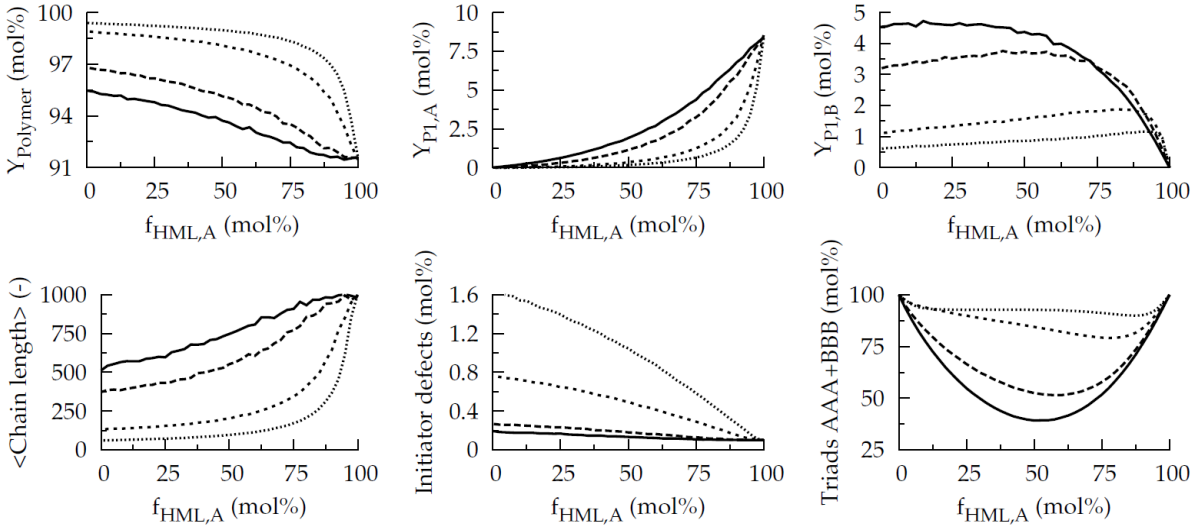

Figure I2: Effect of initial premonomer composition on the yields and properties for the copolymerizations of 1 (possessing no substituents) with 6-9 (possessing EWGs) (see Figures 3, 4 and 5 in Chapter 3); Reaction conditions: $[RO^-]_0/[HML]_0$ = 1, 308 K; $f_{HML,A}$ is defined as $[HML,A]_0/([HML,A]_0+[HML,B]_0)$; HML,A = 1 and HML,B: ——— : 1 with 6; - - - - - : 1 with 7; . . . . . : 1 with 8; ····· : 1 with 9

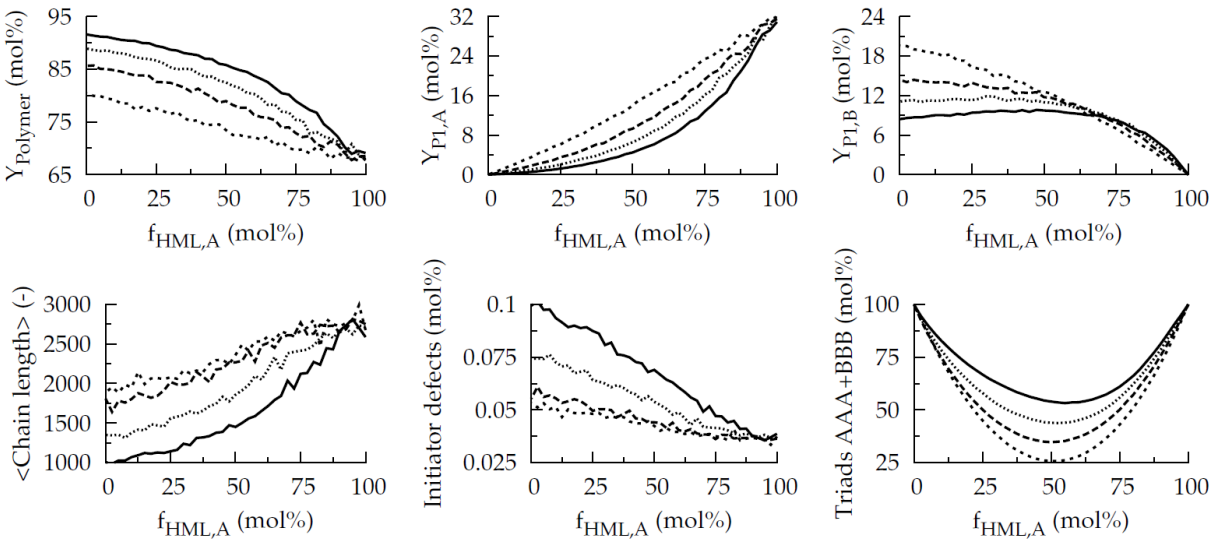

Figure I3: Effect of initial premonomer composition on the yields and properties for the copolymerizations of 2 (possessing Me groups) with 1-5 (possessing EDGs) (see Figures 3, 4 and 5 in Chapter 3); Reaction conditions: $[RO^-]_0/[HML]_0$ = 1, 308 K; $f_{HML,A}$ is defined as $[HML,A]_0/([HML,A]_0+[HML,B]_0)$; HML,A = 2 and HML,B: ——— : 2 with 1; - - - - - : 2 with 3; . . . . . : 2 with 4; ····· : 2 with 5

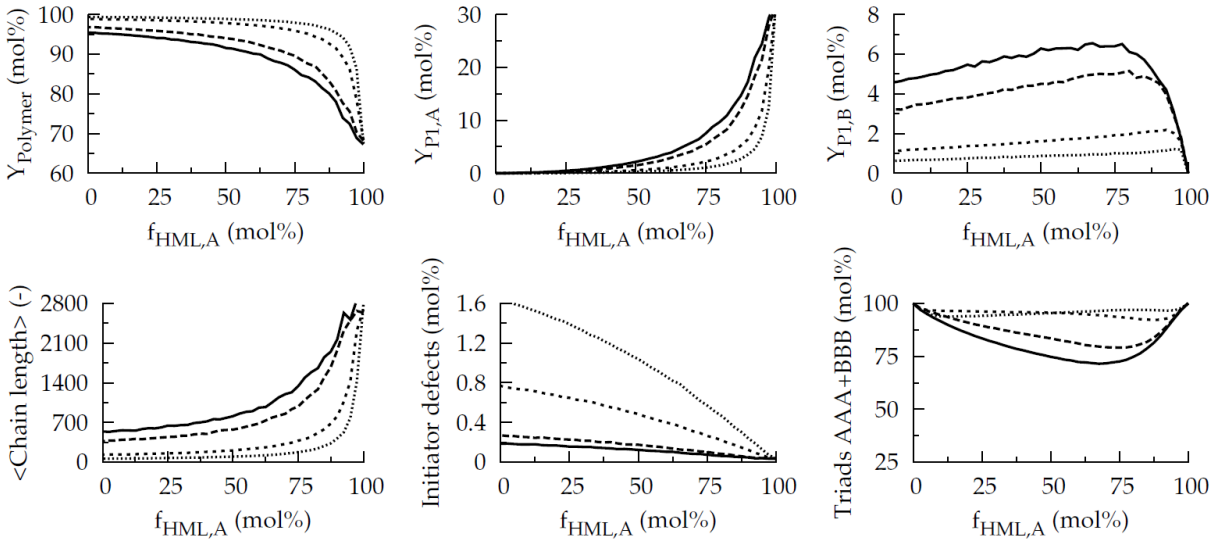

Figure I4: Effect of initial premonomer composition on the yields and properties for the copolymerizations of 2 (possessing Me groups) with 6-9 (possessing EWGs) (see Figures 3, 4 and 5 in Chapter 3); Reaction conditions: $[RO^-]_0/[HML]_0$ = 1, 308 K; $f_{HML,A}$ is defined as $[HML,A]_0/([HML,A]_0+[HML,B]_0)$; HML,A = 2 and HML,B: ——— : 2 with 6; - - - - - : 2 with 7; . . . . . : 2 with 8; ····· : 2 with 9

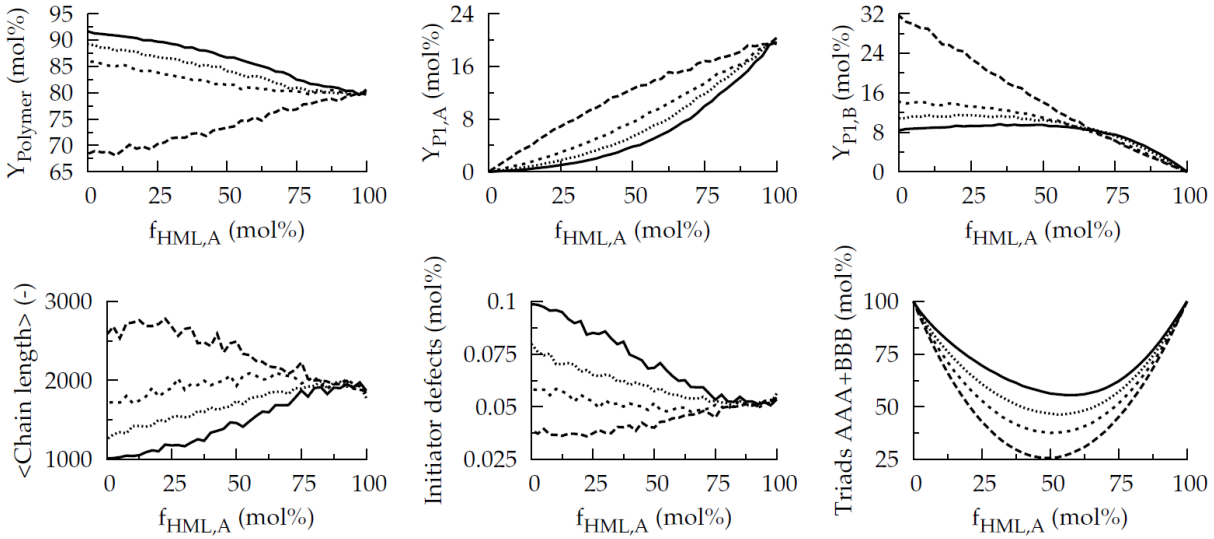

Figure I5: Effect of initial premonomer composition on the yields and properties for the copolymerizations of 4 (possessing OC_1 and OC_{10} groups) with 1-5 (possessing EDGs) (see Figures 3, 4 and 5 in Chapter 3); Reaction conditions: $[RO^-]_0/[HML]_0$ = 1, 308 K; $f_{HML,A}$ is defined as $[HML,A]_0/([HML,A]_0+[HML,B]_0)$; HML,A = 4 and HML,B: ——— : 4 with 1; - - - - - - : 4 with 2; . . . . . : 4 with 3; ····· : 4 with 5

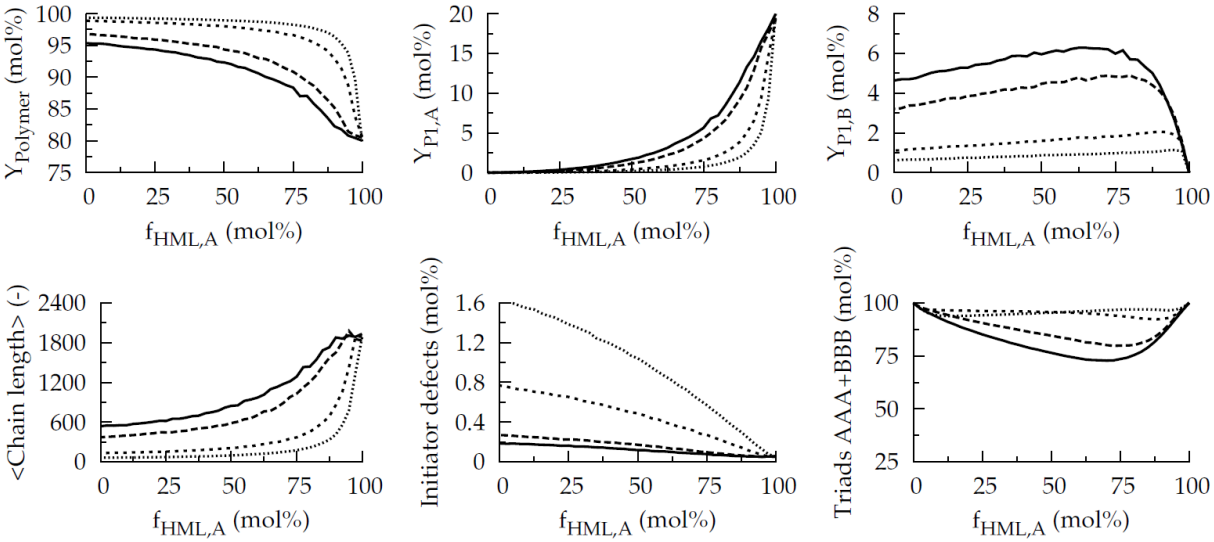

Figure I6: Effect of initial premonomer composition on the yields and properties for the copolymerizations of 4 (possessing OC_1 and OC_{10} groups) with 6-9 (possessing EWGs) (see Figures 3, 4 and 5 in Chapter 3); Reaction conditions: $[RO^-]_0/[HML]_0$ = 1, 308 K; $f_{HML,A}$ is defined as $[HML,A]_0/([HML,A]_0+[HML,B]_0)$; HML,A = 4 and HML,B: ——— : 4 with 6; - - - - - - : 4 with 7; . . . . . : 4 with 8; ····· : 4 with 9

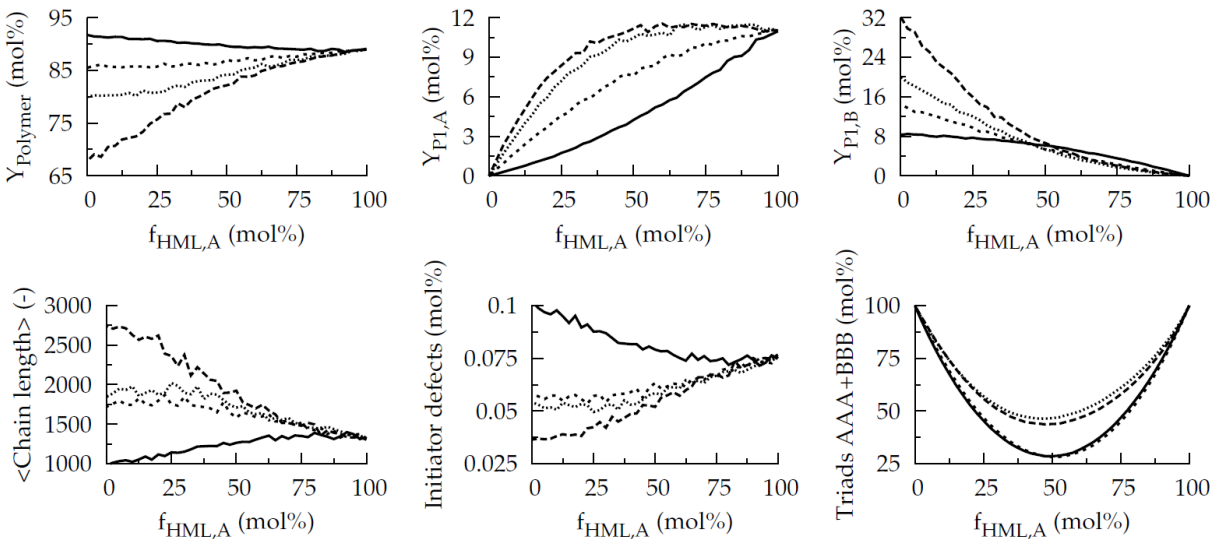

Figure I7: Effect of initial premonomer composition on the yields and properties for the copolymerizations of 5 (possessing OC_1 and SC_1 groups) with 1-4 (possessing EDGs) (see Figures 3, 4 and 5 in Chapter 3); Reaction conditions: $[RO^-]_0/[HML]_0$ = 1, 308 K; $f_{HML,A}$ is defined as $[HML,A]_0/([HML,A]_0+[HML,B]_0)$; HML,A = 5 and HML,B: ——— : 5 with 1; - - - - - : 5 with 2; . . . . . : 5 with 3; ····· : 5 with 4

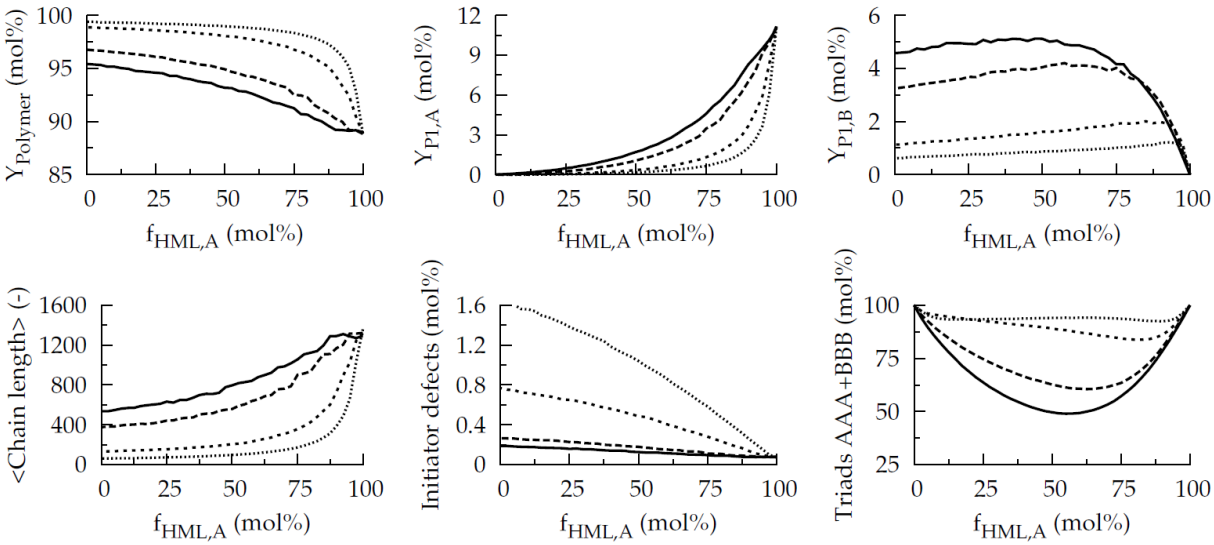

Figure I8: Effect of initial premonomer composition on the yields and properties for the copolymerizations of 5 (possessing OC_1 and SC_1 groups) with 6-9 (possessing EWGs) (see Figures 3, 4 and 5 in Chapter 3); Reaction conditions: $[RO^-]_0/[HML]_0$ = 1, 308 K; $f_{HML,A}$ is defined as $[HML,A]_0/([HML,A]_0+[HML,B]_0)$; HML,A = 5 and HML,B: ——— : 5 with 6; - - - - - : 5 with 7; . . . . . : 5 with 8; ····· : 5 with 9

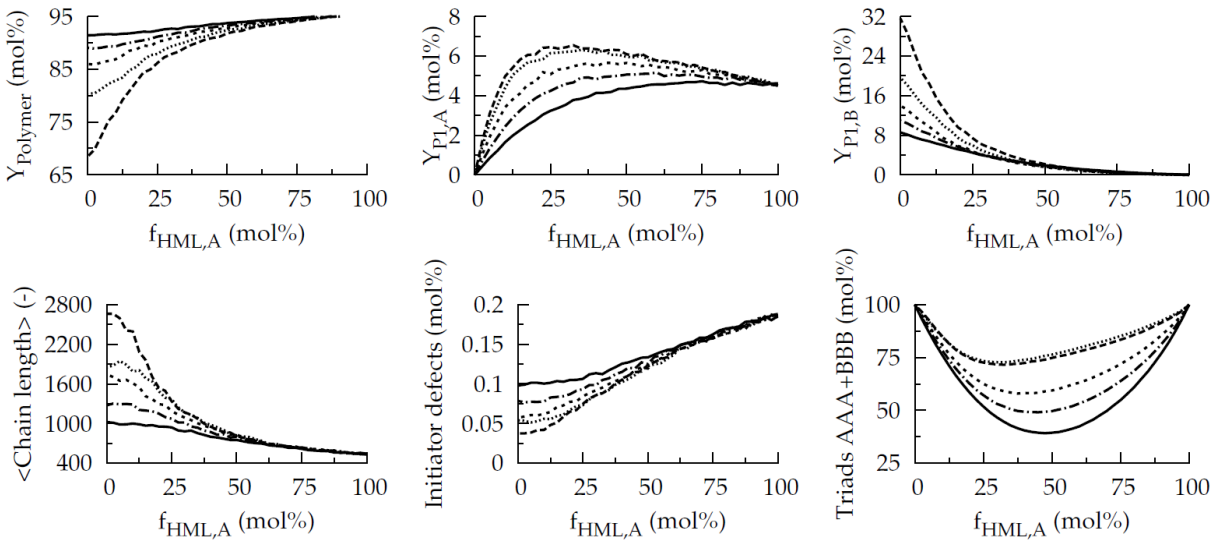

Figure I9: Effect of initial premonomer composition on the yields and properties for the copolymerizations of 6 (possessing an OC_1 group) with 1-5 (possessing EDGs) (see Figures 3, 4 and 5 in Chapter 3); Reaction conditions: $[RO^-]_0/[HML]_0$ = 1, 308 K; $f_{HML,A}$ is defined as $[HML,A]_0/([HML,A]_0+[HML,B]_0)$; HML,A = 6 and HML,B: ——— : 6 with 1; - - - - - : 6 with 2; . . . . . : 6 with 3; ····· : 6 with 4; —·—·— : 6 with 5

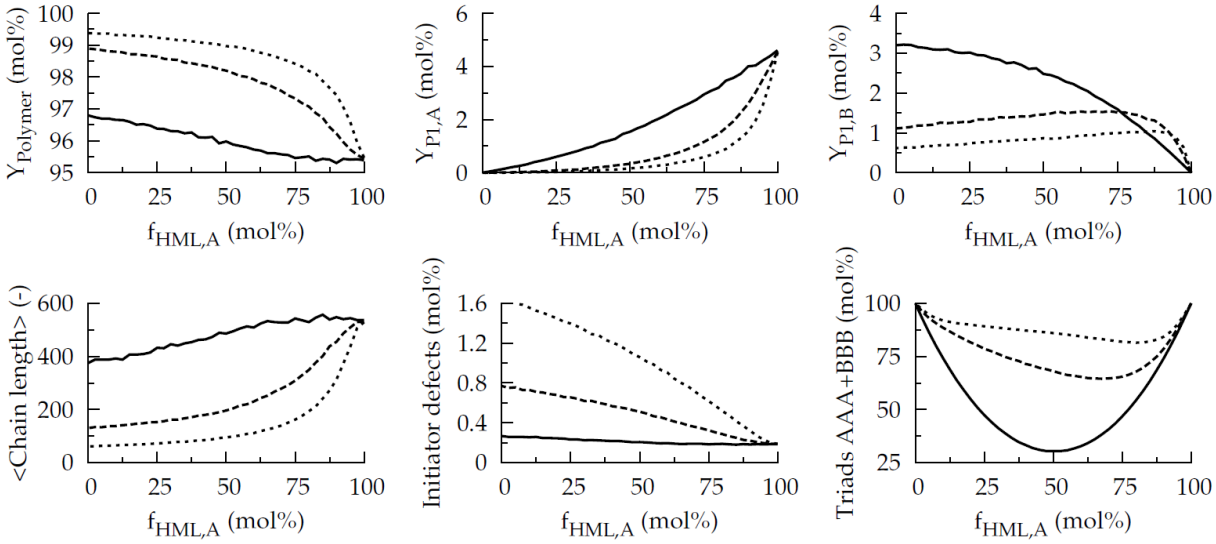

Figure I10: Effect of initial premonomer composition on the yields and properties for the copolymerizations of 6 (possessing an OC_1 group) with 7-9 (possessing EWGs) (see Figures 3, 4 and 5 in Chapter 3); Reaction conditions: $[RO^-]_0/[HML]_0$ = 1, 308 K; $f_{HML,A}$ is defined as $[HML,A]_0/([HML,A]_0+[HML,B]_0)$; HML,A = 6 and HML,B: ——— : 6 with 7; - - - - - : 6 with 8; . . . . . : 6 with 9

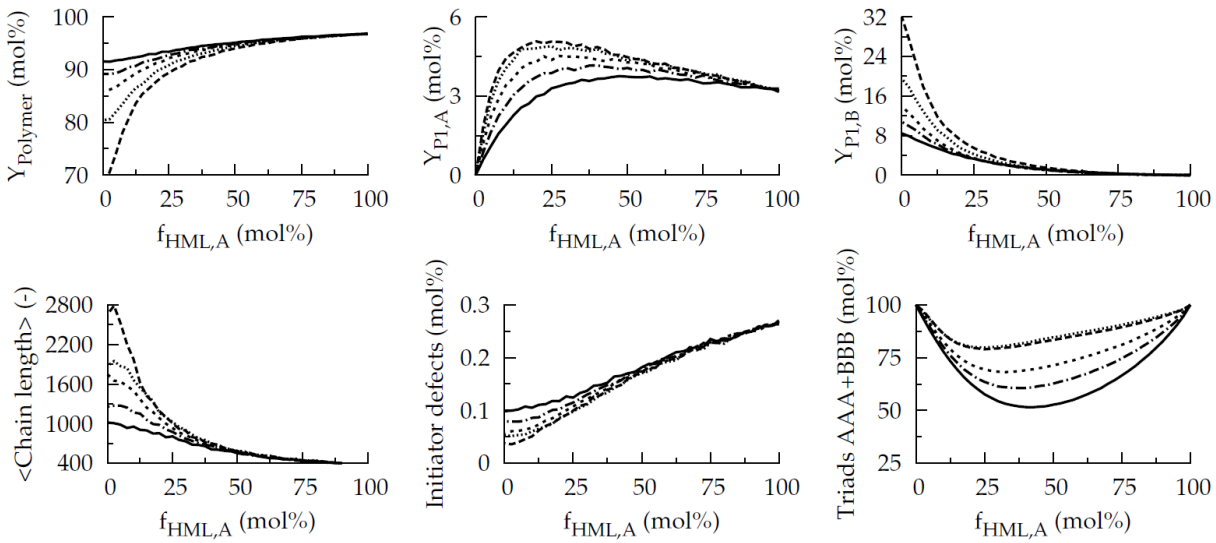

Figure I11: Effect of initial premonomer composition on the yields and properties for the copolymerizations of 7 (possessing OC_1 and Br groups) with 1-5 (possessing EDGs) (see Figures 3, 4 and 5 in Chapter 3); Reaction conditions: $[RO^-]_0/[HML]_0$ = 1, 308 K; $f_{HML,A}$ is defined as $[HML,A]_0/([HML,A]_0+[HML,B]_0)$; HML,A = 7 and HML,B: ——— : 7 with 1; - - - - : 7 with 2; . . . . . : 7 with 3; ····· : 7 with 4; —·—·— : 7 with 5

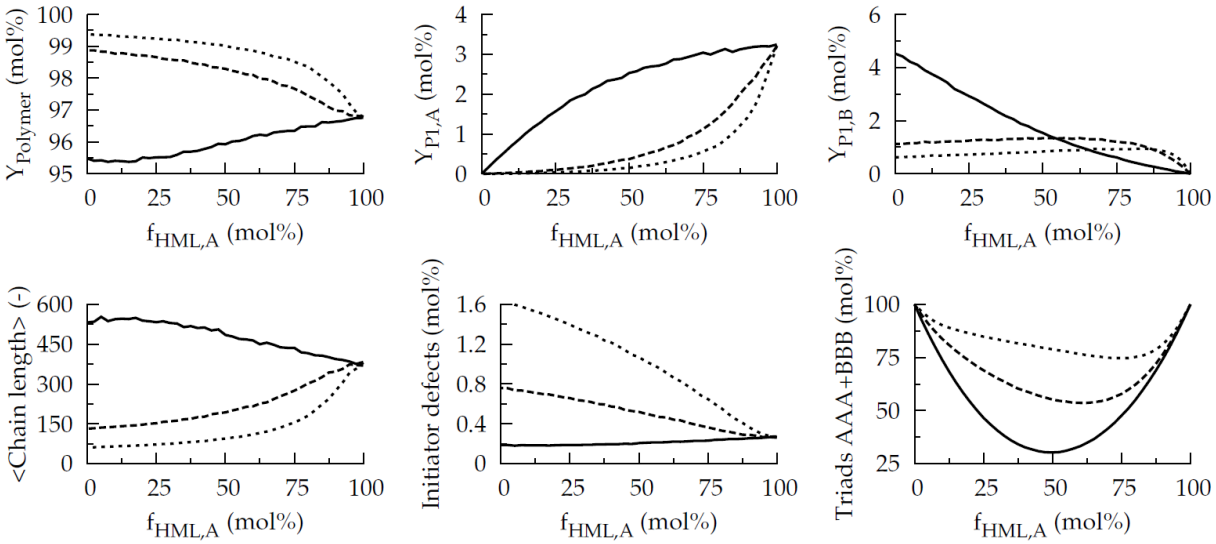

Figure I12: Effect of initial premonomer composition on the yields and properties for the copolymerizations of 7 (possessing OC_1 and Br groups) with 6-9 (possessing EWGs) (see Figures 3, 4 and 5 in Chapter 3); Reaction conditions: $[RO^-]_0/[HML]_0$ = 1, 308 K; $f_{HML,A}$ is defined as $[HML,A]_0/([HML,A]_0+[HML,B]_0)$; HML,A = 7 and HML,B: ——— : 7 with 6; - - - - : 7 with 8; . . . . . : 7 with 9

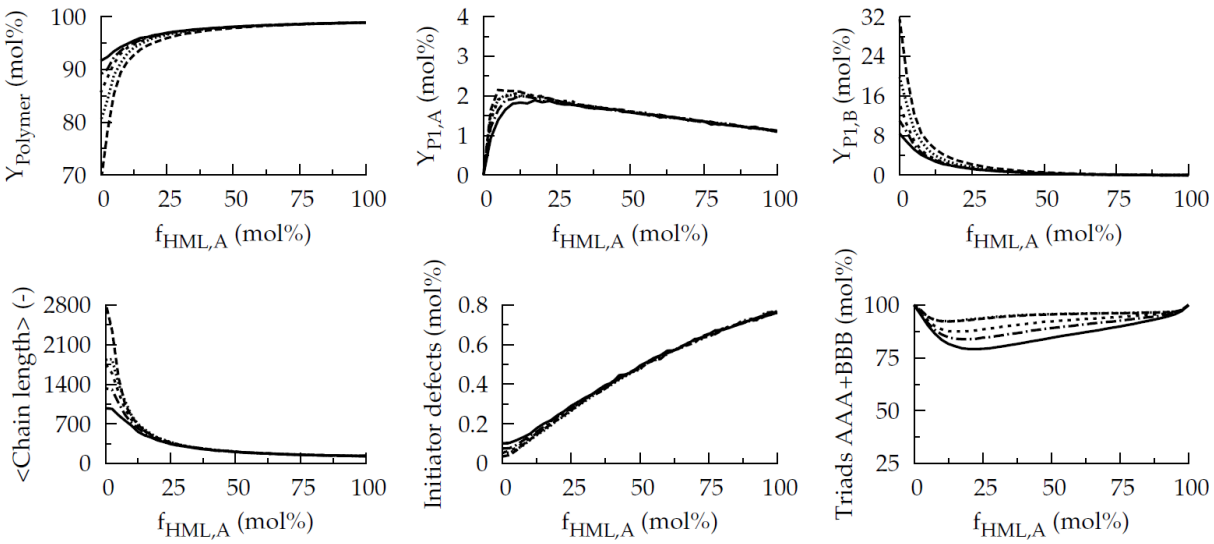

Figure I13: Effect of initial premonomer composition on the yields and properties for the copolymerizations of 8 (possessing a Br group) with 1-5 (possessing EDGs) (see Figures 3, 4 and 5 in Chapter 3); Reaction conditions: $[RO^-]_0/[HML]_0$ = 1, 308 K; $f_{HML,A}$ is defined as $[HML,A]_0/([HML,A]_0+[HML,B]_0)$; HML,A = 8 and HML,B: ——— : 8 with 1; - - - - - : 8 with 2; . . . . . : 8 with 3; ····· : 8 with 4; —·—·— : 8 with 5

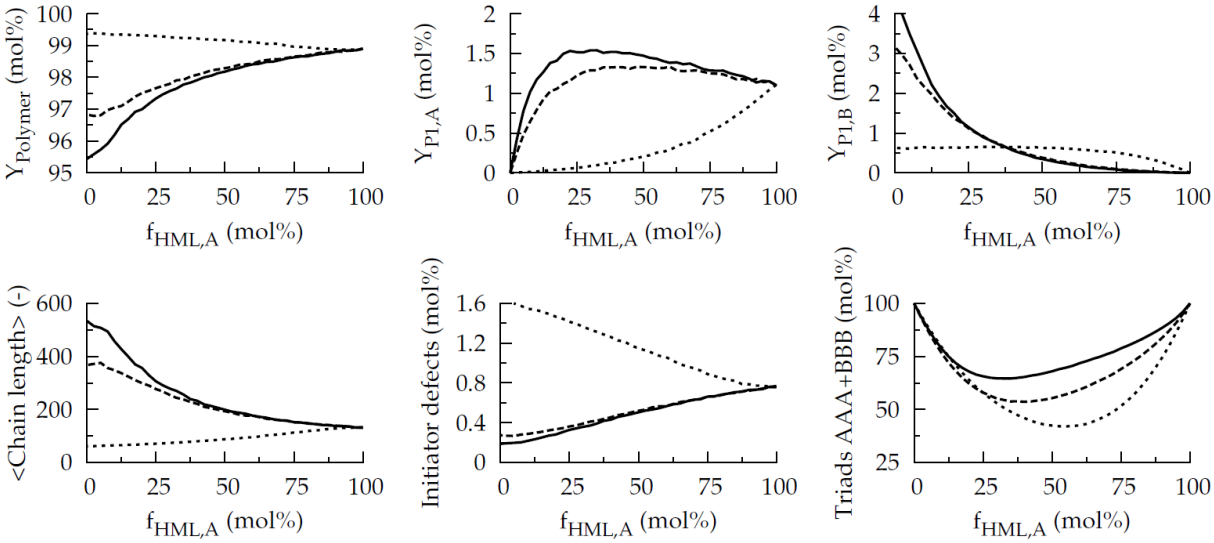

Figure I14: Effect of initial premonomer composition on the yields and properties for the copolymerizations of 8 (possessing a Br group) with 6-9 (possessing EWGs) (see Figures 3, 4 and 5 in Chapter 3); Reaction conditions: $[RO^-]_0/[HML]_0$ = 1, 308 K; $f_{HML,A}$ is defined as $[HML,A]_0/([HML,A]_0+[HML,B]_0)$; HML,A = 8 and HML,B: ——— : 8 with 6; - - - - - : 8 with 7; . . . . . : 8 with 9

Appendix J: Supporting maps for the effect of the base on the copolymerization

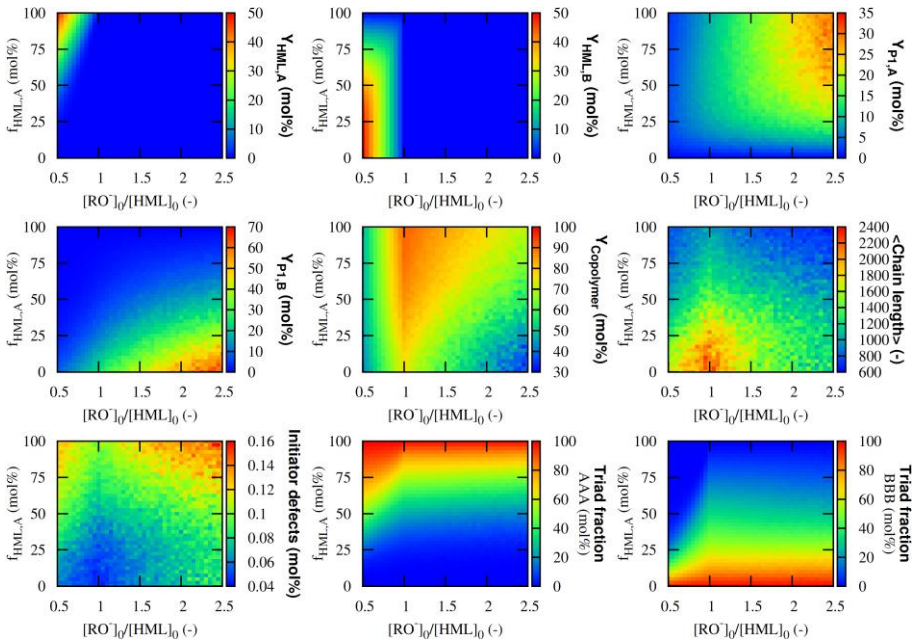

Figure J1: Effect of the base and the initial premonomer composition on the yields and properties for the copolymerization of 1 with 2 (see Figures 3, 4 and 5 in Chapter 3); Reaction conditions: 308 K; $f_{HML,A}$ is defined as $[HML,A]_0/([HML,A]_0+[HML,B]_0)$

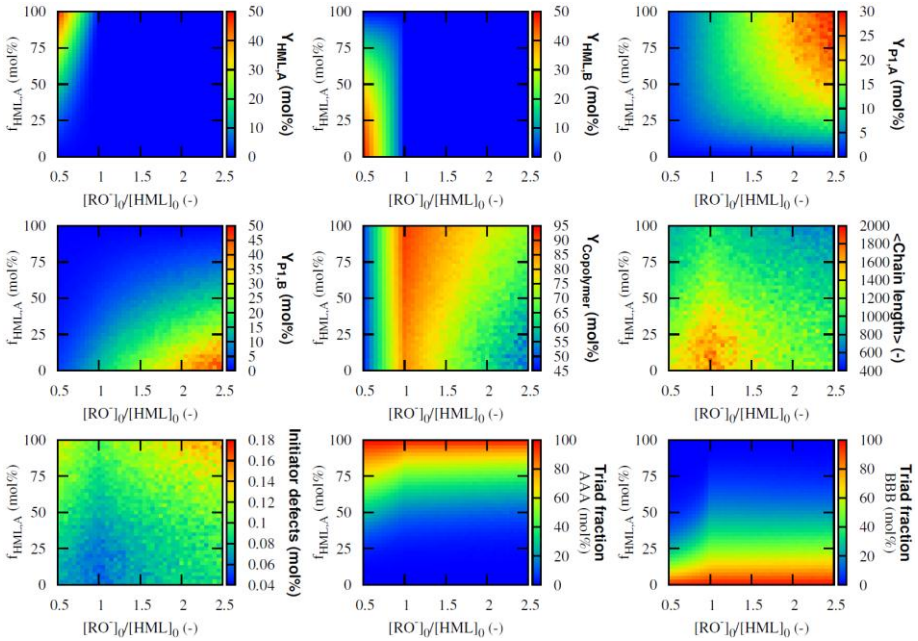

Figure J2: Effect of the base and the initial premonomer composition on the yields and properties for the copolymerization of 1 with 3 (see Figures 3, 4 and 5 in Chapter 3); Reaction conditions: 308 K; $f_{HML,A}$ is defined as $[HML,A]_0/([HML,A]_0+[HML,B]_0)$

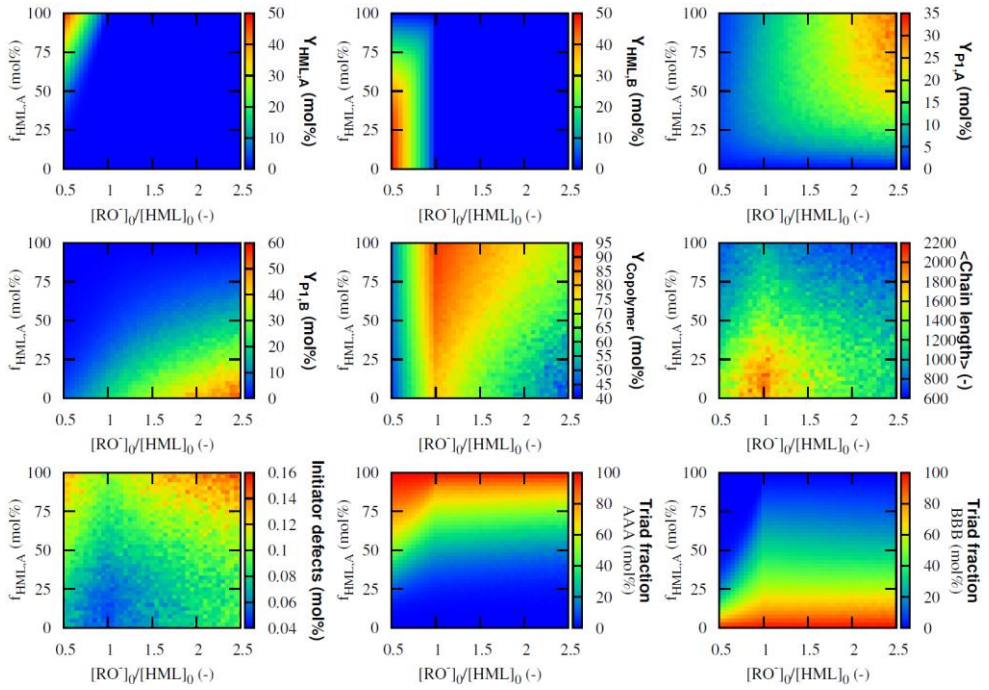

Figure J3: Effect of the base and the initial premonomer composition on the yields and properties for the copolymerization of 1 with 4 (see Figures 3, 4 and 5 in Chapter 3); Reaction conditions: 308 K; $f_{HML,A}$ is defined as $[HML,A]_0/([HML,A]_0+[HML,B]_0)$

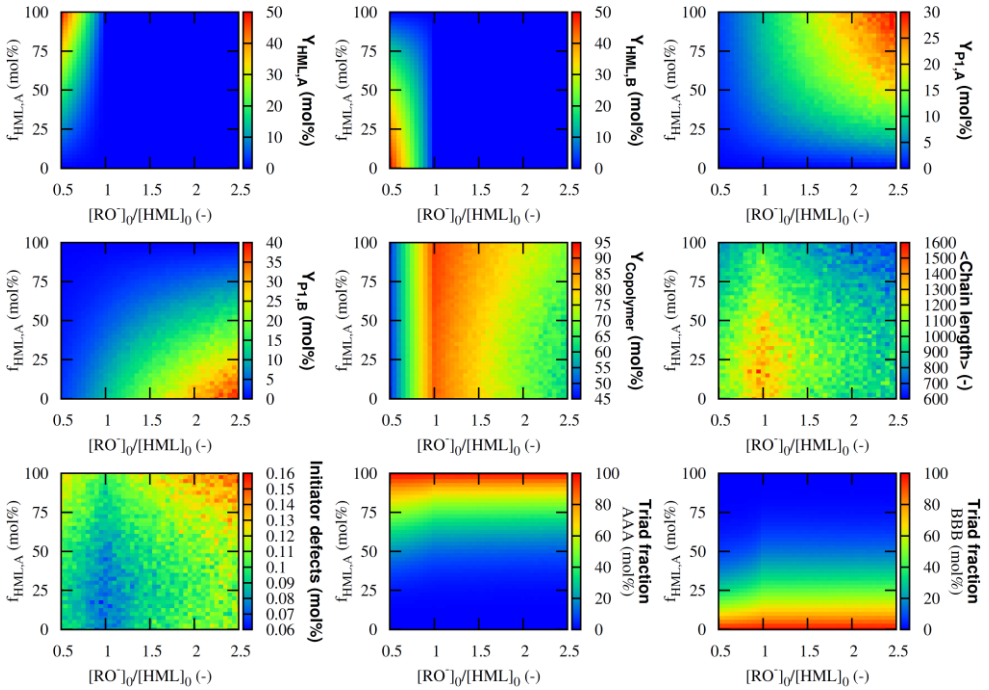

Figure J4: Effect of the base and the initial premonomer composition on the yields and properties for the copolymerization of 1 with 5 (see Figures 3, 4 and 5 in Chapter 3); Reaction conditions: 308 K; $f_{HML,A}$ is defined as $[HML,A]_0/([HML,A]_0+[HML,B]_0)$

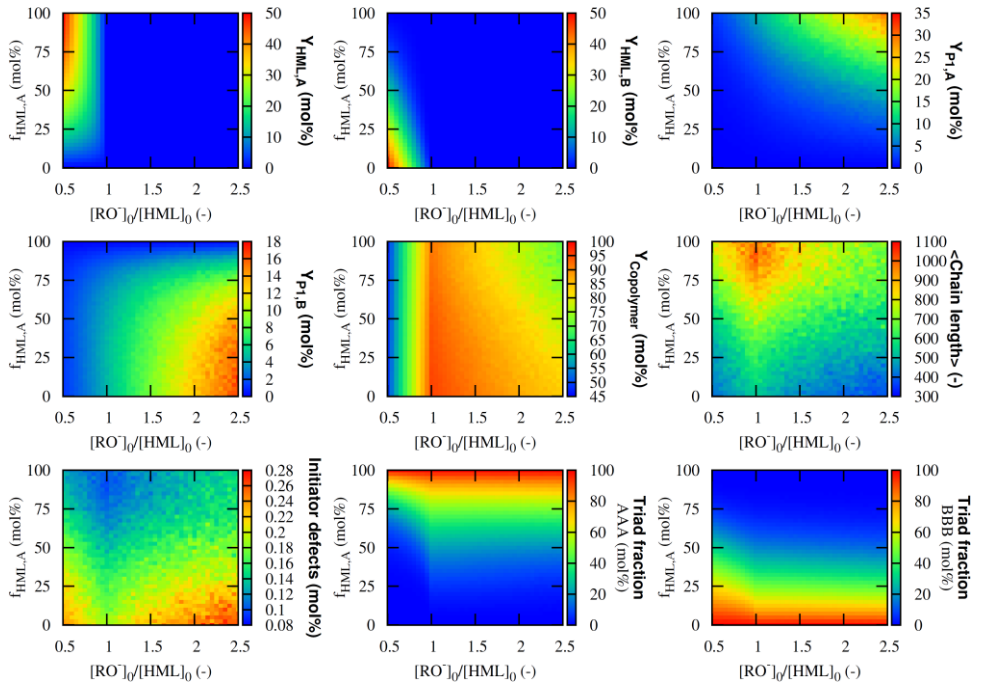

Figure J5: Effect of the base and the initial premonomer composition on the yields and properties for the copolymerization of 1 with 6 (see Figures 3, 4 and 5 in Chapter 3); Reaction conditions: 308 K; $f_{HML,A}$ is defined as $[HML,A]_0/([HML,A]_0+[HML,B]_0)$

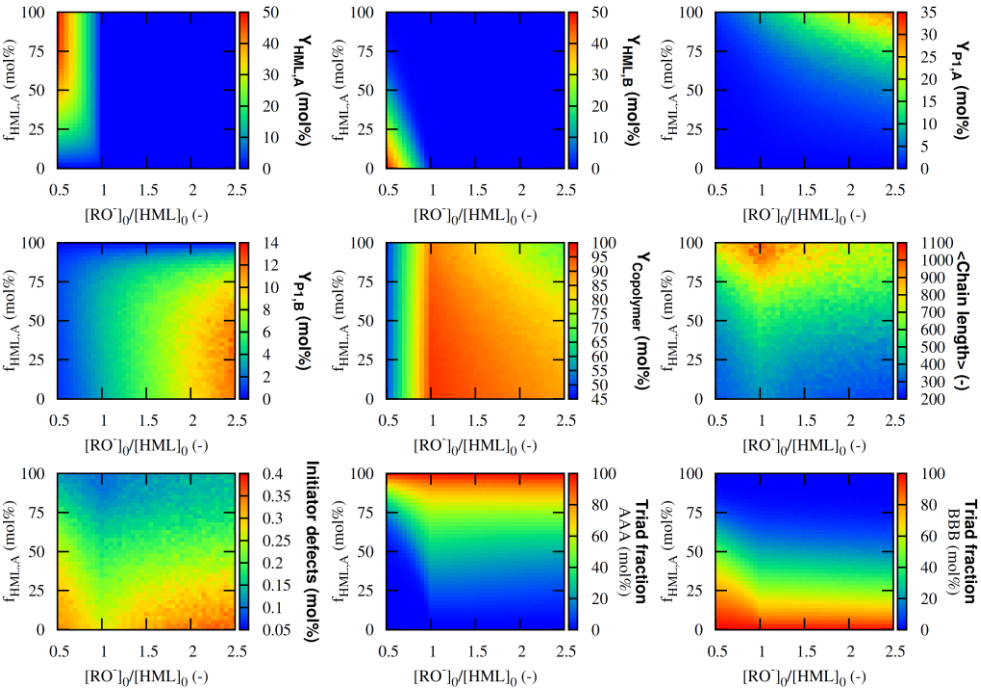

Figure J6: Effect of the base and the initial premonomer composition on the yields and properties for the copolymerization of 1 with 7 (see Figures 3, 4 and 5 in Chapter 3); Reaction conditions: 308 K; $f_{HML,A}$ is defined as $[HML,A]_0/([HML,A]_0+[HML,B]_0)$

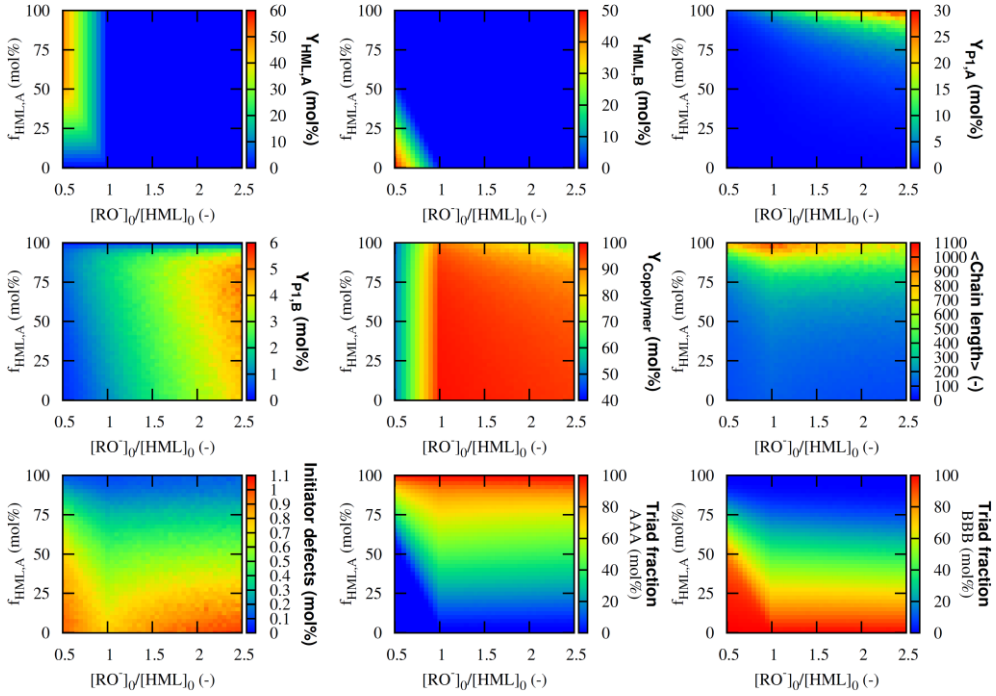

Figure J7: Effect of the base and the initial premonomer composition on the yields and properties for the copolymerization of 1 with 8 (see Figures 3, 4 and 5 in Chapter 3); Reaction conditions: 308 K; $f_{HML,A}$ is defined as $[HML,A]_0/([HML,A]_0+[HML,B]_0)$

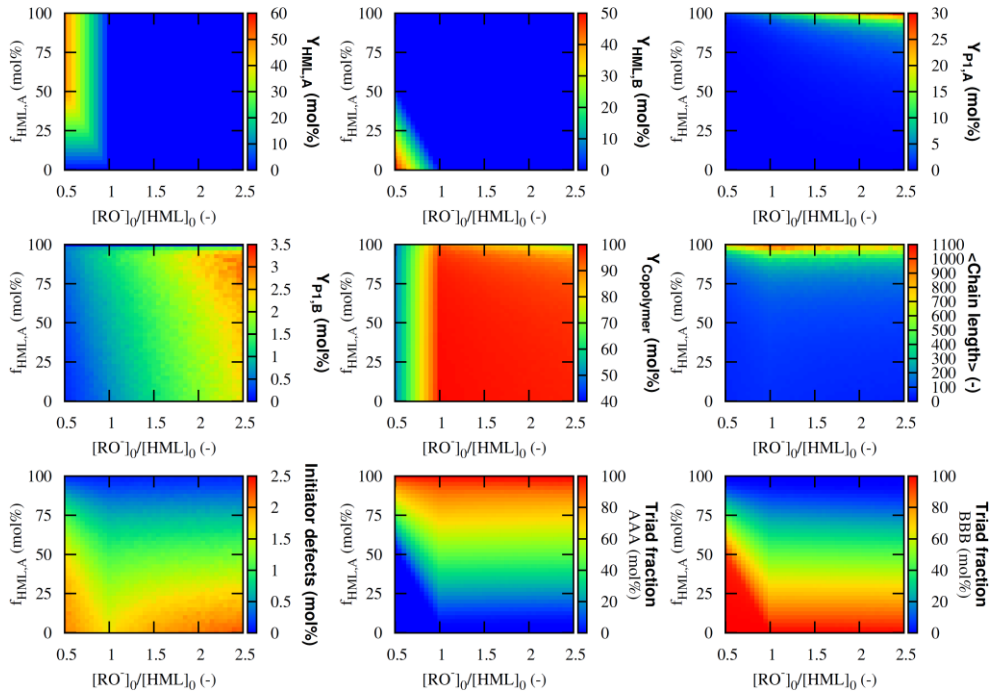

Figure J8: Effect of the base and the initial premonomer composition on the yields and properties for the copolymerization of 1 with 9 (see Figures 3, 4 and 5 in Chapter 3); Reaction conditions: 308 K; $f_{HML,A}$ is defined as $[HML,A]_0/([HML,A]_0+[HML,B]_0)$

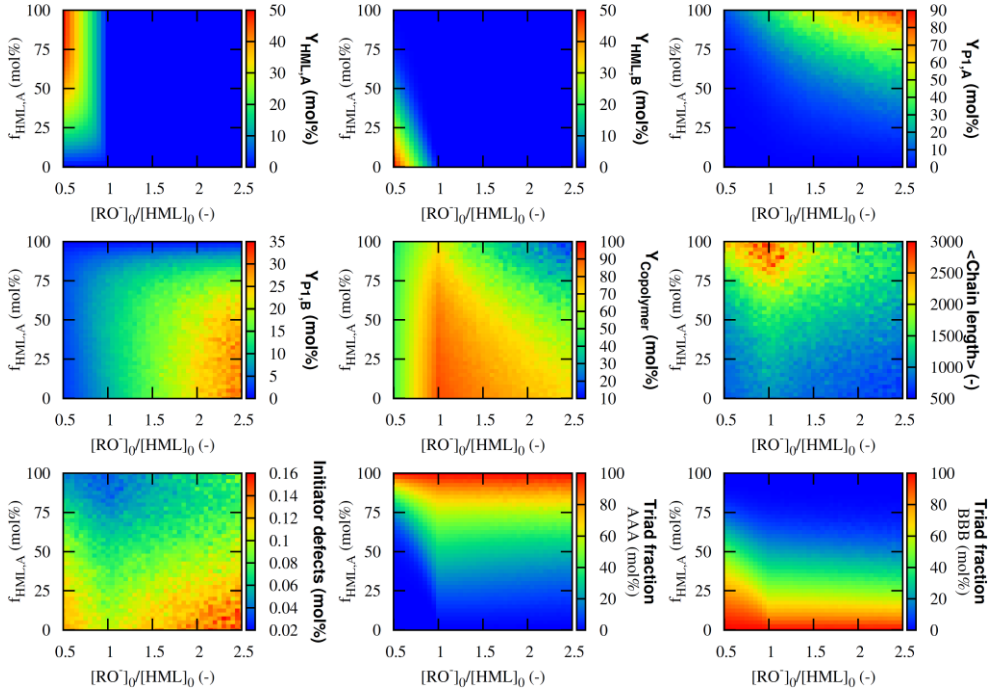

Figure J9: Effect of the base and the initial premonomer composition on the yields and properties for the copolymerization of 2 with 1 (see Figures 3, 4 and 5 in Chapter 3); Reaction conditions: 308 K; $f_{HML,A}$ is defined as $[HML,A]_0/([HML,A]_0+[HML,B]_0)$

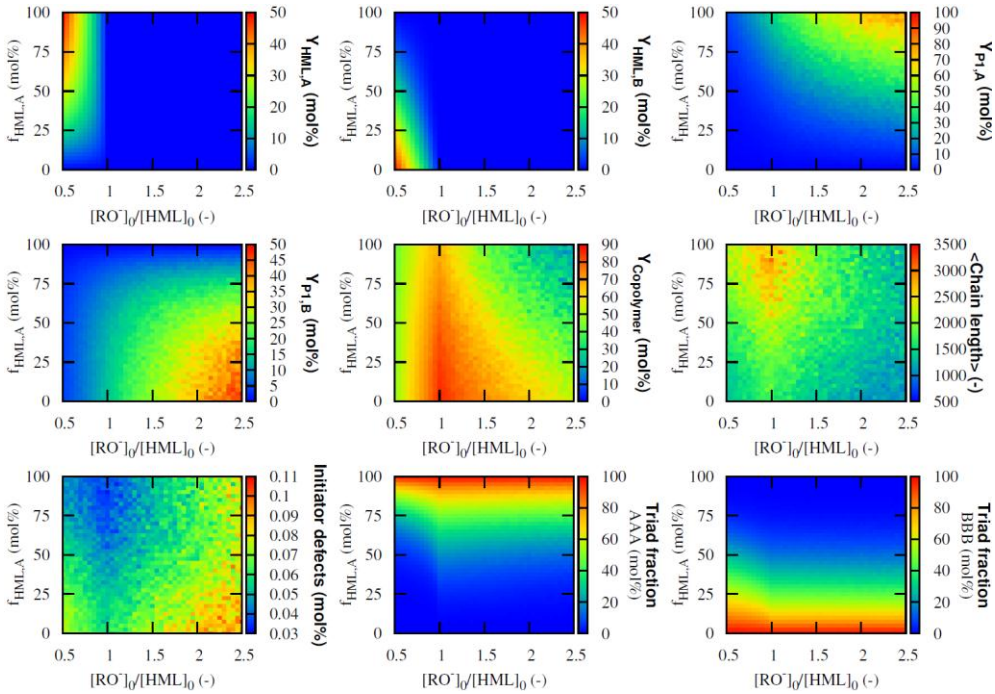

Figure J10: Effect of the base and the initial premonomer composition on the yields and properties for the copolymerization of 2 with 3 (see Figures 3, 4 and 5 in Chapter 3); Reaction conditions: 308 K; $f_{HML,A}$ is defined as $[HML,A]_0/([HML,A]_0+[HML,B]_0)$

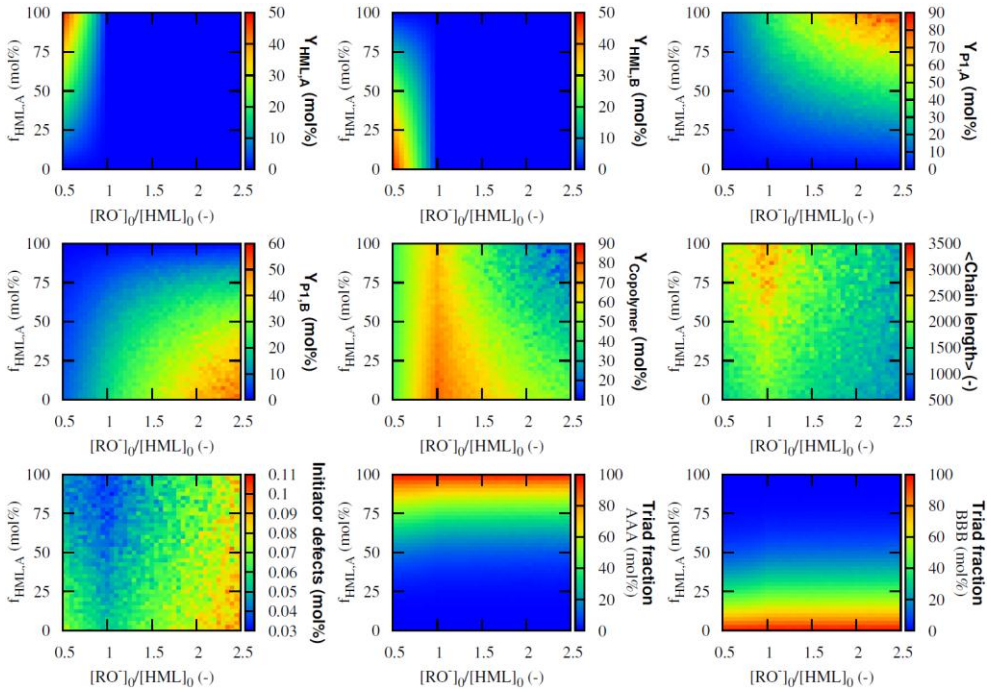

Figure J11: Effect of the base and the initial premonomer composition on the yields and properties for the copolymerization of 2 with 4 (see Figures 3, 4 and 5 in Chapter 3); Reaction conditions: 308 K; $f_{HML,A}$ is defined as $[HML,A]_0/([HML,A]_0+[HML,B]_0)$

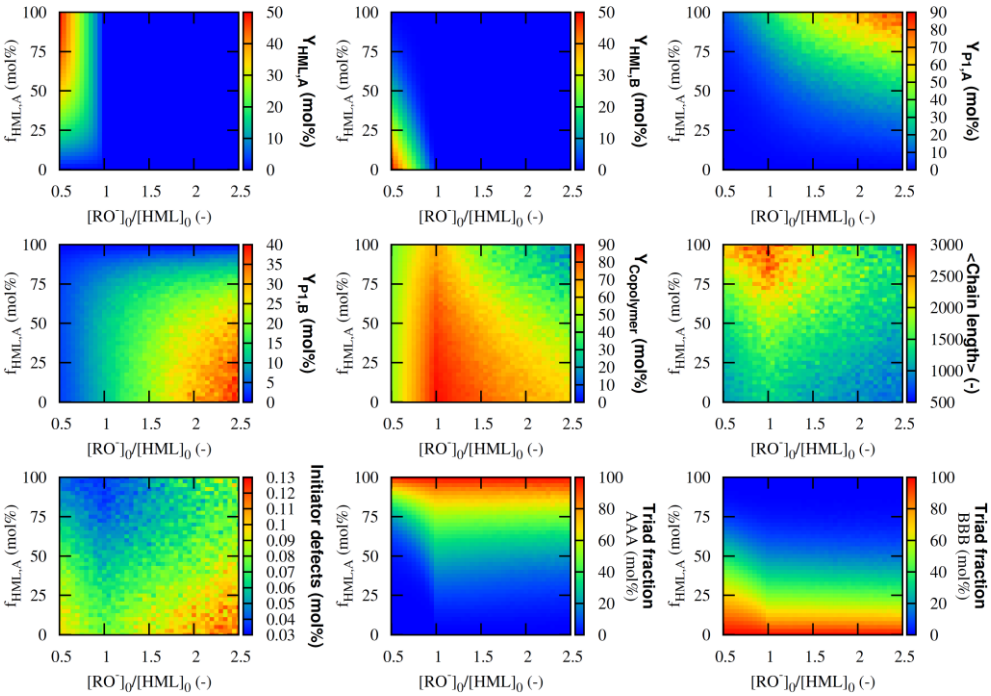

Figure J12: Effect of the base and the initial premonomer composition on the yields and properties for the copolymerization of 2 with 5 (see Figures 3, 4 and 5 in Chapter 3). Reaction conditions: 308 K; $f_{HML,A}$ is defined as $[HML,A]_0/([HML,A]_0+[HML,B]_0)$

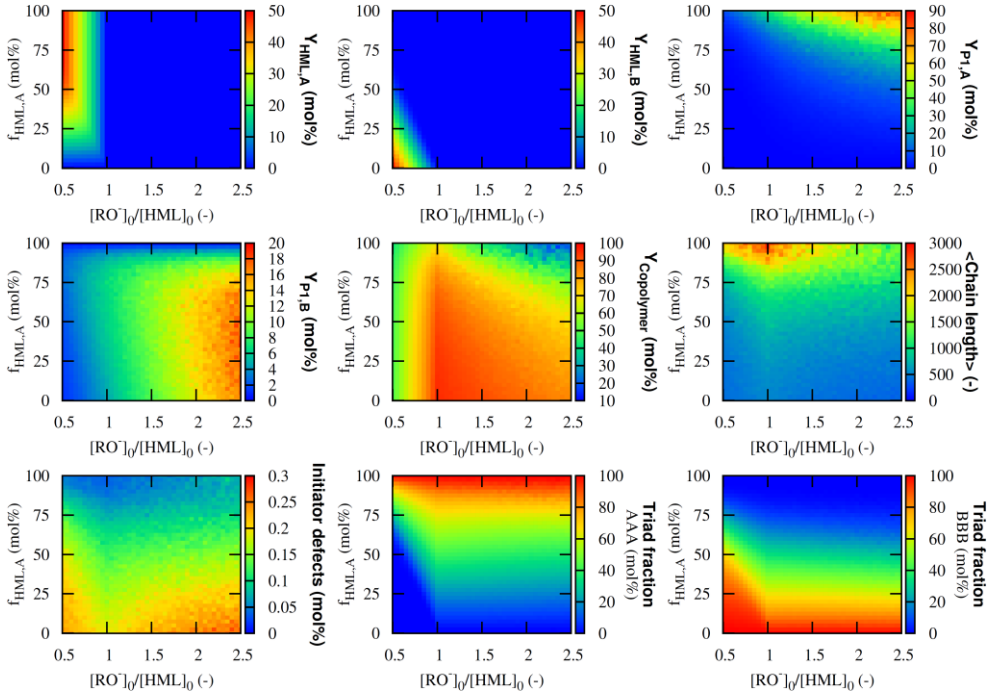

Figure J13: Effect of the base and the initial premonomer composition on the yields and properties for the copolymerization of 2 with 6 (see Figures 3, 4 and 5 in Chapter 3); Reaction conditions: 308 K; $f_{HML,A}$ is defined as $[HML,A]_0/([HML,A]_0+[HML,B]_0)$

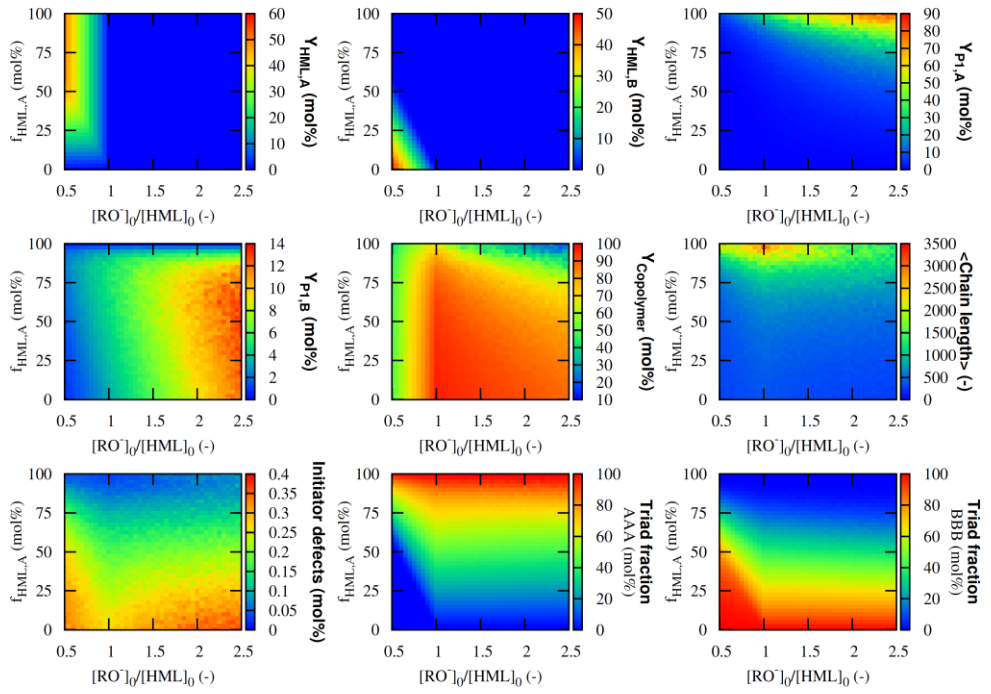

Figure J14: Effect of the base and the initial premonomer composition on the yields and properties for the copolymerization of 2 with 7 (see Figures 3, 4 and 5 in Chapter 3); Reaction conditions: 308 K; $f_{HML,A}$ is defined as $[HML,A]_0/([HML,A]_0+[HML,B]_0)$

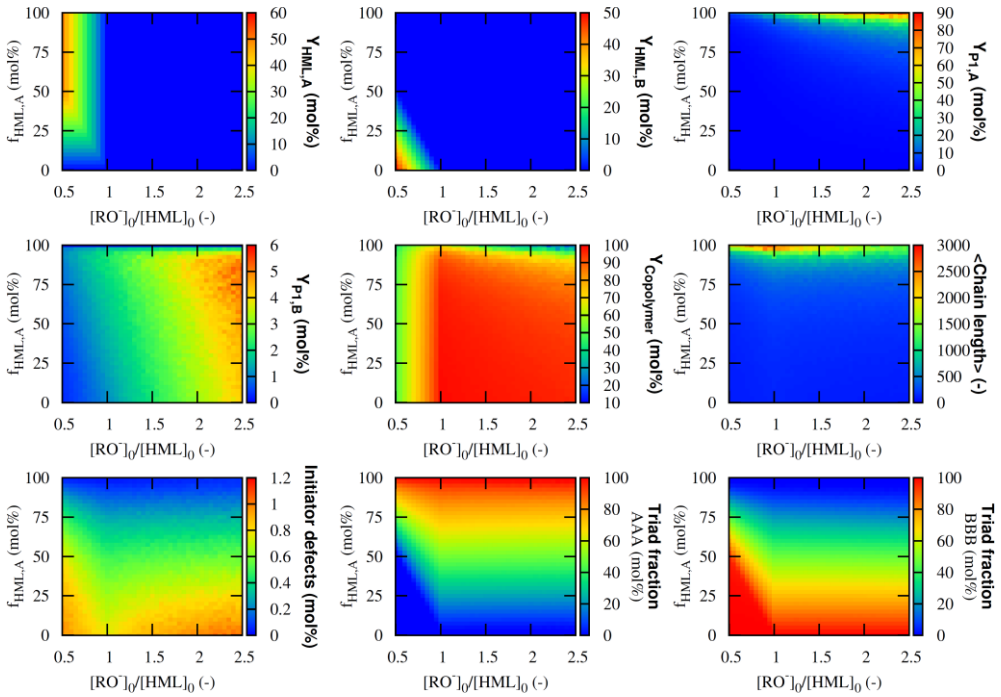

Figure J15: Effect of the base and the initial premonomer composition on the yields and properties for the copolymerization of 2 with 8 (see Figures 3, 4 and 5 in Chapter 3); Reaction conditions: 308 K; $f_{HML,A}$ is defined as $[HML,A]_0/([HML,A]_0+[HML,B]_0)$

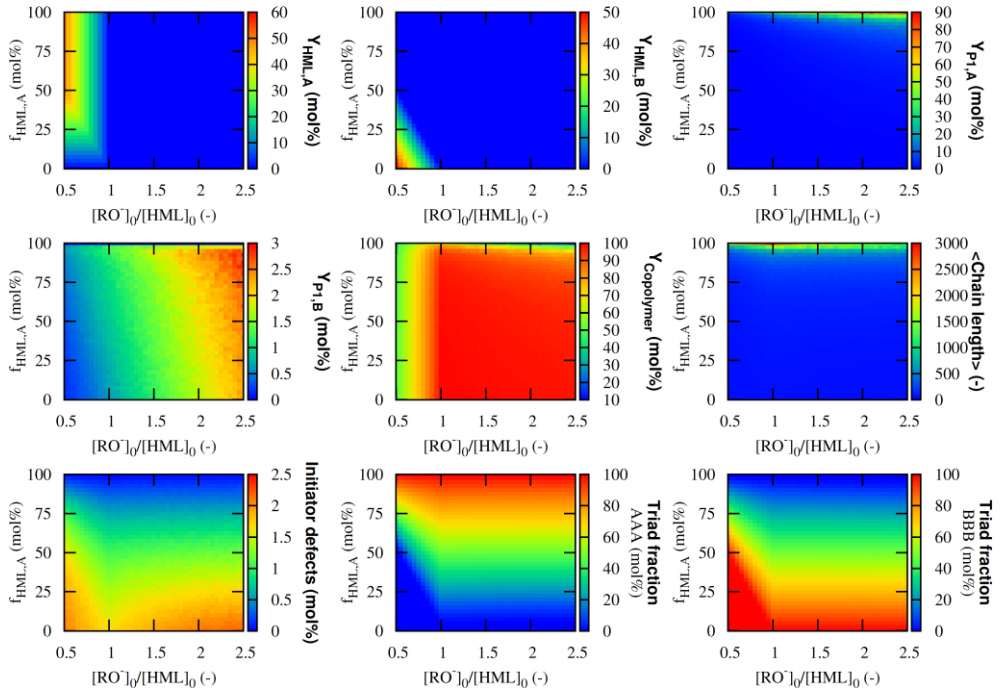

Figure J16: Effect of the base and the initial premonomer composition on the yields and properties for the copolymerization of 2 with 9 (see Figures 3, 4 and 5 in Chapter 3); Reaction conditions: 308 K; $f_{HML,A}$ is defined as $[HML,A]_0/([HML,A]_0+[HML,B]_0)$

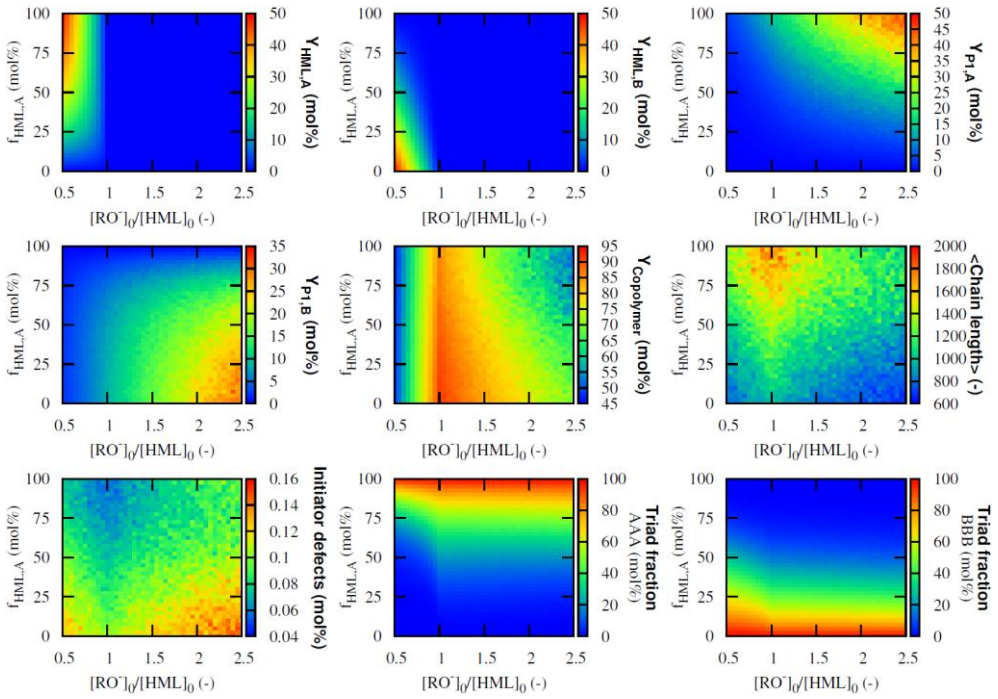

Figure J17: Effect of the base and the initial premonomer composition on the yields and properties for the copolymerization of 3 with 1 (see Figures 3, 4 and 5 in Chapter 3); Reaction conditions: 308 K; $f_{HML,A}$ is defined as $[HML,A]_0/([HML,A]_0+[HML,B]_0)$

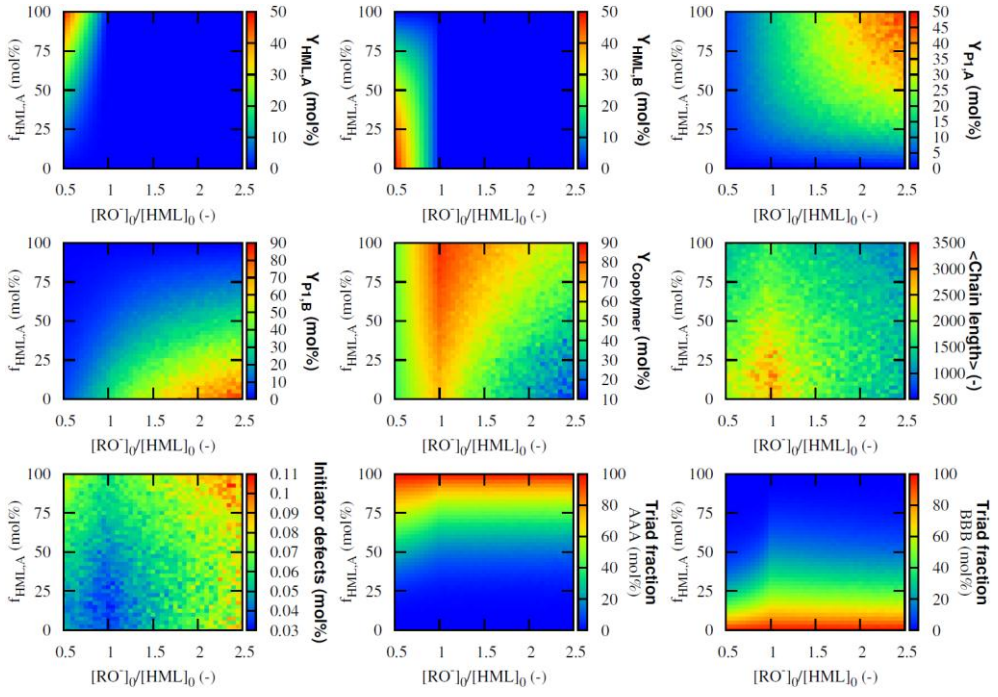

Figure J18: Effect of the base and the initial premonomer composition on the yields and properties for the copolymerization of 3 with 2 (see Figures 3, 4 and 5 in Chapter 3); Reaction conditions: 308 K; $f_{HML,A}$ is defined as $[HML,A]_0/([HML,A]_0+[HML,B]_0)$

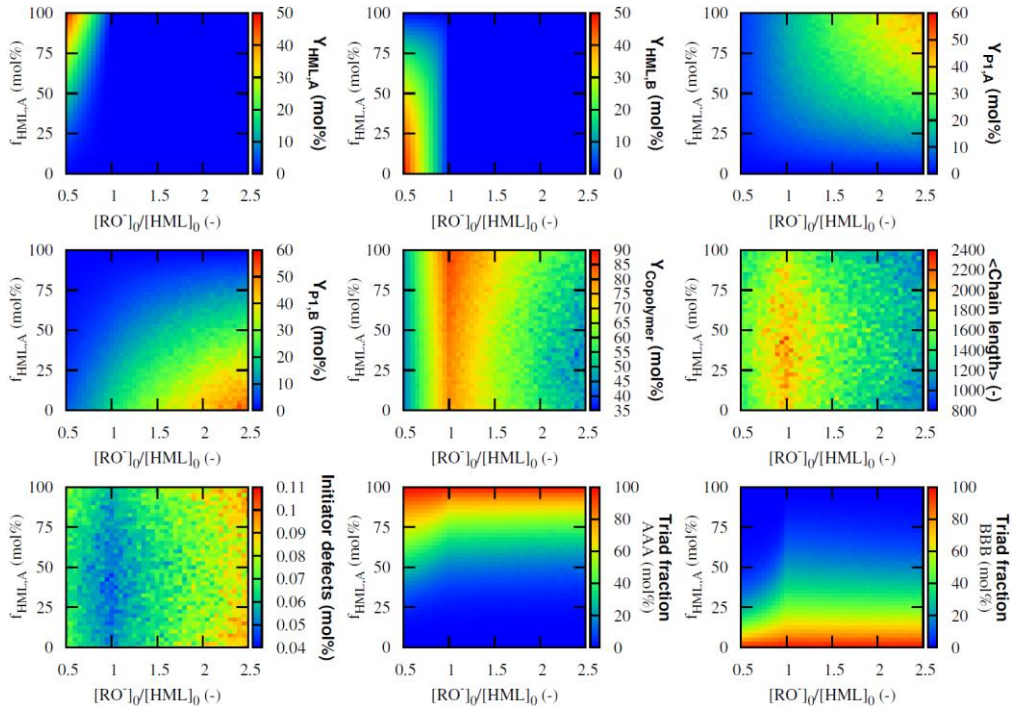

Figure J19: Effect of the base and the initial premonomer composition on the yields and properties for the copolymerization of 3 with 4 (see Figures 3, 4 and 5 in Chapter 3); Reaction conditions: 308 K; $f_{HML,A}$ is defined as $[HML,A]_0/([HML,A]_0+[HML,B]_0)$

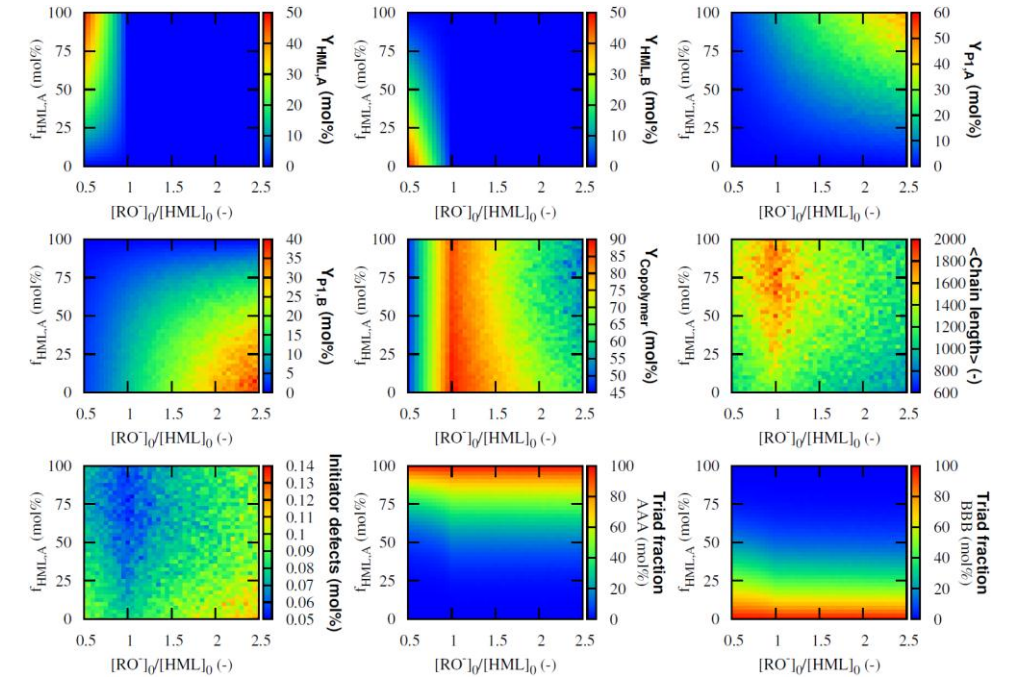

Figure J20: Effect of the base and the initial premonomer composition on the yields and properties for the copolymerization of 3 with 5 (see Figures 3, 4 and 5 in Chapter 3); Reaction conditions: 308 K; $f_{HML,A}$ is defined as $[HML,A]_0/([HML,A]_0+[HML,B]_0)$

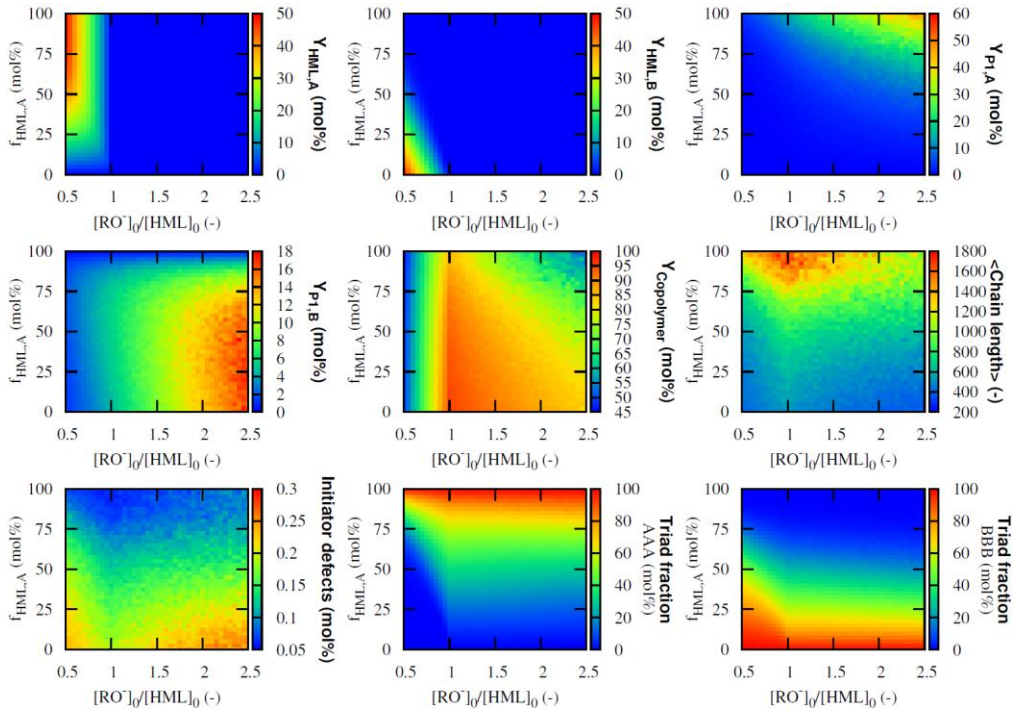

Figure J21: Effect of the base and the initial premonomer composition on the yields and properties for the copolymerization of 3 with 6 (see Figures 3, 4 and 5 in Chapter 3); Reaction conditions: 308 K; $f_{HML,A}$ is defined as $[HML,A]_0/([HML,A]_0+[HML,B]_0)$

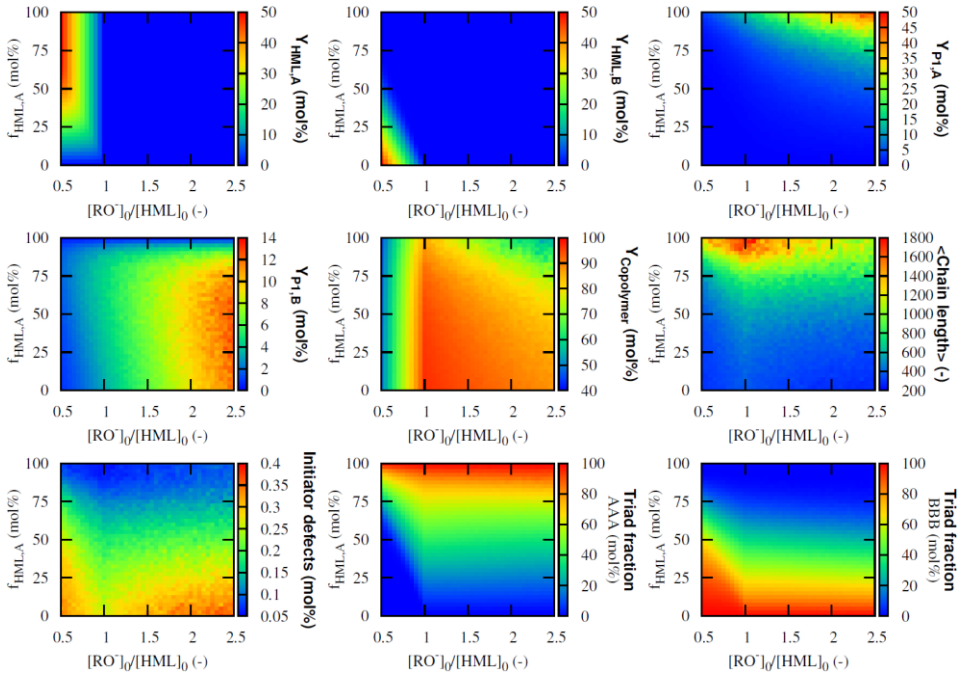

Figure J22: Effect of the base and the initial premonomer composition on the yields and properties for the copolymerization of 3 with 7 (see Figures 3, 4 and 5 in Chapter 3); Reaction conditions: 308 K; $f_{HML,A}$ is defined as $[HML,A]_0/([HML,A]_0+[HML,B]_0)$

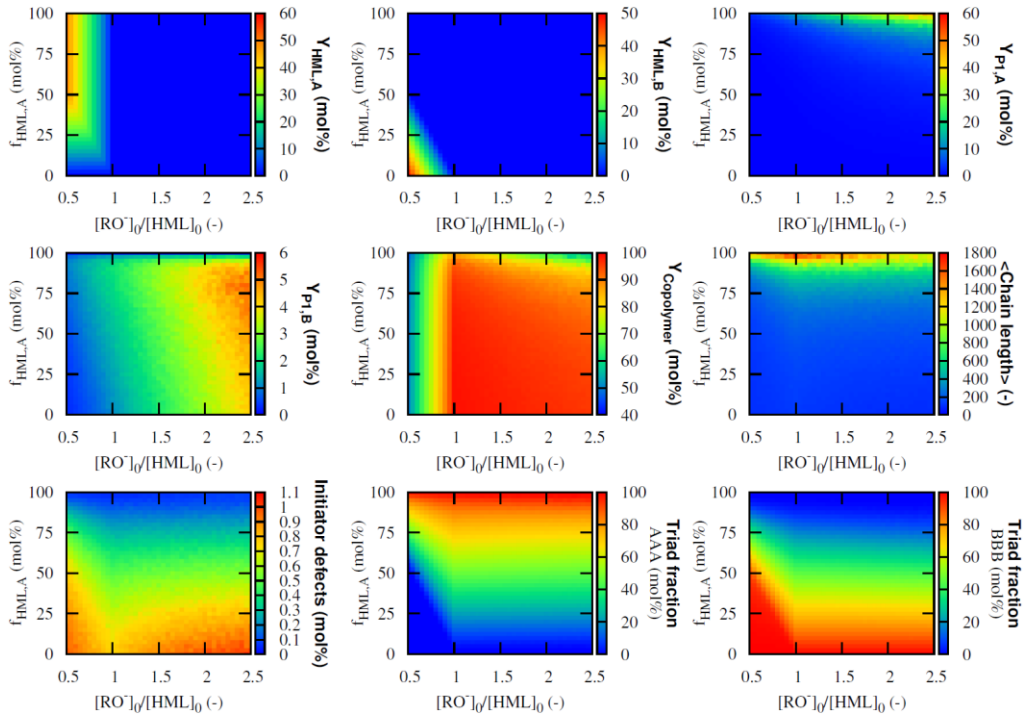

Figure J23: Effect of the base and the initial premonomer composition on the yields and properties for the copolymerization of 3 with 8 (see Figures 3, 4 and 5 in Chapter 3); Reaction conditions: 308 K; $f_{HML,A}$ is defined as $[HML,A]_0/([HML,A]_0+[HML,B]_0)$

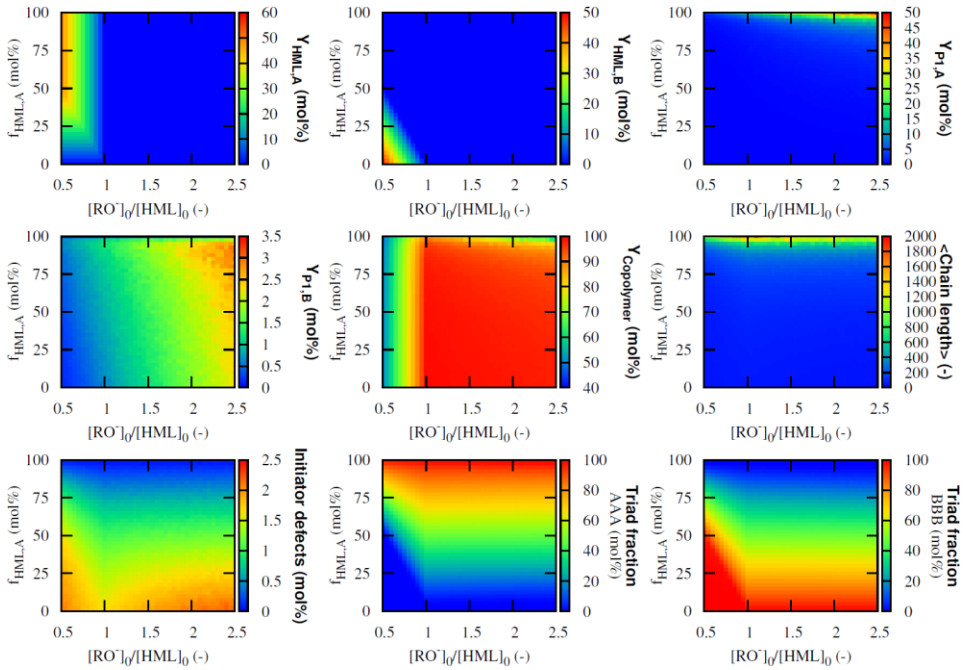

Figure J24: Effect of the base and the initial premonomer composition on the yields and properties for the copolymerization of 3 with 9 (see Figures 3, 4 and 5 in Chapter 3); Reaction conditions: 308 K; $f_{HML,A}$ is defined as $[HML,A]_0/([HML,A]_0+[HML,B]_0)$

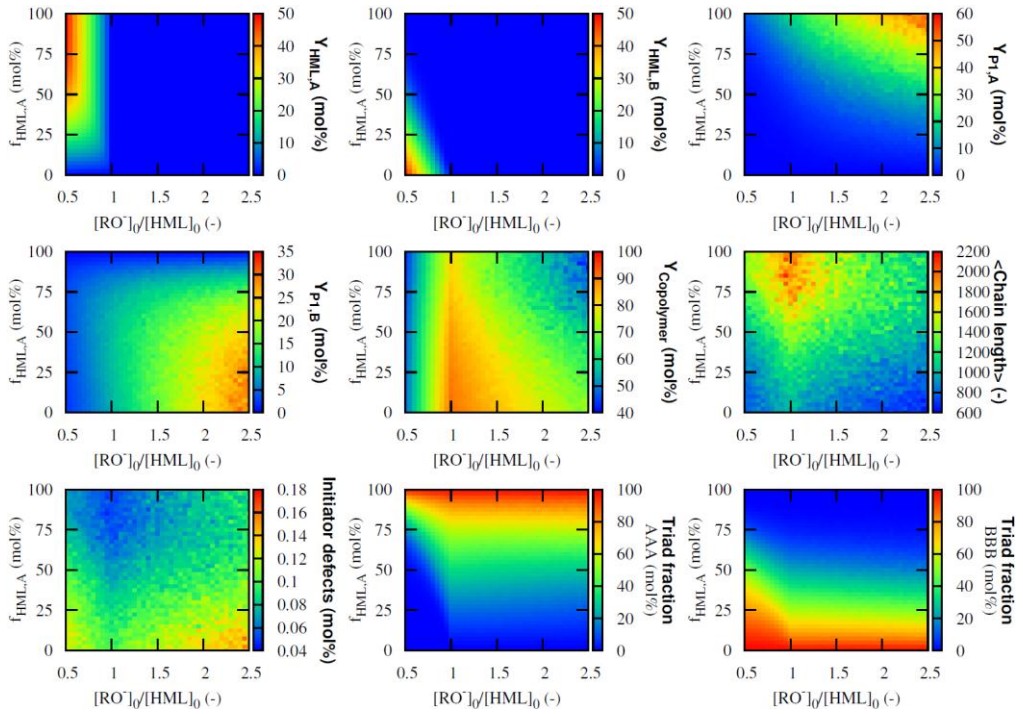

Figure J25: Effect of the base and the initial premonomer composition on the yields and properties for the copolymerization of 4 with 1 (see Figures 3, 4 and 5 in Chapter 3); Reaction conditions: 308 K; $f_{HML,A}$ is defined as $[HML,A]_0/([HML,A]_0+[HML,B]_0)$

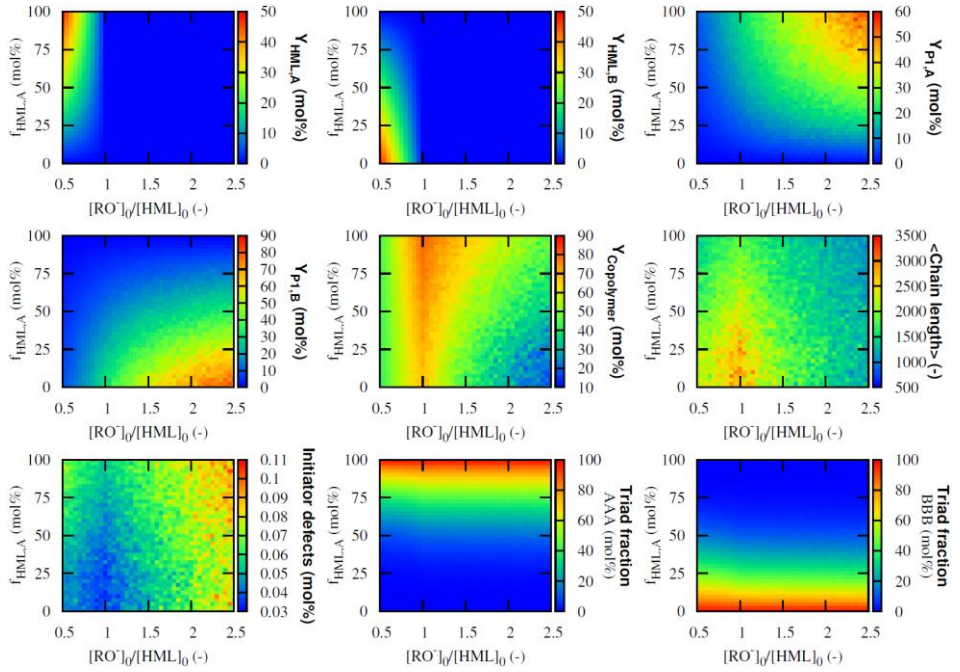

Figure J26: Effect of the base and the initial premonomer composition on the yields and properties for the copolymerization of 4 with 2 (see Figures 3, 4 and 5 in Chapter 3); Reaction conditions: 308 K; $f_{HML,A}$ is defined as $[HML,A]_0/([HML,A]_0+[HML,B]_0)$

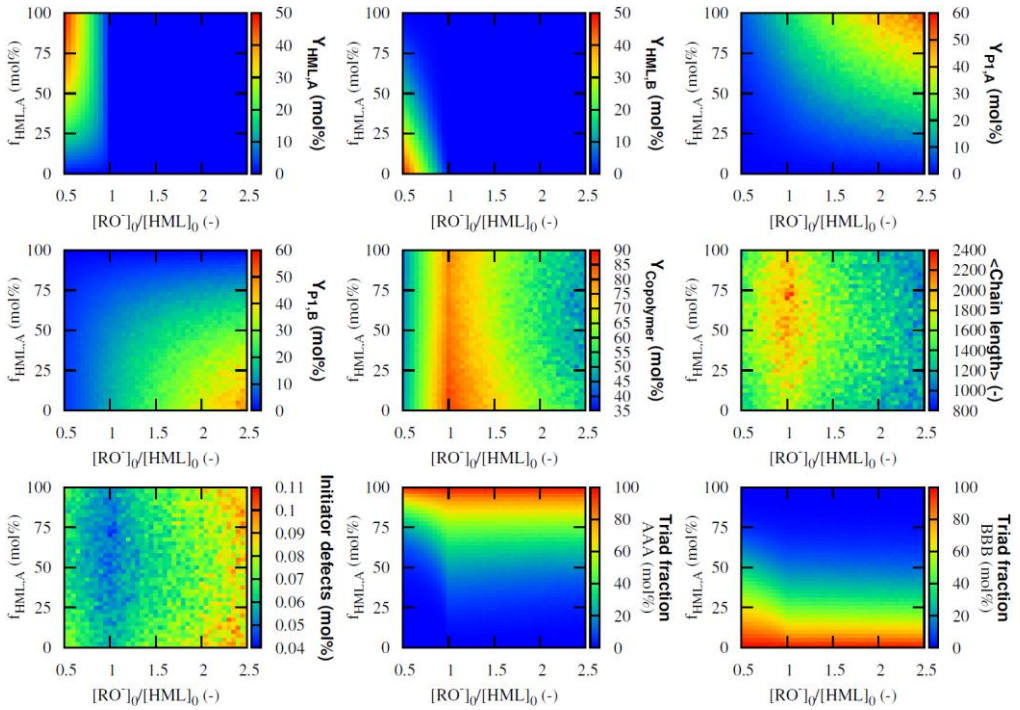

Figure J27: Effect of the base and the initial premonomer composition on the yields and properties for the copolymerization of 4 with 3 (see Figures 3, 4 and 5 in Chapter 3); Reaction conditions: 308 K; $f_{HML,A}$ is defined as $[HML,A]_0/([HML,A]_0+[HML,B]_0)$

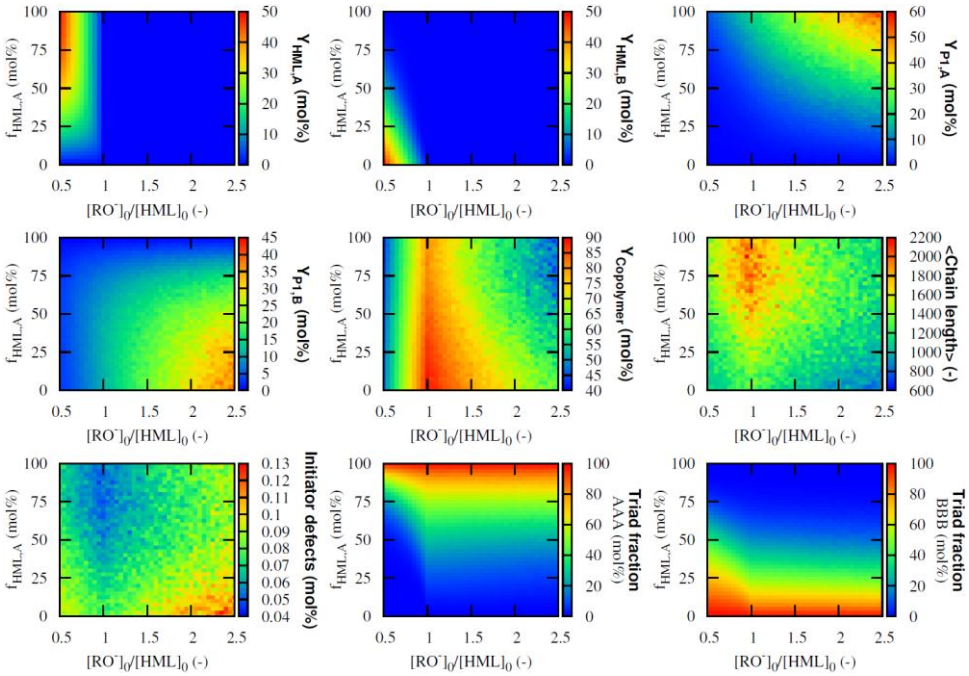

Figure J28: Effect of the base and the initial premonomer composition on the yields and properties for the copolymerization of 4 with 5 (see Figures 3, 4 and 5 in Chapter 3); Reaction conditions: 308 K; $f_{HML,A}$ is defined as $[HML,A]_0/([HML,A]_0+[HML,B]_0)$

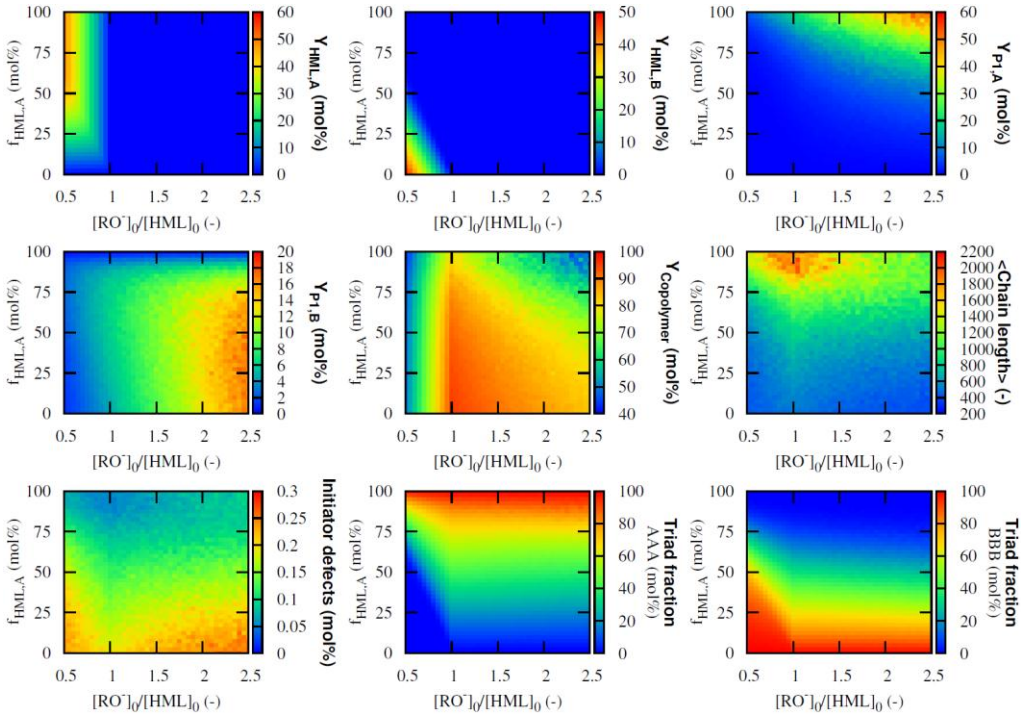

Figure J29: Effect of the base and the initial premonomer composition on the yields and properties for the copolymerization of 4 with 6 (see Figures 3, 4 and 5 in Chapter 3); Reaction conditions: 308 K; $f_{HML,A}$ is defined as $[HML,A]_0/([HML,A]_0+[HML,B]_0)$

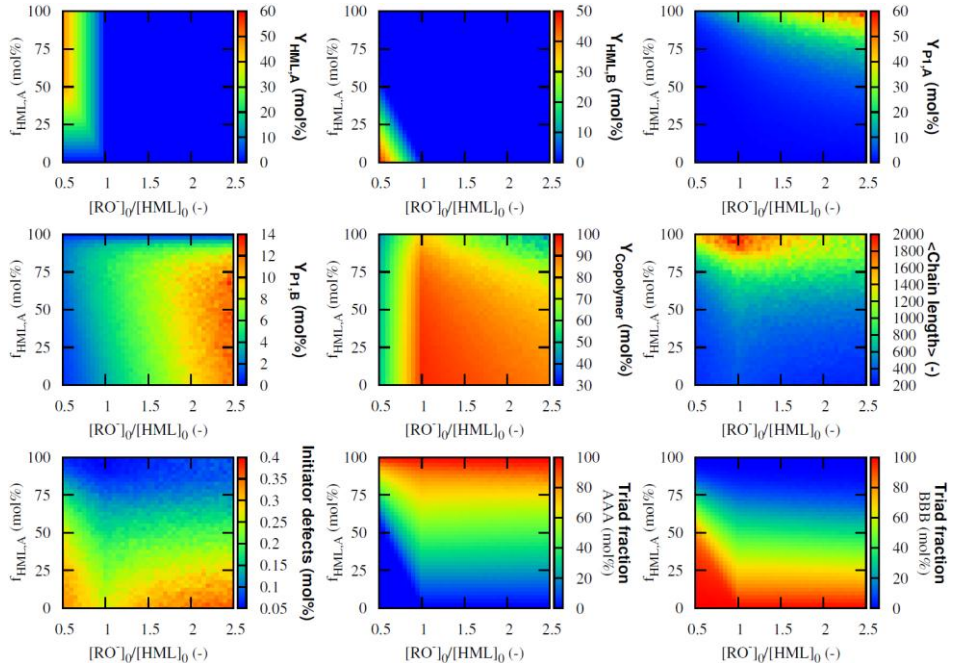

Figure J30: Effect of the base and the initial premonomer composition on the yields and properties for the copolymerization of 4 with 7 (see Figures 3, 4 and 5 in Chapter 3); Reaction conditions: 308 K; $f_{HML,A}$ is defined as $[HML,A]_0/([HML,A]_0+[HML,B]_0)$

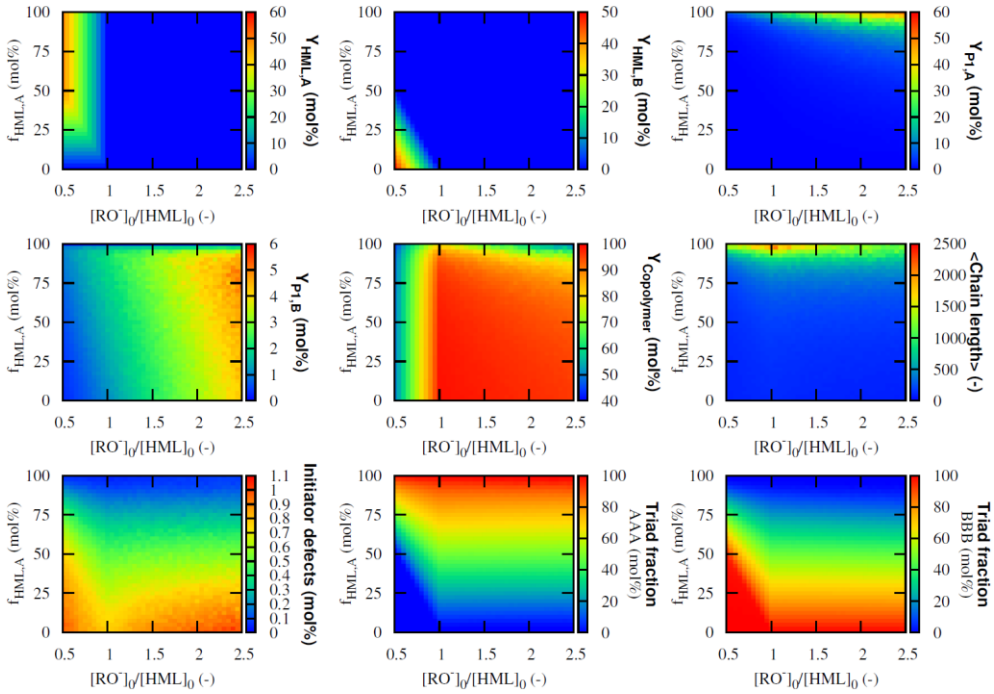

Figure J31: Effect of the base and the initial premonomer composition on the yields and properties for the copolymerization of 4 with 8 (see Figures 3, 4 and 5 in Chapter 3); Reaction conditions: 308 K; $f_{HML,A}$ is defined as $[HML,A]_0/([HML,A]_0+[HML,B]_0)$

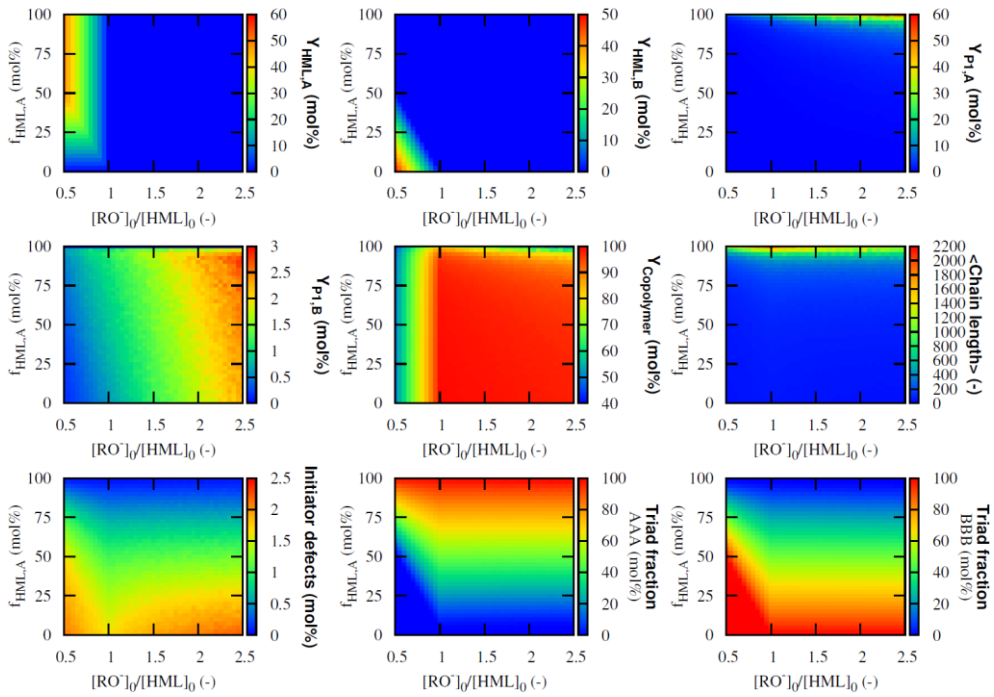

Figure J32: Effect of the base and the initial premonomer composition on the yields and properties for the copolymerization of 4 with 9 (see Figures 3, 4 and 5 in Chapter 3); Reaction conditions: 308 K; $f_{HML,A}$ is defined as $[HML,A]_0/([HML,A]_0+[HML,B]_0)$

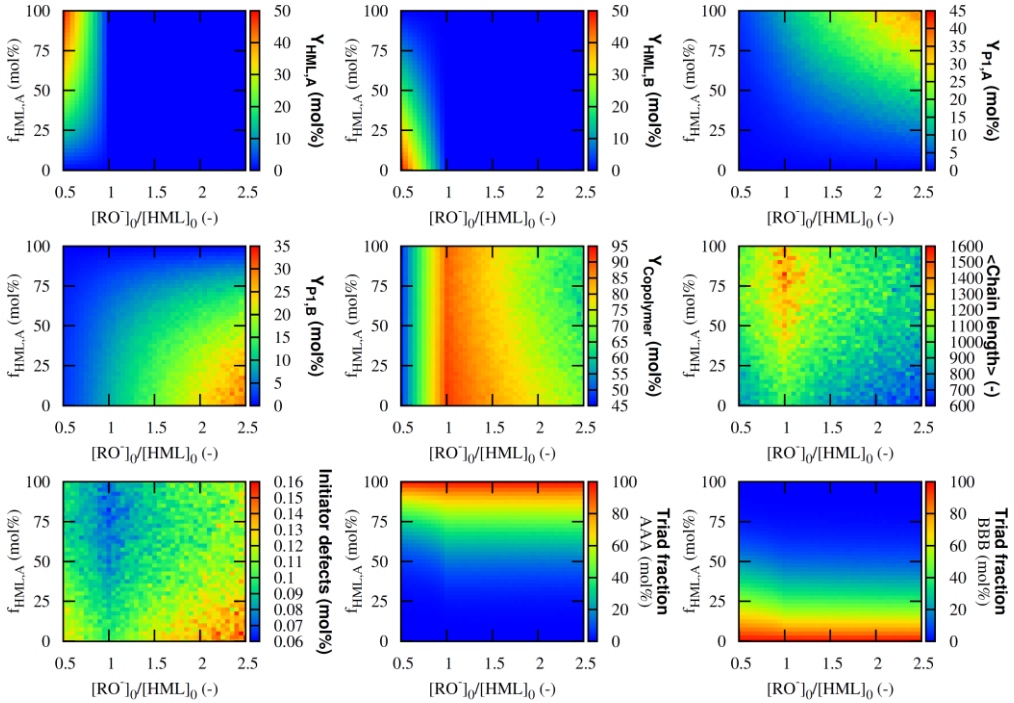

Figure J33: Effect of the base and the initial premonomer composition on the yields and properties for the copolymerization of 5 with 1 (see Figures 3, 4 and 5 in Chapter 3); Reaction conditions: 308 K; $f_{HML,A}$ is defined as $[HML,A]_0/([HML,A]_0+[HML,B]_0)$

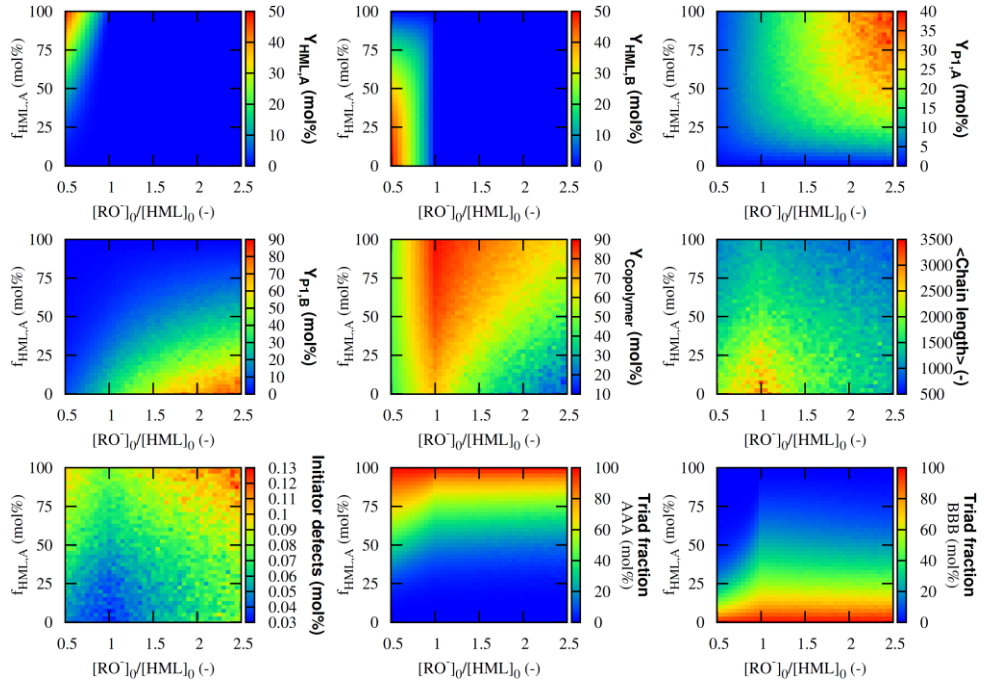

Figure J34: Effect of the base and the initial premonomer composition on the yields and properties for the copolymerization of 5 with 2 (see Figures 3, 4 and 5 in Chapter 3); Reaction conditions: 308 K; $f_{HML,A}$ is defined as $[HML,A]_0/([HML,A]_0+[HML,B]_0)$

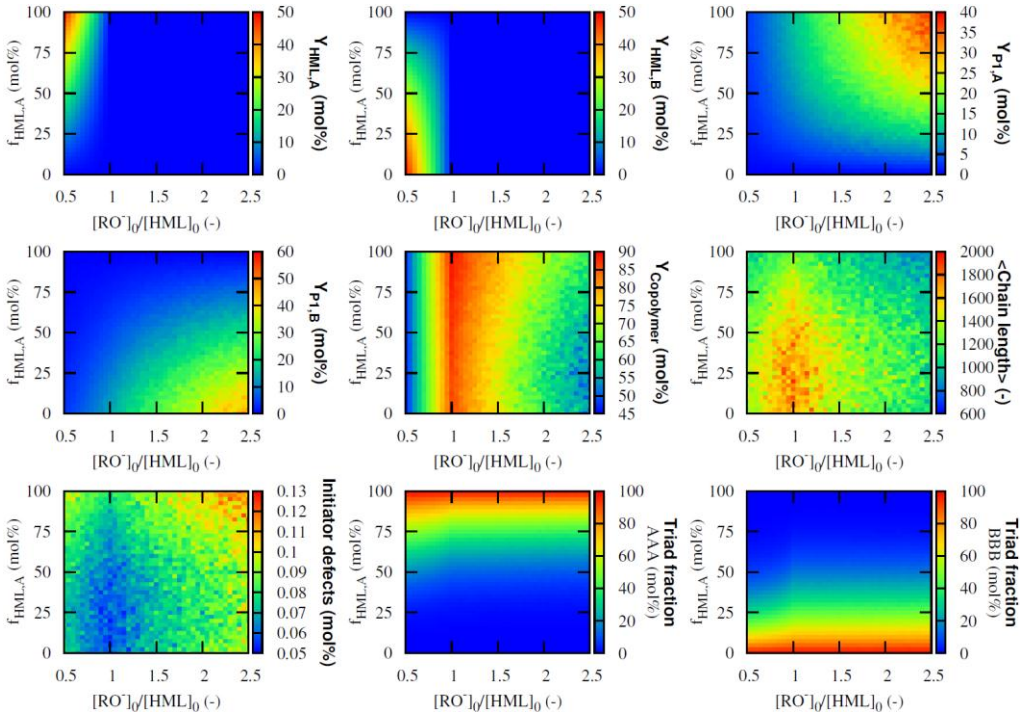

Figure J35: Effect of the base and the initial premonomer composition on the yields and properties for the copolymerization of 5 with 3 (see Figures 3, 4 and 5 in Chapter 3); Reaction conditions: 308 K; $f_{HML,A}$ is defined as $[HML,A]_0/([HML,A]_0+[HML,B]_0)$

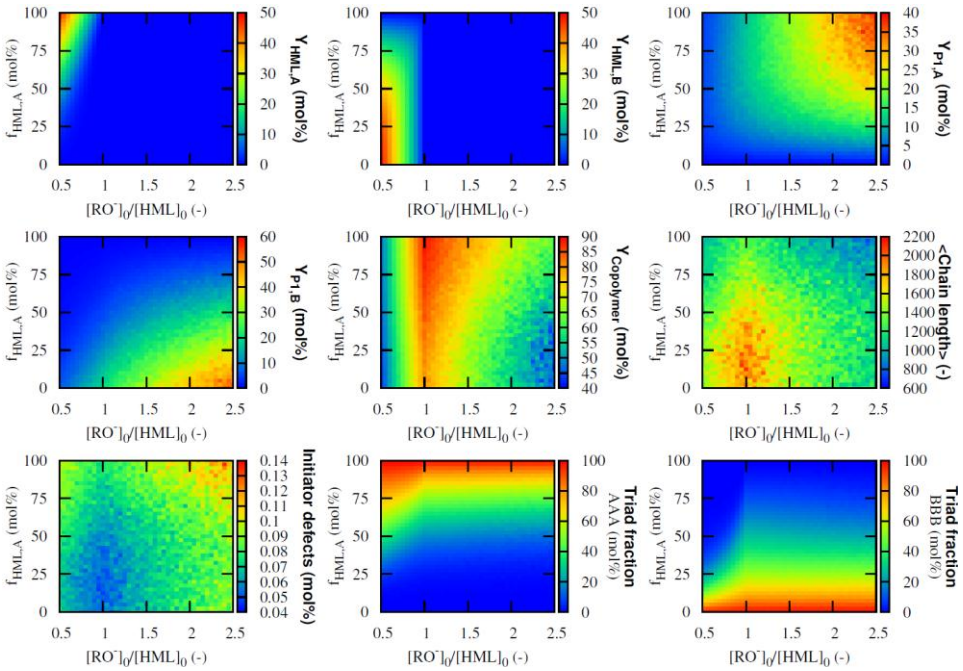

Figure J36: Effect of the base and the initial premonomer composition on the yields and properties for the copolymerization of 5 with 4 (see Figures 3, 4 and 5 in Chapter 3); Reaction conditions: 308 K; $f_{HML,A}$ is defined as $[HML,A]_0/([HML,A]_0+[HML,B]_0)$

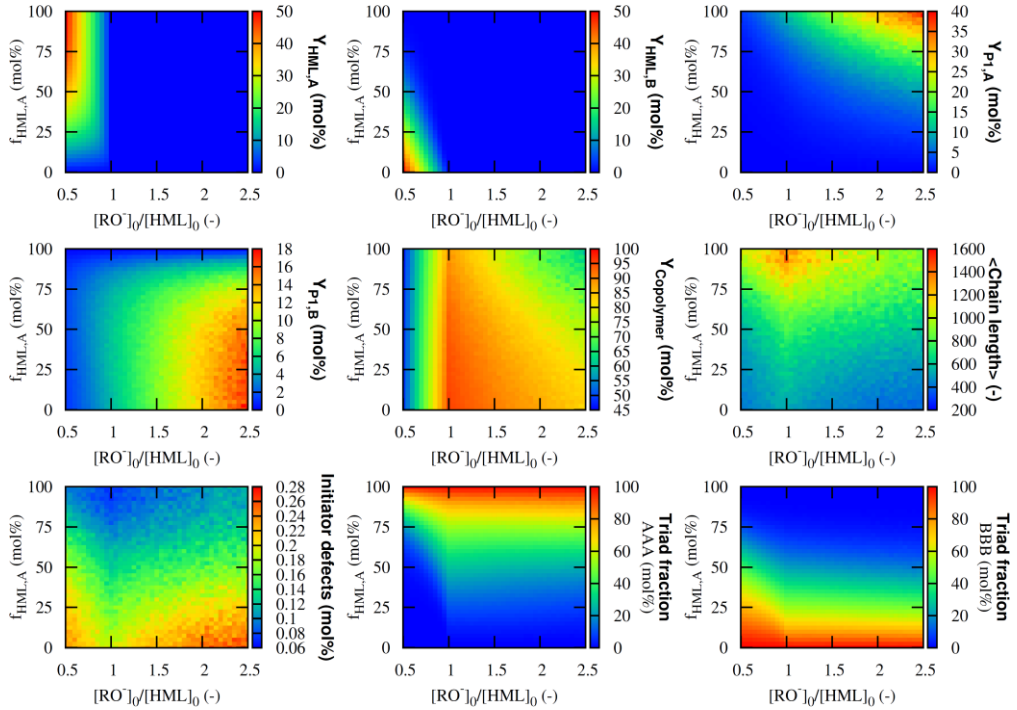

Figure J37: Effect of the base and the initial premonomer composition on the yields and properties for the copolymerization of 5 with 6 (see Figures 3, 4 and 5 in Chapter 3); Reaction conditions: 308 K; $f_{HML,A}$ is defined as $[HML,A]_0/([HML,A]_0+[HML,B]_0)$

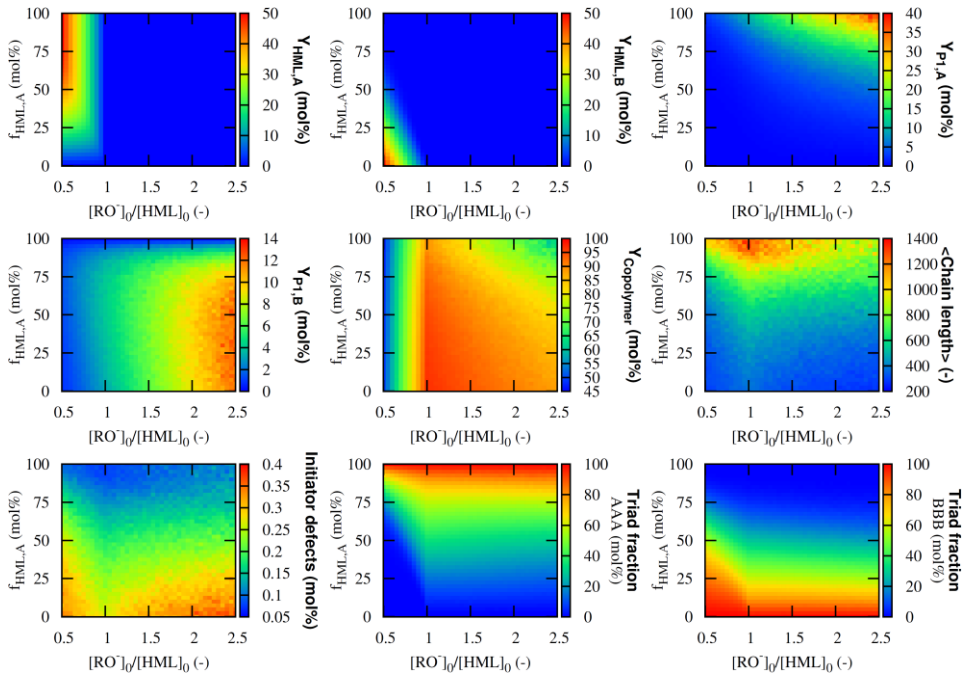

Figure J38: Effect of the base and the initial premonomer composition on the yields and properties for the copolymerization of 5 with 7 (see Figures 3, 4 and 5 in Chapter 3); Reaction conditions: 308 K; $f_{HML,A}$ is defined as $[HML,A]_0/([HML,A]_0+[HML,B]_0)$

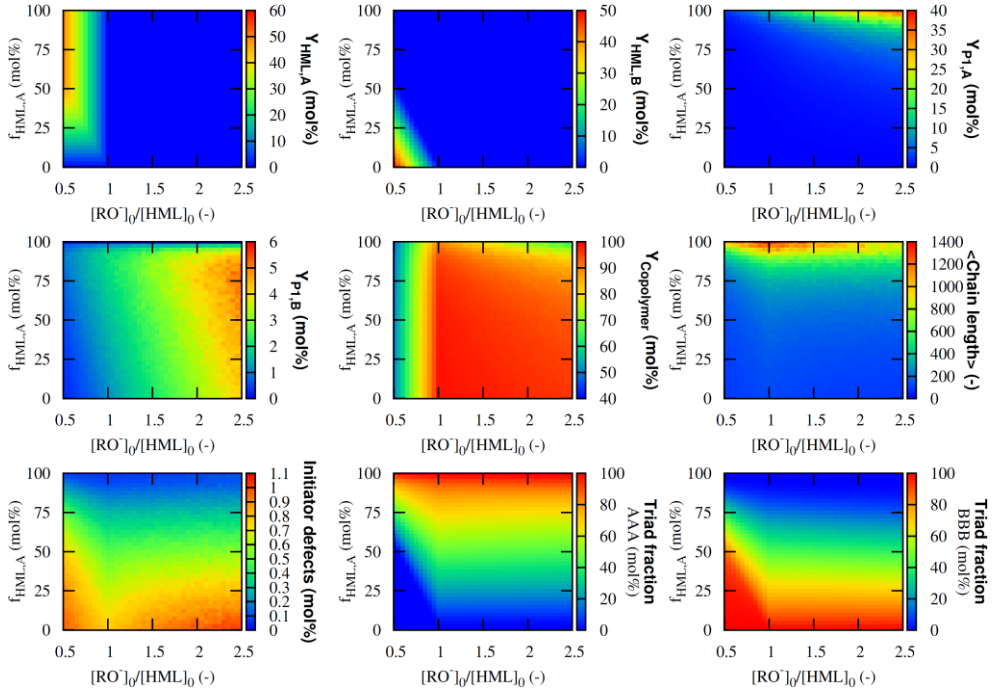

Figure J39: Effect of the base and the initial premonomer composition on the yields and properties for the copolymerization of 5 with 8 (see Figures 3, 4 and 5 in Chapter 3); Reaction conditions: 308 K; $f_{HML,A}$ is defined as $[HML,A]_0/([HML,A]_0+[HML,B]_0)$

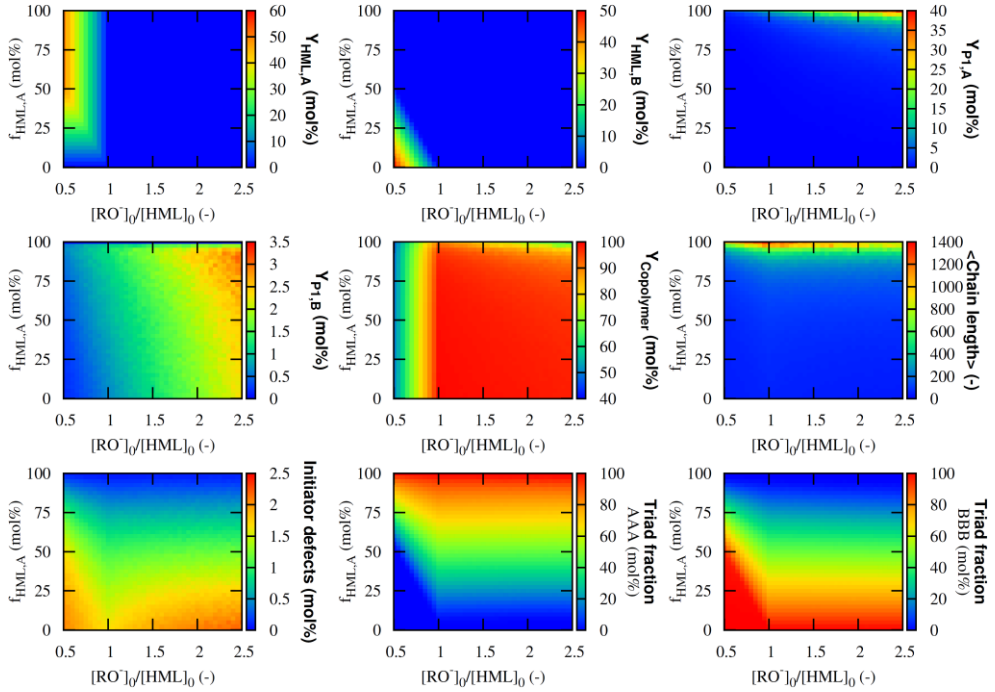

Figure J40: Effect of the base and the initial premonomer composition on the yields and properties for the copolymerization of 5 with 9 (see Figures 3, 4 and 5 in Chapter 3); Reaction conditions: 308 K; $f_{HML,A}$ is defined as $[HML,A]_0/([HML,A]_0+[HML,B]_0)$

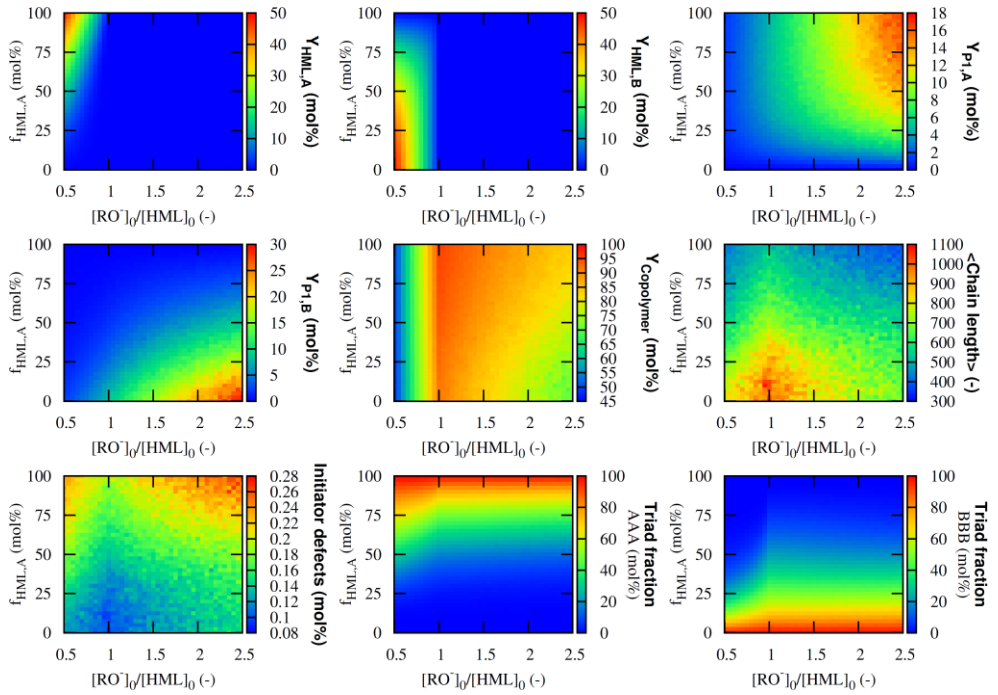

Figure J41: Effect of the base and the initial premonomer composition on the yields and properties for the copolymerization of 6 with 1 (see Figures 3, 4 and 5 in Chapter 3); Reaction conditions: 308 K; $f_{HML,A}$ is defined as $[HML,A]_0/([HML,A]_0+[HML,B]_0)$

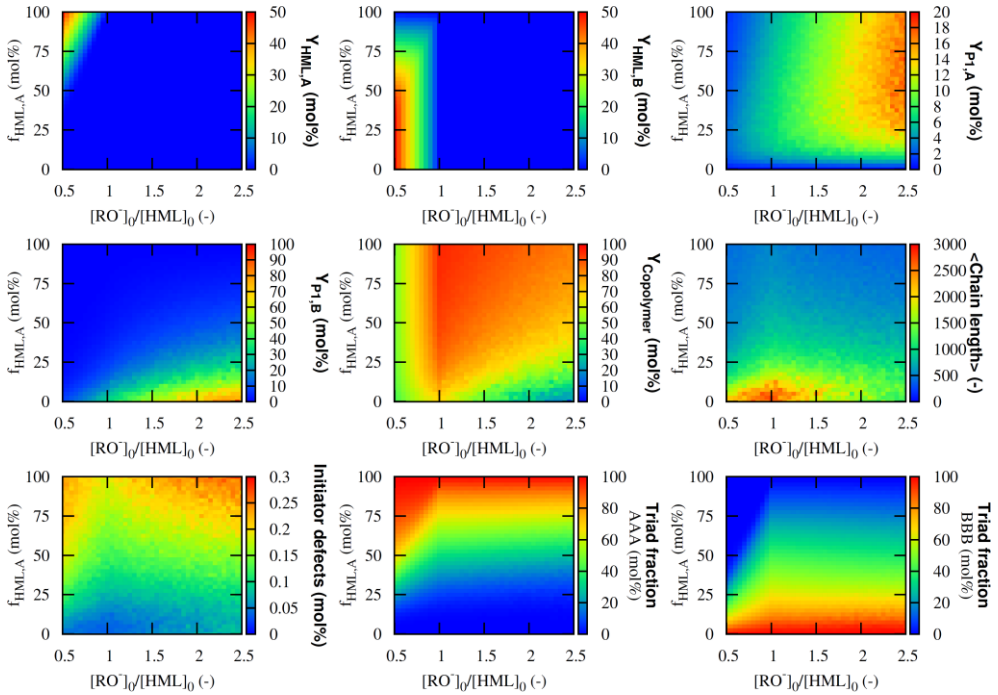

Figure J42: Effect of the base and the initial premonomer composition on the yields and properties for the copolymerization of 6 with 2 (see Figures 3, 4 and 5 in Chapter 3); Reaction conditions: 308 K; $f_{HML,A}$ is defined as $[HML,A]_0/([HML,A]_0+[HML,B]_0)$

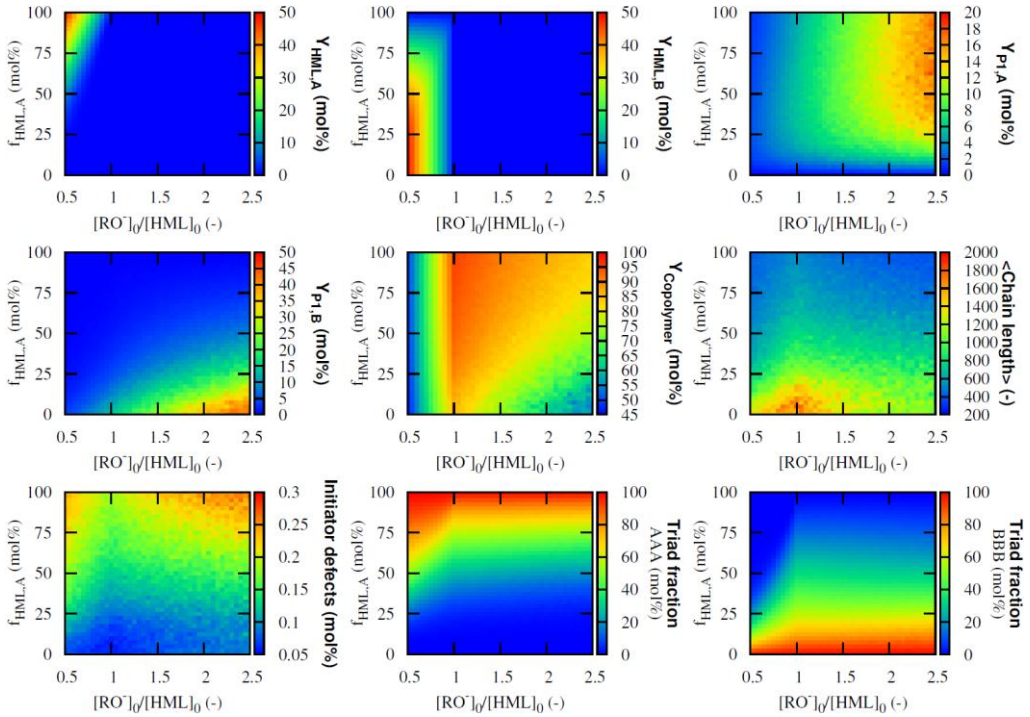

Figure J43: Effect of the base and the initial premonomer composition on the yields and properties for the copolymerization of 6 with 3 (see Figures 3, 4 and 5 in Chapter 3); Reaction conditions: 308 K; $f_{HML,A}$ is defined as $[HML,A]_0/([HML,A]_0+[HML,B]_0)$

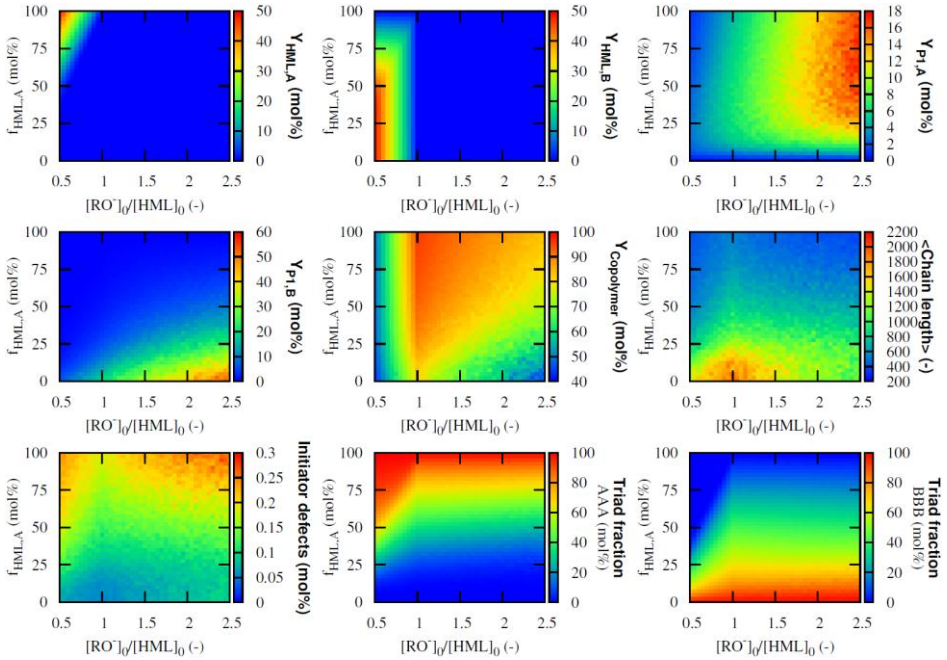

Figure J44: Effect of the base and the initial premonomer composition on the yields and properties for the copolymerization of 6 with 4 (see Figures 3, 4 and 5 in Chapter 3); Reaction conditions: 308 K; $f_{HML,A}$ is defined as $[HML,A]_0/([HML,A]_0+[HML,B]_0)$

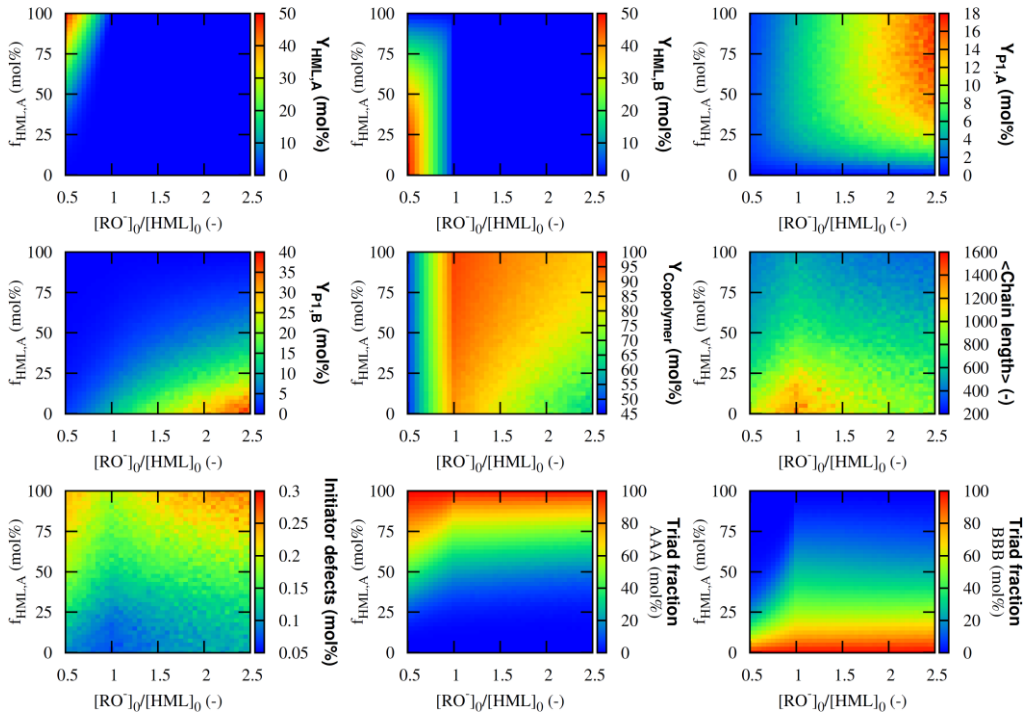

Figure J45: Effect of the base and the initial premonomer composition on the yields and properties for the copolymerization of 6 with 5 (see Figures 3, 4 and 5 in Chapter 3); Reaction conditions: 308 K; $f_{HML,A}$ is defined as $[HML,A]_0/([HML,A]_0+[HML,B]_0)$

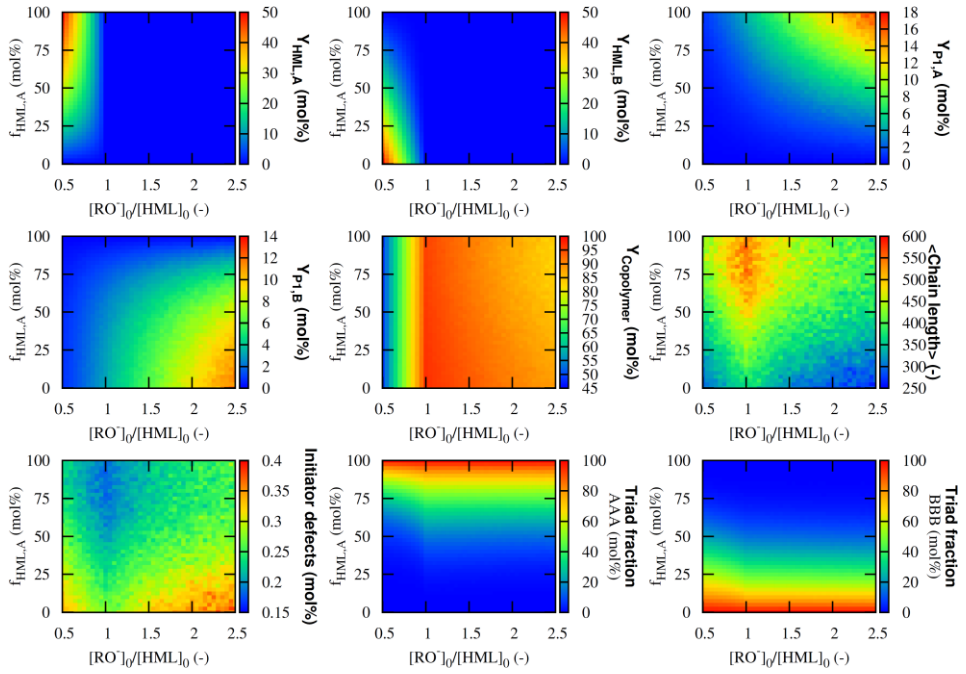

Figure J46: Effect of the base and the initial premonomer composition on the yields and properties for the copolymerization of 6 with 7 (see Figures 3, 4 and 5 in Chapter 3); Reaction conditions: 308 K; $f_{HML,A}$ is defined as $[HML,A]_0/([HML,A]_0+[HML,B]_0)$

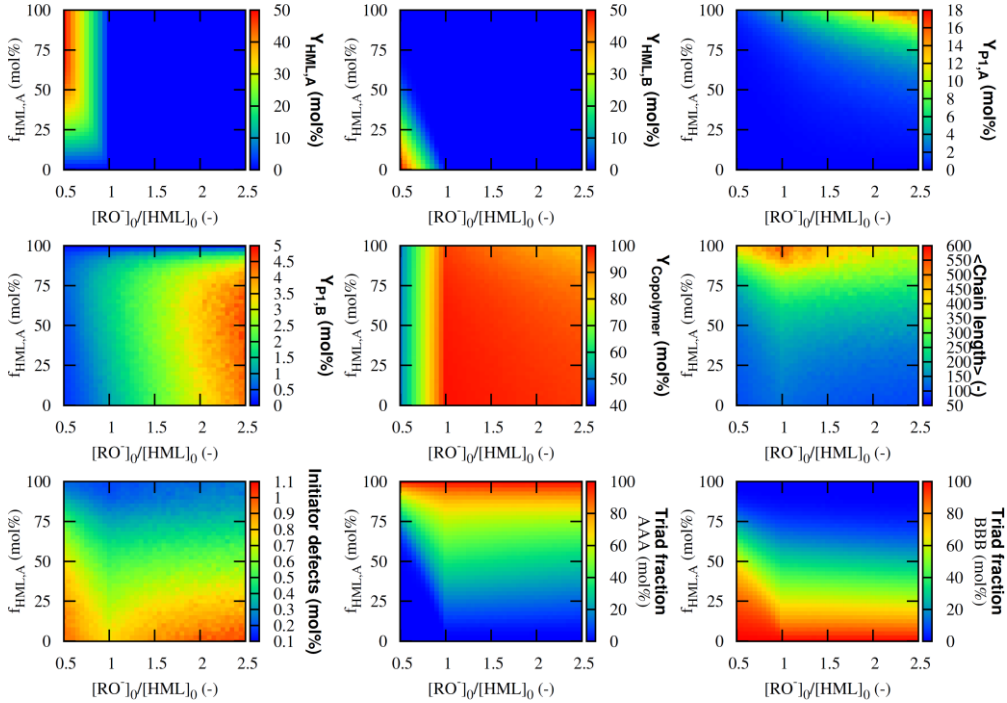

Figure J47: Effect of the base and the initial premonomer composition on the yields and properties for the copolymerization of 6 with 8 (see Figures 3, 4 and 5 in Chapter 3); Reaction conditions: 308 K; $f_{HML,A}$ is defined as $[HML,A]_0/([HML,A]_0+[HML,B]_0)$

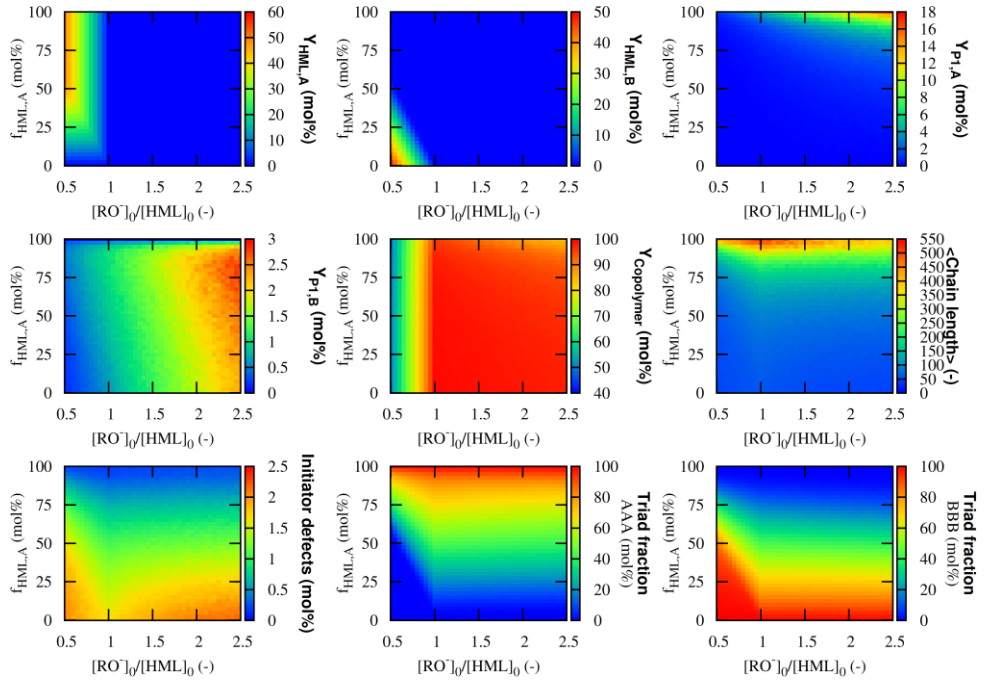

Figure J48: Effect of the base and the initial premonomer composition on the yields and properties for the copolymerization of 6 with 9 (see Figures 3, 4 and 5 in Chapter 3); Reaction conditions: 308 K; $f_{HML,A}$ is defined as $[HML,A]_0/([HML,A]_0+[HML,B]_0)$

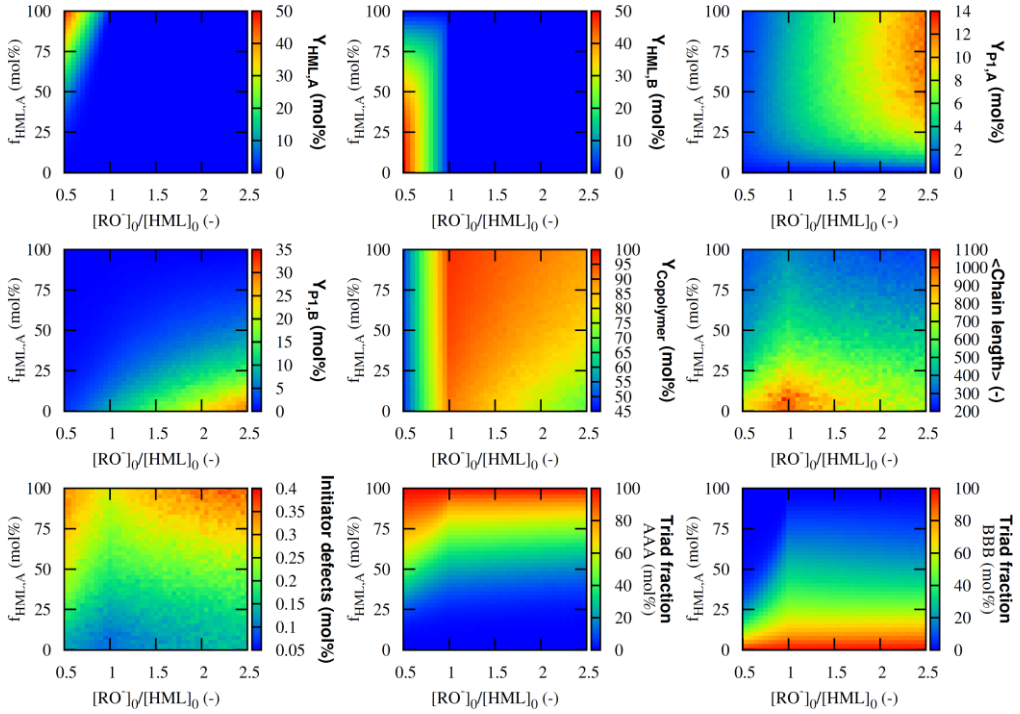

Figure J49: Effect of the base and the initial premonomer composition on the yields and properties for the copolymerization of 7 with 1 (see Figures 3, 4 and 5 in Chapter 3); Reaction conditions: 308 K; $f_{HML,A}$ is defined as $[HML,A]_0/([HML,A]_0+[HML,B]_0)$

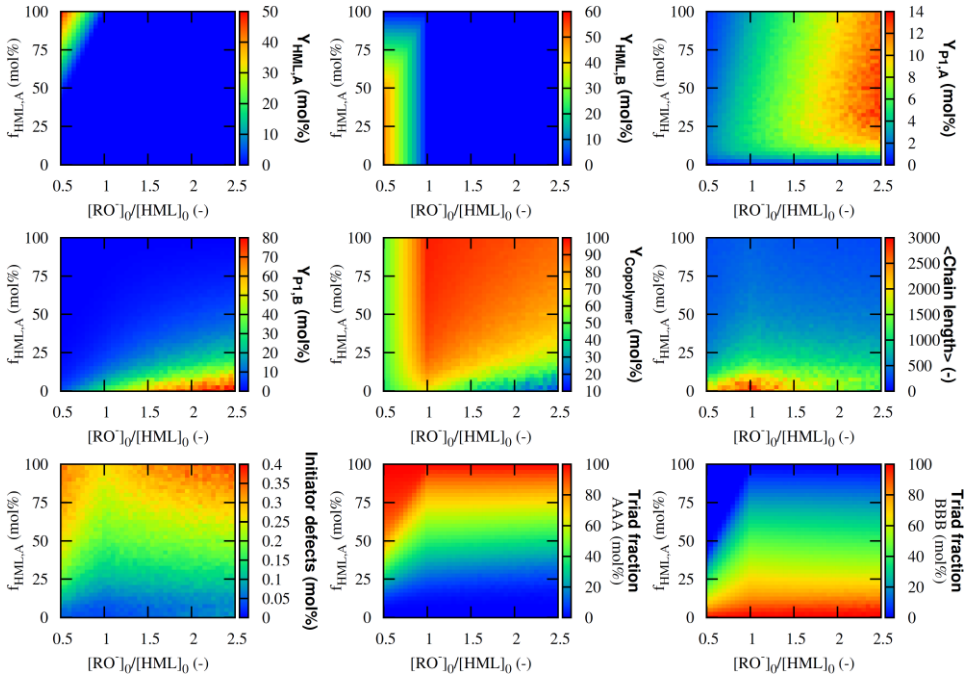

Figure J50: Effect of the base and the initial premonomer composition on the yields and properties for the copolymerization of 7 with 2 (see Figures 3, 4 and 5 in Chapter 3); Reaction conditions: 308 K; $f_{HML,A}$ is defined as $[HML,A]_0/([HML,A]_0+[HML,B]_0)$

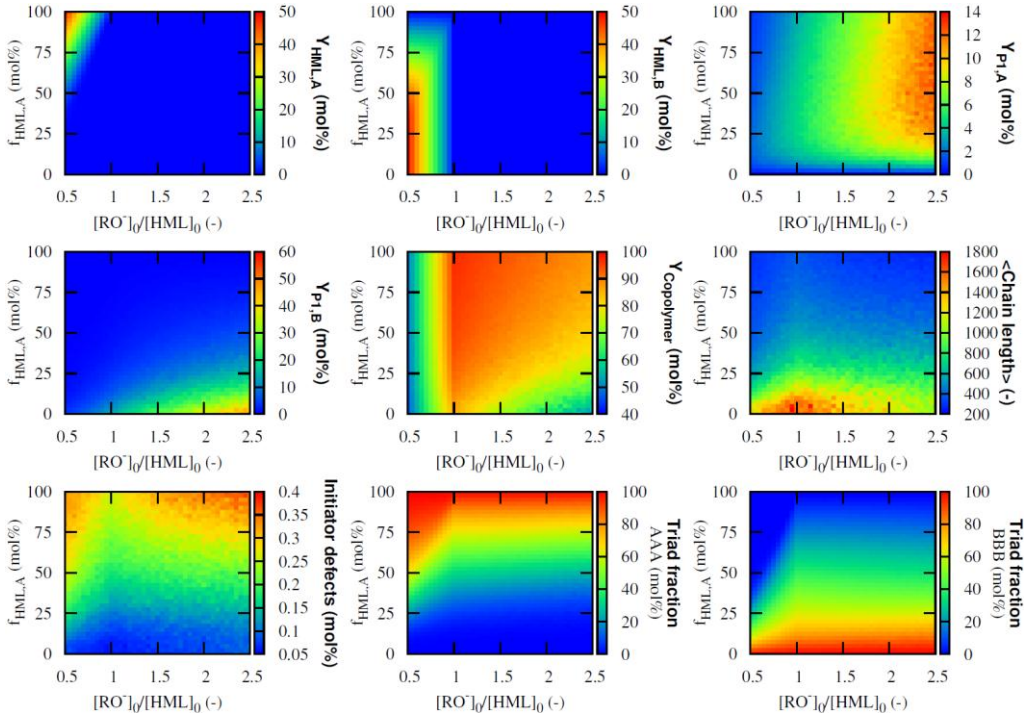

Figure J51: Effect of the base and the initial premonomer composition on the yields and properties for the copolymerization of 7 with 3 (see Figures 3, 4 and 5 in Chapter 3); Reaction conditions: 308 K; $f_{HML,A}$ is defined as $[HML,A]_0/([HML,A]_0+[HML,B]_0)$

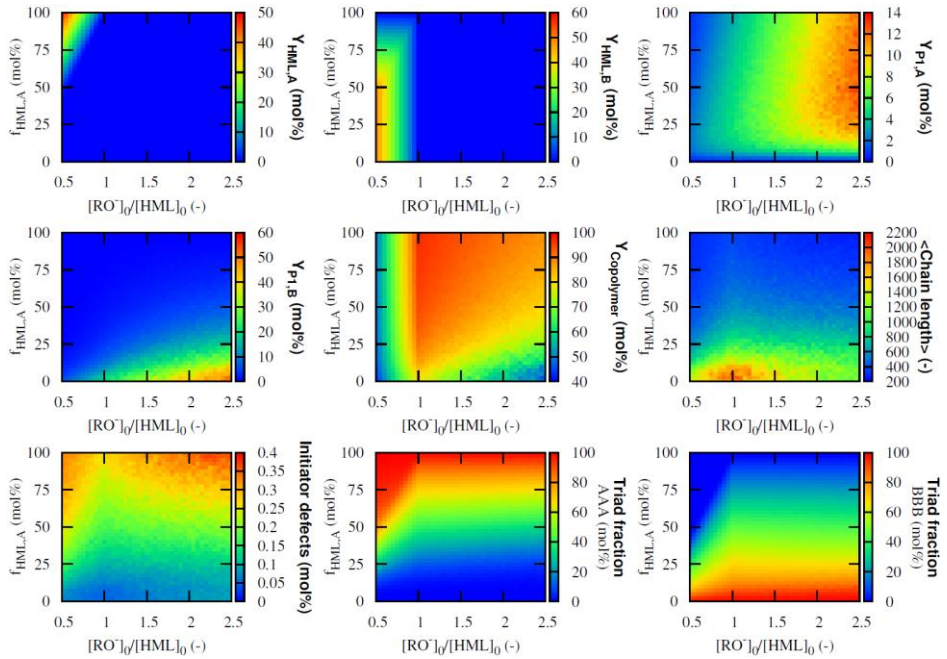

Figure J52: Effect of the base and the initial premonomer composition on the yields and properties for the copolymerization of 7 with 4 (see Figures 3, 4 and 5 in Chapter 3); Reaction conditions: 308 K; $f_{HML,A}$ is defined as $[HML,A]_0/([HML,A]_0+[HML,B]_0)$

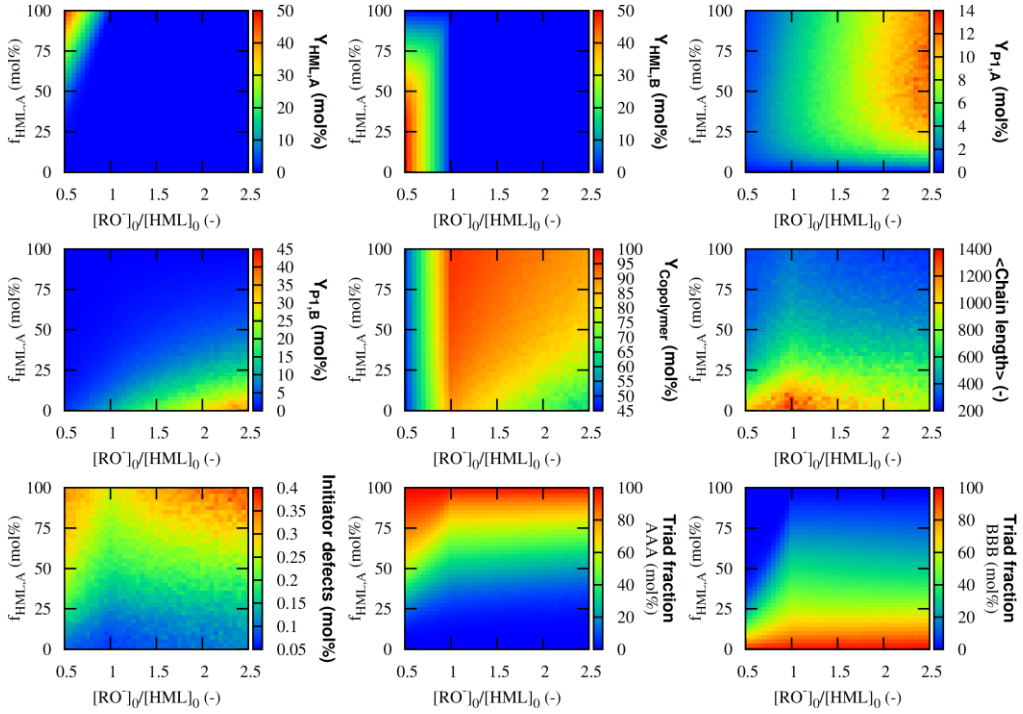

Figure J53: Effect of the base and the initial premonomer composition on the yields and properties for the copolymerization of 7 with 5 (see Figures 3, 4 and 5 in Chapter 3); Reaction conditions: 308 K; $f_{HML,A}$ is defined as $[HML,A]_0/([HML,A]_0+[HML,B]_0)$

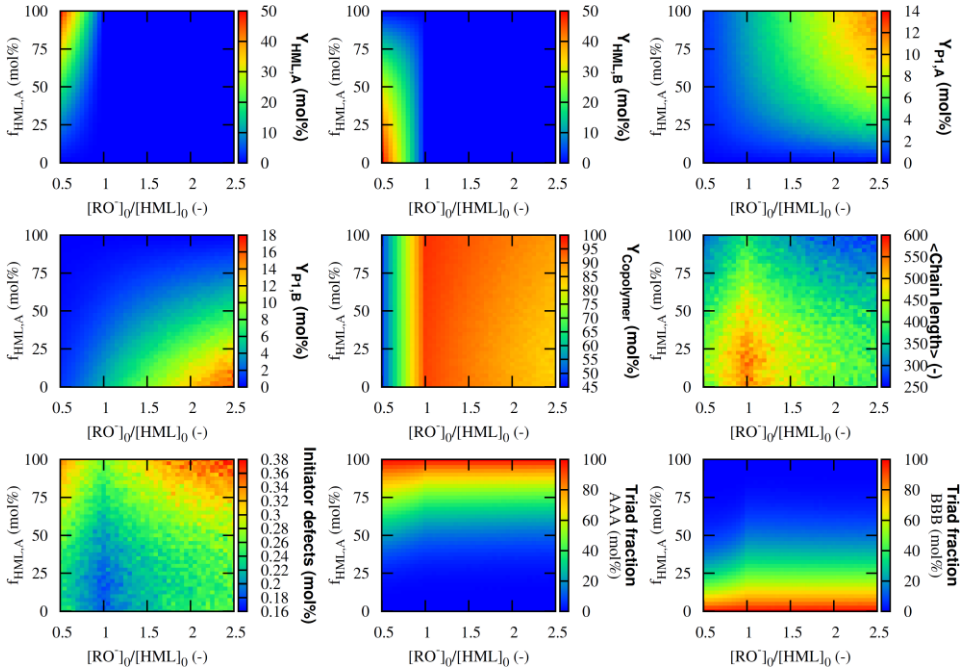

Figure J54: Effect of the base and the initial premonomer composition on the yields and properties for the copolymerization of 7 with 6 (see Figures 3, 4 and 5 in Chapter 3); Reaction conditions: 308 K; $f_{HML,A}$ is defined as $[HML,A]_0/([HML,A]_0+[HML,B]_0)$

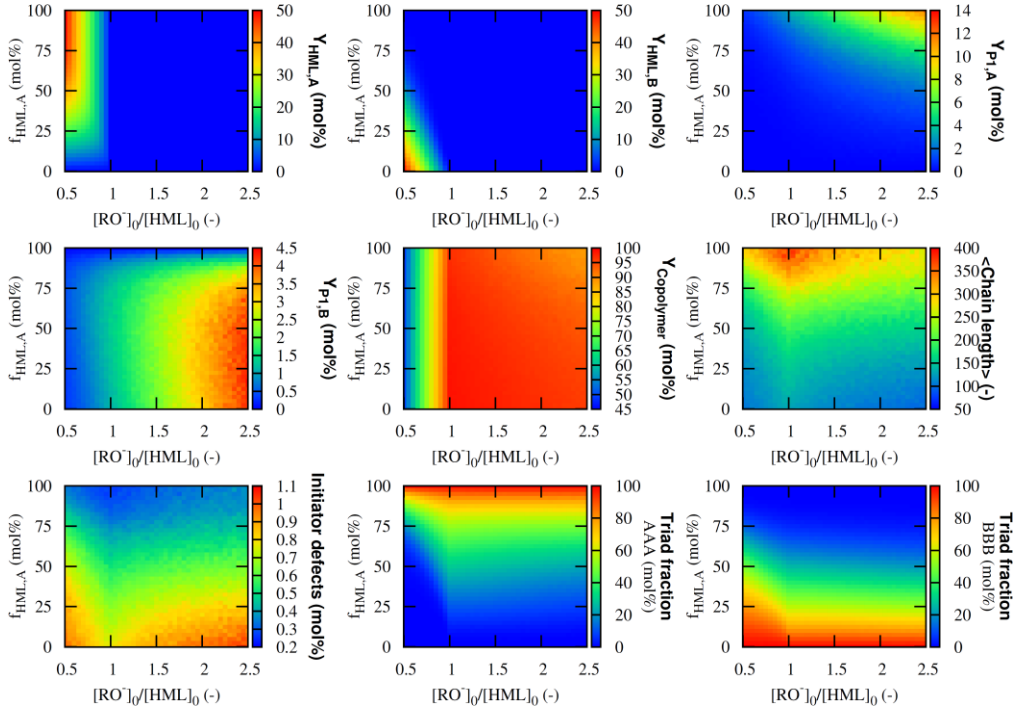

Figure J55: Effect of the base and the initial premonomer composition on the yields and properties for the copolymerization of 7 with 8 (see Figures 3, 4 and 5 in Chapter 3); Reaction conditions: 308 K; $f_{HML,A}$ is defined as $[HML,A]_0/([HML,A]_0+[HML,B]_0)$

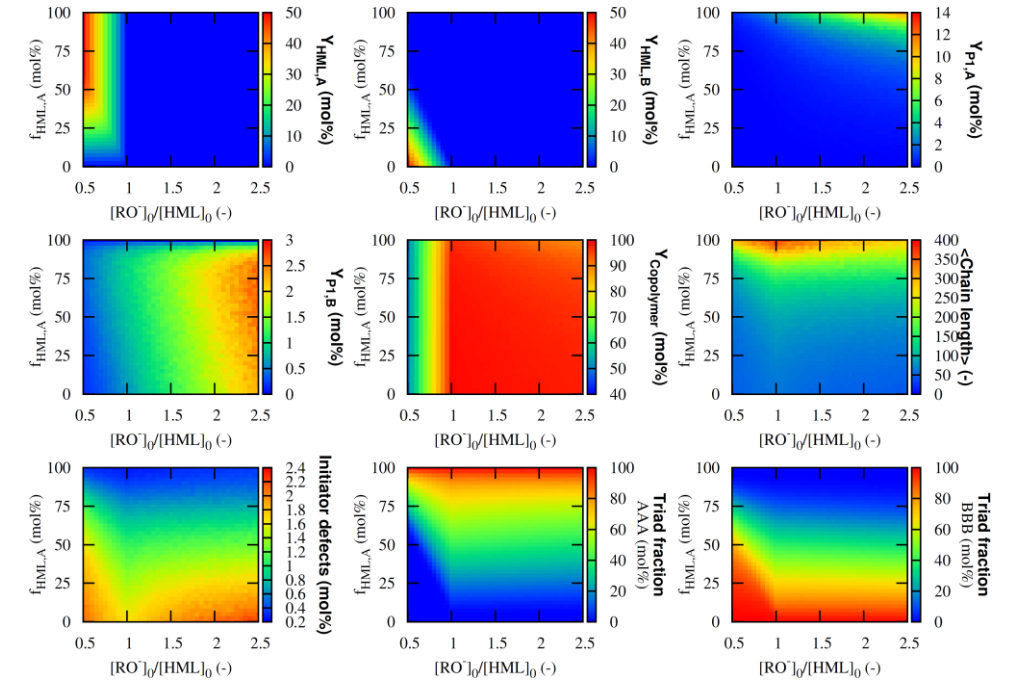

Figure J56: Effect of the base and the initial premonomer composition on the yields and properties for the copolymerization of 7 with 9 (see Figures 3, 4 and 5 in Chapter 3); Reaction conditions: 308 K; $f_{HML,A}$ is defined as $[HML,A]_0/([HML,A]_0+[HML,B]_0)$

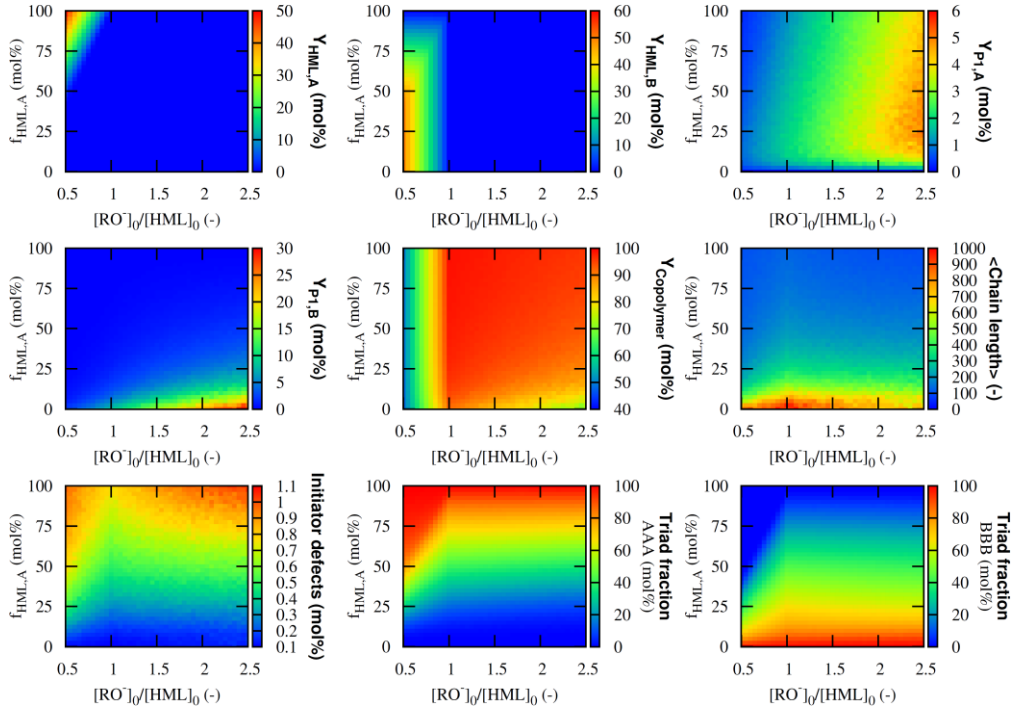

Figure J57: Effect of the base and the initial premonomer composition on the yields and properties for the copolymerization of 8 with 1 (see Figures 3, 4 and 5 in Chapter 3); Reaction conditions: 308 K; $f_{HML,A}$ is defined as $[HML,A]_0/([HML,A]_0+[HML,B]_0)$

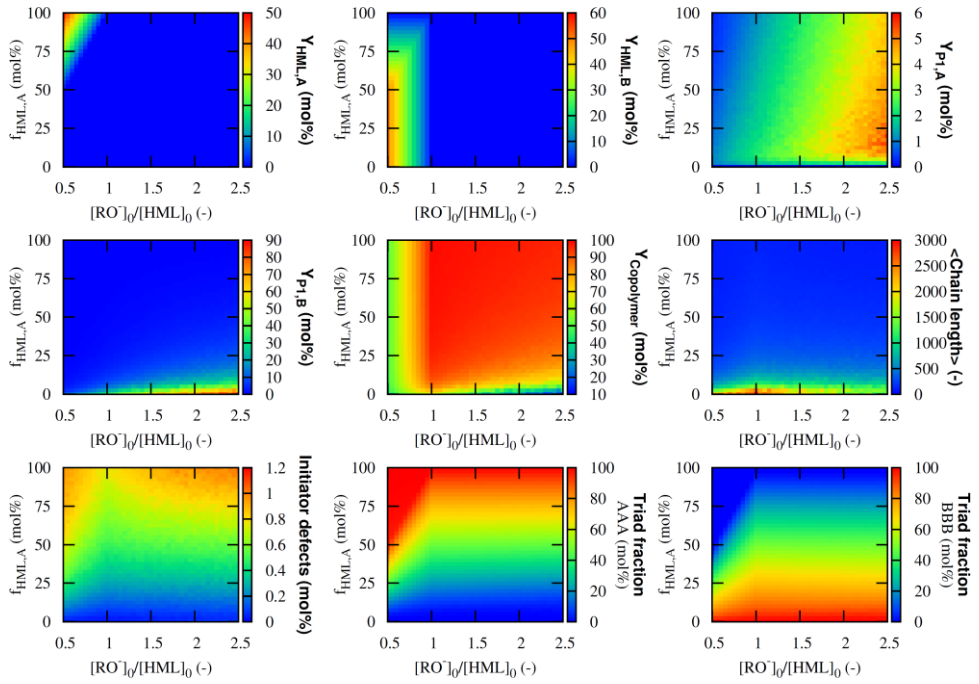

Figure J58: Effect of the base and the initial premonomer composition on the yields and properties for the copolymerization of 8 with 2 (see Figures 3, 4 and 5 in Chapter 3); Reaction conditions: 308 K; $f_{HML,A}$ is defined as $[HML,A]_0/([HML,A]_0+[HML,B]_0)$

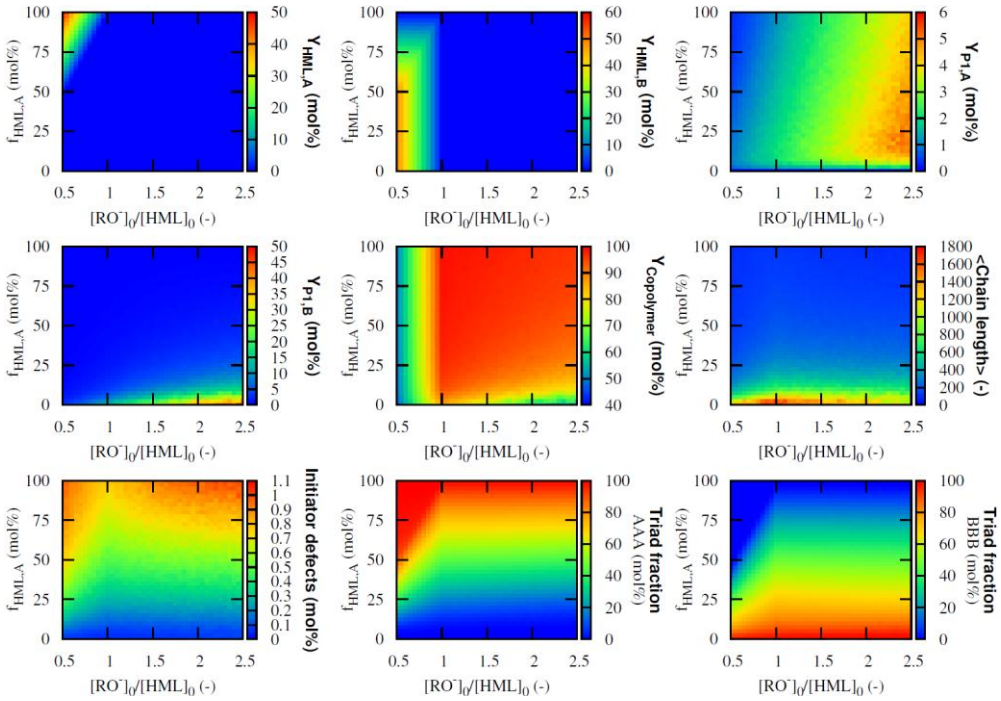

Figure J59: Effect of the base and the initial premonomer composition on the yields and properties for the copolymerization of 8 with 3 (see Figures 3, 4 and 5 in Chapter 3); Reaction conditions: 308 K; $f_{HML,A}$ is defined as $[HML,A]_0/([HML,A]_0+[HML,B]_0)$

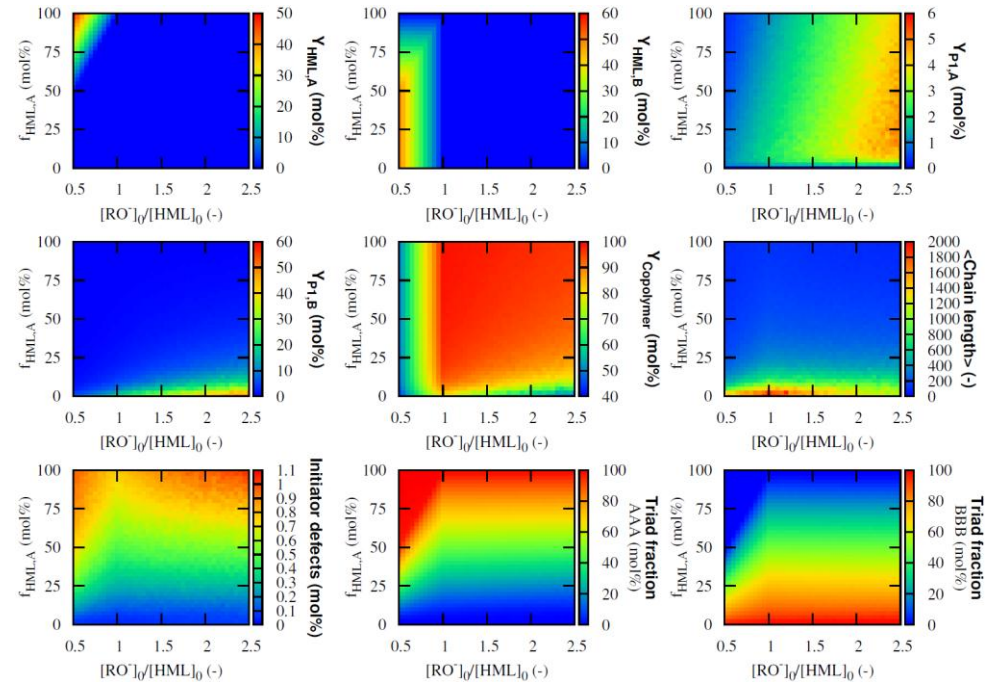

Figure J60: Effect of the base and the initial premonomer composition on the yields and properties for the copolymerization of 8 with 4 (see Figures 3, 4 and 5 in Chapter 3); Reaction conditions: 308 K; $f_{HML,A}$ is defined as $[HML,A]_0/([HML,A]_0+[HML,B]_0)$

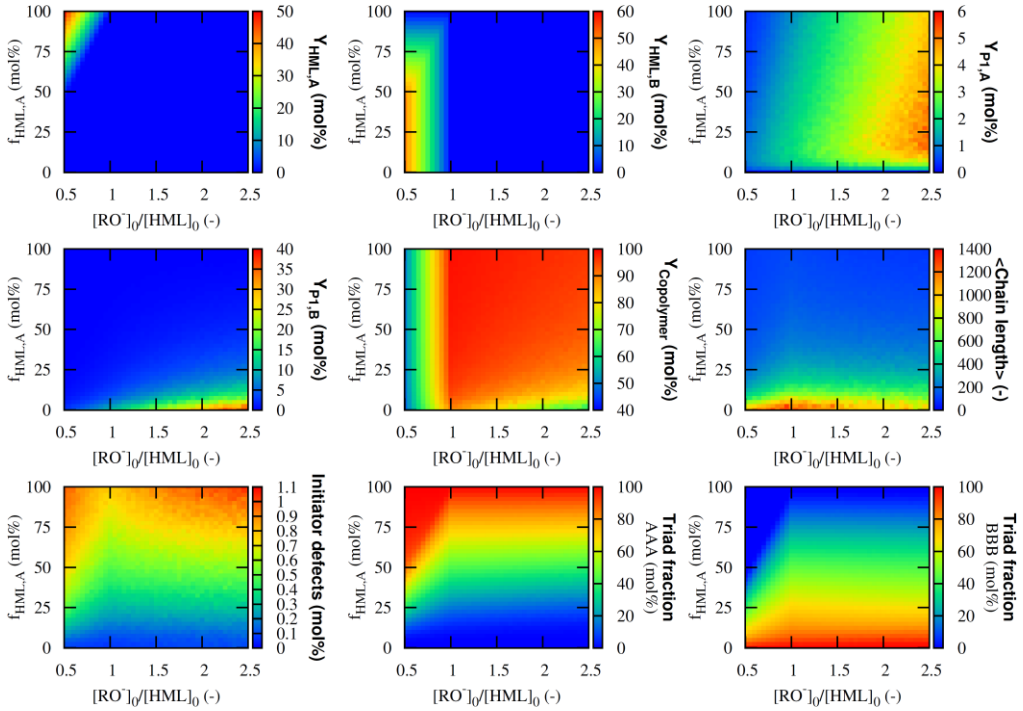

Figure J61: Effect of the base and the initial premonomer composition on the yields and properties for the copolymerization of 8 with 5 (see Figures 3, 4 and 5 in Chapter 3); Reaction conditions: 308 K; $f_{HML,A}$ is defined as $[HML,A]_0/([HML,A]_0+[HML,B]_0)$

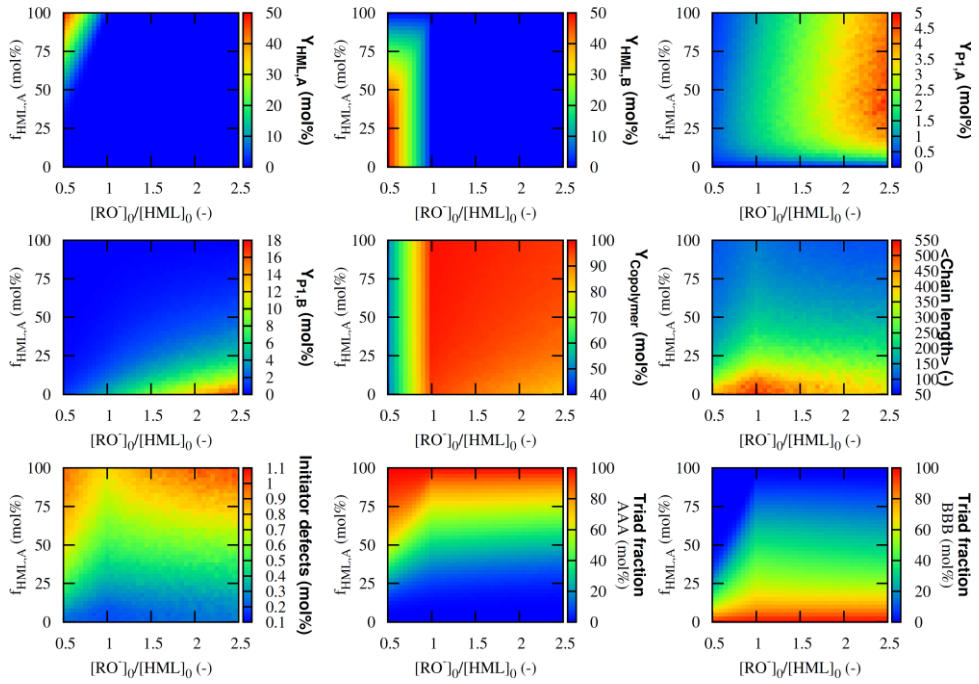

Figure J62: Effect of the base and the initial premonomer composition on the yields and properties for the copolymerization of 8 with 6 (see Figures 3, 4 and 5 in Chapter 3); Reaction conditions: 308 K; $f_{HML,A}$ is defined as $[HML,A]_0/([HML,A]_0+[HML,B]_0)$

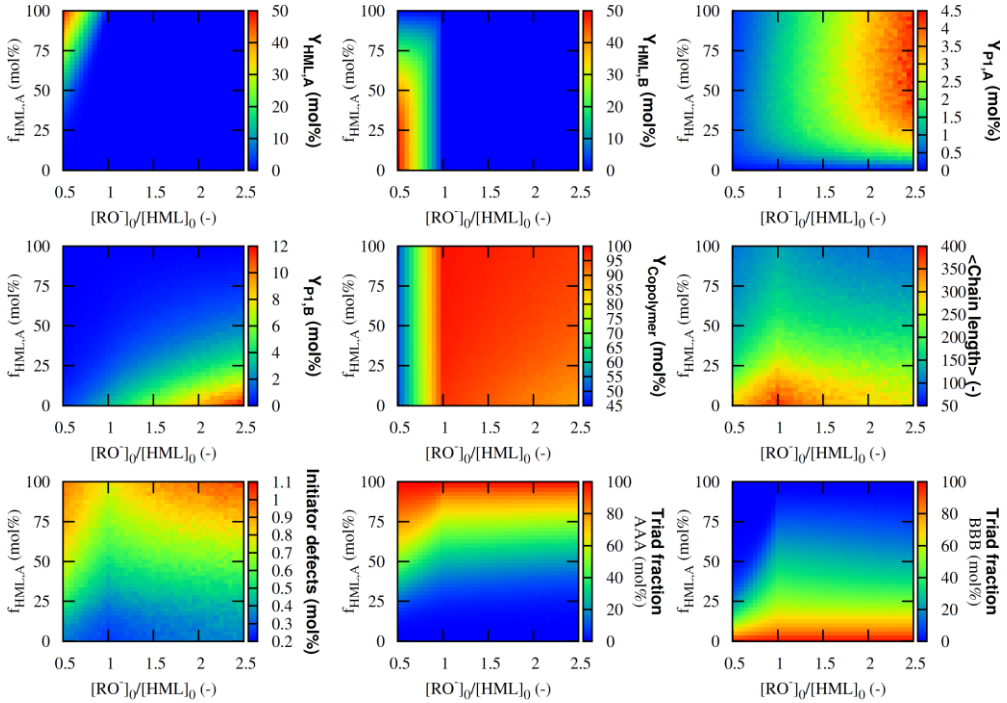

Figure J63: Effect of the base and the initial premonomer composition on the yields and properties for the copolymerization of 8 with 7 (see Figures 3, 4 and 5 in Chapter 3); Reaction conditions: 308 K; $f_{HML,A}$ is defined as $[HML,A]_0/([HML,A]_0+[HML,B]_0)$

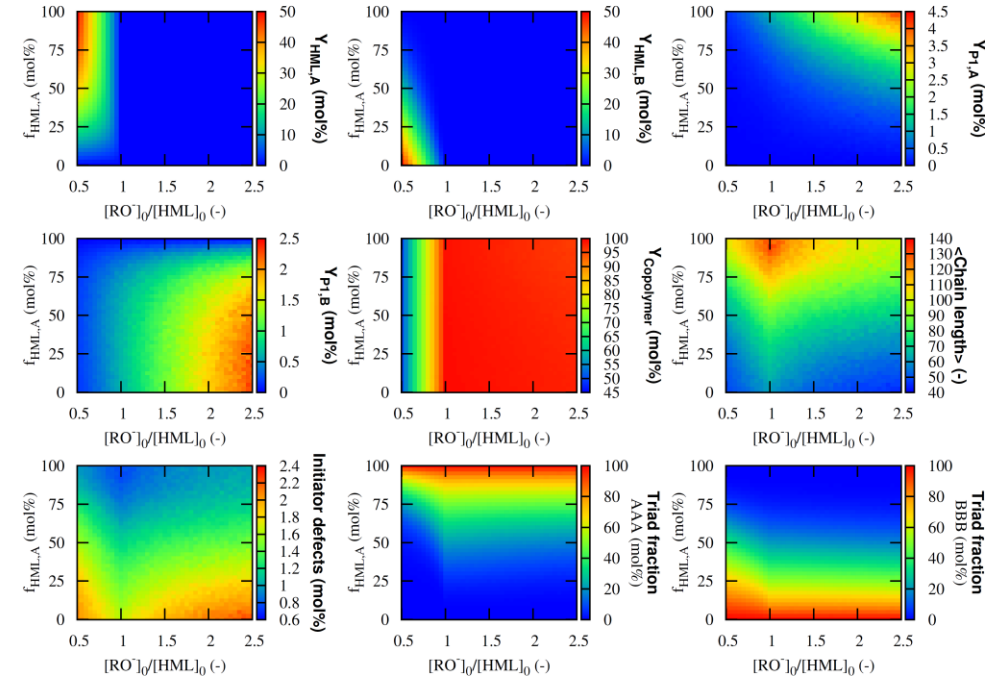

Figure J64: Effect of the base and the initial premonomer composition on the yields and properties for the copolymerization of 8 with 9 (see Figures 3, 4 and 5 in Chapter 3); Reaction conditions: 308 K; $f_{HML,A}$ is defined as $[HML,A]_0/([HML,A]_0+[HML,B]_0)$

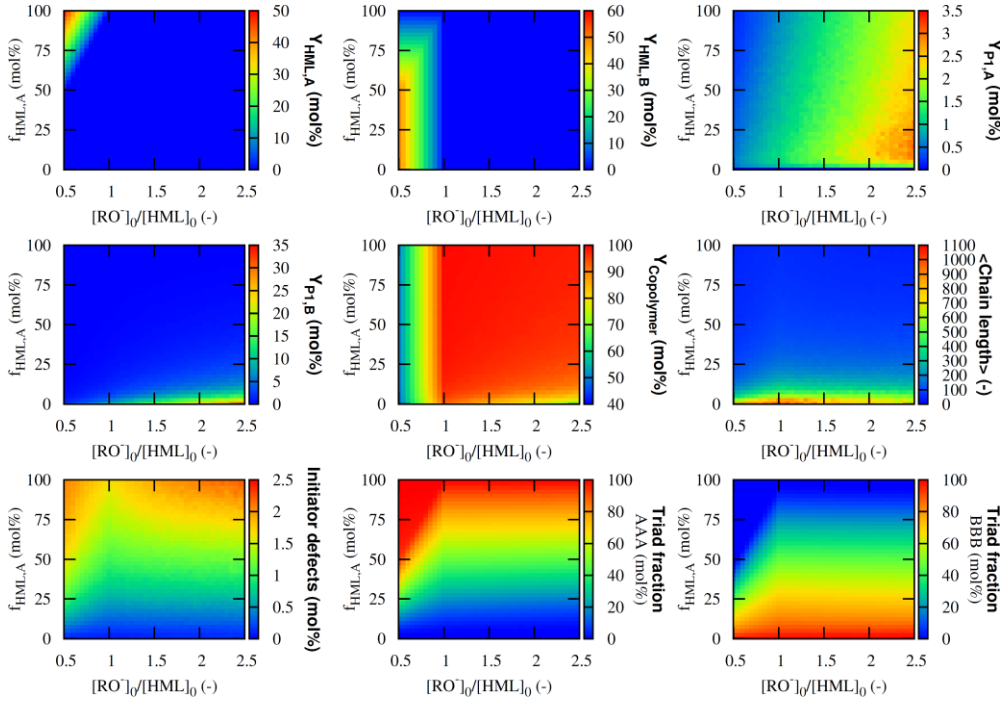

Figure J65: Effect of the base and the initial premonomer composition on the yields and properties for the copolymerization of 9 with 1 (see Figures 3, 4 and 5 in Chapter 3); Reaction conditions: 308 K; $f_{HML,A}$ is defined as $[HML,A]_0/([HML,A]_0+[HML,B]_0)$

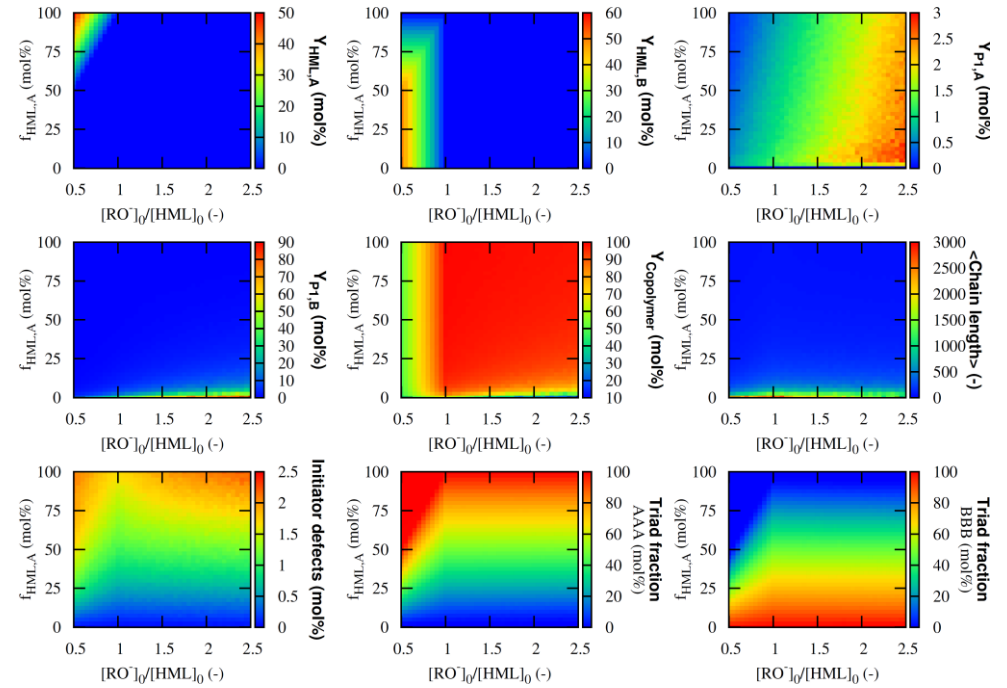

Figure J66: Effect of the base and the initial premonomer composition on the yields and properties for the copolymerization of 9 with 2 (see Figures 3, 4 and 5 in Chapter 3); Reaction conditions: 308 K; $f_{HML,A}$ is defined as $[HML,A]_0/([HML,A]_0+[HML,B]_0)$

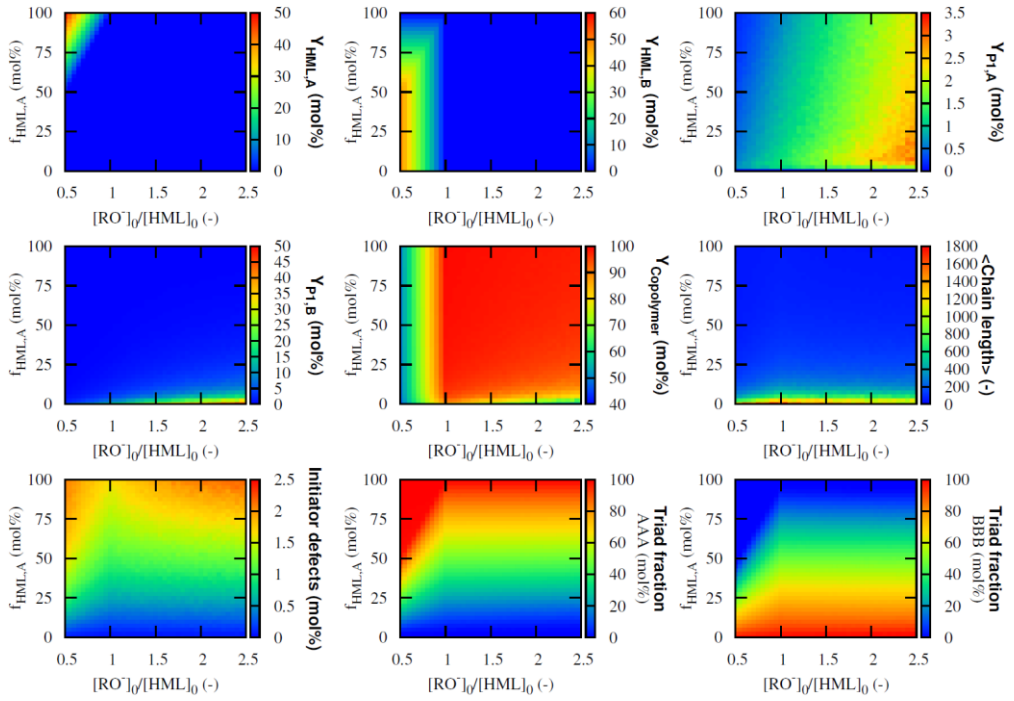

Figure J67: Effect of the base and the initial premonomer composition on the yields and properties for the copolymerization of 9 with 3 (see Figures 3, 4 and 5 in Chapter 3); Reaction conditions: 308 K; $f_{HML,A}$ is defined as $[HML,A]_0/([HML,A]_0+[HML,B]_0)$

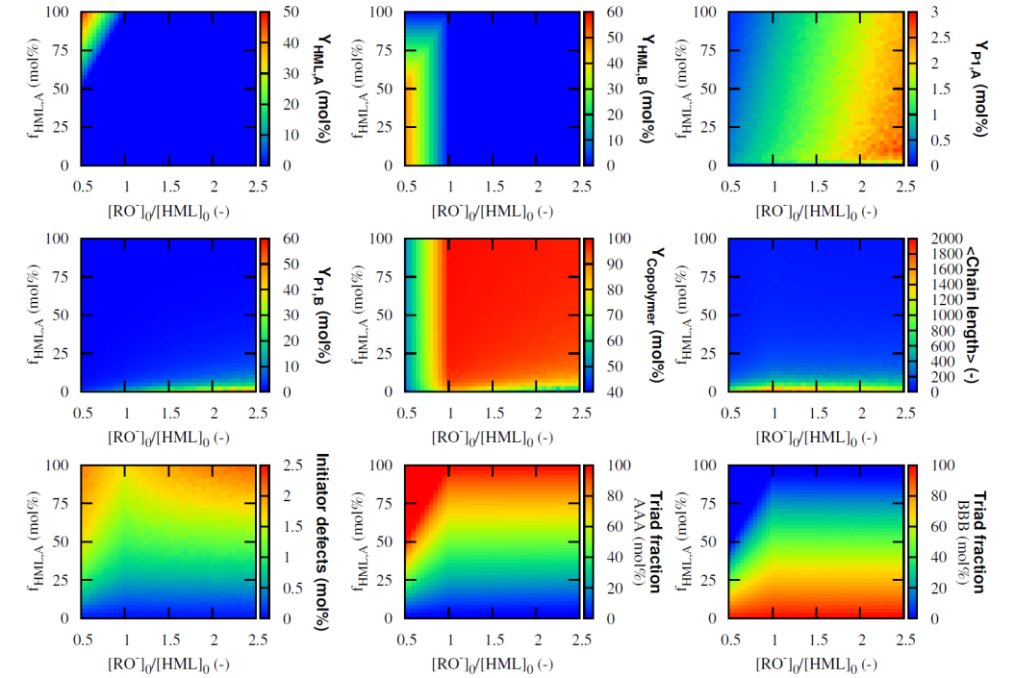

Figure J68: Effect of the base and the initial premonomer composition on the yields and properties for the copolymerization of 9 with 4 (see Figures 3, 4 and 5 in Chapter 3); Reaction conditions: 308 K; $f_{HML,A}$ is defined as $[HML,A]_0/([HML,A]_0+[HML,B]_0)$

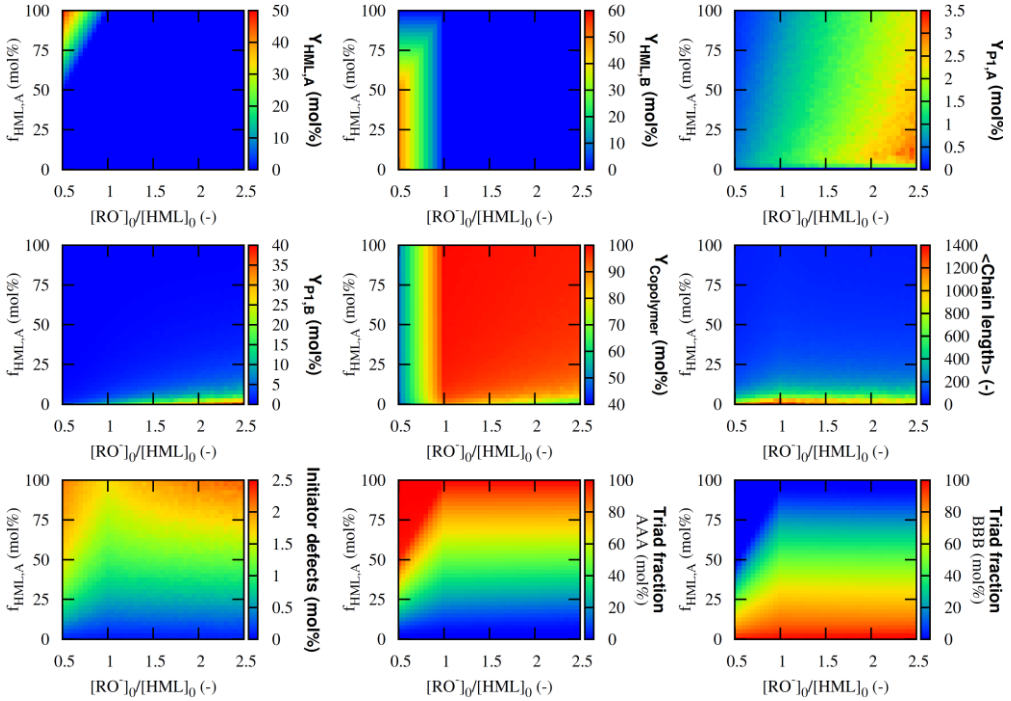

Figure J69: Effect of the base and the initial premonomer composition on the yields and properties for the copolymerization of 9 with 5 (see Figures 3, 4 and 5 in Chapter 3); Reaction conditions: 308 K; $f_{HML,A}$ is defined as $[HML,A]_0/([HML,A]_0+[HML,B]_0)$

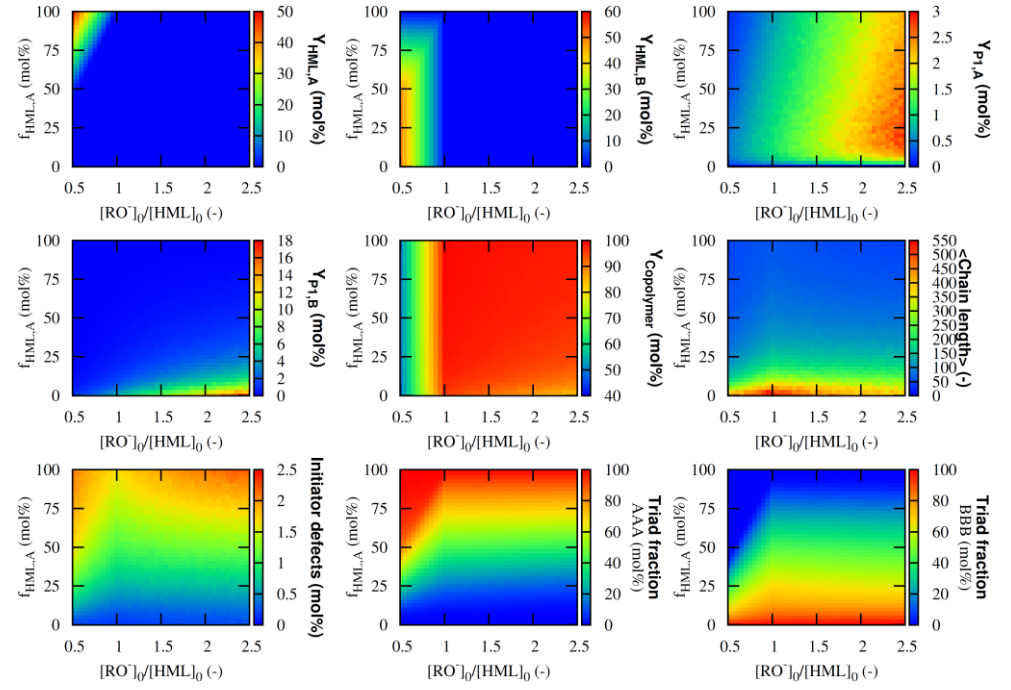

Figure J70: Effect of the base and the initial premonomer composition on the yields and properties for the copolymerization of 9 with 6 (see Figures 3, 4 and 5 in Chapter 3); Reaction conditions: 308 K; $f_{HML,A}$ is defined as $[HML,A]_0/([HML,A]_0+[HML,B]_0)$

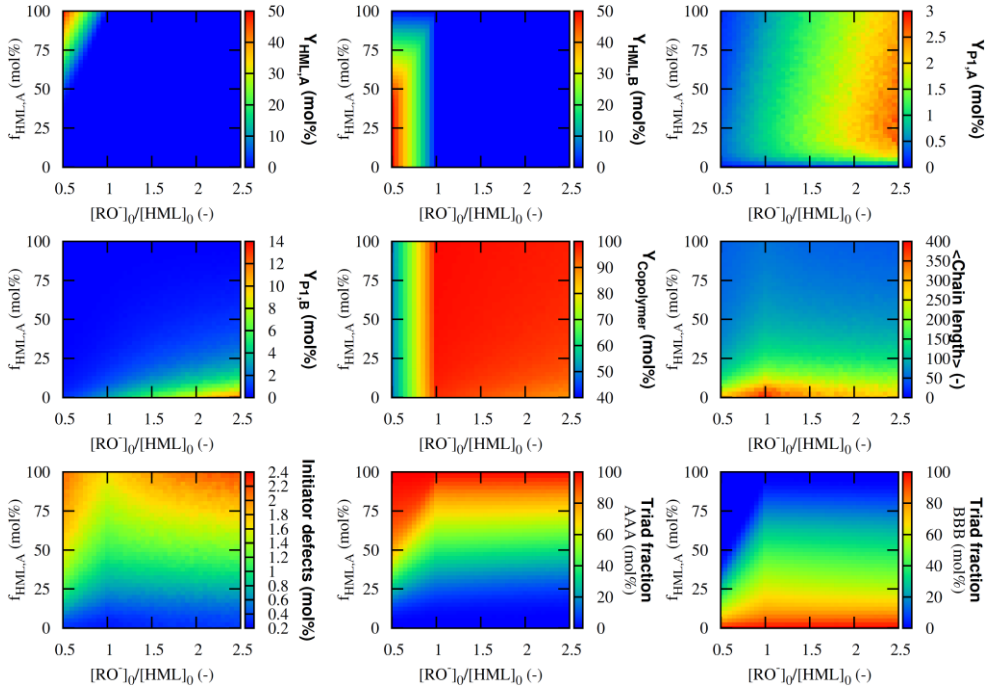

Figure J71: Effect of the base and the initial premonomer composition on the yields and properties for the copolymerization of 9 with 7 (see Figures 3, 4 and 5 in Chapter 3); Reaction conditions: 308 K; $f_{HML,A}$ is defined as $[HML,A]_0/([HML,A]_0+[HML,B]_0)$

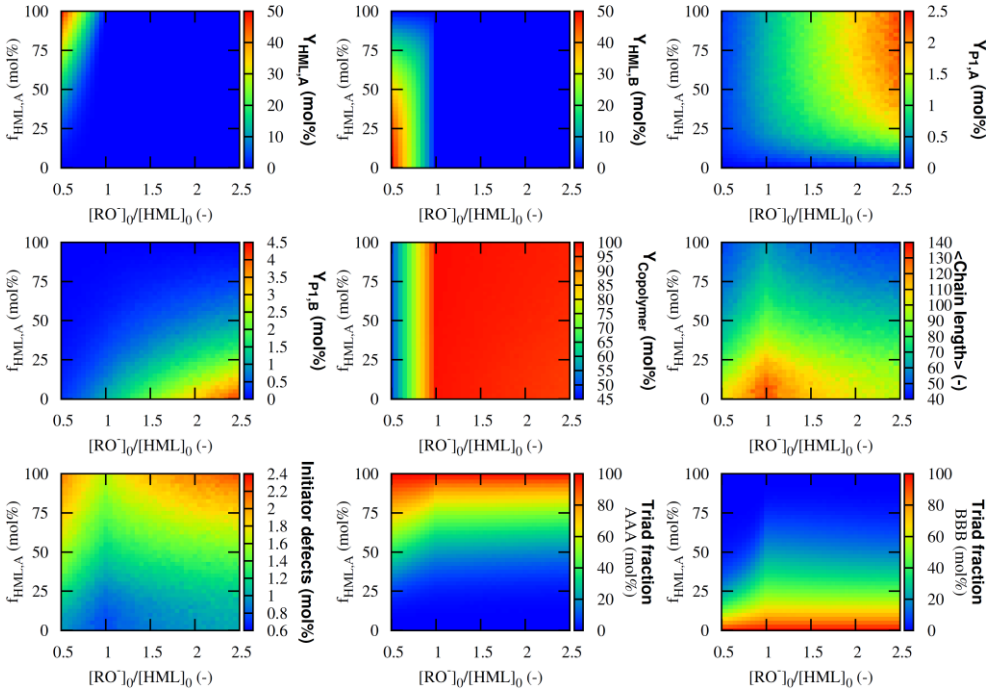

Figure J72: Effect of the base and the initial premonomer composition on the yields and properties for the copolymerization of 9 with 8 (see Figures 3, 4 and 5 in Chapter 3); Reaction conditions: 308 K; $f_{HML,A}$ is defined as $[HML,A]_0/([HML,A]_0+[HML,B]_0)$

Appendix K: Supporting maps for the effect of the Hammett substituent constant σ on the copolymerization

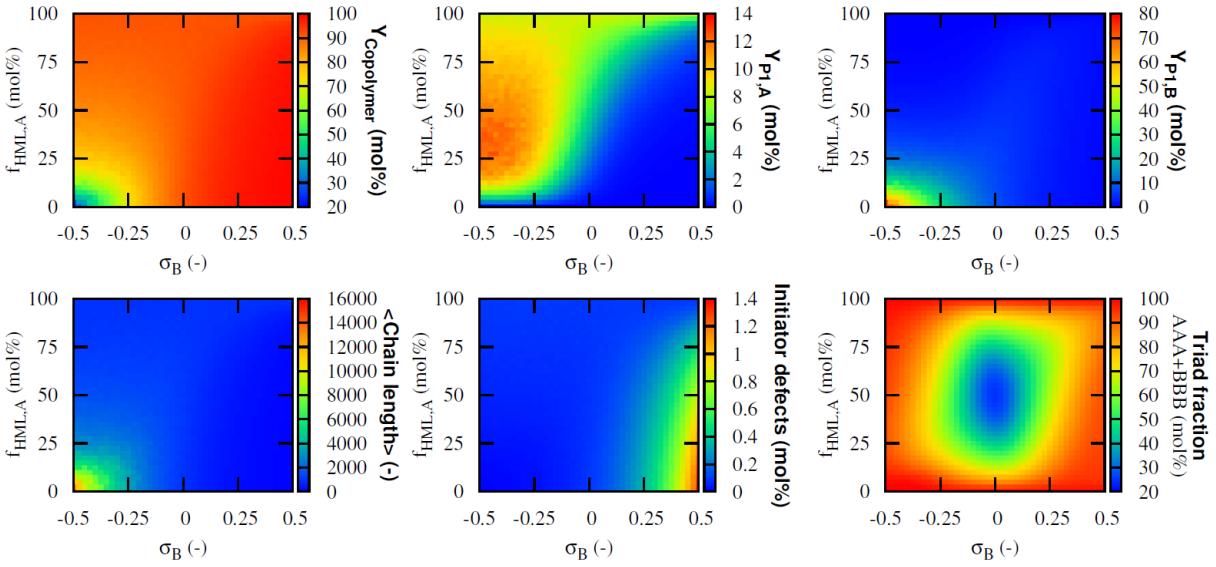

Figure K1: Effect of the Hammett substituent constant σ_B and the initial premonomer composition on the yields and properties for the copolymerization of 1 (see Figures 3, 4 and 5 in Chapter 3); Reaction conditions: $[RO^-]_0/[HML]_0$ = 1, 308 K; $f_{HML,A}$ is defined as $[HML,A]_0/([HML,A]_0+[HML,B]_0)$

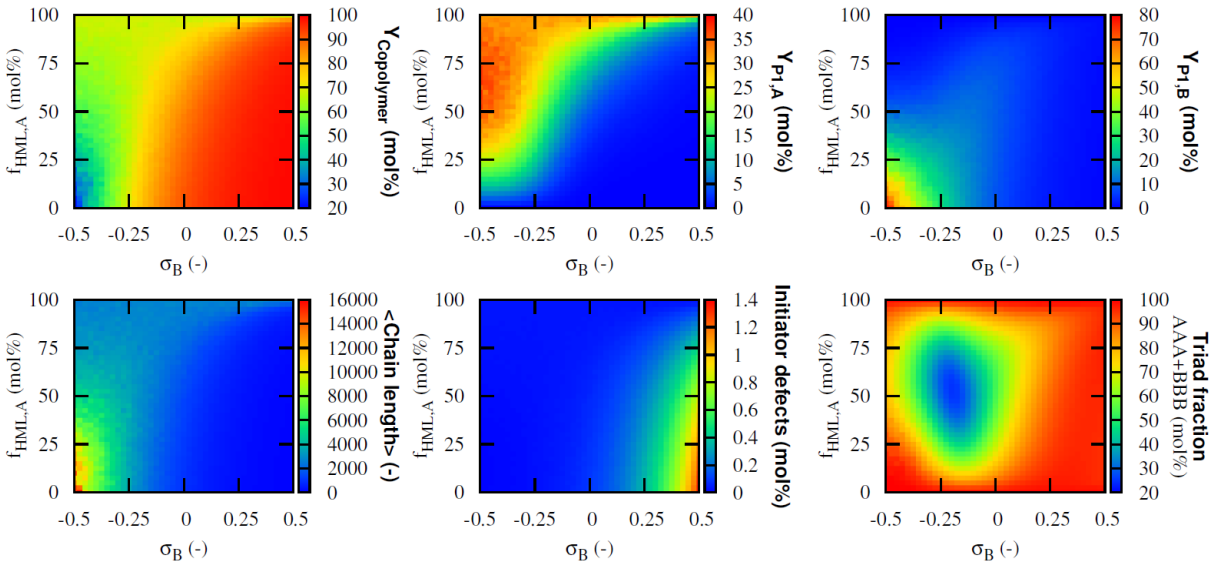

Figure K2: Effect of the Hammett substituent constant σ_B and the initial premonomer composition on the yields and properties for the copolymerization of 2 (see Figures 3, 4 and 5 in Chapter 3); Reaction conditions: $[RO^-]_0/[HML]_0$ = 1, 308 K; $f_{HML,A}$ is defined as $[HML,A]_0/([HML,A]_0+[HML,B]_0)$

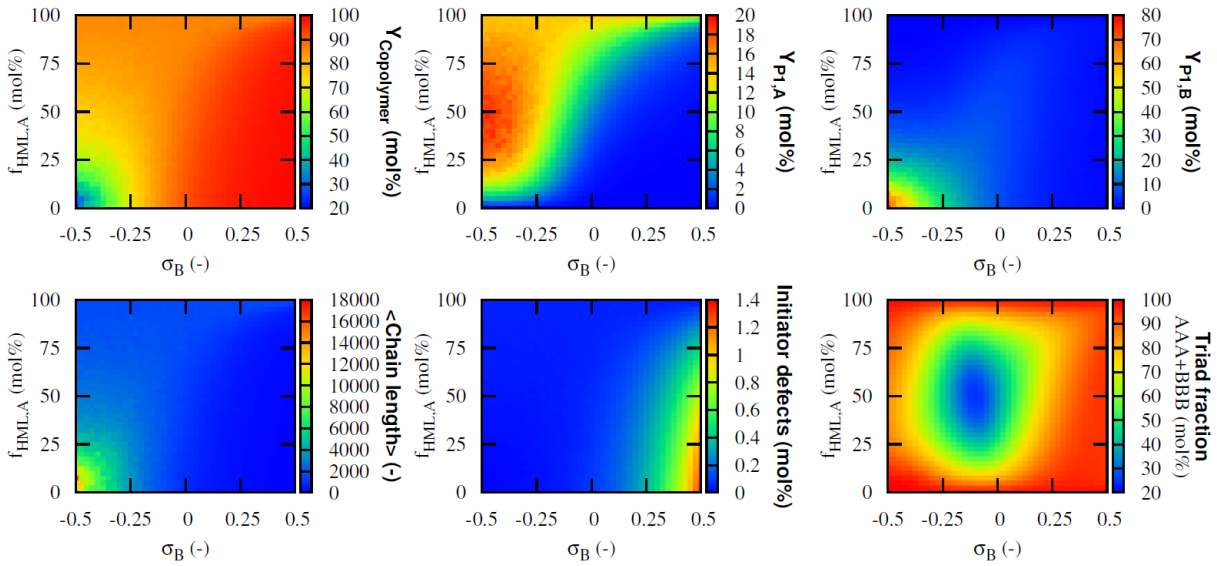

Figure K3: Effect of the Hammett substituent constant σ_B and the initial premonomer composition on the yields and properties for the copolymerization of 3 (see Figures 3, 4 and 5 in Chapter 3); Reaction conditions: $[RO^-]_0/[HML]_0$ = 1, 308 K; $f_{HML,A}$ is defined as $[HML,A]_0/([HML,A]_0+[HML,B]_0)$

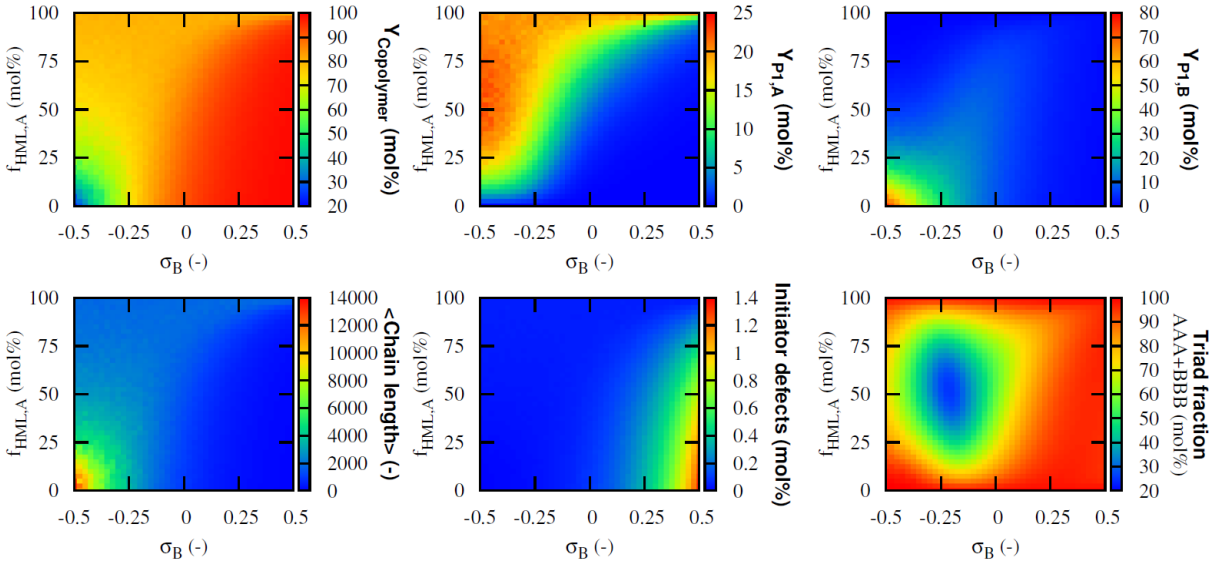

Figure K4: Effect of the Hammett substituent constant σ_B and the initial premonomer composition on the yields and properties for the copolymerization of 4 (see Figures 3, 4 and 5 in Chapter 3); Reaction conditions: $[RO^-]_0/[HML]_0$ = 1, 308 K; $f_{HML,A}$ is defined as $[HML,A]_0/([HML,A]_0+[HML,B]_0)$

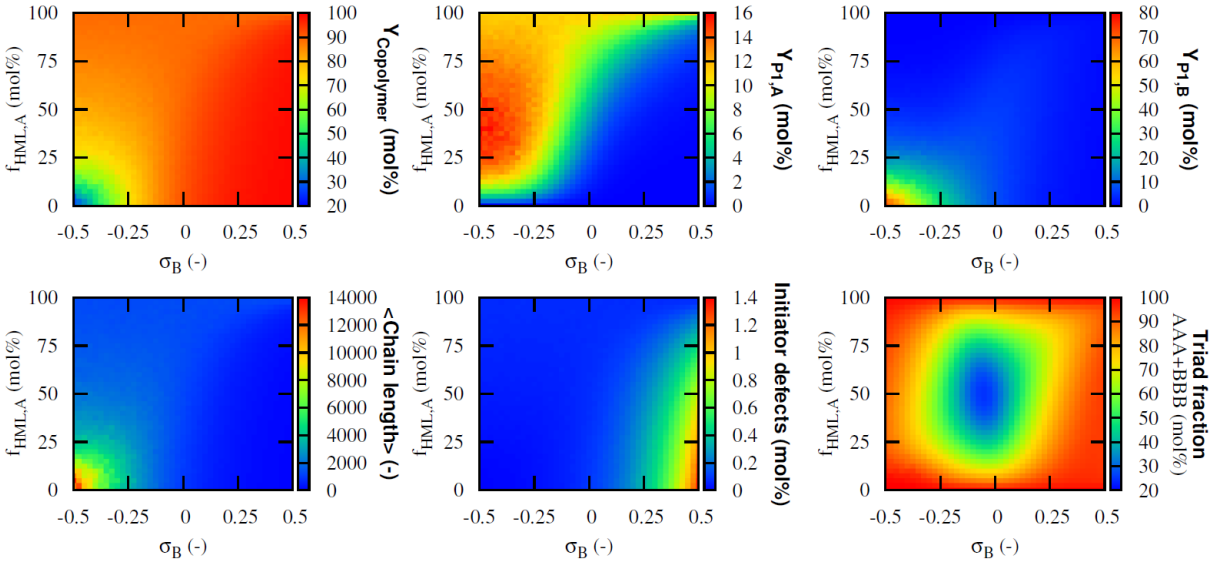

Figure K5: Effect of the Hammett substituent constant σ_B and the initial premonomer composition on the yields and properties for the copolymerization of 5 (see Figures 3, 4 and 5 in Chapter 3); Reaction conditions: $[RO^-]_0/[HML]_0$ = 1, 308 K; $f_{HML,A}$ is defined as $[HML,A]_0/([HML,A]_0+[HML,B]_0)$

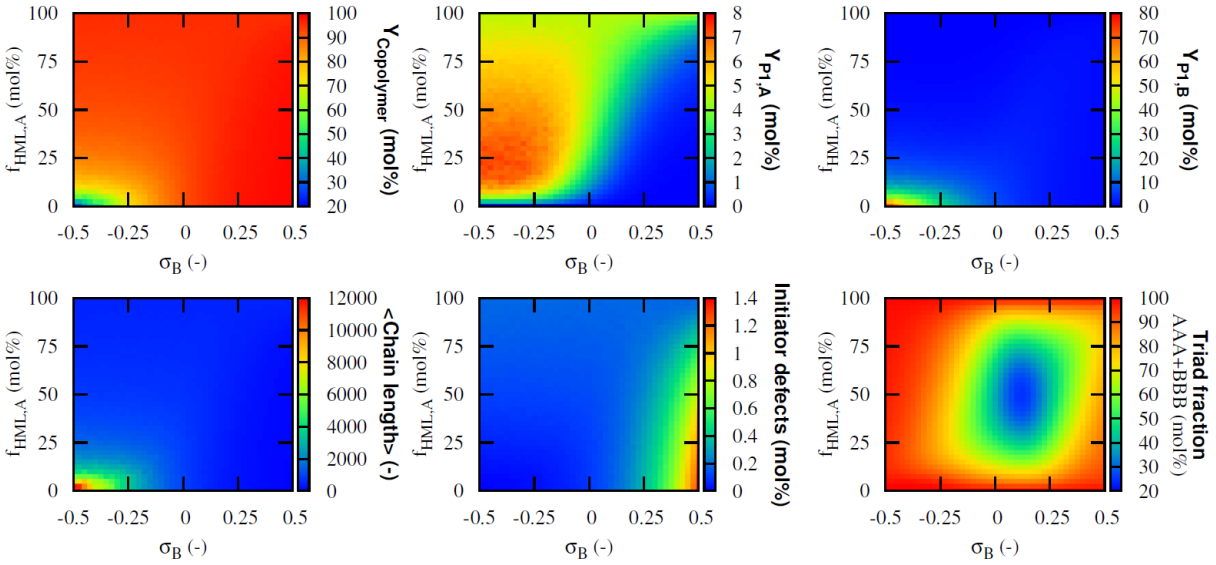

Figure K6: Effect of the Hammett substituent constant σ_B and the initial premonomer composition on the yields and properties for the copolymerization of 6 (see Figures 3, 4 and 5 in Chapter 3); Reaction conditions: $[RO^-]_0/[HML]_0$ = 1, 308 K; $f_{HML,A}$ is defined as $[HML,A]_0/([HML,A]_0+[HML,B]_0)$

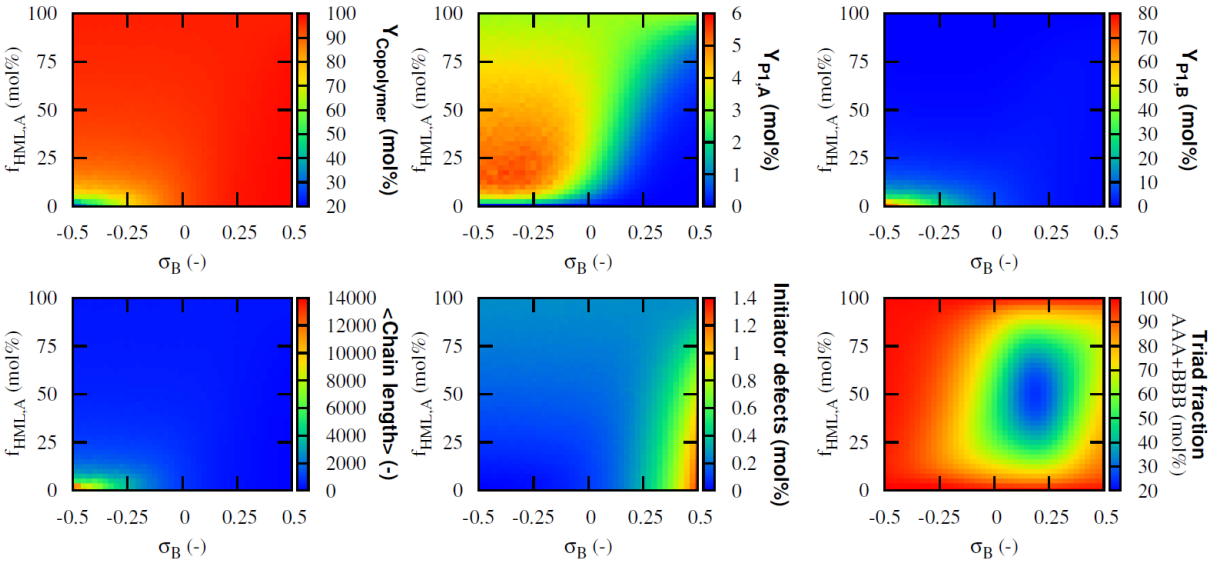

Figure K7: Effect of the Hammett substituent constant σ_B and the initial premonomer composition on the yields and properties for the copolymerization of 7 (see Figures 3, 4 and 5 in Chapter 3); Reaction conditions: $[RO^-]_0/[HML]_0$ = 1, 308 K; $f_{HML,A}$ is defined as $[HML,A]_0/([HML,A]_0+[HML,B]_0)$

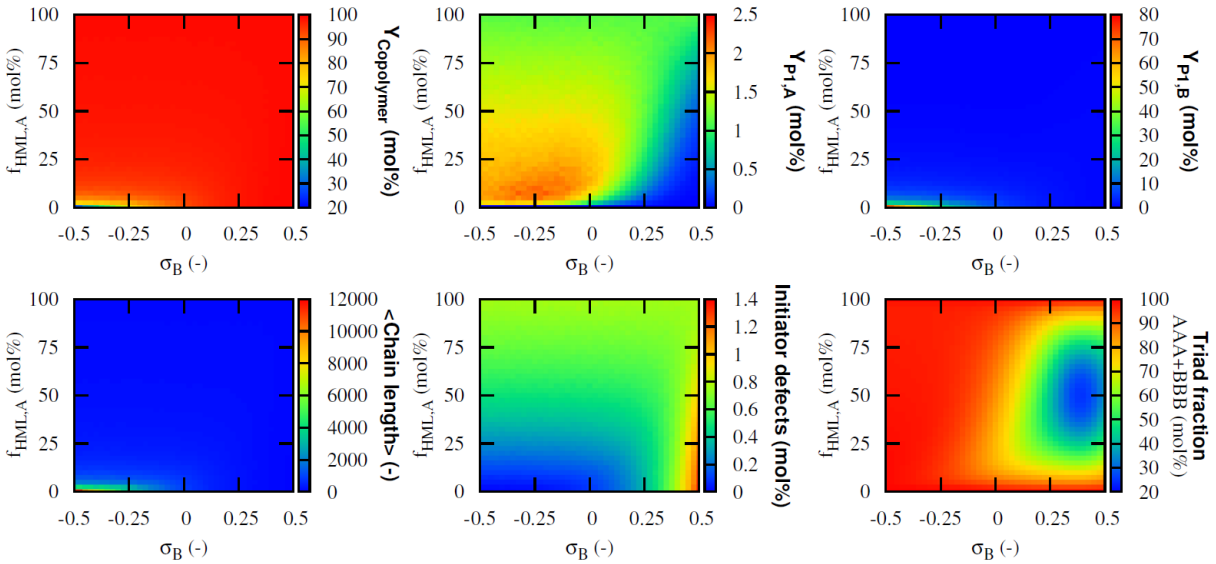

Figure K8: Effect of the Hammett substituent constant σ_B and the initial premonomer composition on the yields and properties for the copolymerization of 8 (see Figures 3, 4 and 5 in Chapter 3); Reaction conditions: $[RO^-]_0/[HML]_0$ = 1, 308 K; $f_{HML,A}$ is defined as $[HML,A]_0/([HML,A]_0+[HML,B]_0)$

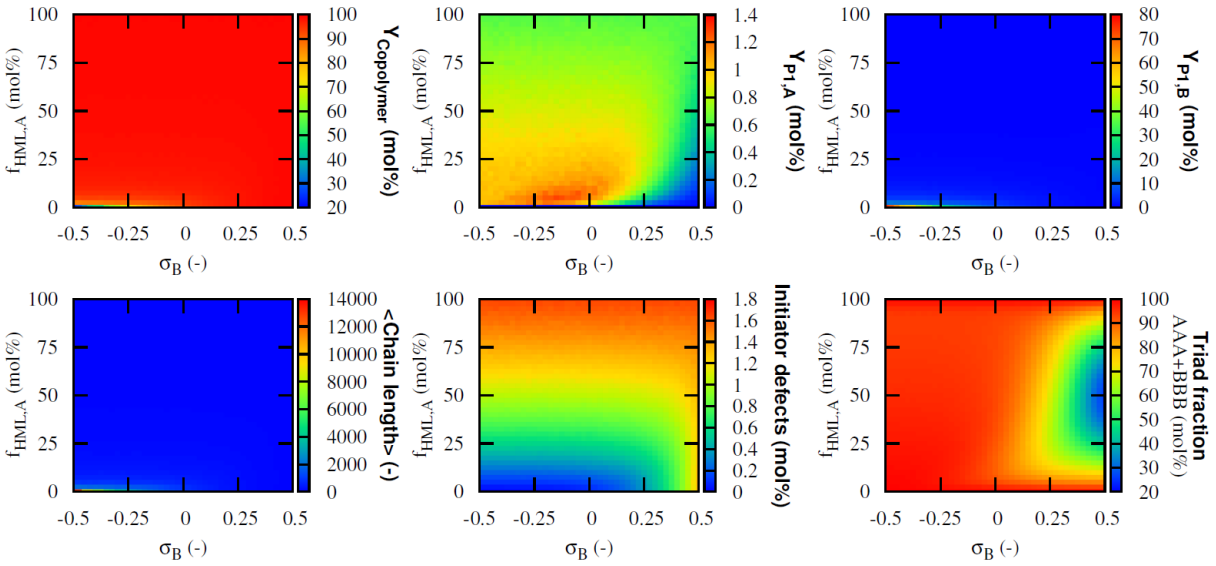

Figure K9: Effect of the Hammett substituent constant σ_B and the initial premonomer composition on the yields and properties for the copolymerization of 9 (see Figures 3, 4 and 5 in Chapter 3); Reaction conditions: $[RO^-]_0/[HML]_0$ = 1, 308 K; $f_{HML,A}$ is defined as $[HML,A]_0/([HML,A]_0+[HML,B]_0)$

Appendix L: Triads for the copolymerization of identically substituted premonomers

Figure L1 shows the triads for the copolymerization using DTC-MO and DTC-ODMO as comonomers after final elimination. It should be noted that for the precursor copolymer 8 triads can be distinguished. However, the total AAA+BBB triad fractions remains the same for both types of copolymers. In particular, in case a random copolymer is obtained, both for the precursor polymer and the conjugated polymer obtained after final elimination this fraction equals 25%. Moreover, due to symmetry the center two triads in Figure L1 each contribute for 25%, whereas the top and bottom two only contribute each for 12.5%. Hence, the fraction of the AAA+BBB triads is 25%, as is also the case for regiorandom MDMO-PPV.

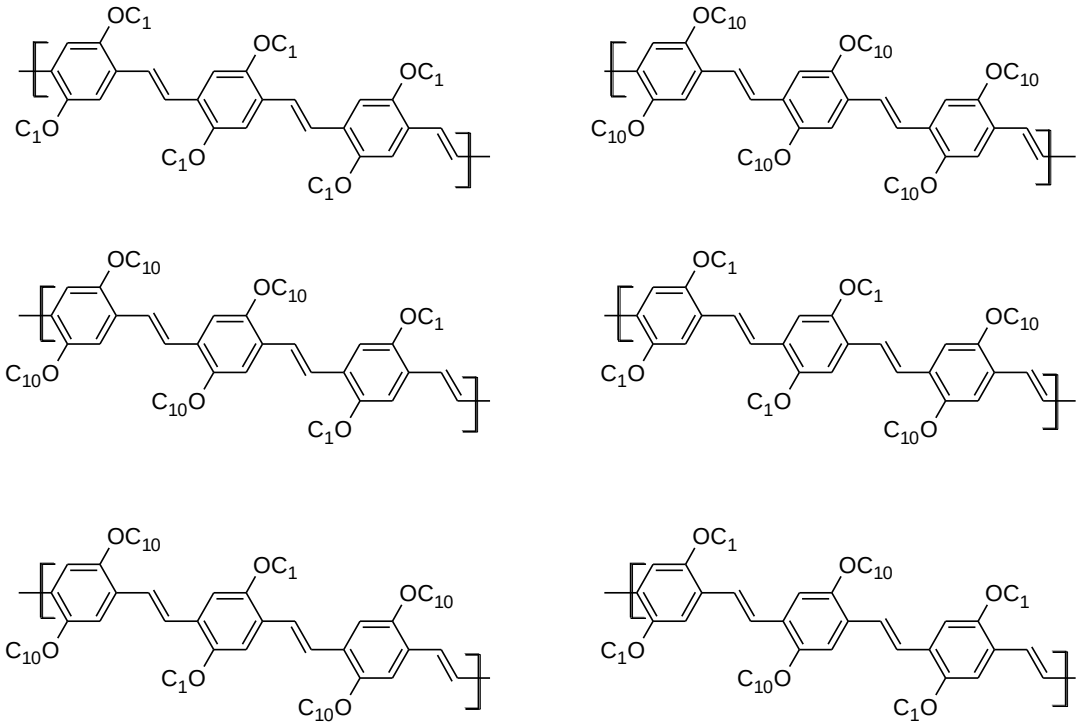

Figure L1: Triads for copolymerization using DTC-MO and DTC-ODMO (see Figure 4 in Chapter 4) after final elimination

Appendix M: Bivariate description

The first extension of the reported kMC model is the calculation of the CC-CLD (CC: chemical composition), i.e. the number fraction of polymer chains having a given chain length and given number of monomer A/B units. Such distributions were used to study FRP copolymerization and living polymerization.[1] In this work, the approach of Chaffey-Millar et al.,[2] which was used for the basic kMC algorithm,[3] is extended to obtain the bivariate distribution. For every chain length in the tree data structure reported by Chaffey-Millar et al.,[2] a sub-tree data structure is defined to locate and update the second variable (either composition or amount of cross-propagations) with logarithmic complexity.

Although both the bivariate and the individual tracking extension can be run in parallel in one simulation, they are sharing the same initial number of monomers. This implies that a small sample for visualization of the gradient, may be insufficient for the calculation of the CLD. Hence, the CLD and its average properties, and the CC-CLD, are calculated from the bivariate solver with a large initial amount of monomer molecules. In a subsequent small but representative sample simulation, typically 1000 polymer chains are simulated for (gradient) visualization.

References

1. Szymanski, R. *E-polymers* **2009**, 044.
2. Chaffey-Millar, H.; Stewart D.; Chakravarty, M. M. T; Keller, G.; Barner-Kowollik, C. *Macromol. Theor. Simul.* **2007**, 16, 6, 575-592.
3. Van Steenberge, P.; Vandenbergh, J.; D'hooge, D. R.; Reyniers, M.-F.; Adriaensens, P. J.; Lutsen, L.; Vanderzande, D. J. M.; Marin, G. B. *Macromolecules* **2011**, 44, 8716-8726.

Appendix N: Time evolution of matrix 'ReactionEventHistory'

Initially, the matrix elements of 'ReactionEventHistory' are equal to 0, i.e., the absence of monomer or any reaction event. When the k-th initiator radical R_0 propagates, ReactionEventHistory' (k,1) is altered to either 1 or 2 depending on the monomer selected (A = 1 and B = 2; e.g. the reaction event shown in Scheme N1 at t = t_1). Instead, in case propagation with a macroradical is selected as the next reaction step, the number k of the reacting macromolecule is determined using a search algorithm of linear complexity based on the work of Gillespie.[1] The chain length of the selected macromolecule k can easily be determined from the matrix 'ReactionEventHistory' because ReactionEventHistory(k,l+1) is 0 before executing the propagation event. In a final step, ReactionEventHistory(k,l+1) becomes 1 or 2 depending on whether A or B is incorporated (e.g. reaction event shown in Scheme N1 at t = t_2). Similarly, upon deactivation/activation a value of 3/4 is assigned without transfer of the entire chain composition to a different container (e.g. reaction event shown in Scheme N1 at t = t_3). On the other hand, for termination reactions the values 5 and 6 are used depending on the termination mode being recombination or disproportionation.

It should be mentioned that less memory is needed if only the last deactivation reaction event is stored, i.e. along the simulation the label 3 is removed upon activation. This has been implemented as a user option, in such way ATRPs can be simulated for higher targeted chain lengths (TCLs).

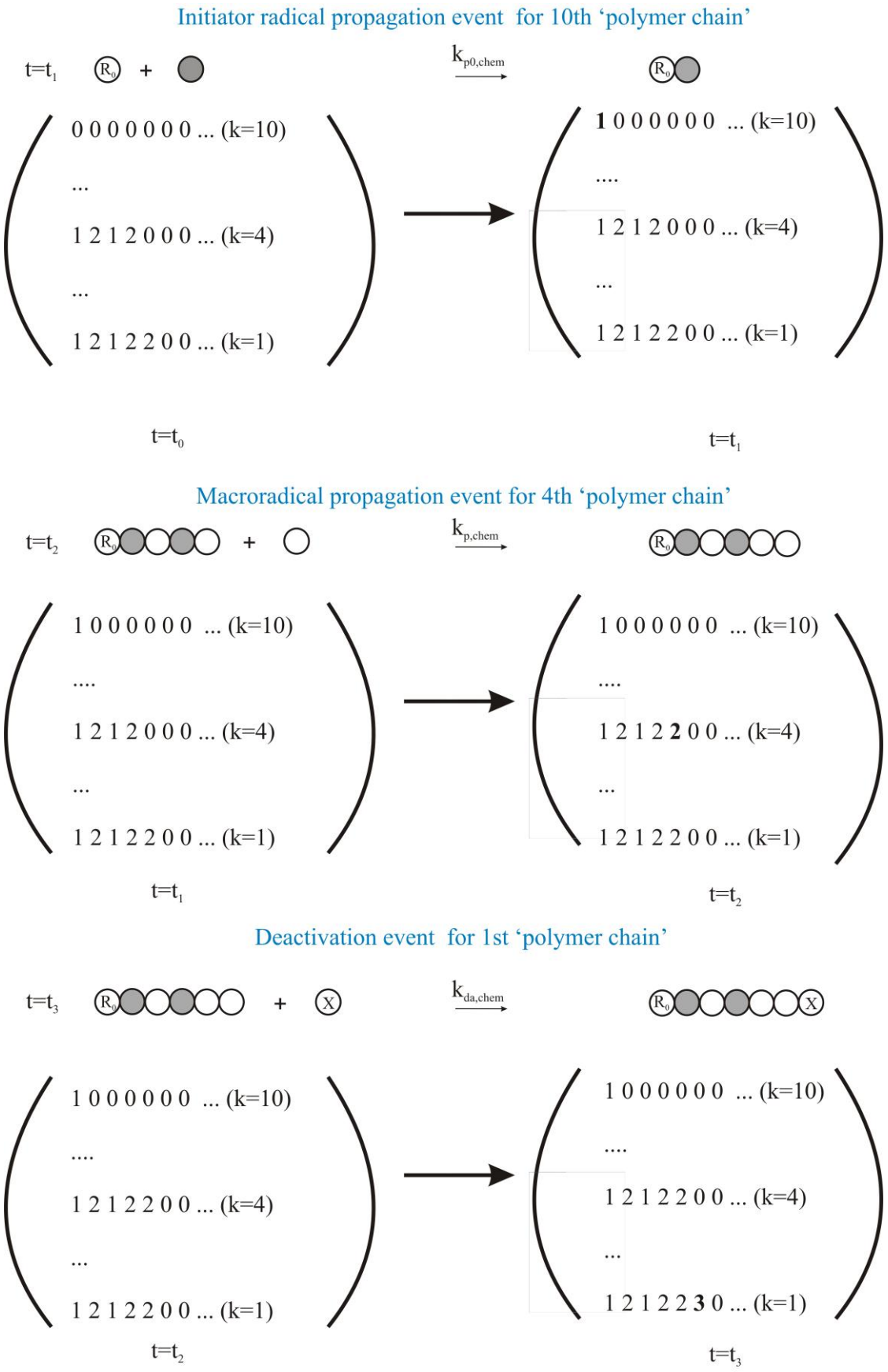

Scheme N1: Principle of individual tracking of macromolecules

When a termination event takes place, the terminated chains in ‘ReactionEventHistory’ are copied to a separate container ‘DeadPolymer’ to allow an easy separation of dead and dormant polymer chains. For the recombination products specific treatment is however necessary. The first macroradical recombining is copied to the first empty row of ‘DeadPolymer’, while the second terminating macroradical is transferred to the same row but mirrored, taking into account that the two recombination event labels have to be in the middle of the dead polymer chain.

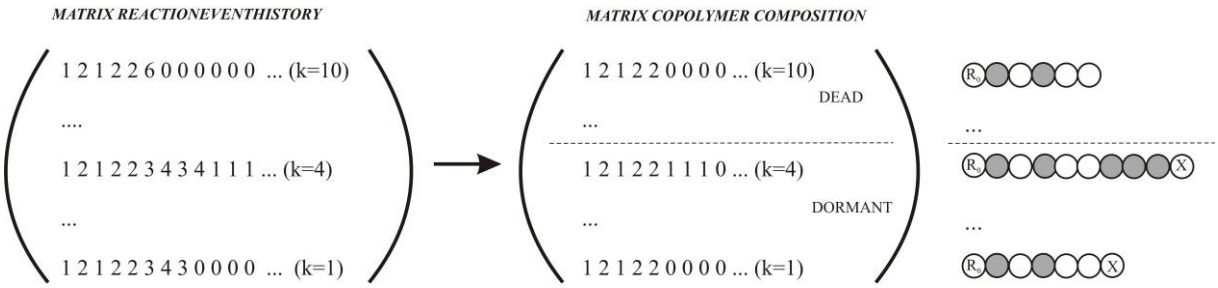

Scheme N2: Principle of the calculation of the copolymer composition

The copolymer composition of all chains is subsequently obtained by copying ‘DeadPolymer’ in the upper part of a third matrix ‘CopolymerComposition’ and copying the dormant polymer molecules from ‘ReactionEventHistory’ in the lower part after removing the excessive event labels (3-6). Such approach allows a visualization of the dead and dormant polymer chains (Scheme N2). At the same time the chain length of each polymer chain is obtained by counting the total number of monomer units per chain.

References

1. Gillespie, D. T. *J. Phys. Chem.* **1977**, 81, 25, 2340-2361.

Appendix O: Necessity of the calculation of the minimum of $GD_{B\ to\ A}$, $GD_{A\ to\ B}$, $GD'_{B\ to\ A}$ and $GD'_{A\ to\ B}$ per chain

For every polymer chain k in 'CopolymerComposition', four normalized linear gradient deviation values ($GD_{B\ to\ A}$, $GD_{A\ to\ B}$, $GD'_{B\ to\ A}$ and $GD'_{A\ to\ B}$) have to be calculated:

$$GD_{B\,to\,A}(k) = \sum_{l=1}^{i} \frac{1}{2} \frac{\left|S_A(k,l) - S_{A,ideal,B\,to\,A}(k,l)\right| + \left|S_B(k,l) - S_{B,ideal,B\,to\,A}(k,l)\right|}{i^2} \quad \text{(O1)}$$

$$GD_{A\,to\,B}(k) = \sum_{l=1}^{i} \frac{1}{2} \frac{\left|S_A(k,l) - S_{A,ideal,A\,to\,B}(k,l)\right| + \left|S_B(k,l) - S_{B,ideal,A\,to\,B}(k,l)\right|}{i^2} \quad \text{(O2)}$$

$$GD'_{B\,to\,A}(k) = \sum_{l=1}^{i} \frac{1}{2} \frac{\left|S'_A(k,l) - S'_{A,ideal,B\,to\,A}(k,l)\right| + \left|S'_B(k,l) - S'_{B,ideal,B\,to\,A}(k,l)\right|}{i^2} \quad \text{(O3)}$$

$$GD'_{A\,to\,B}(k) = \sum_{l=1}^{i} \frac{1}{2} \frac{\left|S'_A(k,l) - S'_{A,ideal,A\,to\,B}(k,l)\right| + \left|S'_B(k,l) - S'_{B,ideal,A\,to\,B}(k,l)\right|}{i^2} \quad \text{(O4)}$$

In each equation, a comparison is made between the actual amount of A and B as a function of (chain) position l ($S_{A/B}$) and the amount of the theoretical ideal linear gradient profile ($S_{A/B,ideal}$) given in Figure N2 in Appendix N. The first two equations relate to an evaluation from 'left to right', whereas the last two relate to an evaluation from 'right to left'. A further distinction is made whether (from 'left to right') a 'A to B' or 'B to A' reference gradient is used. In this way, as explained below, the linear gradient quality of the considered copolymer chain k can be calculated by selecting the minimum value of these four averages.

To illustrate the necessity of the calculation of the minimum of four linear gradient deviation values ($GD_{B\ to\ A}$, $GD_{A\ to\ B}$, $GD'_{B\ to\ A}$ and $GD'_{A\ to\ B}$; Equation O1-O4) a comparison is made between following five methods:

$$GD_1(k) = GD_{B\,to\,A}(k) \quad \text{(O5)}$$

$$GD_2(k) = GD_{A\,to\,B}(k) \quad \text{(O6)}$$

$$GD_3(k) = GD'_{BtoA}(k) \qquad \text{(O7)}$$

$$GD_4(z) = GD'_{AtoB}(k) \qquad \text{(O8)}$$

$$GD_5(k) = \min\left\{GD_{BtoA}(k),\quad GD_{AtoB}(k), GD'_{BtoA}(k),\quad GD'_{AtoB}(k)\right\} \qquad \text{(O9)}$$

The first four methods (O5-O8) correspond to a single evaluation per chain k, whereas the last method (O9) is the one used in Chapter 5, i.e., the minimal value of $GD_{B\ to\ A}$, $GD_{A\ to\ B,}$ $GD'_{B\ to\ A}$ and $GD'_{A\ to\ B}$ is used per chain. For all five methods the average value is obtained by:

$$< GD_m^* >= \sum_{k=1}^{k_{max}} \frac{GD_k(k)}{k_{max}} \qquad \text{(O10)}$$

Note that $<GD_5^*>$ is the same as <GD*> in Chapter 5, i.e. no rescaling with 0.175 is performed yet.

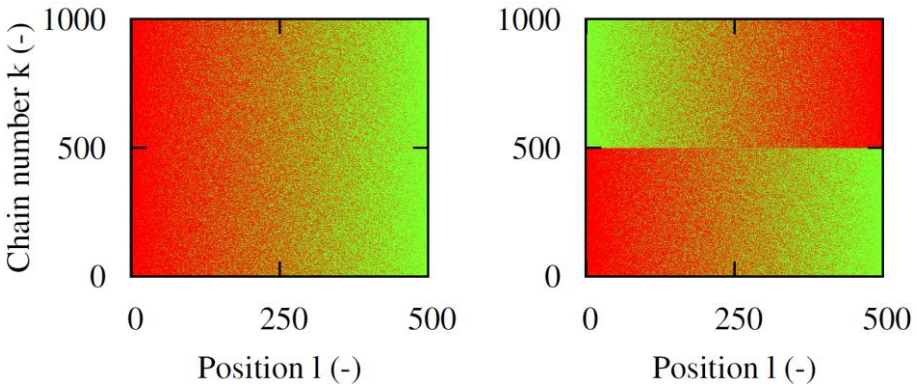

Figure O1: left: 'perfect' linear 'B to A' gradient (TCL = 500); right: same but with half of the polymer chains plotted in the opposite direction; red: monomer B, green: monomer A; these both copolymers should be evaluated the same with respect to linear gradient quality

For a 'perfect' linear B to A gradient (TCL = 500) as shown in Figure M1 (left), the corresponding evolutions of $<GD_m^*>$ (m = 1,…,5) with 'conversion' are given in Figure O2. Here a 'conversion' of e.g. 0.10/0.20/… corresponds to the copolymer when selecting only the first fifty/hundred/… columns of Figure O1 (left). It can be seen that at low 'conversion' a 'right to left' evaluation is necessary, since $GD'_{A\ to\ B}$ leads to the minimal GD value. As indicated in Chapter 5, 'right to left' evaluations are denoted by a prime. On the other hand, at

higher conversions $GD_{B\ to\ A}$, which corresponds to a 'left to right' evaluation, leads always to the lowest value. Note that for Figure O1(left) a <GD> value of 0.01 results. Hence, in order to correctly calculate the gradient quality of these copolymers it is already necessary to include one 'left to right' and one 'right to left' evaluation.

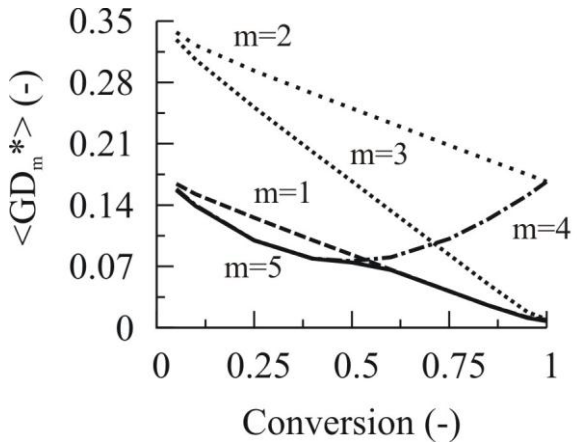

Figure O2: Five different methods (Equation O6-O10) for the evaluation of the average linear gradient deviation (<GD*>) as a function of 'conversion' leading to the copolymer shown in Figure M1 (left); here 'conversion' of e.g. 0.10/0.20/… corresponds to the copolymer when selecting only the first fifty/hundred/… columns; m is the number of the method; m = 5: method used in Chapter 5 (here not rescaled with 0.175)

Table O1 shows that for the copolymer presented in Figure O1 (right) all four evaluations are however necessary. This copolymer is in 'reality' the same as Figure O1 (left) and should thus have the same <GD*> value of 0.01. The only difference is that here half of the polymer chains are plotted in the opposite direction. It can be seen that in the first four cases a value of ca. 0.09 results, which is significantly higher than the correct value of 0.01 which is obtained in case the criterion is used as discussed in Chapter 5. Only via the latter criterion the computer evaluation corrects automatically for polymer chains being stored in the matrix 'CopolymerComposition' in the 'wrong way' before <GD*> is calculated. For completeness, it is mentioned here that in Figure O2 the maximal value for the minimum of the 4 gradient evaluations (m = 1,…,4) is 0.175.

Table O1: Average linear gradient deviation (<GD*>) for copolymer Figure O1 (right) and different criteria; m is the number of the criterion; m = 5: criterion used in Chapter 5; 0.01 should be obtained (same value as Figure O1 (left))

Criterion m	<GD*>
1	0.09
2	0.09
3	0.09
4	0.09
5	**0.01**

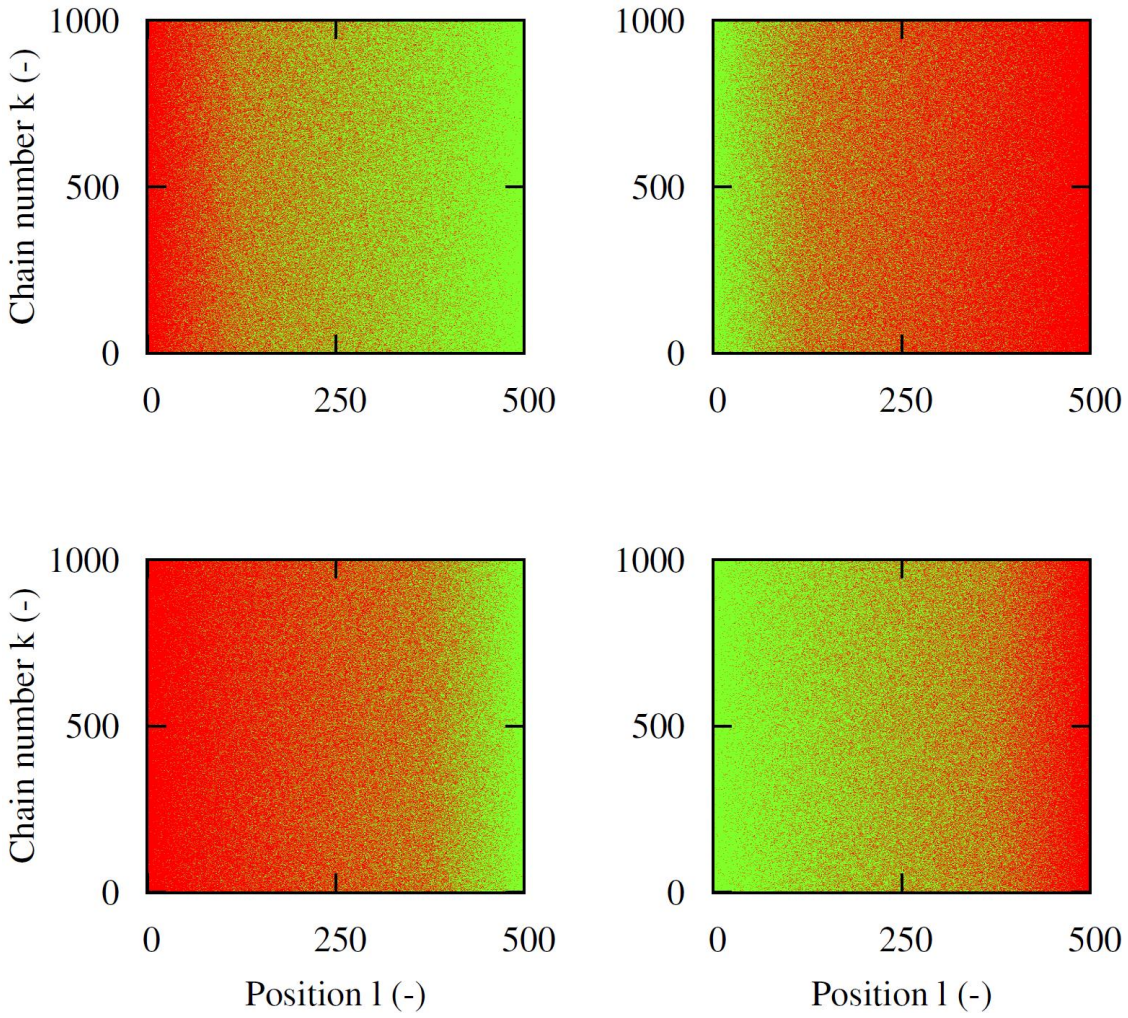

Figure O3: top left: based on Equation O11-O12; top right: same equations both with A and B switched; bottom: switch of position at which the probabilities are equal to 0.5 from 125 to 375; red: monomer B, green: monomer A; these copolymers have the same linear gradient quality

Hence, it is clear that in general all four deviations have to be taken into account. The latter can also be concluded from Table O2 which shows the $<GD_m^*>$ (m = 1,…,5) values in case the four copolymers shown in Figure O3 are compared. These copolymers have the same linear gradient quality, since they are all piecewise linear gradient copolymers based on the same probabilities for the comonomer present. For example, the top left copolymer corresponds to the following piecewise probabilities (with i = 500) for A and B:

$$p_A(l,i) = \frac{0.5(l-1)}{\frac{i}{4}-1} = 1 - p_B(l,i) \qquad (1 \le l \le i/4) \qquad \text{(O11)}$$

$$p_A(l,i) = 1 - \frac{2(i-l)}{3i} = 1 - p_B(l,i) \qquad (i/4 \le l \le i) \qquad \text{(O12)}$$

Note that at a position of i/4 both probabilities become equal to 0.5 and as l increases more A is present in the copolymer. The top right copolymer is based on the same equations but with A and B switched. The bottom two copolymers are obtained by switching the position at which both probabilities are the same from i/4 to 3/4 i. It can be seen that the criterion of Chapter 5 (m = 5) leads to a unique value of 0.052. Moreover, close inspection of the table shows that the criterion takes into account the consideration mentioned in Chapter 5, since the $<GD_m^*>$ (m = 1,…,4) values are permuted per column.

Table O2: Average linear gradient deviation (<GD*>) for copolymers of Figure O3 for different criteria; m is the number of the criterion; m = 5: criterion used in Chapter 5 without rescaling

	$<GD_m^*>$			
Criterion	top left	top right	bottom left	bottom right
1	0.219	0.112	**0.052**	0.073
2	**0.052**	0.073	0.219	0.112
3	0.112	0.219	0.073	**0.052**
4	0.073	**0.052**	0.112	0.219
5	**0.052**	**0.052**	**0.052**	**0.052**

Appendix P: Instantaneous and cumulative monomer unit profiles for theoretical ideal linear gradient profile

For a perfect linear gradient 'B to A' copolymer (plotted from 'left to right') with all polymer chains having a chain length i, the probability that A is present at (chain) position l (l = 1, …, i) is defined as:

$$p_{A,ideal,BtoA}(l,i) = \frac{l-1}{i-1} = 1 - p_{B,ideal,BtoA}(l,i) \qquad \text{(P1)}$$

in which $p_{B,ideal,\ B\ to\ A}$ is the probability that B is present, which in turn decreases linearly with position l. However, as explained in Appendix R, only for sufficiently high chain lengths these probabilities can be approached using random numbers. For example, Figure P1 shows the result of such generation for two targeted chain lengths (TCL = 100 and 500). In both cases, at the first positions the polymer is rich in monomer B (2; red), whereas a gradual change to the exclusive presence of monomer A (1; green) takes places at the last positions. It can be seen that a higher TCL implies a smoother transition from 'B to A' and thus allows a better mimicking of the ideal probabilities.

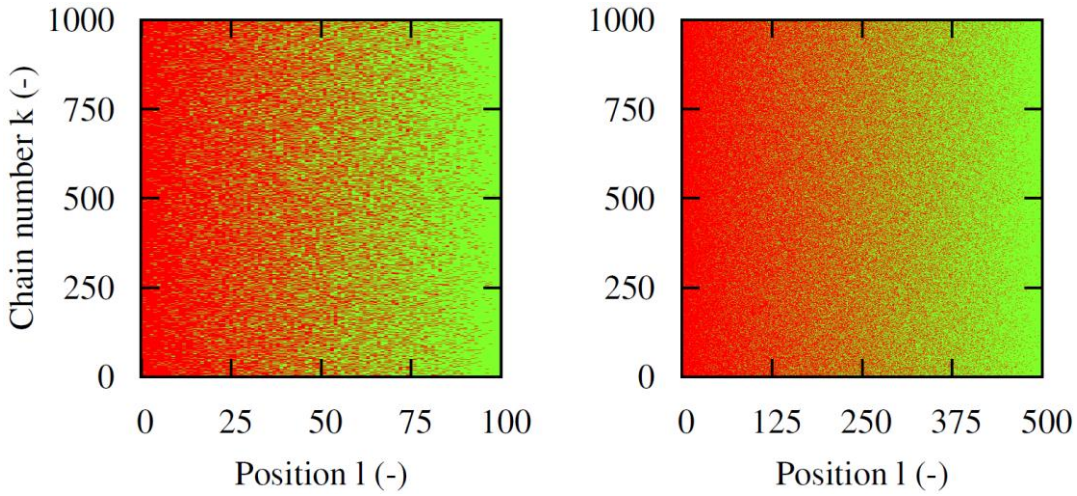

Figure P1: Random numbers based generation of the ideal linear 'B to A' gradient for 1000 polymer molecules all having a chain length of (left) 100 (right) 500; related to Equation (P1); red: monomer B, green: monomer A; right: better linear gradient (see Appendix R)

Based on Equation P1, the theoretical amount of monomer A/B that has to be present up to a position l (from 'left to right') for a polymer chain k with length i can be calculated as follows:

$$S_{A,ideal,BtoA}(i,l)=\sum_{l'=1}^{l} p_{A,ideal,BtoA}(l',i)=\frac{(l-1)l}{2(i-1)} \qquad \text{(P2)}$$

$$S_{B,ideal,BtoA}(i,l)=\sum_{l'=1}^{l} p_{B,ideal,BtoA}(i,l')=\sum_{l'=1}^{l}\frac{(l'-1)}{(i-1)}=\frac{i}{2}-\frac{(i-l)(i-l-1)}{2(i-1)} \qquad \text{(P3)}$$

in which i depends on k only. For simplicity, in the remaining equations i always refers to i(k).

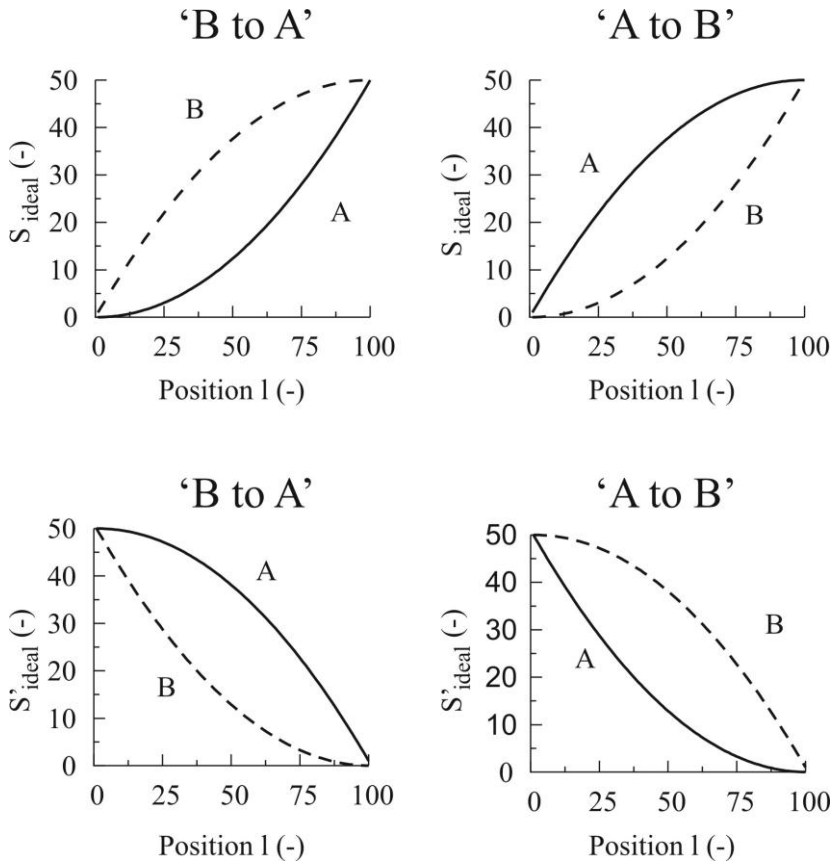

Figure P2: Theoretical amount of monomer A/B for ideal linear 'B to A' (left) and 'A to B' (right) perfect gradient copolymer chain; i = 100; the perfect gradient copolymer chains are considered from 'left to right'; top 2 plots used for 'left to right' evaluation of the linear gradient quality of a 'actual' copolymer chain; bottom 2 plots are used for 'right to left' evaluation

For a chain length *i* of 100, these ideal cumulative values for a ‘B to A’ gradient copolymer chain are shown in Figure P2 (left top). Similarly, for a perfect ‘A to B’ gradient copolymer, again plotted from ‘left to right’, Figure P2 (right top) is obtained, which is based on Equation (P4) and (P5):

$$S_{A,ideal,AtoB}(k,l) = S_{B,ideal,BtoA}(k,l) \qquad \text{(P4)}$$

$$S_{B,ideal,AtoB}(k,l) = S_{A,ideal,BtoA}(k,l) \qquad \text{(P5)}$$

However, as explained in Appendix O, a proper linear gradient evaluation also requires the comparison with four other linear gradient profiles. To obtain e.g. the same linear gradient quality for the copolymer of Figure O1 (left) in Appendix M and the same copolymer but with half of the copolymer chains artificially plotted from ‘left to right’ (Figure O1 (right)) the profiles shown in the bottom of Figure P2 are also needed:

$$S'_{A,ideal,AtoB}(i,l) = S_{B,ideal,AtoB}(i,i-l+1) \qquad \text{(P6)}$$

$$S'_{B,ideal,AtoB}(i,l) = S_{A,ideal,AtoB}(i,i-l+1) \qquad \text{(P7)}$$

$$S'_{A,ideal,BtoA}(i,l) = S'_{B,ideal,AtoB}(i,l) \qquad \text{(P8)}$$

$$S'_{B,ideal,BtoA}(i,l) = S'_{A,ideal,AtoB}(i,l) \qquad \text{(P9)}$$

In these equations, the prime is used to refer to a ‘right to left’ evaluation instead of a ‘left to right’ evaluation. These four equations are plotted in the bottom of Figure P2 and have the same shape as those plotted in the top underlining that the calculation accounts for the considerations explained in Chapter 5.

In other words, an ‘actual’ copolymer chain k can only be regarded as an ideal linear gradient copolymer chain in case its cumulative amounts of A and B vary similarly to either the left or right subplots of Figure P2 depending on whether this chain has ‘B to A’ or ‘A to B’ linear gradient character from ‘left to right’. The calculation of the actual cumulative amounts is discussed below.

For a simulated copolymer chain with chain length i (e.g. the k-th polymer chain in the matrix CopolymerComposition) a cumulative amount of monomer A, $S_A(k,l)$, can be calculated as follows in case an evaluation is performed from 'left to right':

$$S_A(k,l) = \sum_{l'=1}^{l} \left[2 - CopolymerComposition(k,l')\right] \qquad \text{with } l = 1, \ldots, i \qquad \text{(P10)}$$

For each position *y* where a monomer A is present, the value of S_A is increased by unity while no contribution is added if a monomer B is present. Analogously, for B the following equation can be derived:

$$S_B(k,l) = \sum_{l'=1}^{l} \left[CopolymerComposition(k,l') - 1\right] \qquad \text{with } l = 1, \ldots, i \qquad \text{(P11)}$$

Furthermore, for an evaluation from 'right to left' the following similar equations result:

$$S'_A(k,l) = \sum_{l'=i}^{l} \left[2 - CopolymerComposition(k,l')\right] \qquad \text{with } l = 1, \ldots, i \qquad \text{(P12)}$$

$$S'_B(k,l) = \sum_{l'=i}^{l} \left[CopolymerComposition(k,l') - 1\right] \qquad \text{with } l = 1, \ldots, i \qquad \text{(P13)}$$

in which the prime in S' denotes again the evaluation from 'right to left'.

Appendix Q: Functional form for gradient evaluation

As explained in Appendix O, for the gradient evaluation of a copolymer chain k the equations O1-O4 are used. For example, Equation O1 allows to calculate per polymer chain the linear gradient deviation in case a 'B to A' gradient is the reference and a 'left to right' evaluation is performed. In what follows the functional form of Equation O1 is explained. A similar explanation can be given for the other three equations.

First, both the cumulative amount of A and B ($S_{A/B}$) are compared with the corresponding ideal reference amount (here $S_{A/B\ ideal,\ B\ to\ A}$) for a given position i in the polymer chain, which are subsequently used to calculate the average:

$$\frac{1}{2}\left(\left|S_A(k,l)-S_{A,ideal,BtoA}(k,l)\right|+\left|S_B(k,l)-S_{B,ideal,BtoA}(k,l)\right|\right) \qquad \text{(Q1)}$$

After summation over all positions for that polymer chain, this value is divided by the chain length i to express the deviation per monomer unit for the considered polymer chain:

$$\sum_{l=1}^{i}\frac{1}{2}\frac{\left(\left|S_A(k,l)-S_{A,ideal,BtoA}(k,l)\right|+\left|S_B(k,l)-S_{B,ideal,BtoA}(k,l)\right|\right)}{i} \qquad \text{(Q2)}$$

However, a second deviation by i is necessary since $S_{A/B}$ scales with i:

$$\sum_{l=1}^{i}\frac{1}{2}\frac{\left(\left|S_A(k,l)-S_{A,ideal,BtoA}(k,l)\right|+\left|S_B(k,l)-S_{B,ideal,BtoA}(k,l)\right|\right)}{i^2} \qquad \text{(Q3)}$$

In such way, it is avoided that polymer chains with a high chain length but good linear gradient quality are badly evaluated. As explained above, reproducing of the ideal linear gradient by the probabilities of Equation P1 is better for higher TCLs. However, in case the second division by i (here TCL) is not taken into account the criterion would regard ideal linear gradients for high TCls as worse, as illustrated in Figure Q1:

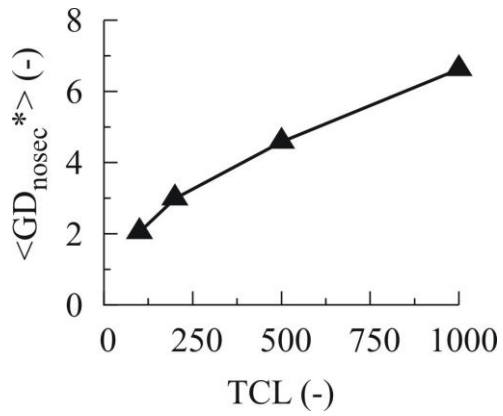

Figure Q1: Average linear gradient deviation without a second scaling with i (<GD_{nosec} *>) for the copolymer reproduced based on Equation (N1) at different TCLs

Appendix R: Effect of targeted chain length on mimicking of an ideal gradient copolymer

Figure R1 shows the <GD> value for gradient copolymers obtained based on Equation (O1) for different TCLs. For all TCls, a value close to zero is obtained with an improved linear gradient quality at higher TCLs. The latter can be understood based on the fact that to short polymer chains do not allow a 'continuous' linear gradient character as needed by Equation (O1).

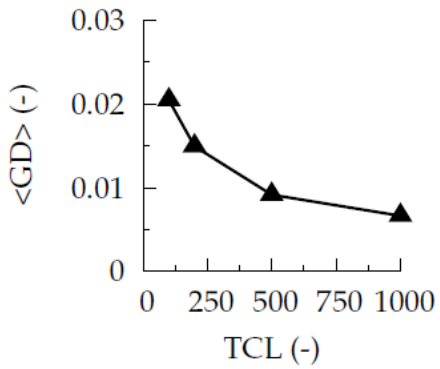

Figure R1: Average linear gradient deviation (<GD>) for gradient copolymers obtained based on Equation (O1) for different targeted chain lengths (TCLs); TCL = 100 (Figure P1 (left) in Appendix P), 200, 500 (Figure P1 (right) in Appendix P) and 1000

For a TCL of 500, it follows however that a value of 0.008 (ca. 0.01) is obtained, which can be considered as sufficiently low. Hence, the corresponding copolymer (Figure P1 (right) in Appendix P) can be safely regarded as an ideal linear gradient copolymer.

Appendix S: Variance of GD distribution

Figure S1 shows the variance of the GD distribution, defined as:

$$s^2 = \sum_{k=1}^{k=N} \frac{\left(\frac{\langle GD(k) \rangle}{0.175} - \frac{\langle GD^* \rangle}{0.175} \right)^2}{N-1} \qquad \text{(S1)}$$

as a function of conversion for the ATRP corresponding to Figures 5-9 in Chapter 5. It can be seen that a value of approximately 0.01 is obtained from low conversion onwards, which is three times lower than the average value, <GD>. This indicates that a narrow GD distribution is obtained.

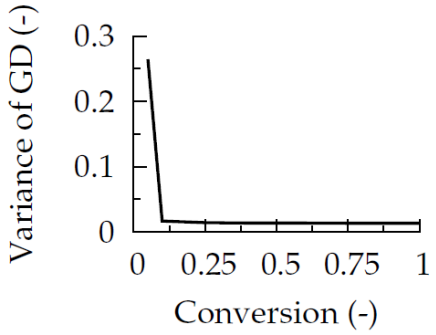

Figure S1: Variance of GD distribution corresponding to Figures 5-9 in Chapter 5

Appendix T: Effect of activation rate coefficient on the polymer properties

Figure T1 shows the PDI, end-group functionality and <GD> profile for various activation rate coefficients $k_{a,chem}$ for a fixed $k_{da,chem}$ of 10^6 L mol^{-1} s^{-1}. In each simulation, the activation of tertiary dormant species ($k_{a,chem,BX}$) is assumed ten times faster than for secondary species ($k_{a,chem,AX}$). The <GD> and PDI profile display a minimum situated at $k_{a,chem}$ equal to 10^{-1} L mol^{-1} s^{-1}. On the other hand, the end-group functionality decreases as a function of $k_{a,chem}$ and therefore cannot be used to assess the linear gradient quality. Compared to Figure 13 in Chapter 5 (fixed $k_{da,chem}$ of 10^7 L mol^{-1} s^{-1}) higher PDI and thus <GD> values are obtained.

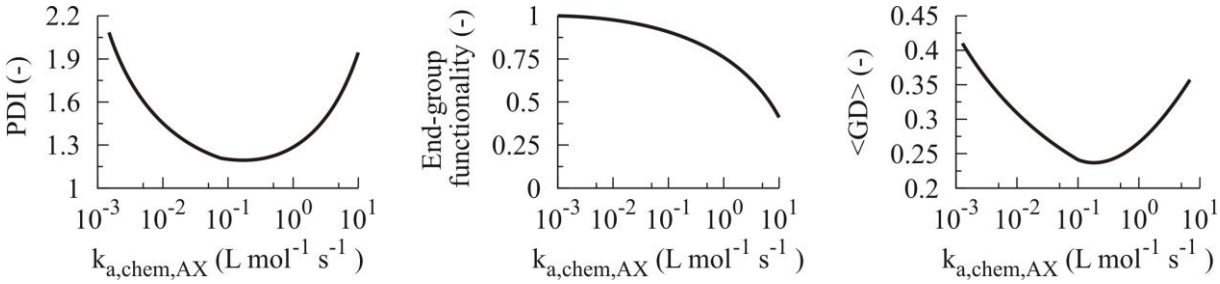

Figure T1: left: PDI; middle: end-group functionality; right: <GD> as a function of $k_{a,chem,AX}$ at a conversion of 1; $[A+B]_0/[R_0X]_0/[Cu(I)L_yX]_0$ = 100/1/1 with $[A]_0 = [B]_0$ and $[Cu(II)L_yX_2]_0 = 0$; $k_{da,chem} = 10^6$ L mol^{-1} s^{-1} and $k_{a,chem,BX} = 10\ k_{a,chem}$

Appendix U: Statistical significance of regression

U.1. Regression

To decide if the correlation of <GD> with PDI for a TCL of 100 is significantly different from the correlation for a TCL of 500, statistics should be used. Non-weighted linear regressions are performed for three data sets:

1. The data set for TCL = 100 with $N_1 = 20$ data points
2. The data set for TCL = 500, with $N_2 = 20$ data points
3. The combined data set, with $N_1+N_2 = 40$ data points

For convenience, PDI and <GD> are denoted respectively x and y from here on. Via Equation U1, the parameters β_0 and β_1 can be fitted to the data set.

$$y = \beta_0 + \beta_1 x \qquad \text{(U1)}$$

It is assumed that the (regression) model errors are normally distributed and with unknown but equal variance. The estimates for β_0 and β_1 are denoted respectively b_0 and b_1. Hence, for each set of data, values for b_0 and b_1 will be obtained. To calculate the parameters, helping variables are calculated in Table U1:

Table U1: Helping variables to determine linear regression parameters.

	TCL = 100	TCL = 500	Combined
$\sum x_i$	23.39	23.46	46.85
$\sum y_i$	4.44	3.73	8.16
$\sum x_i y_i$	5.27	4.54	9.81
$\sum x_i^2$	27.55	27.85	55.40
$\sum y_i^2$	1.02	0.78	1.80

Based on these sums, following averages are defined for N data points:

$$\overline{x} = \frac{\sum x_i}{N} \qquad \text{(U2)}$$

$$\overline{y} = \frac{\sum y_i}{N} \qquad \text{(U3)}$$

$$\overline{xy} = \frac{\sum x_i y_i}{N} \qquad \text{(U4)}$$

$$\overline{x^2} = \frac{\sum x_i^2}{N} \qquad \text{(U5)}$$

$$\overline{y^2} = \frac{\sum y_i^2}{N} \qquad \text{(U6)}$$

These averages[1,2] allow to estimate b_0 and b_1 according to Equations U7 and U8:

$$b_0 = \bar{y} - b_1\bar{x} \qquad \text{(U7)}$$

$$b_1 = \frac{\overline{xy} - \bar{x}\cdot\bar{y}}{\overline{x^2} - \bar{x}^2} \qquad \text{(U8)}$$

The found parameters are given in Table U2 with 99% probability.

Table U2: Regression parameters and 99% confidence interval (α = 0.01).

	TCL = 100	TCL = 500	Combined
b_0	-0.28 ± 0.02	-0.41 ± 0.02	-0.35 ± 0.12
b_1	0.43 ± 0.02	0.50 ± 0.02	0.47 ± 0.09

It is clear that the confidence intervals of the parameters of the separate regressions do not overlap, hence it can be expected that the data for TCL = 100 and the data for TCL = 500 should not be combined into a single data set. As illustrated below, the difference in the correlations for TCL = 100 and TCL = 500 is significant.

U.2. Chow test

The Chow test[3] is an F-test and determines if two linear regressions differ significantly by using the null hypothesis that k parameters β_0, β_1,… are the same for both data sets.

Without going in detail, the Chow test statistic T is constructed as:

$$T = \frac{\left(\frac{S_3 - (S_1 + S_2)}{k}\right)}{\left(\frac{S_1 + S_2}{N_1 + N_2 - 2k}\right)} \qquad \text{(U9)}$$

In which:

1. S_1 is the sum of squared residuals of the first data set (TCL = 100)
2. S_2 is the sum of squared residuals of the second data set (TCL = 500)
3. S_3 is the sum of squared residuals of the combined data set
4. k is the number of parameters in the regression model (2)

The denominator characterizes the sum of squared residuals by performing separate regressions while the numerator characterizes the reduction in sum of squared residuals by performing separate regressions. Because the S_i are all χ^2 distributed, the Chow test statistic follows an F distribution with degrees of freedom k and N_1+N_2-2k, i.e.:

$$\frac{\left(\frac{S_3-(S_1+S_2)}{k}\right)}{\left(\frac{S_1+S_2}{N_1+N_2-2k}\right)} \sim F(2,36) \qquad \text{(U10)}$$

The S_i are calculated using the earlier defined helping variables and regression parameters (Tables U1 and U2):

$$S_i = \Sigma(y_i - \hat{y}_i)^2 = \Sigma y_i^2 - b_0 \Sigma y_i - b_1 \Sigma x_i y_i \qquad \text{(U11)}$$

In which $\hat{y}_i$ is the <GD> value according to Equation U1, i.e. the regression value. The found values for S_i are given in Table U3.

Table U3: Sum of residual squares for the separate and combined data sets.

	TCL = 100	TCL = 500	Combined
S	0.0011	0.0020	0.0175

The test statistic is then:

$$F(2,36) = \frac{\left(\frac{0.0175-(0.0011+0.0020)}{2}\right)}{\left(\frac{0.0011+0.0020}{20+20-4}\right)} = 84.08 \qquad \text{(U12)}$$

The critical F value with a significance level of 1% is $F(2,36)_{crit} = 5.25$. For values of the test statistic lower than the critical F value, the null hypothesis is accepted. For values of the test statistic higher than the critical value, the null hypothesis is rejected. Hence, the null hypothesis, i.e. β_0 and β_1 are the same for both data sets, can be rejected with 99% probability. Table U4 illustrates the effect of α on the critical F value.

Table U4: Critical F value as a function of the significance level of the test.

α	$F(2,36)_{crit}$
5% (Significant)	3.26
1% (Very/strongly significant)	5.25

Hence, the (PDI,<GD>) data for TCL = 100 and TCL = 500 must be described using different correlations, meaning that there is a clear effect of the TCL on the correlation of PDI with <GD>.

References

1. Taerwe, L. Waarschijnlijkheidsrekening en statistiek, Cursustekst Universiteit Gent, 2003.
2. Dingens, P. Beginselen der waarschijnlijkheidsrekening en der mathematische statistiek, Cursustekst Universiteit Gent, 1960
3. Chow, G.C. *Econometrica* **1960**, 28, 3, 591-605.

Glossary

α,ω-macro-diradical recombination:

Term coined by the group of Rehahn for the recombination of linear macrodiradicals possessing radical centers at each chain end. The reaction product is not a dead polymer molecule, but a new, longer, α,ω-macrodiradical.

1,6-elimination:

Analogously to the conventional 1,2-elimination to form a vinyl bond, the substrate for an 1,6-elimination is a p-xylene and the reaction product is a quinoid type molecule breaking aromaticity during the 1,6-elimination.

Apparent rate coefficient:

Rate coefficient related to the observed kinetics, i.e., rate coefficient determined by the intrinsic chemical rate coefficient and transport phenomena.

Arrhenius coefficient:

$k = A\ exp(-E_A/RT)$ with k the rate coefficient of the reaction step, R the universal gas constant, T the temperature and A the pre-exponential factor; E_A the Arrhenius activation energy.

Atom transfer radical polymerization (ATRP):

Polymerization technique allowing ’controlled’ polymer properties, i.e., a low value for the polydispersity index and a high livingness. ATRP is based on an atom transfer of the end-group functionality via a transition metal complex, i.e., the ATRP catalyst.

Biradical:

Molecule possessing two radical centers which are interacting with each other through mesomery.

Branch:

Defined for non-networked polymers, a linear part of a polymer chain formed by a branching reaction, such as radical transfer to polymer or backbiting.

Catalyst:

A species which is regenerated at the end of a closed reaction sequence.

Chain length of a polymer molecule:

The number of repeating units (coming from the (co)monomer(s)) in a polymer molecule.

Chain transfer:

Reaction leading to transfer of the radical center between two species.

Chemical composition – chain length distribution (CC-CLD):

Type of distribution in which the variables are the chain length and the chemical composition. Specifically for linear copolymerization, the chemical composition is the (fractional) monomer composition for a given chain length. Specifically for weakly branched homopolymerization, the chemical composition is the number of short chain branches for a given chain length.

Chemical composition distribution (CCD):

Describes the number fraction of polymer chains as a function of their fractional monomer composition. The broadness of the CCD is an indication of the compositional homogeneity of the polymer product.

Compositional drift:

The deviation of the copolymer composition from the monomer composition in the feed.

Conjugation length:

Length of the conjugated system along the polymer backbone.

Conjugated polymer:

Polymer possessing alternating single and double carbon-carbon bonds, possessing high conductivity and thus opto-electronic properties. Typically the conjugated system resides on the backbone, although side chain conjugation has been reported as well.

Copolymerization:

Denoting the polymerization of multiple monomers. However, often the term is used to denote the polymerization of two monomers.

Cumulative copolymer composition profile:

The fraction of monomer A cumulatively incorporated in the copolymer, $F_{A,cum}$, as a function of the fraction of monomer A in the monomer feed, f_A. The polymerization time is an implicit parameter in this representation.

Deactivation of a radical:

CRP specific reaction leading to incorporation of end-group functionality and the disappearance of a radical center.

Dead polymer molecule:

Polymer molecule without end-group functionality.

Diradical:

Molecule possessing two radical centers which are not interacting with each other through mesomery.

Dead polymer molecule:

Polymer molecule without end-group functionality X

Dormant polymer molecule:

Polymer molecule possessing end-group functionality X

Elementary reaction step:

The irreducible act of reaction in which reactants are transformed into products directly,

i.e., without passing through an intermediate that is susceptible to isolation.

End-group functionality:

Functional group allowing further chemical modification (mostly a halogen atom in ATRP);

part allowing livingness.

Geometric mean:

The geometric mean of N real numbers x_i (1, …, N) is defined as $(x_1 \cdot x_2 \cdot \ldots \cdot x_{N-1} \cdot x_N)^{1/N}$.

Glass transition temperature:

A second-order phase transition through which a strong restriction of mobility of the polymer molecules is obtained. Below this temperature a glassy amorphous solid is obtained. Above this temperature a rubbery amorphous solid is obtained. Gradient copolymers are characterized by broad glass transition temperature ranges.

Gradient copolymer:

Mostly pertaining to linear polymer chains, denoting a gradual change in the monomer composition along the polymer chain.

Gradient deviation:

A deviation (with respect to the theoretical ideal linear gradient profile) of the cumulative monomer composition of a single chain.

Hole mobility:

Pertaining to the mobility of holes in the p-donor phase as opposed to the mobility of electrons in the n-donor phase. Due to overall charge neutrality, at least one of the mobilities is limiting energy conversion in an opto-electronic device, usually the p-type material, such as PPV.

Homo-termination:

Denoting the termination of similar species. For homopolymerization, it refers to an equal chain length of the recombining species. In the case of copolymerization of two monomers A and B, the termination between macroradicals ending in the same monomer unit is often termed "homo-termination", as opposed to cross-termination denoting the termination a macroradical ending in A and a macroradical ending in B.

Ideal ATRP:

A polymerization via the ATRP mechanism in which a polymer is obtained in which all polymer chains possess the same predetermined chain length and end-group functionality. This requires instantaneous ATRP initiation and absence of termination reactions.

Ideal gradient copolymer chain:

Chain obtained by sampling from the probabilities dictated by the theoretical ideal linear gradient profile.

Instantaneous copolymer composition:

The fraction of monomer A instantaneously incorporated in the copolymer, $F_{A,inst}$, as a function of the fraction of monomer A in the monomer feed, f_A. The polymerization time is an implicit parameter in this representation.

Kinetic Monte Carlo (kMC):

Monte Carlo method to simulate the time evolution of processes occurring in nature. The KMC method is essentially the same as the dynamic Monte Carlo method and the Gillespie algorithm, the difference is in terminology and application area. The KMC algorithm is also known as the residence-time algorithm, the *n*-fold way or the Bortz-Kalos-Lebowitz (BKL) algorithm.

Mayo-Lewis equation:

A widely used closed-form analytical expression to describe the instantaneous copolymer composition $F_{A,inst}(f_A)$. It is based on the quasi-steady state approximation of the individual macroradical terminal unit types and depends only the (propagation) reactivity ratios $r_1 = k_{11}/k_{12}$ and $r_2 = k_{22}/k_{21}$.

Polymer molecule:

A molecule built from many monomers.

Macroradical:

Polymer molecule possessing a radical center.

Mechanism:

Is used to describe a reaction network or a reaction sequence or the stereochemistry of an elementary reaction step.

Microstructure:

The entirety of structural characteristics of a polymer on the molecular level. They determine the morphological, rheological, thermal and physical properties of polymers.

Monomer conversion:

Monomer consumed with respect to initial amount.

Monomer sequence:

A fixed-order series of monomers of arbitrary number and identity.

Monomer sequence distribution:

The number fraction of a sequence with given length as a function of every possible monomer sequence.

Monte Carlo algorithm:

A randomized algorithm with deterministic running time and characterized by output which may be incorrect with a certain (typically small) probability. E.g. coin-tossing.

Number chain length distribution of the polymer:

Number fraction of polymer molecules as a function of chain length.

Polydispersity:

For polydispersity equal to unity, there is a unique chain length and the number, mass and z average chain length coincide. For polydispersities higher than unity, the polymer chains are distributed with respect to their chain length and the averages of the CLD do not coincide.

Poly(phenylene vinylene) PPV:

The most used conjugated polymer.

Propagation of a radical:

Reaction leading to chain growth, i.e. addition to monomer.

Rate coefficient:

Coefficient of proportionality for the calculation of a reaction rate.

Reaction channel:

Term used in kinetic Monte Carlo method literature to denote the reaction possibilities of a chemically reacting system. During the course of simulation, multiple firings of reaction events occur through the reaction channels.

Reaction event:

Term used in kinetic Monte Carlo method literature to denote the firing of a single reaction by a computer simulation.

Regioregularity:

Term mostly pertaining to the repetitive nature of the placement of side chains onto a polymer backbone. Predominantly related to the environment of a monomer unit in a polymer, which can be investigated using NMR spectroscopy.

Reversible Addition Fragmentation chain Transfer-Chain Length Dependent-Termination (RAFT-CLD-T)'- technique:

An accurate method for measuring apparent termination rate coefficients as a function of chain length and conversion using reversible addition-fragmentation chain transfer polymerization.

Segment:

A monomer sequence consisting of a single type of monomer unit (either A or B but not both), also called a block.

Segment length distribution:

The number fraction of a segment as a function of the segment length. The segment length is defined as the highest length of a consecutive series of monomers of the same type, i.e. …BAAAB… is a segment of length 3.

Sequence:

See ‘monomer sequence’.

Stochastic process:

As opposed to a deterministic process, describing a process which can only evolve in one way. In a stochastic process, there are several (often infinitely many) directions in which the process may evolve.

Termination of radicals:

Reaction leading to the formation of (a) dead polymer molecule(s) with the disappearance

of two radical reactive centers.

Theoretical ideal linear gradient profile:

Probability density function of the fraction of monomer A or B along a theoretical chain.

Topology:

Specifically for polymers, topology is closely related to polymer architecture and includes linear, short chain branched, long chain branched, networked, armed/star, brush, comb-like, grafted and dendritic polymers.

Triad distribution:

Monomer sequence distribution of length 3.

Univariate:

Referring to a function of only one variable. Functions involving more than one variable are called multivariate. Specifically for distributions, in the case of only two random variables, this is called a bivariate distribution, but generalizes to any number of random variables, giving a multivariate distribution.